

Modeling and Optimization of Turning Duplex Stainless Steels

Von der Fakultät Konstruktions-, Produktions- und Fahrzeugtechnik
der Universität Stuttgart zur Erlangung der
Würde eines Doktors der Ingenieurwissenschaften (Dr.-Ing.)
genehmigte Abhandlung

Vorgelegt von
M. Sc. Rastee Dalshad Ali (Koyee)
aus Erbil, Kurdistan-Irak

Hauptberichter: Univ.-Prof. Dr.-Ing. Prof. h. c. mult. Dr. h. c. mult. Uwe Heisel i. R.
Mitberichter: Prof. Dr. rer. nat. Siegfried Schmauder

Tag der mündlichen Prüfung: 14.04.2015

Institut für Werkzeugmaschinen der Universität Stuttgart
2015

Vorwort

Hiermit möchte ich all denen meinen Dank aussprechen, die mich bei der Entstehung dieser Arbeit unterstützt und zu ihrem Gelingen beigetragen haben. In diesem Zusammenhang sei dem Deutsche Akademische Austauschdienst für die finanzielle Unterstützung und Förderung gedankt.

Dem Leiter des Institutes, Univ.-Prof. Dr.-Ing. Prof. h. c. mult. Dr. h. c. mult. Uwe Heisel i. R. gilt mein besonderer Dank für die Möglichkeit zur Durchführung der Arbeit und den dafür notwendigen Freiraum ebenso wie für die Übernahme des Hauptberichtes und die dabei entstandenen Anregungen.

Herrn Prof. Dr. rer. nat. Siegfried Schmauder danke ich sehr herzlich für die teilweise Betreuung meiner Arbeit. Seine freundliche Unterstützung meiner wissenschaftlichen Tätigkeit, seine ständige Bereitschaft zu fachlichen Diskussionen mit vielen wertvollen Ratschlägen und konstruktiven Anregungen haben maßgeblich zur Realisierung dieser Arbeit beigetragen.

Herrn Dipl.-Ing Dipl.-Gwl. Rocco Eisseler, meinem langjährigem Kollege und Gruppenleiter, danke ich für zahlreiche konstruktive fachliche Diskussionen, die ebenso wie seine Tipps zu formalen Aspekten der schriftlichen Ausarbeitung eine wertvolle Hilfe geleistet haben.

Ein herzlicher Dank gebührt weiterhin meinen Kollegen und Freunden, durch die ich meine Promotionszeit in schöner Erinnerung behalten werde. Frau Inge Özdemir, Herrn Dr.-Ing. Michael Schaal, Herrn Dipl.-Ing. Atanas Mishev, Herrn Dipl.-Ing. (FH) Jens Großmann, Herrn Rolf Bauer und Herrn Dr.-Ing. Johannes Rothmund vielen Dank für Ihre Freundschaft und Hilfsbereitschaft.

Mein ganz besonderer Dank gilt letztlich meinem Vater Dalshad sowie meinen Geschwistern, Dipl. Rasper, Dipl.-Ing. Rawand, Dr. Rawa, Dipl.-Ing. Rawen und B.Sc. Suham, und meinen Cousins Dr. Narmin Koye, Dr. Bahzad Koye und Dr. Kurdo Koye für ihre fortwährende liebevolle Unterstützung. Ihr Verständnis, ihre oft endlose Geduld sowie ihre unermüdliche moralische Aufbauarbeit haben mir den notwendigen familiären Rückhalt zur Durchführung dieser Arbeit gegeben.

Stuttgart, im April 2015

Rastee D. Ali (Koyee)

Für die Seele meiner Mutter

Bahar Hammadamin Muhammad

Ehrenwörtliche Erklärung

Hiermit erkläre ich, dass ich die vorliegende Arbeit selbstständig verfasst und keine anderen als die angegebenen Hilfsmittel genutzt habe. Alle wörtlich oder inhaltlich übernommenen Stellen habe ich als solche gekennzeichnet. Ich versichere außerdem, dass ich die vorliegende Arbeit keiner anderen Prüfungsbehörde vorgelegt habe und, dass die Arbeit bisher auch auf keine andere Weise veröffentlicht wurde. Ich bin mir der moralischen und gesetzlichen Konsequenzen einer falschen Aussage bewusst.

Legal statement

I solemnly declare that I have produced this work all by myself. Ideas taken directly or indirectly from other sources are marked as such. This work has not been shown to any other board of examiners so far and has not been published yet. I am fully aware of moral and legal consequences of making a false declaration.

Datum: 29.01.2015

Rastee D. Ali (Koyee)

Contents

Nomenclature	X
Extended Abstract	XIX
1 Einleitung	XIX
2 Forschungsmethodik	XX
2.1 Hypothesen	XXI
2.2 Gliederung der Dissertation	XXI
2.3 Die Vorgehensweisen	XXII
3 Zusammenfassung	XXIX
Summary	XXXI
1 Introduction	1
1.1 Frame of reference	4
1.1.1 Metal cutting	5
1.2 Background and aim	24
1.3 Research approach	25
1.4 Research hypothesis	26
1.5 Research questions	27
1.6 Research delimitations	28
1.7 Outline of the dissertation	28
2 State of the art in machining modeling and optimization: A review	32
2.1 Input-output parameter relationship of modeling tools	33
2.1.1 Statistical regression	34
2.1.2 Neural network	39
2.1.3 Fuzzy set theory	43
2.2 Finite element modeling of chip formation processes	47
2.2.1 Basics of FEM formulations and remeshing techniques	49
2.2.2 Historical perspective	52

2.2.3	Scales of the machining modeling	52
2.2.4	Simulation software & phases of metal cutting FEA	53
2.2.5	Advantages and problems associated with numerical cutting modeling	54
2.2.6	Input models and identification of input parameters	56
2.3	Determination of optimal or near-optimal cutting conditions	62
2.3.1	Taguchi Method	63
2.3.2	Response surface methodology (RSM)	68
2.3.3	Nature-inspired meta-heuristic algorithms	73
2.3.4	Multiple Attribute Decision Making (MADM) methods	86
2.4	A systematic methodology for modeling and optimization of cutting processes	102
3	Experimental details	106
3.1	Workpiece materials	106
3.1.1	Mechanical properties and chemical compositions	106
3.1.2	Temperature-dependent physical and mechanical properties of the workpiece materials	107
3.2	Machine tool and cutting tool	110
3.3	Design of experiments (DOE)	112
3.3.1	Full factorial design	112
3.3.2	Taguchi designs	113
3.3.3	D-Optimal design	115
3.4	Measurement of the machining performance characteristics	116
3.4.1	Measurement of cutting forces and effective cutting power	116
3.4.3	Measurement of surface quality characteristics	117
3.4.4	Measurement of the flank wear	118
3.4.5	Infrared temperature measurement system	120
3.4.6	Chip thickness and chip serration ratio	121
4	Experimental investigation and multi-objective optimization of turning DSSs: A case study	122
4.1	Pareto optimality	122

4.2	Performance characteristics	123
4.2.1	Specific cutting pressures	123
4.2.2	The width of maximum flank wear land (VB_{\max})	125
4.3	Bat Algorithm for multi-objective optimization of turning DSSs.	130
4.4	Interim conclusions	132
5	Universal Characteristics Index	134
5.1	Estimation of the chip volume ratio	135
5.2	Universal characteristics index	137
5.2.1	TOPSIS	138
5.2.2	VIKOR method	139
5.2.3	GRA	139
5.2.4	UC	139
5.2.5	Fuzzy-MADM	140
5.3	Optimization	142
5.4	Interim conclusions	145
6	Taguchi-MADM-Meta-heuristic concept	146
6.1	Taguchi method	146
6.2	VIKOR method	150
6.3	Meta-heuristic optimization	152
6.4	Interim conclusions	155
7	Application of Fuzzy-MADM approach in optimizing surface quality of stainless steels	157
7.1	Proposed methodology	157
7.2	Results and discussions	160
7.2.1	Computation of the MSQCI	160
7.2.2	Fuzzy-MADM method	162
7.3	Confirmation tests	166
7.4	Interim conclusions	167

8	Sustainability-based multi-pass optimization of cutting DSSs	169
8.1	Performance characteristics	170
8.2	Phase I: Parametric cutting investigations	172
8.2.1	Effect of control factors on performance characteristics	173
8.2.2	Parametric optimization of performance characteristics	178
8.3	Phase II: Economics of cutting DSSs	180
8.4	Phase III: Operational sustainability index	182
8.4.1	Optimization of OSI using CSNNS	185
8.5	Interim conclusions	189
9	Numerical modeling and optimization of turning DSSs	193
9.1	3D FEM prediction of the chip serration	194
9.2	3D FEM prediction of the chip serration	198
9.3	Inverse identification of 3D FEM input parameters	202
9.3.1	Proposed methodology	207
9.3.2	Extension of FANNS: a case study	215
9.4	Inverse identification of Usui's wear model constants	215
9.5	Numerical optimization of turning DSSs	217
9.5.1	Selective control factors	218
9.5.2	Results and discussions	220
9.5.3	Numerical machining performance measure	227
9.6	Interim conclusions	230
10	Conclusions	233
11	References	238
12	Appendix A: Supplementary tabulations	A1

Nomenclature

List of Latin symbols:

Symbol	Unit	Definition
A	MPa	Initial yield strength
A^-		Negative ideal solution
A^*		Positive ideal solution
A_a	€/m ² .Month)	Monthly rent
A_c	mm ²	Cutting area
A_l		Loudness
a_p	mm	Depth of cut
b		Bias
B		Strain hardening coefficient
C		Strain rate coefficient
C^*		Closeness to the ideal solution
CB		Chip-breaker type
C_f		A constant function of cutting length
CI		Consistency Index
CM		Cooling medium
c_n		Coefficient of regression equations
C_p	J/kg. K	Heat capacity
CR		Consistency Ratio
$\%C_2$		Percentage of ON state of the machine
d	mm	Outside diameter
D	MPa	Cockcroft-Latham material constant
$D_{crit.}$	MPa	Critical damage value
DV		Degree of diversification
e		Error terms in regression and neural network analyses
E	J	Energy
e_c	J/mm ³	Cutting energy

Symbol	Unit	Definition
E_c	€/kWh	Electricity cost
E_j		Entropy of attribute j
$\%E$		Percentage error
F_c	N	Main cutting force
F_f	N	Feed cutting force
f_q		Frequency
f_r	mm/rev	Feed rate
F_t	N	Thrust cutting force
$\%F_t$		Percentage increase in thrust cutting force
g^*		Global best
<i>Geo.</i>		Insert shape
<i>GRG</i>		Grey relational grade
H		Chip serration ratio
h	mm	Chip thickness
h_{tc}	N/(mm.sec.K)	Thermal contact conductance
I		Intensity of light of a firefly
I_c	A	Line current
<i>JAS</i>	hrs	Annual operating hours
k		Order of neural network layers
K_1	€	Main time-related costs
$k_{1,1}$	MPa	Specific cutting pressure for 1mm ² cutting area
K_2	€	Fixed or the workpiece-related costs
K_3	€	Tool-related costs
k_b	m ² kg/(sec ² K)	Boltzmann constant
k_{bB}	€	Procurement cost
k_{bE}	€	Operational cost
k_{bR}	€	Space cost
k_{bW}	€	Cost of maintenance and repair

Symbol	Unit	Definition
k_c	MPa	Specific cutting pressure
k_{ET}	€	Cost of the spare parts
k_f	MPa	Specific feed pressure
K_F	€	Total production cost
k_k	€/hrs	Coolant cost
K_L	€	Labor cost
K_M	€	Machine hour-rate cost
K_{ML}	€	Machine and wage rate cost
K_n		Number of control factors
K_r	degree	Cutting edge anle
KT	μm	Depth of the crater wear
k_t	MPa	Specific thrust pressure
k_{th}	$\text{W}/(\text{m}^2.\text{K})$	Thermal conductivity
k_{WH}	€	Cost of the tool holder
k_{WP}	€	Cost of the cutting insert
L		Number of levels
L_c	mm	Length of cut
L_m	€/hrs	Hourly wage of labor
l_r	mm	Approach length
L_s	mm	Sample length
L_t	mm	Travel length
m	units	Number of the production units
m		Thermal softening exponent in JC model
MRR	mm^3/min	Material removal rate
N	rpm	Rotational speed
n_p		Number of cutting passes
N_t		Number of experimental trials
Ob		Response variable

Symbol	Unit	Definition
P_a		Probability
P_c	W	Cutting power
P_e	W	Effective power
P_M	W	Motor power
PN		Preference number
P_r		Pulse emission
P_{sp}	W	Net spindle power
$\%P_p$		Percentage of the procurement cost
$\%P_r$		Percentage decrease in flow stress
Q_m	m ²	Machine-tool basement area
Q_{NN}		VIKOR index predicted by neural networks
Q_V		VIKOR index
$\%q_i$		Percentage of the interest rate
R		Chip volume ratio
r	€	Amount of non-wage costs of the machine operator
R^2		Coefficient of determination
Ra	μm	Arithmetic average roughness
$R_{adj.}$		Adjusted coefficient of determination
R_c	N	Resultant cutting force
RI		Random Index
R_i		Regret measure
Rt	μm	Highest roughness point from the mean
Rz	μm	Average absolute value of five peaks and valleys
r_ε	mm	Nose radius
\tilde{R}		Centroid
S^-		Negative ideal alternative
S^*		Positive ideal alternative
S_i		Utility measure
T	min	Tool life

Symbol	Unit	Definition
t_a	hrs	Working time
t_{bB}	hrs	Machine utilization time
t_c	min	Cutting time
t_e	min	Production time or time per unit
t_g	min	Basic time
t_h	min	Main process time
t_i	min	Idle time
t_l	years	Economic machine life
T_m	°C	Melting temperature
T_r	°C	Reference temperature
t_n	min	Auxiliary process time
t_q		Target of the neural network
t_{rB}	min	set-up time
t_{rV}	min	Nonproductive set-up activities time
t_{rW}	min	Tool change time
t_{vM}	min	Machine set-up time
t_{WZ}	min	Time that passes till a single tool is changed
U_c		Utility constant
U_l	V	Line voltage
V		Mean square of neural network error
VB	μm	Average width of the flank wear land
VB_{\max}	μm	Maximum width of the flank wear land
VB_n	μm	Average width of the notch wear land
v_c	m/min	Cutting speed
v_s	m/sec	Sliding velocity
w		Weight of the attributes
W	μm	Wear
x		Number of machines

Symbol	Unit	Definition
x^*		Individual best
Z_s		Number of cutting edges per insert

List of Greek symbols:

Symbol	Unit	Definition
α_n	degree	Normal rake angle
α_{rand}		Randomization parameter
α_z		Step size scaling factor in Cuckoo Search algorithm
β_a		Firefly attractiveness
β_r		Random vector drawn from a uniform distribution
β_w	degree	Wedge angle
δ_r		Euclidean distance between fireflies
Δ		Deviation squence
Δ_c	degree	Chip flow angle
ε		Equivalent plastic strain
$\dot{\varepsilon}$		Equivalent plastic strain rate
$\dot{\varepsilon}_0$	sec ⁻¹	Reference plastic strain rate
ε_f		Effective strain
$\dot{\varepsilon}_p$		Von Mises equivalent plastic strain
ϕ	N/(mm.sec)	Heat flux
Φ	J	Conducted heat
ϕ_n	degree	Normal shear angle
ϕ_s	degree	Shear angle
$\dot{\phi}_p$	W/m ³	Volumetric heat generation
γ_a		Randomization parameter in Firefly Algorithm
γ_c	degree	Relief or clearance angle
η	dB	Signal to Noise ratio
κ_t		Taylor-Quinney coefficient
λ		Expectation of occurrence
Λ		Inertia function

Symbol	Unit	Definition
λ_i	degree	Inclination angle
λ_w		Wavelength in Bat Algorithm
μ		Friction coefficient
μ_A		Membership function of set A
μ_c		Coulomb friction coefficient
μ_s		Shear friction coefficient
$\bar{\theta}_T$	°C	Mean tool face temperature
ρ_m	kg/m ³	Density
ρ		Degree of uncertainty
σ_1	MPa	Principal stress
σ_n	MPa	Normal stress
$\bar{\sigma}$	MPa	Von Mises equivalent stress
ς		Learning parameter
τ_f	MPa	Frictional stress
v		Random number drawn from a uniform distribution
Ω		Acceleration constant
ξ		Weight of the strategy
ψ		Activation function of neurons
ψ_g		Random number drawn from Gaussian distribution
ζ		Learning rate
ζ_g		Grey relational coefficient

List of abbreviations:

Abbreviation	Description
AAD	Absolute Average Deviation
AHP	Analytical Hierarchy Process
ALE	Arbitrary Lagrangian-Eulerian
ANN	Artificial Neural Networks
ANOM	Analysis of Means
ANOVA	Analysis of Variance
APSO	Accelerated Particle Swarm Optimization

Abbreviation	Description
BUE	Built-up edge
CS	Cuckoo Search
CSNNS	Cuckoo Search Neural Network Systems
CV	Crisp Value
DC	Discontinuous Chips
DOE	Design of Experiment
DOF	Degree of Freedom
DSS	Duplex Stainless Steel
FA	Firefly Algorithm
FANNS	Firefly Algorithm Neural Network System
FEM	Finite Element Method
FIS	Fuzzy Inference System
GRA	Grey Relational Analysis
GTMA	Graph Theory and Matrix Approach
JMatPro	Java-based Material Properties
LB	Lower Bound
LCFC	Long Cylindrical and Flat helical Chips
LHCS	Long Helical Chip Segments
LM	Lower Medium
LRSC	Long Ribbon and Snarled Chips
LSC	Long Spiral Chips
MADM	Multiple Attribute Decision Making
MH	Moderately High
ML	Moderately Low
MLP	Multi-Layer Perceptron
MOBA	Multi-Objective Bat Algorithm
MOO	Multi-Objective Optimization
MPCI	Multi-Performance Characteristics Index
MSE	Mean Square Error
MSQCI	Multi-Surface Quality Characteristics Index
OA	Orthogonal Array
OSI	Operational Sustainability Index
PF	Pareto Front

Abbreviation	Description
RMSE	Root Mean Square Errors
RSM	Response Surface Methodology
SA	Simulated Annealing
SCFC	Short Cylindrical and Flat helical Chips
SHCS	Short Helical Chip Segments
SRSC	Short Ribbon and Snarled Chips
SS	Sum of Squares
SSC	Short Spiral Chips
STDV	Standard Deviation
TOPSIS	Technique for Order Preference by Similarity to Ideal Solution
UB	Upper Bound
UC	Utility Concept
UCI	Universal Characteristics Index
UM	Upper Medium
VH	Very High
VL	Very Low

Extended Abstract

1 Einleitung

Der Mensch nutzt seit rund 5000 Jahren das Metall Eisen. Aber erst im 18. Jahrhundert stoßen Wissenschaftler in kurzer Folge auf eine ganze Reihe zuvor unbekannter Metalle. Im Jahr 1751 entdeckte z.B. der schwedische Wissenschaftler Axel Cronstedt das Element Nickel. 1778 folgte sein Landsmann Karl Wilhelm Scheele mit dem Element Molybdän. 1797 fand der Franzose Nicola-Louis Vauquelin ein neues Metall, das er Chrom nannte. Im 19. Jahrhundert experimentierten mehrere Metallurgen erfolgreich mit Eisen-Chrom Legierungen. Zwar zeigt sich, dass sie besonderes rostbeständig sind, allerdings waren die Gründe hierfür noch nicht bekannt.

1912 wurde den beiden Deutschen Edward Maurer und Beno Strauß ein Patent auf austenitische Chrom-Nickel-Stähle erteilt. Noch heute machen die austenitischen Sorten rund 65% der Weltproduktion an rostfreiem Stahl aus. 1913 wurde in England erstmals martensitischer rostfreier Stahl hergestellt. Der Entdecker dieser Neuerung war Harry Brearley. Ungefähr zur selben Zeit, nämlich 1915, entwickelten die US-Amerikaner Becket und Dantsaizen ferritische rostfreie Stähle. Auf sie entfallen 30% der weltweiten Erzeugung. Bis 1920, also in weniger als einem Jahrzehnt, bildete sich auf diese Weise der hauptsächliche Anwendungsgebiete.

1930 entwickelten schwedische Metallurgen Stahlsorten, die sowohl ein ferritisches als auch ein austenitisches Gefüge in einer Legierung vereinen, und bezeichneten diese als rostfreie Duplexstähle. Duplexstähle revolutionierten zunächst die Zellstoff- und Papierindustrie durch die Verfügbarkeit beständiger Bauteile. Heute bewähren sie sich in einer ganzen Reihe von Anwendungen, z.B. in der petrochemischen Industrie oder bei der Meerwasser-Entsalzung, also dort wo sowohl eine besondere Korrosionsbeständigkeit als auch eine hohe Festigkeit erforderlich sind.

Seit 1990 findet eine zweite Generation von rostfreien Duplexstähle immer mehr breiteren Einsatz als Alternative zu den konventionellen rostfreien Stählen. Die Gründe hierfür sind:

1. Geringere Preise durch einen geringeren Anteil an Nickel,
2. Höhere Zugfestigkeit und

3. Deutlich höhere Korrosionsbeständigkeit gegen durch Chlorid induzierte Spannungskorrosion als dies bei austenitischen rostfreien Stählen der Fall ist.

Andererseits sind die rostfreien Duplexstähle normalerweise schwerer zerspanbar als austenitische Sorten mit einer vergleichbaren Korrosionsbeständigkeit. Die Gründe sind: große Zähigkeit, niedrige Wärmeleitfähigkeit, hohe Streckgrenzwerte (ca. zweimal höher als austenitische rostfreie Stähle), spezielle Mikrostruktur (weiches Ferrit neben hartem Austenit), geringer Schwefel- und Phosphorgehalt, starke Tendenz zu Bildung von Aufbauschneiden und eine hohe Kaltverfestigungsrate.

Aufgrund der hohen Zähigkeit bilden sich oftmals beim Zerspanen lange Band- oder Wirrspäne aus, die sich um das Werkstück oder den Werkzeughalter wickeln können. Die Problematik verschärfte sich besonders bei Schlichtoperationen mit geringen Vorschüben und Schnitttiefen. In der automatisierten Fertigung verringert dies die Produktivität aufgrund von Maschinenstillstandszeiten sowie geringer Prozesssicherheit in erheblichem Maße.

2 Forschungsmethodik

Vor dem Hintergrund der Komplexität von Zerspanungsuntersuchungen, der Grenzen der Theorie spanender Prozesse und analytischer Modelle, der Schwierigkeiten bei der Modellierung und Optimierung von Parametern des Zerspanungsprozesses und der Notwendigkeit von zusätzlichen Kenntnissen über die Zerspanung von duktilen und kaltverfestigten Materialien, wird in der vorliegenden Dissertation die Zerspanung von rostfreien Duplexstählen am Beispiel des Drehens systematisch untersucht. Neuentwickelte Modellierungs- und Optimierungsverfahren werden systematisch verwendet, um die Zerspanbarkeit rostfreier Duplexstähle präziser abbilden zu können. Das abschließende Ziel der vorliegenden Arbeit ist es, dem Prozessplaner ein Hilfsmittel an die Hand zu geben, mit dem er, unter Berücksichtigung mehrerer und sich häufig widersprechender Leistungsmerkmale, die optimalen Prozessparameter für die Drehbearbeitung von Duplexstählen finden kann. Auf Ein- und Ausgangskenngrößen basierende Modellierungs- sowie Optimierungsverfahren, multikriterielle Entscheidungsstrategien (MKES) und Finite-Elemente-Simulationen wurden hier intensiv angewandt. Solche MKES, die mit der Fuzzy-Set-Theorie in Verbindung stehen, werden ebenfalls vorgeschlagen, um damit eine Mehrzieloptimierung durchzuführen und für unterschiedliche Schnittbedingungen angepasste Maßnahmen zu erhalten. Ein weiteres Hilfsmittel stellt die Hybridisierung

rechnerischer Modellierungs- sowie Optimierungsverfahren dar. Diese werden im Rahmen der Ansätze zur Zerspanungsoptimierung effektiv angewendet.

2.1 Hypothesen

Ausgehend von der Frage, wie die Verwendung von neu entwickelten Modellierungs- und Optimierungsverfahren für eine effektive Ableitung von optimierten Zerspanungslösungen ermöglicht werden kann, werden systematische Untersuchungen unter Einsatz von neuentwickelten Modellierungs- und Optimierungsverfahren durchgeführt. Zunächst sollen jedoch die folgenden Hypothesen vorgestellt werden:

1. Statistische Regression und metaheuristische Optimierungsverfahren können zu einer Reihe von nicht dominanten Zerspanungslösungen führen.
2. Fuzzylogik ist vorteilhaft zur Beseitigung der Diskrepanz in der Rangordnung von Alternativen unter dem Einsatz von MKES.
3. Das Taguchi-MKES-metaheuristische Konzept kann praktischerweise für Mono- und Mehrzieloptimierungen verwendet werden.
4. Merkmale der Oberflächenqualität können effizient optimiert werden, wenn MKES mit der Fuzzy-Set-Theorie gekoppelt werden.
5. Die Multipass-Zerspanung kann nachhaltig optimiert werden, wenn eine systematische Hybridisierung des Modells der Ein- und Ausgangskenngrößen sowie der Optimierung und der MKES durchgeführt wird.
6. Es ist ausreichend, die JMatPro Software, MKES und Modelle sowie Optimierungsansätze für Ein- und Ausgangskenngrößen zur Rückwärtsidentifikation von FEM-Eingangskenngrößen zu benutzen.

2.2 Gliederung der Dissertation

Angesichts der breit angelegten Aufgabenstellung ist die Dissertation in 10 Kapitel gegliedert. In Kapitel 1 wird eine kurze Einführung in das Hauptthema gegeben und die bei den Forschungsarbeiten verfolgte wissenschaftliche Methodik behandelt. In Kapitel 2 wird der Stand der Technik zu den Themenbereichen Modellierung und Optimierung von Zerspanprozessen dargestellt. Zudem wird ein Überblick über die Vor- und Nachteile der Verfahren und der abgeleiteten Modellierungs- und Optimierungsansätze gegeben. Im Kapitel 3 werden der verwendete Versuchsaufbau sowie die Details der experimentellen Untersuchungen beschrieben.

Kapitel 4 befasst sich mit experimentellen Untersuchungen zum Längsdrehen von rostfreien Duplexstählen mit beschichteten Wendeschneidplatten. In Kapitel 5 wird die Beseitigung von Diskrepanzen bei der MKES-Rangordnung durch die Ableitung eines allgemeinen Eigenschafts-Zeiger-Index behandelt. In Kapitel 6 wird die Anwendung eines neuen Taguchi-VIKOR- metaheuristischen Konzepts als angemessener Ansatz für die Mono- und Mehrzieloptimierung der Bearbeitung von rostfreien Duplexstählen aufgeführt. In Kapitel 7 wird die Taguchi-Methode in Verbindung mit der Fuzzy-MKES für die Optimierung von Merkmalen der Oberflächengüte angewandt. In Kapitel 8 wird ein systematischer Ansatz vorgelegt, der unterschiedliche Modellierungs- und Optimierungsverfahren integriert, um die Multipass-Zerspanung von rostfreien Duplexstählen nachhaltig zu optimieren. Kapitel 9 befasst sich mit der Rückwärtsidentifikation der FEM-Eingangskenngrößen und der Anwendung der Finite-Elemente-Simulationen, um damit eine hypothetische Optimierungsstudie durchzuführen. In Kapitel 10 werden die Forschungsfragen, welche der vorliegenden Arbeit zugrunde lagen, beantwortet und abschließenden besprochen.

2.3 Die Vorgehensweisen

2.3.1 Die Fledermaus-Mehrzieloptimierung

Im Zusammenhang mit der Haupthypothese stellt sich die erste Forschungsfrage wie folgt: Kann durch die Anwendung der statistischen Regression und des Metaheuristischen Optimierungsverfahren in Mehrzieloptimierungen eine Reihe von nichtdominierten Zerspanungslösungen effektiv gewonnen werden? Um diese Frage angemessen zu beantworten, wird eine experimentelle Untersuchung des Längsdrehens von rostfreien Duplexstählen EN 1.4462 und EN 1.4410 mit beschichteten Wendeschneidplatten durchgeführt. Mit Hilfe des Fledermaus-Mehrziel-Algorithmus (MOBA) werden Bewertungskriterien wie beispielsweise die Zerspankraftkomponenten und die maximale Verschleißmarkenbreite optimiert und die Pareto Grenzen der nicht dominierten Optimierungslösungen ermittelt. Die parametrischen Einflüsse von Größen wie Schnittgeschwindigkeit, Vorschub und Kühlmedium auf die Bewertungskriterien werden mit Hilfe von dreidimensionalen Diagrammen dargestellt.

Erste Ergebnisse zeigen, dass die Werte von nicht nutzbringenden Bewertungskriterien bei der Zerspanung des Werkstoffs EN 1.4410 im Allgemeinen höher liegen, als beim Werkstoff EN 1.4462. Zudem zeigt die Nasszerspanung im Vergleich zur Trockenzerspanung eine Verbesserung der Gesamtbearbeitungsleistung durch geringere Zerspankraftkomponenten und die

Steigerung der Werkzeugstandzeit. Drittens wird nach der Regressionsanalyse ein MOBA zur Modellierung eingesetzt. Ergebnisse zeigen, dass der MOBA sehr effizient und sehr zuverlässig ist. Er führt effizient zu vielen optimalen Lösungen. Abhängig vom Entscheidungsträger-vorzug wird die optimale Schnittbedingung identifiziert.

2.3.2 Der allgemeine Eigenschaftenzeiger

Die zweite Forschungsfrage lautet: Ist die Anwendung von Fuzzylogik vorteilhaft zur Beseitigung von Widersprüchlichkeiten in der Rangordnung beim Einsatz von MKES? Als beispielhafter Zerspanungsprozess wird hierzu das Plandrehen bei konstanter Schnittgeschwindigkeit herangezogen. Das Plandrehen zeichnet sich im Vergleich zum Außenlängsdrehen durch eine bessere Wirtschaftlichkeit, höhere Oberflächengüte und kürzere Hauptzeit aus. Leistungsmerkmale wie Spanraumzahl, resultierende Schnittkraft, spezifische Schnittkraft und Netto-Spindelleistung sollen gleichzeitig optimiert werden.

Unter den vielen maßgeblichen Leistungsmerkmalen ist die Spanraumzahl eine der wichtigsten. Die Spanraumzahl gibt Auskunft über die Sperrigkeit der Späne. Sie wird aus dem Verhältnis von Spänevolumen zu Spanungsvolumen gebildet. Allerdings ist die messtechnische Erfassung des Spänevolumens in der Praxis nicht einfach. Um dieses zumindest hinreichend abschätzen zu können, wird deshalb eine neue Methode vorgeschlagen. Zunächst werden qualitative Informationen über die Späne in einer Spanbruchtabelle dargestellt. Anschließend werden die Späne gemäß den bekannten Standardspanformen klassifiziert. Dann kommt die Fuzzylogik zum Einsatz, wobei Regeln formuliert werden, um die qualitativen Informationen zu fuzzifizieren. Abschließend werden die fuzzifizierten Daten im Fuzzy-Inferenz-System zu quantitativen Daten defuzzifiziert und zur Vorhersage der Spanraumzahl genutzt.

Die unterschiedlichen Leistungsmerkmale werden zudem mit Hilfe von MKES wie TOPSIS, VIKOR, GRA und UA in einem einzelnen MKES-Index zusammengeführt. Basierend auf einer unterschiedlichen MKES-Präferenz und der Tatsache, dass keine MKES als optimales Verfahren anzusehen ist, wird schließlich die Mamdani-Fuzzy-Begründung genutzt, um den Widerspruch zwischen den MKES aufzulösen und einen allgemeinen Index abzuleiten. Dieser Index wird als allgemeiner Eigenschaftenzeiger (UCI) bezeichnet. Der optimierte UCI wird anhand der Ergebnisse von zwei weiteren Optimierungsverfahren validiert.

Bei diesen Verfahren handelt es sich um:

1. Die Methode der gewichteten Summen ergänzt durch eine simulierte Abkühlung und

2. Statistische Regression ergänzt durch eine simulierte Abkühlung.

Die Ergebnisse zeigen, dass mit diesem Ansatz die aus anderen anderen Optimierungsverfahren resultierende, durchschnittliche Verbesserung der Leistungsmerkmale übertroffen werden kann. Im Allgemeinen sind durchschnittliche Verbesserungen zwischen 10% und 40% möglich.

Aus diesen Ergebnissen kann geschlossen werden, dass der neue Ansatz wirkungsvoller ist, als die anderen klassischen Ansätze.

2.3.3 Das Taguchi-VIKOR-metaheuristische Konzept

Kann das Taguchi-VIKOR-metaheuristische Konzept praktischerweise für Monoziel- und Mehrzieloptimierungen der Zerspanung von rostfreien Stählen verwendet werden? Dies ist die dritte Frage in der Folge des Erkenntnisgewinns. Zunächst werden hierzu die Schnittbedingungen als Einflussgrößen und das Plandrehen mit konstanter Schnittgeschwindigkeit als Zerspanprozess festgelegt.

Anschließend wurden Zerspanversuche gemäß der Taguchi-Methode durchgeführt. Bei der Taguchi-Methode werden im Wesentlichen orthogonale Felder eingesetzt. Orthogonale Felder sind Teilfaktorpläne, d.h. es werden nicht alle möglichen Kombinationen von Faktorstufen durchgespielt, sondern nur eine genau ausgewählte Teilmenge. Durch diesen Ansatz kann man die Zahl der erforderlichen Experimente erheblich reduzieren. Im konkreten Fall müssen so anstelle von 125 Experimenten nur 25 Experimente durchgeführt werden. Die Leistungsmerkmale, die gleichzeitig optimiert werden sollen, sind die Schnittleistung, die resultierenden Schnittkräfte, die spezifische Schnittenergie und der arithmetische Mittenrauwert. Die Vorgehensweise ist wie folgt:

Im ersten Schritt werden die Monozieloptimierungen nach der Taguchi Methode durchgeführt. Die Taguchi-Methode, das sogenannte Robust Design, ist eine Technik, deren Ziel es ist, Produkte und Prozesse zu entwickeln, die robust gegen äußere Störeinflüsse sind. Die Taguchi-Methode nutzt das Signal-Rausch-Verhältnis. Es ist definiert als das Verhältnis der vorhandenen mittleren Signalleistung zur vorhandenen mittleren Rauschleistung. Es wird oft im logarithmischen Maßstab dargestellt. Danach werden Mittelwertanalyse und Varianzanalyse der Signal-Rausch-Verhältnisswerte durchgeführt. Eine Maximierung des Mitten-Signal-Rausch Verhältnisses minimiert die Verlustkosten und optimiert die Steuerungsgröße.

Im zweiten Schritt wird die Mehrzieloptimierung durchgeführt und hierzu die VIKOR-Methode eingesetzt. VIKOR gehört zu einer Kompromissklassifizierung der MKES. Sie beginnt mit einer Datennormalisierung auf Werte zwischen 0 und 1. Anschließend werden die Gewichte der einzelnen Leistungsmerkmale mit Hilfe der Entropiegewichtsmethode berechnet. Anschließend erfolgt die statistische Kalkulation der Utility, Regret und des VIKOR-Index und der entsprechenden Rangordnung der Alternativen. Man kann diesen Index auch als Schwerzerspanbarkeitsindex bezeichnen. Je kleiner der Wert des VIKOR-Index desto besser. Es handelt sich um einen Index, der genau darauf hinweist, wo sich der optimale Schnittparameterbereich befindet.

Der dritte Schritt, um die wirkungsvollsten metaheuristischen Optimierungsverfahren zu ermitteln und die exakten Schnittbedingungen zu bestimmen, besteht darin, drei neuentwickelte, metaheuristische Algorithmen anzuwenden und ihre Leistung zu vergleichen. Die betrachteten drei neuentwickelten, metaheuristischen Optimierungsverfahren sind der Glühwürmchen-Algorithmus, die beschleunigte Partikel-Schwarm-Optimierung und der Kuckuck-Suchalgorithmus. Diese Algorithmen wurden entsprechend der gegebenen Entscheidungsvariablen, Zielfunktionen und Zwänge eingesetzt. Die Ergebnisse zeigten, dass der Kuckuck-Suchalgorithmus die anderen Optimierungsalgorithmen übertrifft.

Zusammenfassend wird bewiesen, dass das Taguchi-VIKOR-metaheuristische Konzept praktischerweise für Monoziel- und Mehrzieloptimierung der Zerspanung rostfreier Stähle verwendet werden kann.

2.3.4 Die Optimierung von Merkmalen der Oberflächengüte

Die vierte Frage befasst sich mit der Optimierung von Merkmalen der Oberflächengüte. Unter Zuhilfenahme von MKES und Fuzzy-Set-Theorie werden die Größen zur Bewertung der Oberflächengüte namentlich der arithmetische Mittenrauwert, die gemittelte Rautiefe und die maximale Rautiefe parallel optimiert. Zu diesem Zweck wird ein neuer Ansatz dargestellt.

Der Zerspanungsprozess wird wiederum das Plandrehen mit konstanter Schnittgeschwindigkeit und als Eingangsgrößen die Schnittbedingungen festgelegt. Taguchi-Versuchspläne werden verwendet, um den gesamten Hauptparameterraum mit einer geringen Anzahl von Versuchen abarbeiten zu können.

Die Vorgehensweise, die sogenannte Methodik, gliedert sich in fünf Stufen: die erste Stufe erledigt die Vorverarbeitung der Daten. Diese beinhaltet die Versuchsplanung und die Festle-

gung der Leistungsmerkmale. Im zweiten Schritt werden MKES, wie GTMA und AHP-TOPSIS benutzt, um einen allgemeinen Index für die Merkmale der Oberflächengüte zu bestimmen. Es stellt sich die Frage, warum hier zwei MKES genutzt werden: Es gibt kein MKES als globales Verfahren, das für alle Arten von Mehrzieloptimierungsproblemen geeignet ist. Aus diesem Grund ist der Entscheidungsablauf immer mit Unsicherheiten behaftet. Um dieses Problem zu lösen, wird im zweiten Schritt die Fuzzy-Set-Theorie herangezogen. Alle Merkmale der Oberflächengüte müssen in Fuzzy-Trapeznummern überführt werden und unter Einhaltung von 10%-Unsicherheit im Entscheidungsablauf konvertieren. Dann wird die Methode der Gewichteten Summen zur Ableitung von Kompromisslösungen verwendet und die geometrischen Eigenschaften der Trapeznummern werden zur Defuzzifizierung der Indizes genutzt. Schließlich werden die defuzzifizierten Zahlen nachbearbeitet. Die Nachbearbeitung befasst sich mit der Anwendung der Mittelwert- und Varianzanalyse sowie der Verifikation der optimierten Ergebnisse.

Nach der Anwendung und Verifikation des Ansatzes, wird die erreichte Verbesserung der Merkmale der Oberflächengüte ermittelt. Hier zeigt sich, dass Verbesserungen von bis zu 30% bei der Oberflächengüte möglich sind. Deshalb kann zusammengefasst werden, dass die beschriebene Vorgehensweise zielführend ist.

2.3.5 Die nachhaltige Optimierung der Multipass-Zerspanung

Im Zusammenhang mit den Hypothesen stellt sich die fünfte Frage: ist es möglich, durch eine systematische Hybridisierung des Modells und der Optimierung der Ein- und Ausgangskenngrößen und durch die MKES die Multipass-Zerspanung nachhaltig zu optimieren?

Wie bei den zuletzt beschriebenen Vorgehensweisen, wird zunächst die experimentelle Methodik festgelegt. Die Experimente werden am Beispiel des Plandrehens bei konstanter Schnittgeschwindigkeit im Mehrschnittverfahren durchgeführt. Bekanntermaßen sind die Zusammenhänge zwischen den Eingang- und Ausganggrößen bei der Zerspanung stark nichtlinear. Außerdem müssen noch kategorische Faktoren zu den Versuchsplänen und Zerspanungsmodellen hinzugefügt werden. Dazu werden D-Optimale Versuchspläne als sehr geeignet angesehen. Die D-Optimalen Versuchspläne werden nicht mit einem festen Schema generiert, sondern iterativ aufgebaut. Allerdings sind die Vorteile, wie freie Wahl für die Zahl der Stufen pro Einflussfaktor, freie Wahl des mathematischen Modells, freie Wahl der Stu-

fenabstände wesentlich größer, als die Nachteile, wie beispielsweise zu wenig Versuchspunkte in der Mitte des Versuchsraumes und die Abhängigkeit von Rechenalgorithmen.

Die Steuerungsfaktoren sind hier numerisch und kategorisch. Erstmals werden Leistungsmerkmale, wie die prozentuale Erhöhung der radialen Schnittkraft, die Spanraumzahl, die Wirkleistung und die maximale Verschleißmarkenbreite, in der Zerspanungsoptimierung der rostfreien Duplexstähle genutzt.

Die Vorgehensweise des Studiums vollzieht sich systematisch in drei Phasen. In Phase 1 werden mathematische Modelle für die Leistungsmerkmale mit der Response-Surface-Methode (RSM) entwickelt, die Wechselwirkungseffekte zwischen Schnittbedingungen und Leistungsmerkmalen mit Hilfe von dreidimensionalen Diagrammen analysiert und eine parametrische Optimierung der Leistungsmerkmale unter Verwendung des Kuckuck-Suchalgorithmus durchführt. In der Phase 2 werden umfassende Modelle zur Kalkulation von Produktionskosten und Produktionsraten entwickelt. Um den Konflikt zwischen dem Wunsch nach minimierten Produktionskosten und maximierter Produktionsrate überwinden zu können, wird TOPSIS als Optimierungsansatz vorgeschlagen. Die Betriebsmittel-belegungszeit, die Hauptzeitkosten, die Werkzeug- und Werkzeugwechselkosten werden für die Herstellung einer Zahl von 12.000 Stück optimiert und hieraus die beste Alternativ identifiziert. Ein Ansatz zur Modellierung und Optimierung eines Betriebsnachhaltigkeitsindex (BNI) wird in der dritten Phase der Vorgehensweise präsentiert. Zuerst wird durch die Anwendung der Mamdani-Implikation ein neuer Index für die nachhaltige Mehrschnitt-Zerspanung von rostfreien Stählen abgeleitet. Durch das BNI kann genau bestimmt werden, wo der Bereich nachhaltiger Zerspanungsparameter liegt. Der nächste Schritt beinhaltet die Modellierung und Optimierung. Ein neues Verfahren nutzt ein künstliches neuronales Netz mit integriertem Kuckuck-Suchalgorithmus (CSNNS). Das BNI kann gleichzeitig und effizient durch den entwickelten CSNNS modelliert und optimiert werden.

Schließlich kann festgehalten werden, dass die systematische Hybridisierung des Modells und der Optimierung der Ein- und Ausgangskenngrößen sowie die MKES Methoden die Zerspanung der rostfreien Duplexstähle nachhaltig optimieren können.

2.3.6 Die Rückwärtsidentifikation der FEM-Eingangskenngrößen

Die nächste Anwendung der Modellierung und Optimierung behandelt die Rückwärtsidentifikation von FEM-Eingangskenngrößen. Für die Zerspanungssimulation ist es ein wesentlicher

Vorteil, Eingangskenngrößen wie die Thermokontakt-Leifähigkeit, den Coulombschen Reibkoeffizienten, den Schub-Reibkoeffizienten, den Taylor-Quinney-Koeffizienten, die Festigkeitsabnahme und das Cockcroft-Latham-Schadenskriterium und deren Wechselwirkung mit den gegebenen Schnittbedingungen zu kennen.

Bevor die FEM-Simulation erstellt wird, werden die mechanischen und physikalischen Eigenschaften der Werkstoffe als Funktion der Temperatur ermittelt. Zu diesem Zweck wurde JMatPro eine Java-basierte Software zur Herleitung von Materialeigenschaften genutzt. Physikalische Eigenschaften, wie die Wärmeleitfähigkeit, der thermische Ausdehnungs-koeffizient und die spezifische Wärmekapazität, werden als Funktionen der Temperatur dargestellt. Auch wurden die mechanischen Eigenschaften, wie Fließkurven, Elastizitätsmodul und Poissonzahl als Funktion der Temperatur ausgedrückt. Aus diesen wichtigen Informationen wird zunächst ein Textfile erzeugt, um dieses dann in die Keyword-Datei der aktuellen Simulation kopieren zu können.

Um die Eignung von JMatPro für Bereitstellung von Daten für Zerspanungssimulationen zu bewerten, wurde die FE-Simulation unter ähnlichen Eingangsgrößen mit dem Johnson-Cook-Model verglichen. Die Ergebnisse zeigen, dass die JMatPro-basierte Simulation die Johnson-Cook Simulation übertrifft, besonders wenn die Späne-Morphologie als Bewertungskriterium herangezogen wird.

Zur Rückwärtsidentifikation von FEM-Eingangskenngrößen wird ein L_{18} -Taguchi-Versuchsplan verwendet. Nach den experimentellen Untersuchungen und Simulationsrechnungen werden für beide Fälle die prozentualen Fehler zwischen Schnittkraft, Temperatur an der Werkzeugspitze und Spandicke gerechnet und als Leistungsmerkmale definiert. Dann wird die VIKOR-Methode verwendet, um alle prozentualen Fehleranteile zu einem Index zu konvertieren. Dieser Index ist eine Funktion der Eingangsgrößen und wird mit dem neuentwickelten FANNS (Firefly Algorithm Neural Network System) optimiert. Am Ende dieser Phase werden die Ergebnisse validiert.

Nach Abschluss der beschriebenen Vorgehensweise, werden die FEM-Eingangskenngrößen rückwärts identifiziert und die prozentualen Fehleranteile drastisch reduziert. Die Rückwärtsidentifikation wirkt sich mit einer Fehlerminimierung von -60% bis -200% bis auf minimal $\pm 10\%$ aus.

Es kann deshalb gesagt werden, dass die vorgeschlagene Vorgehensweise die Eingangskenngrößen sehr effektiv identifiziert und die Fehleranteile der FEM-Rechnung zehn bis zwanzigfach reduziert.

2.3.7 Hypothetische FEM-Optimierung

In der zweiten Phase der FEM-Studie wird eine neue Vorgehensweise zur FEM-basierten Optimierung beschrieben. Einflussgrößen wie Spänebrecher, die Form der Wendeschneidplatte, das Kühlschmiermedium, die Schnittgrößen und Neigungswinkel werden durch den intensiven Einsatz von Taguchi-Optimierungsmethoden und Fuzzylogik optimiert. Die Bewertungskriterien sind in diesem Fall resultierende Schnittkraft, Spannung, Schnitttemperatur und Verschleißrate. Eine neue Maßnahme wird von diesen Merkmalen abgeleitet. Es werden 81 Regeln je Werkstoff formuliert und in das Mamdani-Fuzzy-Inferenz-System integriert. Die Ausgabe der Defuzzifizierung wird als numerischer Zerspanungsleistungsindex (NZLI) bezeichnet.

Nach der Durchführung der FEM-Simulationen und Ableitung des NZLI, wird eine Mittelwertanalyse des NZLI durchgeführt. Je größer der Wert des NZLI ist, desto besser. Abschließend zeigen die Ergebnisse, dass die Vorgehensweise für die weitere Entwicklung und Verbesserung des Zerspanungsprozesses verwenden werden kann.

3 Zusammenfassung

In der vorliegenden Dissertation wurden Untersuchungen zur Bearbeitung von Duplex-Edelstählen unter Anwendung unterschiedlicher und systematisch gut strukturierter Modelle und Optimierungsmethoden durchgeführt. Das Hauptziel, nämlich die Bereitstellung von optimalen Bearbeitungsparametern für Duplex-Edelstähle, wurde unter Verwendung unterschiedlicher Methoden verfolgt. Hierzu zählten eine umfassende statistische Versuchsplanung zur Durchführung der erforderlichen experimentellen Untersuchungen sowie, als besondere Herausforderung, die Integration von insgesamt sechs unterschiedlichen Ansätzen zur Erstellung von Modellen und Optimierungsalgorithmen in einem System. Dies waren zum einen die Verwendung der statistischen Regression und des Multi-Objektive Fledermaus-Algorithmus, um Sätze von nicht dominierten, optimalen Lösungen beim Zerspanen von zwei unterschiedlichen Duplex-Stählen (normal EN 1.4462 und super EN 1.4410) zu erhalten. Zweitens war dies die Ableitung von Fuzzy-Implikationsregeln zur universellen Indizierung, um zum einen

Diskrepanz aus dem Ranking von vier unterschiedlichen attributiven Entscheidungsverfahren zu beseitigen und zum anderen die optimalen Schnittbedingungen zum Plandrehen des austenitischen EN 1.4404 und der beiden Werkstoffe Duplex EN 1.4462 und 1.4410 bei konstanter Schnittgeschwindigkeit definieren zu können. Drittens wurde ein Taguchi-VIKOR-metaheuristisches Konzept vorgeschlagen und auf die Mono- und Multi-Objektive Optimierung der drei oben genannten Werkstoffe eingesetzt. Viertens wurde ein neuartiges, auf der Fuzzy-Set-Theorie beruhendes Konzept angewandt, um die Oberflächengüte von Bauteilen aus den genannten Werkstoffen zu optimieren. Fünftens wurde das Plandrehen von Duplexstählen bei konstanter Schnittgeschwindigkeit in Wiederholversuchen unter Verwendung von hybridisierten Methoden zur statistischen Berechnung, Modellierung und Optimierung nachhaltig verbessert. Hierzu wurde ein neuer Nachhaltigkeitsindex definiert und eingeführt sowie ein neuronales Netzwerk basierend auf einer neuartigen Cuckoo-Search-Methode für die Modellierung und Optimierung eingesetzt. Abschließend wurden Finite-Elemente-Simulationen zum Drehen von Duplexstählen durchgeführt und ein neues Verfahren zur inversen Identifizierung der Eingangsparameter vorgeschlagen. Optimierungstechniken der Statistik und Informatik wurden eingesetzt, um die Differenz zwischen experimentell und numerisch gewonnenen Ergebnissen zu minimieren. Die Studie hat sich auch mit der hypothetischen Anwendung von Finite-Elemente-Simulationen bei der Identifikation optimaler Bedingungen für das Zerspanen von rostfreien Duplex-Edelstählen befasst.

Summary

The global production of stainless steel nearly doubles every ten years and a high growth rate, which has exceeded that of other metals and alloys, indicate the importance of such alloy classes. While there is no controversy over the significant contribution of stainless steels to the well-being of humanity, there is still a lot of room for research works intended to optimize the application of alloys to the manufacturing processes. Owing to the importance of machining as one of the most important classes of manufacturing processes, the cutting of stainless steels attracted a lot of attention long ago. However, there still remain some families of alloys of which their machining has not been thoroughly investigated yet. Belonging to the family of alloys and combining properties such as high strength, high corrosion resistance and a relatively low price of modern duplex stainless steels have made the material an attractive alternative to the more widely used family of austenitic stainless steels. In spite of the importance and popularity potential, investigations on the machining of modern duplex stainless steels have attracted little attention until very recently.

On the other hand, with the onset of more and more powerful computers and superior software, enthusiasm for computer modeling and the optimization of machining processes has continued to grow. The interest in computer modeling and optimization is justified by the fact that perceptive achievement of the optimal process performance is rarely possible, even for a highly skilled operator. Moreover, the large number of variables as well as the complex and stochastic nature of the machining process make the decision-making process more difficult. Therefore, an alternative approach is frequently used to identify the relationship between the performance characteristics of the process and the control factors via mathematical models and/or to represent the dynamics of the system via simulation, after the performance of the process has been optimized using a suitable optimization algorithm.

In the present dissertation, machining investigations into duplex stainless steels are performed under different and systematically well-structured modeling and optimization frameworks. Focusing on the main objective of finding optimum machining process parameters and comprehensively applying the statistical design of experiments to design the experiments, the study tackles the challenge of integrating modeling and optimization algorithms using six different approaches. Firstly, sets of non-dominated optimal solutions are obtained during cutting standard EN 1.4462 and super EN 1.4410 duplex grades employing statistical regres-

sion and Multi-Objective Bat Algorithm. Secondly, fuzzy implication rules are used to derive a universal characteristics index to simultaneously eliminate the discrepancy among the ranking system of four multiple attribute decision-making methods and define the optimum cutting condition during the facing of austenitic EN 1.4404, duplex EN 1.4462 and 1.4410 stainless steels at constant cutting speeds. Thirdly, the Taguchi-VIKOR-Meta-heuristic concept is proposed and applied to the mono- and multi-objective optimization of austenitic and duplex stainless steels. Fourthly, a novel approach based on the fuzzy set theory is applied to optimize the multiple surface quality characteristics of austenitic and duplex stainless steels. Fifthly, the multi-pass facing of duplex stainless steels at constant cutting speeds is sustainably optimized using the hybridization of statistical and computation modeling as well as optimization techniques. A new sustainability index is defined and a novel Cuckoo Search for neural network system algorithms is employed for the modeling and optimization. Lastly, the finite element simulation of turning duplex stainless steels is performed, and a novel procedure of the inverse identification of the input parameters is proposed. Statistical and computational optimization techniques are employed to minimize the percentage difference between experimental and numerical results. The study also covers the hypothetical application of finite element simulations in defining the optimum criteria during cutting duplex stainless steels.

1 Introduction

There is no doubt that stainless steels are an important class of alloys. Their importance is manifested in the plenitude of applications that rely on their use. From low-end applications, like cooking utensils and furniture, to very sophisticated ones, such as space vehicles, the use of stainless steels is indispensable. In fact, the omnipresence of stainless steels in our daily life makes it impossible to enumerate their applications [Lula86]. The importance of stainless steels may be more appreciated by looking at the compound annual growth rate of the world stainless steel production in the last six decades as shown in Figure 1.1.

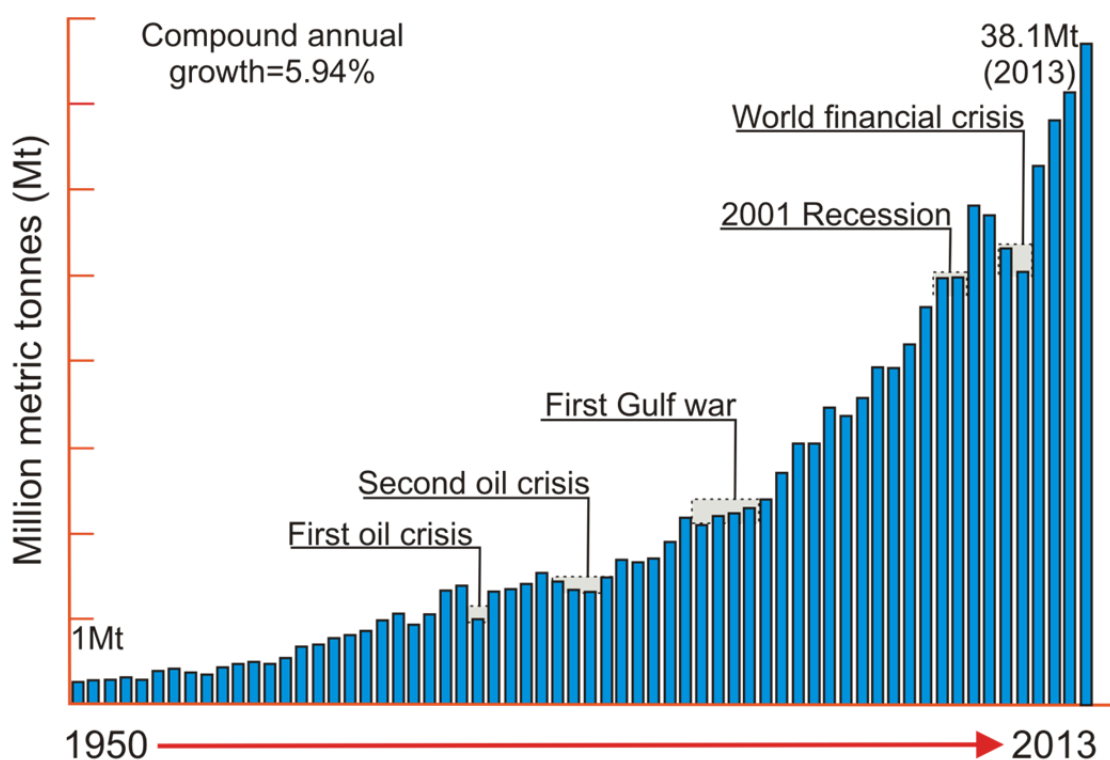


Figure 1.1: Compound annual growth rate of world stainless melt shop production (slab/ingot equivalent): 1950 – 2013 in Mt [Issf13].

Certain relationships between the per-capita consumption of stainless steels and the prosperity of the society could be true in various regions of the world. So that the higher the growth domestic product per capita is, the higher the specific consumption of stainless steel is. The boom of stainless steel consumption per-capita in selected countries in the period between 2001 and 2011 is shown in Figure 1.2. It can be seen that certain developing countries appear in the statistics for the first time with significant stainless steel consumption.

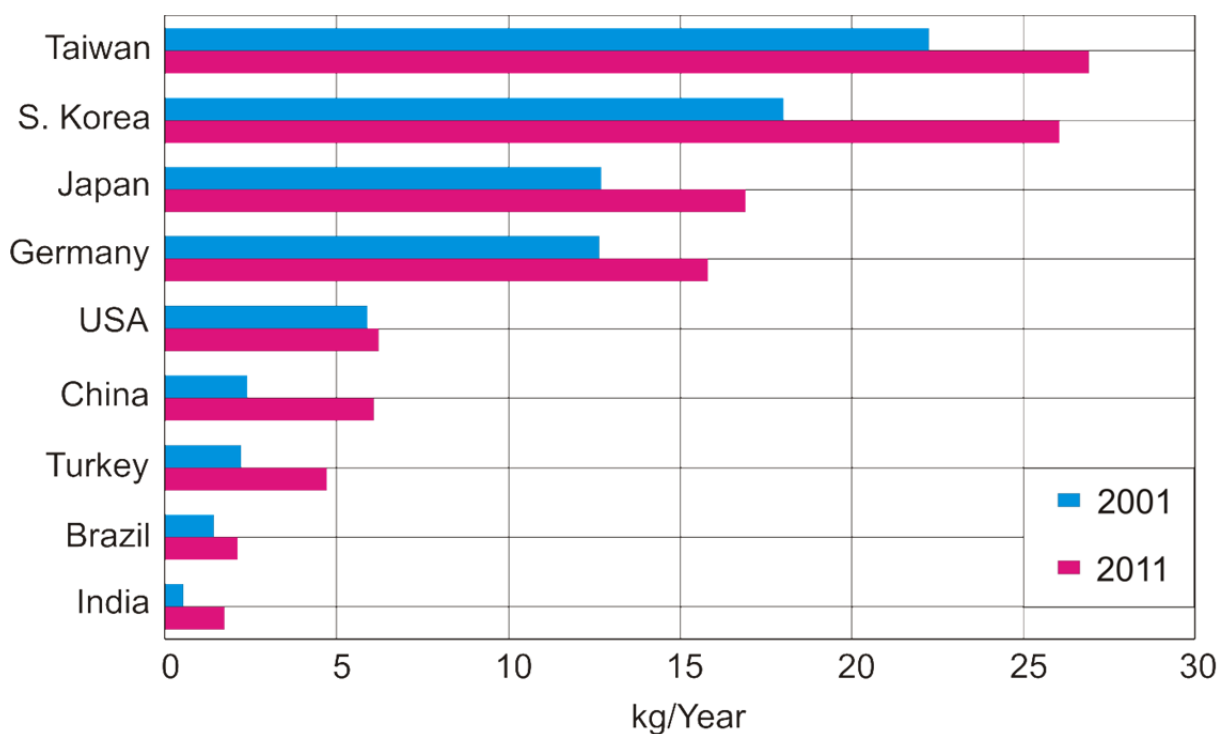


Figure 1.2: Comparison of the per-capita consumption of stainless steel in selected countries [Rasc12].

Compared to alloy steels, stainless steels are chemically complex. The large number of alloying elements enables a larger range of possible phases or basic crystal structures. It makes the deviation from the behavior of pure iron greater; consequently, the calculations that predict which phases will exist are more difficult. The effect of the alloying elements on the microstructure of stainless steels is summarized in an empirical diagram known as Schöffler-DeLong diagram, see Figure 1.3 [Mcgu08]. Schöffler-DeLong grouped the minor and alloying elements present in stainless steels in two categories. The elements of one group have an effect upon the structure similar to that of nickel. These elements include, for example, nitrogen, manganese, copper, which widen the range of austenite, and are called ‘austenite formers’. The other group contains elements, such as silicon, molybdenum and tungsten, which enlarge the range of ferrite, like chromium, and are thus termed ‘ferrite formers’. The Ni-equivalent term on the y-axis represents the sum of nickel content and the contents of other austenite formers multiplied by coefficients representing their effects as compared to that of nickel. The Cr-equivalent is calculated in an analogous manner. Thus, with the aid of this diagram, the presence of austenite, ferrite and martensite can be easily evaluated depending on the chemical composition and the “proper cooling” [CaCa75].

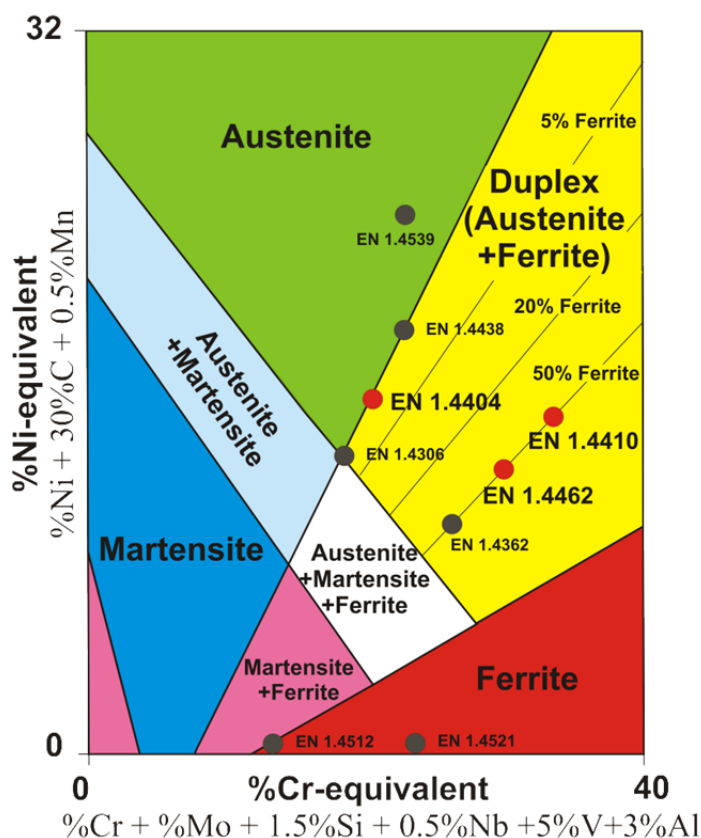


Figure 1.3: Schäffler-DeLong diagram also indicating workpiece materials (red circles).

Based on their microstructure, the wide variety of stainless steel alloys that exist can be classified into five main categories as illustrated in Figure 1.4. Among these families, ferritic stainless steels are the simplest, cheapest stainless steels. In their minimal form, they contain enough chromium to overcome their inherent level of carbon impurity and reach the level of 11% chromium, required for “stainlessness”. Austenitic grades represent the largest group of used stainless steels, making up 65%–70% of the total for the past several years [Grze08]. These steels are generally composed of chromium, nickel and manganese in iron [KaSc06]. Owing to the ferritic-austenitic bi-phased microstructure, duplex stainless steels (DSSs) possess higher mechanical strength and better corrosion resistance than austenitic stainless steels. The applications of and markets for DSSs are continuously increasing due to their outstanding properties and their relatively low costs [ArDe09]. Martensitic stainless steels contain 11–18% Cr, 0.1–1.2% C and small amounts of manganese and nickel [Davi03]. Unlike ferritic and austenitic steels, they are hardenable by heat treatment and are generally used in hardened and tempered conditions [Cobb99]. On the other hand, precipitation-hardening stainless steels are mainly chromium-nickel steels with precipitation-hardening elements, such as copper,

aluminum and titanium. They attain higher strength, toughness and corrosion resistance than strictly martensitic stainless steels [Bram01].

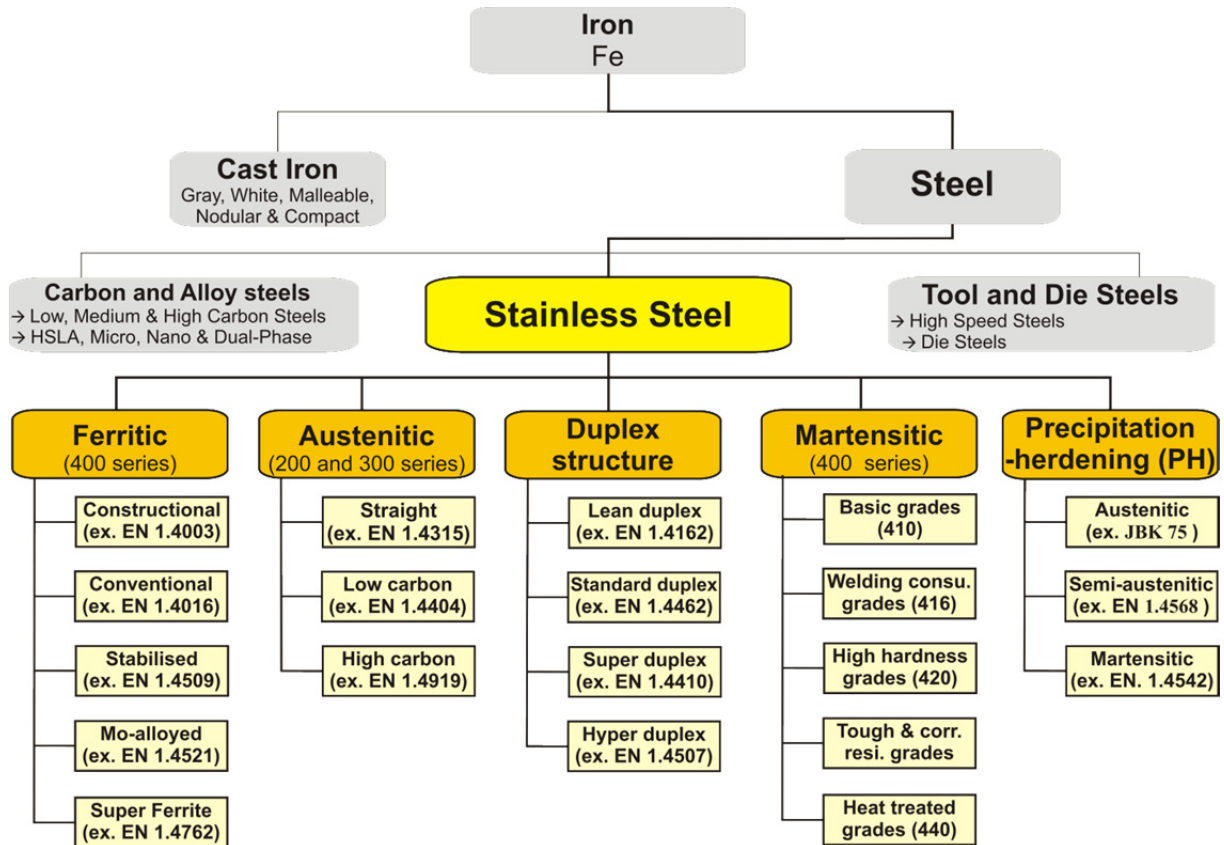


Figure 1.4: Classification chart for stainless steels.

1.1 Frame of reference

Machining is a general term describing a group of manufacturing processes that consist of the removal of material and the modification of the surfaces of a workpiece after it has been produced by various methods [KaSc08]. The importance of machining can be economically envisaged. In the US, for instance, industries spend annually well over \$100 billion to perform metal removal operations because the vast majority of manufactured products require machining at some stage in their production, ranging from relatively rough or nonprecision work, such as cleanup of castings or forgings, to high-precision work, involving tolerances of 0.0025mm or less and high-quality finishes. Thus machining is undoubtedly the most important of the basic manufacturing processes [BIKo13].

The term machinability is often used to describe the easiness with which the work material is machined under a specific set of cutting conditions. The ease of machining different materials

can be compared in terms of the value of tool life, cutting power, surface finish, dimensional accuracy, chip control and part cost under similar cutting conditions. Other criteria can also be employed, for example, cutting temperature, operator safety, etc., see Figure 1.5 [KaSc08].

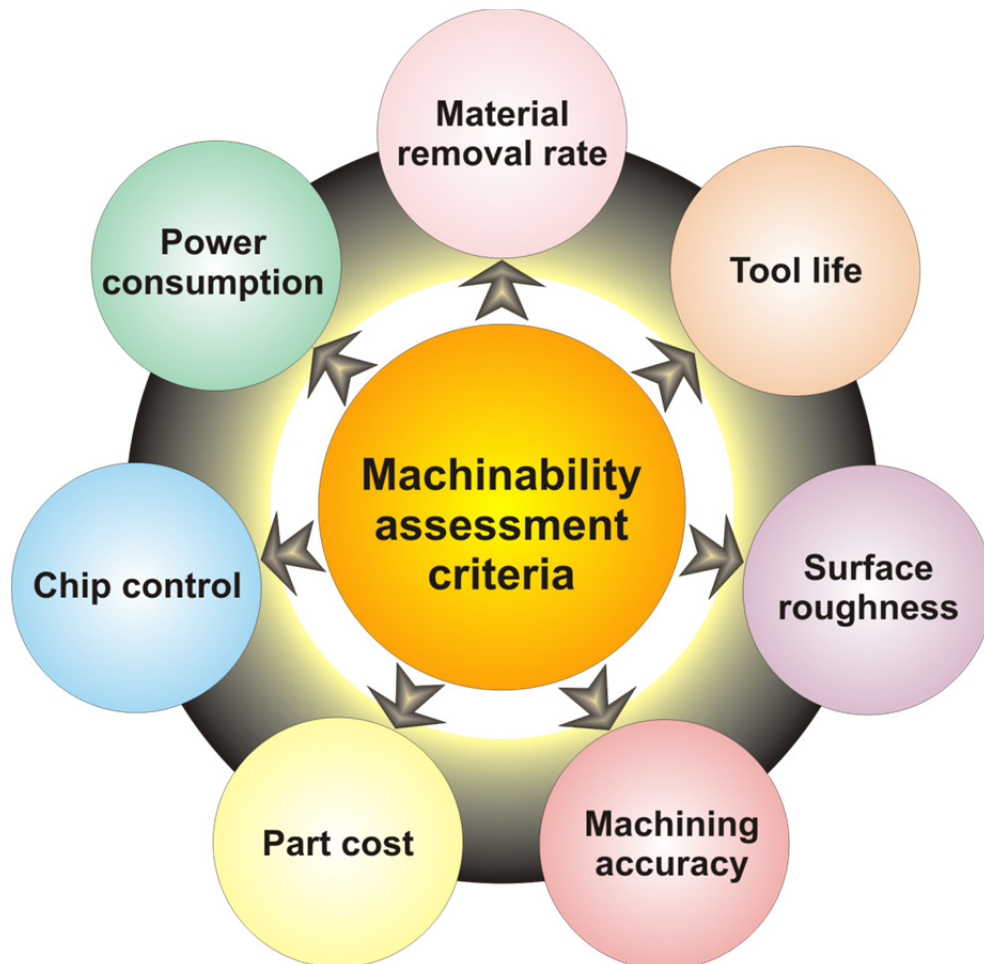


Figure 1.5: Traditionally used machinability assessment criteria [Jawa88].

There are seven traditional machining processes: turning, milling, drilling, sawing, broaching, shaping (planing), and grinding (also called abrasive machining). As an introduction to the field, the following section is intended to describe the fundamentals of metal cutting processes with particular focus on turning processes and the factors influencing the machinability of metals during turning processes.

1.1.1 Metal cutting

In machining, if the workpiece is metal, the process is often called metal cutting or metal removal. The process itself is complex because it has such a wide variety of inputs and outputs. The factors that influence the cutting process are illustrated in Figure 1.6.

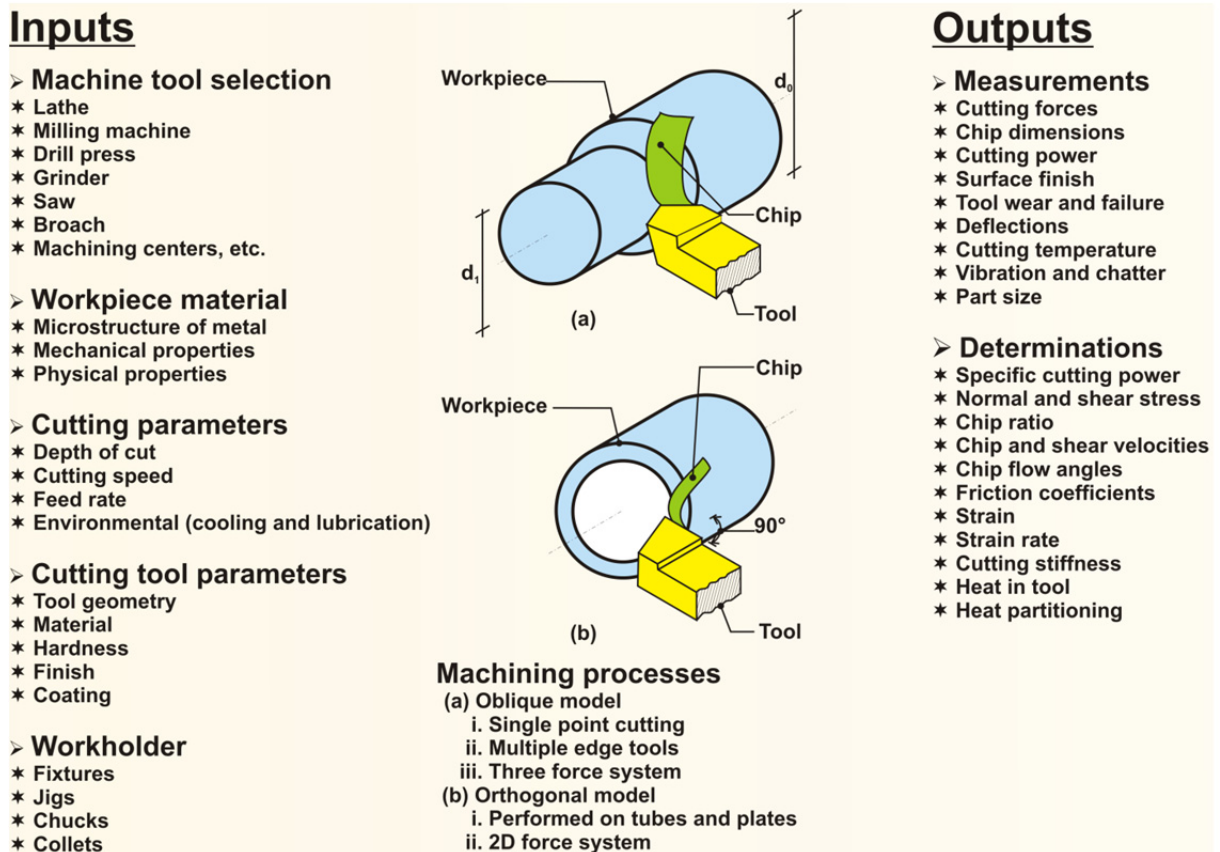


Figure 1.6: Fundamental input and outputs of the metal cutting process.

Although the most common cutting operations are three-dimensional and geometrically complex, the simple case of two-dimensional orthogonal cutting adopted by M. E. Merchant [Merc44] (see Figure 1.7 (a)) is used to explain the general mechanics of metal removal. In orthogonal cutting, the material is removed by a cutting edge that is perpendicular to the direction of relative tool-workpiece motion. In order to continue removing material at a second stage, the tool is taken back to its starting position and fed downwards by the amount f_r , the feed of the process. Perpendicular to f_r , a_p is the depth of cut, which is smaller than or equal to the width of the tool edge. The cutting tool moves to the left along the workpiece at a constant velocity, best known as cutting speed v_c . The surface along which the chip flows is the rake face of the tool. The angle between the rake face and a line perpendicular to the machined surface is called rake angle α_n . The face of the tool that is near the machined surface of the workpiece is the flank face. The angle between the flank face of the tool and the workpiece is called relief or clearance angle γ_c . The angle between the rake face and the flank face is the wedge angle β_w . The sum of the three angles is always equal to 90° [AlBe12, Mark13].

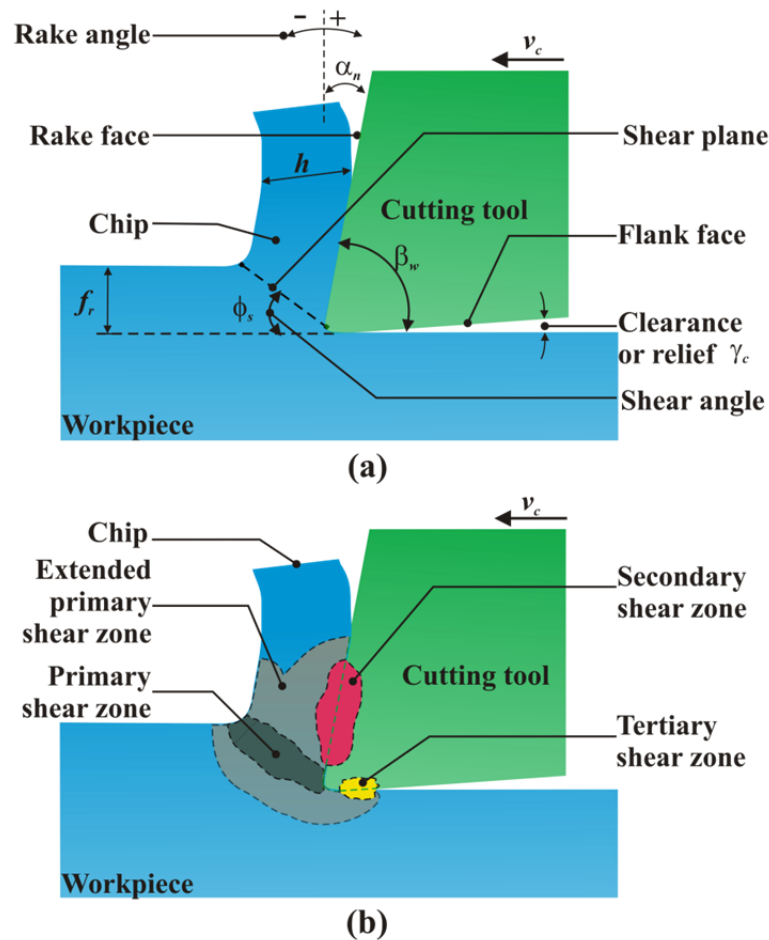


Figure 1.7: Schematic illustration of two-dimensional cutting processes: (a) orthogonal cutting with a well-defined shear plane (b) orthogonal cutting without a well-defined shear plane.

Chip formation in metal cutting is a complex chemical-physical process accompanied by large plastic deformation of the workpiece material and very high strain rates. Basically, there are three deformation zones in the cutting process as shown in the cross-sectional view of the orthogonal cutting (see Figure 1.7 (b)). As the edge of the tool penetrates into the workpiece, the material ahead of the tool is sheared over the primary shear zone to form a chip. The sheared material, i.e., the chip, is partially deformed and moves along the rake face of the tool, which is called secondary deformation zone. The friction area where the flank of the tool rubs the newly machined surface is called tertiary zone [AIBe12, PHLT08].

The engineering approach to characterize plastic deformation in the cutting zone is based on three basic simplifications. The first one, referred to as shear plane model or M.E. Merchant model, was developed in the early 1940s and adopts one shear surface in the shear zone at an angle, ϕ_s (called the shear angle). The work material is assumed to be perfectly plastic, i.e., work hardening does not occur. Moreover, it ignores the built-up edge (BUE), which may be

present, as well as chip curl and depicts tool face friction as being elastic rather than plastic. In 1966, Zorev [Zore63] proposed a ‘fan’-type or pie-shaped shear zone model through replacing curvilinear boundaries by straight lines. Later, Oxley [Oxle89] developed a model with parallel-sided shear bands inclined at a certain angle to the tool motion boundaries [Grze09].

The majority of machining operations involve tool shapes that are three-dimensional, thus the cutting is oblique. The mechanics of complex, three-dimensional oblique cutting operations are usually evaluated by geometrical and kinematic transformation models applied to the orthogonal cutting process. A simplified schematic representation of the oblique cutting process is shown in Figure 1.8.

The process is performed by tools with a tool cutting edge angle of $K_r \neq 90^\circ$ and a tool inclination angle of $\lambda_i \neq 0^\circ$. The rake angle may be measured in more than one plane, and hence more than one rake angle can be defined for a given tool and angle of obliquity. The different rake angles in oblique cutting are called normal (α_n), velocity and effective rake angle. The flow of chip is at an angle to the normal to the cutting edge. The angle between normal to the cutting edge and chip velocity vector is called chip flow angle (Δ_c). The shear angles can also be measured in different planes such as a plane normal to the cutting edge (ϕ_n) and plane of effective rake angle [AlBe12, BlKo13, Grze09, KaSc08].

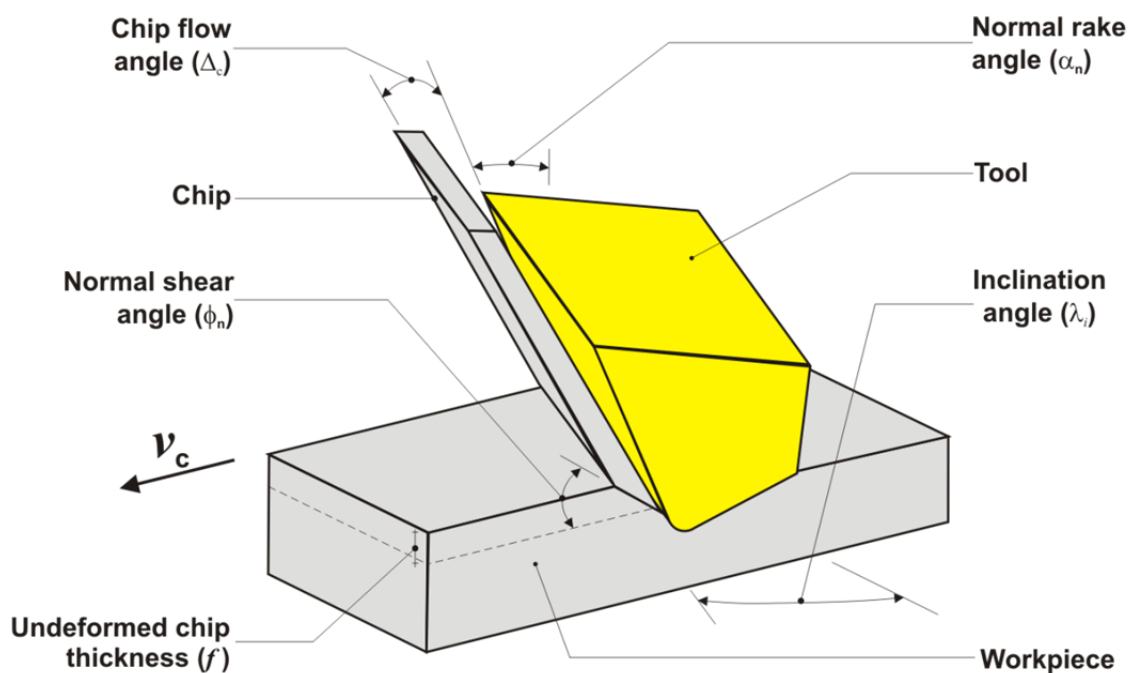


Figure 1.8: Schematic illustration of cutting with an oblique tool.

1.1.1.1 Surface roughness

Roughness refers to the small, finely spaced deviations from the nominal surface that are determined by the material characteristics and the process that formed the surface [Groo10]. It is one of the most important measurable quality characteristics and one of the most frequent customer requirements. Surface roughness greatly affects the functional performance of mechanical parts, such as wear resistance, fatigue strength, ability of distributing and holding lubricant, heat generation and transmission, corrosion resistance, etc.

JIS 1994 has defined six parameters in roughness profiles. The reader should refer to the standard for complete definitions of each parameter [SeCh06]. However, since the ranges of definition seem to be dictated by the physical possibilities of existing measuring instruments, it can be assumed that the definitions can also be extended to values below those, but this must be investigated.

- Ra is the most widely used quantification parameter in surface texture measurement. In the past, it was also known as center line average (CLA) or in the USA as arithmetic average (AA). Ra is the arithmetic average value of the profile departure from the mean line within a sampling length, which can be defined as:

$$Ra = \frac{1}{L_s} \int_0^{L_s} |z(x)| dx \approx \frac{1}{n} \sum_{i=1}^n |z_i| \quad (1.1)$$

where L_s is the sample length, and z is the height from the mean line defined in Figure 1.9.

- Rz is the sum of the average absolute value of the height of the five highest peaks as measured from the average line and the average absolute value of the height of the five lowest valleys within a portion stretching over a sample length (L_s) in the direction in which the average line extends.

$$Rz = \frac{1}{5} \sum_{i=1}^5 |z_{p_i}| + \frac{1}{5} \sum_{i=1}^5 |z_{v_i}| \quad (1.2)$$

where z_{p_i} and z_{v_i} are the highest peaks and deepest valleys respectively.

- Rt is the sum of the height z_{p5} of the highest point from the mean line and the height z_{v5} of the lowest point from the mean line [Groo10, Grou11, WaCh13].

$$Rt = z_{p5} + z_{v5} \quad (1.3)$$

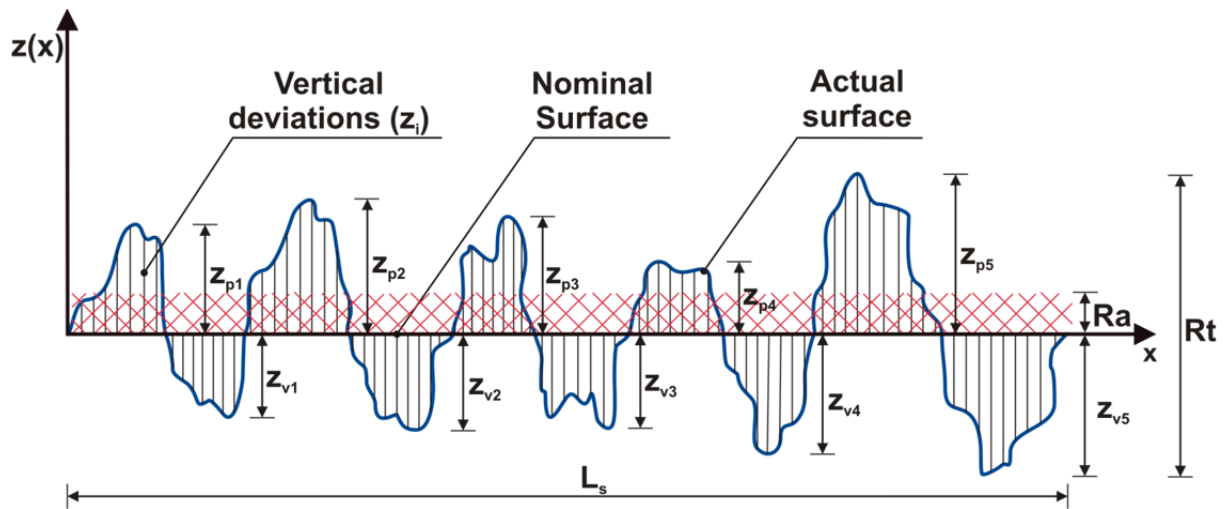


Figure 1.9: Definition of the surface roughness parameters.

1.1.1.2 Energy and power in turning

Turning is a process of removing excess material from the workpiece to produce an axisymmetric surface, in which the workpiece rotates in a spindle and the tool moves in a plane perpendicular to the surface velocity of the workpiece at the tool-workpiece contact point [DiDi08]. Based on the direction of the feed motion, one can differentiate between longitudinal turning, facing and form turning. In the first case there is an axial feed, in the second case a radial feed and in the third case a simultaneous axial and radial feed motion [Chry06]. The first case is used to produce cylindrical surfaces, the second is utilized to produce flat surfaces at the end of the part and perpendicular to its axis, and the third is used to produce various axisymmetric shapes for functional or aesthetic purposes [KaSc06].

It is worthwhile mentioning that during facing operations cutting speed increases linearly from the center to the circumference. Since the surface finish depends on the cutting speed, the surface finish becomes very poor as the tool approaches the center of the workpiece. To maintain a constant surface finish, the facing should be performed at constant cutting speed. For this purpose the rotational speed has to be varied to keep the cutting speed constant. This cutting operation is called facing at constant cutting speed. Through this process, savings of as much as 50% in production time can be achieved as well [Sing11]. The cutting force system in a conventional longitudinal turning and facing operation is shown schematically in Figure 1.10. The main components of the cutting forces are:

- F_c : Main cutting force acting in the direction of the cutting velocity vector. This force is generally the largest force and accounts for 99% of the power required by the process.
- F_f : Feed force acting in the direction of the tool feed. This force is usually about 50% of F_c but accounts for only a small percentage of the power required because feed rates are usually small compared with cutting speeds.
- F_t : Thrust or radial force acting perpendicular to the machined surface. This force is typically about 50% of F_f and contributes very little to power requirements because velocity in the radial direction is negligible.

The resultant cutting force (R_c) and the power required for cutting (P_c) can be calculated from the following equations:

$$R_c = \sqrt{F_c^2 + F_f^2 + F_t^2} \quad (1.4)$$

$$P_c = F_c v_c \quad (1.5)$$

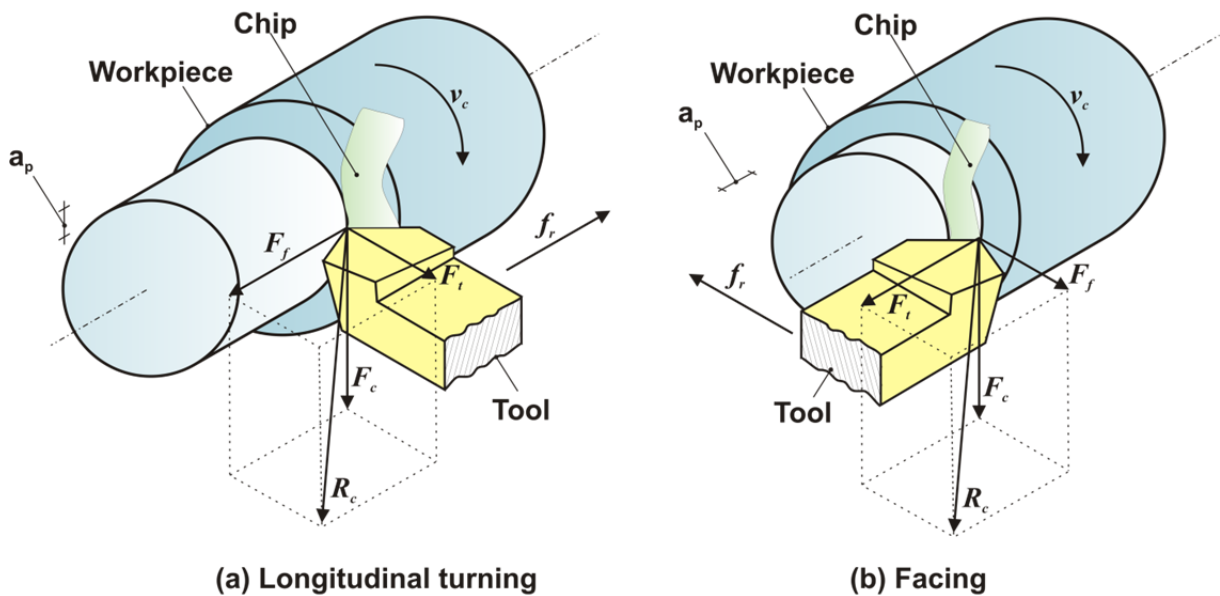


Figure 1.10: (a) Longitudinal turning and (b) facing operations have three measurable components of forces acting on the tool. These forces vary with cutting speed (v_c), feed rate (f_r) and depth of cut (a_p).

The turning energy required to remove a volume of material is given by the cutting power divided by the material removal rate (MRR). In manufacturing technology, this quantity is

generally known as the specific (volumetric) cutting energy (e_c) and both quantities are equivalent to the specific cutting pressure (k_c).

$$e_c = \frac{P_c}{MRR} = \frac{F_c v_c}{f_r a_p v_c} = \frac{F_c}{A_c} = k_c \quad (1.6)$$

where A_c is cross-sectional area of the uncut chip. Similarly, the values of the specific cutting pressures related to the feed forces k_f and thrust forces k_t can be evaluated using the expressions:

$$k_f = \frac{F_f}{A_c} \quad (1.7)$$

$$k_t = \frac{F_t}{A_c} \quad (1.8)$$

The value of the cutting force can also be predicted using the modified Kienzle equation:

$$F = k_{1.1} \left(\frac{v_c}{100} \right)^a (f_r)^{(1-b)} \quad (1.9)$$

where F represents the described cutting and resultant forces, $k_{1.1}$ is the specific cutting pressure for a 1mm^2 cross-sectional area of the cut, and the exponents a and b are model constants [BlKo13, Grze09, Kloc11].

1.1.1.3 Tool wear

During metal cutting, cutting tools are subjected to:

- high localized stresses at the tip of the tool,
- high temperatures, especially along the rake face,
- sliding of the chip along the rake face, and
- sliding of the tool along the newly cut workpiece surface.

These conditions induce tool wear, which is of major consideration in all machining operations, as are mold and die wear in casting and metalworking. Tool wear adversely affects tool life, the quality of the machined surface and its dimensional accuracy, and consequently the economics of cutting operations.

Wear is a gradual process, much like the wear of the tip of an ordinary pencil. The rate of tool wear depends on tool and workpiece materials, tool geometry, process parameters, and the characteristics of the machine tool. Tool wear and the changes in tool geometry during cutting manifest themselves in different ways, generally classified as flank wear, crater wear, nose wear, notching, plastic deformation of the tool tip, chipping, and gross fracture [KaSc06]. Figure 1.11 shows wear forms that occur primarily on turning tools [Kloc11].

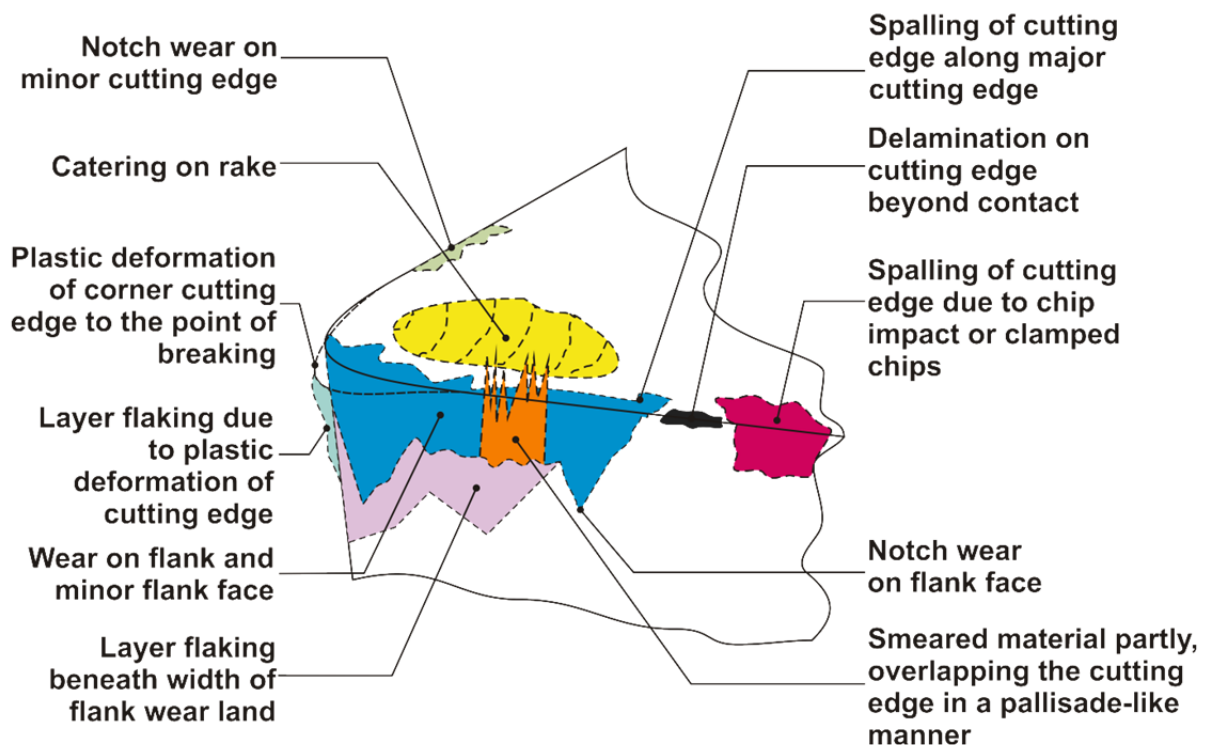


Figure 1.11: Characteristic wear forms at the cutting part during the turning process.

Figure 1.12 is a schematic representation of the dimensions of wear. In particular, we distinguish the width of flank wear land VB , the displacement of cutting edge toward flank face SV_α and rake face SV_γ , the crater depth KT and the crater center distance KM , from which the crater ratio $K = KT/KM$ is formed.

The mechanisms that cause wear at the tool–chip and tool–work interfaces in machining can be summarized as follows:

- Abrasion. This is a mechanical wearing action caused by hard particles in the work material gouging and removing small portions of the tool. This abrasive action occurs in both flank wear and crater wear; it is a significant cause of flank wear.

- Adhesion. When two metals are forced into contact under high pressure and temperature, adhesion or welding occur between them. These conditions are present between the chip and the rake face of the tool. As the chip flows across the tool, small particles of the tool are broken away from the surface, resulting in attrition of the surface.

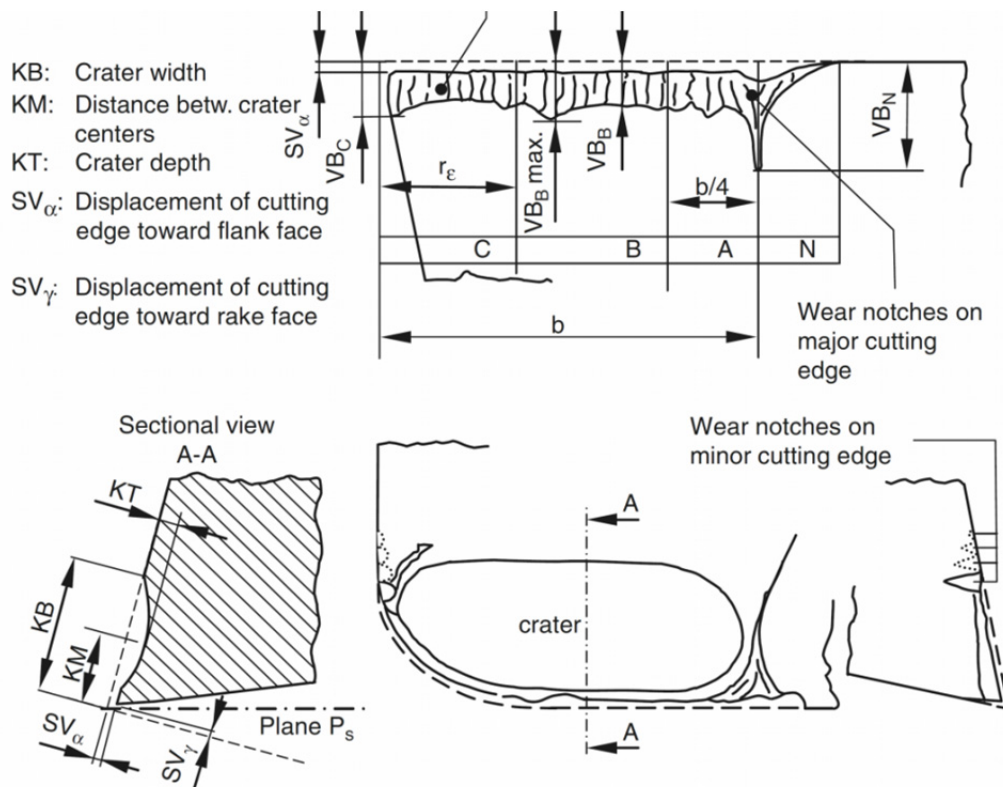


Figure 1.12: Wear forms and measured quantities at the cutting part, according to the DIN ISO 3685 [Kloc11].

- Diffusion. This is a process in which an exchange of atoms takes place across a close contact boundary between two materials. In the case of tool wear, diffusion occurs at the tool–chip boundary, causing the tool surface to become depleted of the atoms responsible for its hardness. As this process continues, the tool surface becomes more susceptible to abrasion and adhesion. Diffusion is believed to be a principal mechanism of crater wear.
- Chemical reactions. The high temperatures and clean surfaces at the tool–chip interface in machining at high speeds can result in chemical reactions, in particular, oxidation, on the rake face of the tool. The oxidized layer, being softer than the parent tool material, is sheared away, exposing new material to sustain the reaction process.
- Plastic deformation. Another mechanism that contributes to tool wear is plastic deformation of the cutting edge. The cutting forces acting on the cutting edge at high tempera-

ture cause the edge to deform plastically, making it more vulnerable to abrasion of the tool surface. Plastic deformation contributes mainly to flank wear.

Most of these tool-wear mechanisms are accelerated at higher cutting speeds and temperatures. From those, diffusion and chemical reaction are especially sensitive to elevated temperatures [Groo10].

1.1.1.4 Chip morphologies in turning

A chip is enormously variable in shape and size in industrial machining operations. The formation of all types of chips involves a shearing of the work material in the region of a plane extending from the tool edge to the position where the upper surface of the chip leaves the work surface. Gray cast iron chips, for example, are always fragmented, and the chips of more ductile materials may be produced as segments, particularly at very low cutting speeds. This discontinuous chip is one of the principal classes of chip forms and has the practical advantage that it is easily cleared from the cutting area. Under the majority of cutting conditions, however, ductile metals and alloys do not fracture on the shear plane, and a continuous chip is produced. Continuous chips may adopt many shapes - straight, tangled or with different types of helix. Often they have considerable strength, and the control of the chip shape is one of the problems confronting machinists and tool designers. Continuous and discontinuous chips are not two sharply defined categories; every shade of gradation between the two types can be observed. Another category of chips is observed when layers of workpiece material are gradually deposited on the tool tip, forming the built-up edge (BUE). As it grows larger, the BUE becomes unstable and eventually breaks apart. Part of the BUE material is carried away by the tool side of the chips; the rest is randomly deposited on the workpiece surface. The cycle of BUE formation and destruction is repeated continuously during the cutting operation until corrective measures are taken [KaSc06, TrWr00].

The formation of chips can be explained in terms of material behavior during the deformation process using appropriate stress-strain curves and relevant fracture mechanisms. As depicted in Figure 1.13 (a), *continuous chips* are related to curve #1 with large plastic flow of the material and the characteristic neck of a tensile specimen developed in region II. This phenomenon is termed by Shaw [Shaw89] as negative strain-hardening in the engineering stress-strain curve. If the plastic flow is not so intensive and the shear strain slightly exceeds the critical value of shear strain, the onset of chip segmentation is observed (partially segmented chips vs.

curve #2). When the entire shear strain decreases further, the chip segmentation starts to develop and the separation of chip segments begins (*elemental chips* vs. #3). In this case, the material necking takes place before the fracture but at a relatively lower shear stress. It should be noted that all three types of chips formed by shearing mechanisms could generally be related to the plastic deformation of the ductile work materials. In contrast, brittle materials only undergo elastic deformation (curve #4), which leads to producing discontinuous chips [Grze09].

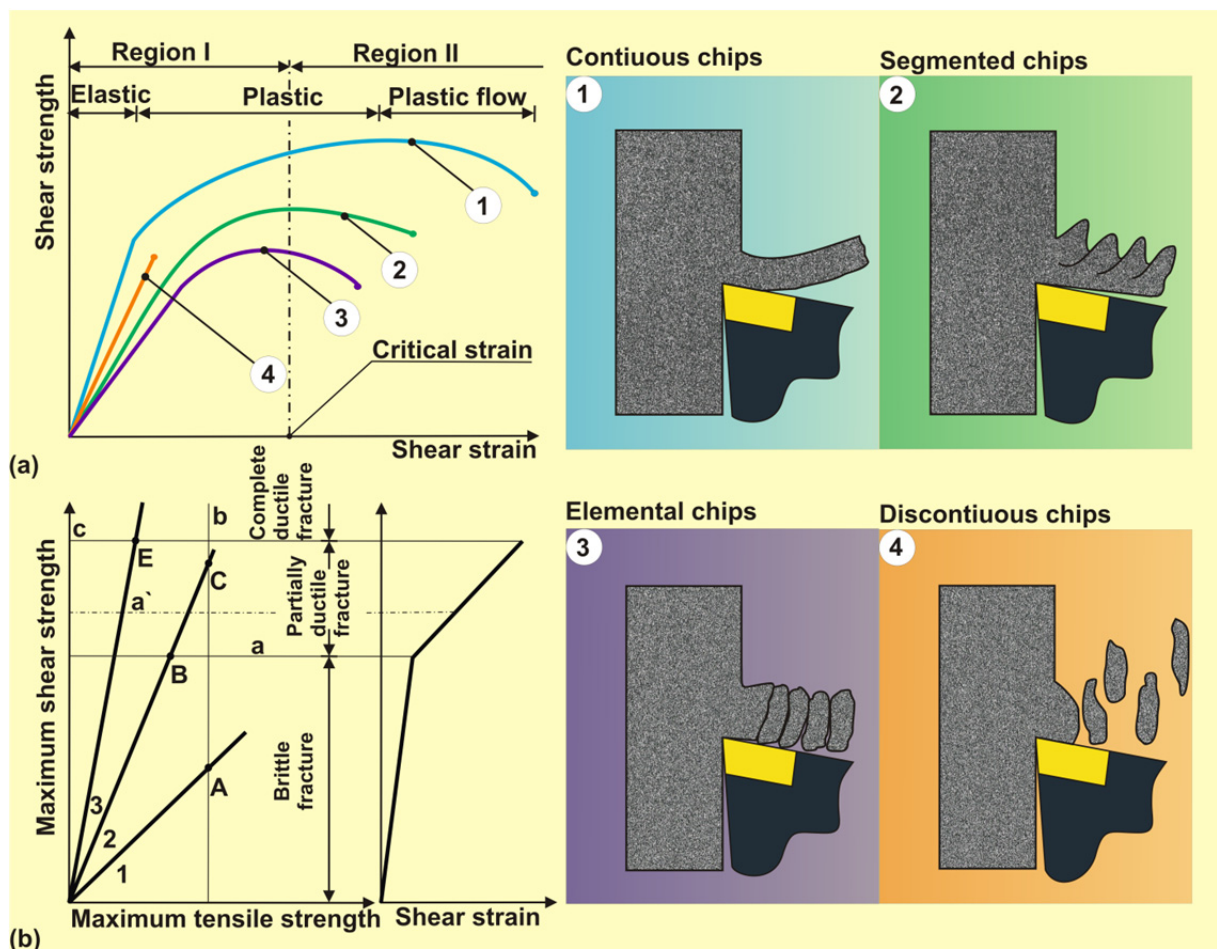


Figure 1.13: (a) Chip formation in terms of stress-strain curves according to Weber and Loladze; and (b) Fridman diagram of the fracture mechanism [Grze08].

All previously selected chip types can also be quantitatively related to the types of material fracture based on the Fridman diagram, shown in Figure 1.13 (b). This diagram utilizes the Tresca criterion for ductile fracture (maximum shear strength on the Y axis) and the maximum tensile strength criterion on the abscissa. Lines a, b and c adequately represent the yield point in shearing (a), the brittle fracture strength (b) and the yield point in shearing for per-

fectly ductile material (c). Additionally, line a' represents some specific case when the shear stress is artificially lowered due to intensive cooling by supplying gaseous or liquid coolants. Inclined lines starting from the origin of such a coordinate system represent simple tension (1), simple compression (2) and simple torsion (3). Consequently, three types of material fracture can be distinguished, namely: brittle fracture in point A, partially ductile fracture in point C because of the linear work-hardening effect and perfect ductile fracture in point E. It can be assumed that these mechanical material states are equivalent to those responsible for the formation of discontinuous, segmented and continuous types [Grze08].

1.1.1.5 Chip volume ratio (R)

With regard to the metal removal rate, one has to distinguish between the volume of the removed material MRR and the space needed for the randomly arranged metal chips. The volume of the removed material identifies the volume occupied by a chip with cross sectional area A_c . The volume of the randomly arranged metal chips removed is greater than the real volume of the same amount of removed material, since in a reservoir the chips are not located next to each other without gaps. The chip volume ratio R defines by what factor the volume of randomly arranged chips is greater than the volume of the removed material.

$$R = \frac{\text{Volume needed for randomly arranged metal chips}}{\text{Material volume of the same amount of metal removal}} \quad (1.10)$$

Figure 1.14 summarizes the most significant chip shapes. Each chip form is assigned to a chip volume ratio R , which defines by what factor the transport volume needed for the specific chip form exceeds the intrinsic material volume of the chip.

The appraisal of the chip form involves two criteria (safety of the operator and transportability). According to this approach, ribbon, snarled and helical chips are not preferred. The desirable chip forms are helical chip segments, spiral chips, pieces of spiral chips and discontinuous chips [TsRe09].




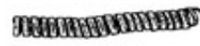




Chip shapes		Chip volume ratio (R)
Ribbon chips		≥ 90
Snarled chips		≥ 90
Flat helical chips		≥ 50
Cylindrical helical chips		≥ 50
Helical chip segments		≥ 25
Spiral chips		≥ 8
Spiral chip segments		≥ 8
Discontinuous chips		≥ 3

Figure 1.14: Chip shapes and chip volume ratios [BBCC09].

1.1.1.6 Economics of turning operations

The economics of machining has been an important area of research in machining starting with the early work of Gilbert [Gilb50]. The main objectives are the minimization of the machining cost, the maximization of the production rate and the maximization of the profit rate. The major constraints are the constraint on surface roughness, forces acting on the tool and machine power. In general, the optimization of machining is a multi-objective problem. The major difficulty in the optimization is the knowledge about the metal cutting behavior. There should be a model to predict the tool life, a model to predict the job quality and a model to predict the forces and temperature of the tool. Figure 1.15 shows the block diagram of the optimization procedure.

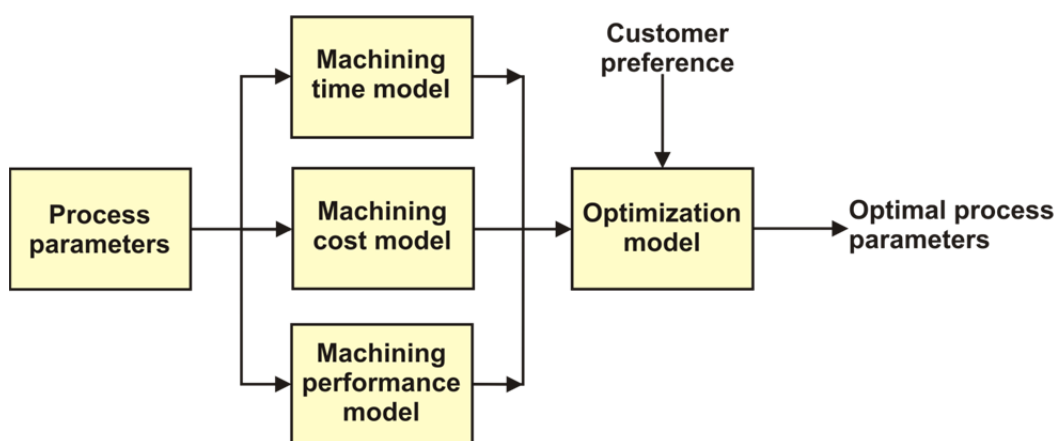


Figure 1.15: Block diagram of the optimization procedure in machining [DiDi08].

- *Machining time model*

In cutting operations, the machine utilization time t_{bB} is defined as the sum of all nominal times that a machine requires to accomplish a specified job. It is composed of the time required to produce m units and the total set-up time t_{rB} :

$$t_{bB} = m.t_e + t_{rB} \quad (1.11)$$

Production time or time per unit t_e can be expressed in terms of the basic time t_g and the idle time t_i as follow:

$$t_e = t_g + t_i \quad (1.12)$$

The basic time t_g is the sum of the main process time t_h and the auxiliary process time t_n .

$$t_g = t_h + t_n \quad (1.13)$$

The main cutting time for turning can be calculated using the following expression:

$$t_h = t_c + C_f \quad (1.14)$$

Here, the cutting time t_c is the time in which the tool is actually cutting. For longitudinal turning operations, the cutting time is defined as:

$$t_c = \frac{L_t}{1000 f_r N} n_p \quad (1.15)$$

where L_t is the total length of tool travel including approach and overrun lengths in mm , n_p is the number of cutting passes, and N is the rotational speed in revolutions per minutes (rpm). Meanwhile, the cutting time for facing a solid cylinder at a constant rotational speed is calculated using the following expression:

$$t_c = \frac{(l_r + d/2)}{1000 f_r N} n_p \quad (1.16)$$

where l_r is the approach length and d is the outside diameter in mm . In facing a solid cylinder at a constant cutting speed, the cutting time (in minutes) is given by the expression:

$$t_c = \frac{\pi}{4000} \cdot \frac{((2l_r + d)^2 + (\frac{1000v_c}{\pi N_{\max}})^2)}{f_r v_c} n_p \quad (1.17)$$

where N_{\max} is the maximum rotational speed of the workpiece. The constant C_f is the function of cut lengths, which are considered in conjunction with the respective feed velocity. The auxiliary process time t_n is the time during which all indirect processes arising during the machining operation (e.g. tightening, measuring, adjusting, pro rata tool change and workpiece change) are executed. The idle time t_i takes all pauses into consideration during which the machine tools are not in operation and the total time required for all irregular events, such as procuring necessary resources. The following relation is considered valid for calculating the idle time:

$$t_i = 0.3(t_h + t_n) \quad (1.18)$$

The total setup time t_{rB} refers to the time required for machine set-up t_{vM} , tool change t_{rW} and nonproductive set-up activities t_{rV} . The latter is often estimated as 30% of the machine set-up and tool change time.

$$t_{rB} = t_{vM} + t_{rW} + t_{rV} \quad (1.19)$$

For a batch of m workpieces per machine, the total tool change time is defined as:

$$t_{rW} = m \cdot t_{WZ} \cdot \frac{t_h}{T} \quad (1.20)$$

where t_{WZ} is the time that passes till a single tool is changed, and both the position correction and the positioning for re-entry have taken place. The tool life T can generally be calculated based on flank wear criteria of $VB=200-600\mu\text{m}$ when cemented carbides are used. The overall working time t_a per x number of machines is described as:

$$t_a = t_e \cdot \frac{m}{x} \quad (1.21)$$

Finally, the following relation is true for the machine utilization time per workpiece or process:

$$t_{bB} = m[1.3(t_c + C_f + t_n) + t_{WZ} \cdot \frac{t_h}{T}] + t_{rV} + t_{vM} \quad (1.22)$$

- *Production cost model*

The typical production cost for a workpiece produced by turning operations is comprised of machine costs, labor cost and tool costs:

$$K_F = K_M + K_L + K_W \quad (1.23)$$

The machine hour-rate describes the costs to be calculated of a machine tool per hour. The machine hour-rate K_M is calculated as follow:

$$K_M = \frac{1}{JAS} \left(\frac{k_{bB}}{t_l} + k_{bW} + k_{bZ} + k_{bR} \right) + k_{bE} \quad (1.24)$$

The annual operating hours JAS of a machine are defined as:

$$JAS = \frac{\text{No. of operation hours}}{\text{Week (w.)}} \times \text{No. of working shifts} \times \frac{\text{No. of working weeks}}{\text{Year}} \quad (1.25)$$

The yearly machine runtime JAS amounts, for example, to 1600–1800 h/a for single-shift operations. In the case of multi-shift operations, the runtime is increased proportionately (e.g. two-shift operations ca. 3200 h/a or three-shift operations ca. 4800 h/a). The procurement costs k_{bB} cover the purchasing, transportation and installation costs. The time t_l is defined as a time frame at which the machine is economically utilizable. The cost of maintenance and repair services k_{bW} can be expressed in terms of the percentage $\% p_p$ of the procurement costs k_{bB} :

$$k_{bW} = \frac{p_p}{100} \cdot k_{bB} \quad (1.26)$$

Assumed interest rates can be set at the current value of the machine, also of a non-depreciated element, as a calculated average based on the procurement price at the full interest rate ($\% q_i$):

$$k_{bZ} = 0.5 \cdot \% q_i \cdot k_{bB} \quad (1.27)$$

To calculate the space cost k_{bR} , planning estimations should take account of the required machine area Q_m in m^2 and the monthly rent A_a per m^2 :

$$k_{bR} = 12 \cdot Q_m \cdot A_a \quad (1.28)$$

The operating cost k_{bE} includes the costs of operation energy, lighting and coolant k_k . The electricity costs can be estimated based on the effective cutting power P_M , the standard cost of electricity E_c in euro/kWh and the percentage $\%C_2$ of being in ON state:

$$k_{bE} = P_M \cdot E_c \cdot \%C_2 + k_k \quad (1.29)$$

Labor cost K_L is calculated as follows:

$$K_L = L_m(1+r) \quad (1.30)$$

where L_m is the gross hourly wage, and r as the amount of the nonwage cost of the operator. This applies if a new factor that summarizes the machine cost and the wage rate per hour in terms of previously defined time scales is formulated as:

$$K_{ML} = K_M + \frac{t_{rB} + t_a}{t_{bB}} \cdot K_L \quad (1.31)$$

The costs of typical indexable carbide cutting tools are comprised of the cost of tool holders k_{WH} , inserts k_{WP} and spare parts k_{ET} :

$$K_W = k_{WH} + k_{WP} + k_{ET} \quad (1.32)$$

The total insert costs are defined as:

$$k_{WP} = \frac{m \cdot t_h \cdot K_{WSP}}{0.8 \cdot T \cdot Z_s} \quad (1.33)$$

where K_{WSP} is the cost of an insert, Z_s is the number of usable cutting edges per insert, and 0.8 is a safety factor accounts for uncertainty in tool life. The spare parts costs are often expressed in terms of the percentage of tool holder and insert costs. The final production cost per unit is obtained by adding the terms in Eqs. 20-35:

$$K_F = \frac{1}{m} [t_{bB} \cdot K_M + (t_{rB} + t_a) \cdot K_L + k_{WH} + \frac{m \cdot t_h \cdot K_{WSP}}{0.8 \cdot T \cdot Z_s} + k_{ET}] \quad (1.34)$$

Using the previous relationships, one can define the main time-related costs as:

$$K_1 = (K_M + \frac{1}{x} K_L) \cdot t_h \quad (1.35)$$

the fixed or the workpiece-related costs as:

$$K_2 = \frac{1}{m} (K_M + \frac{1}{x} K_L) (t_{rM} + t_{rV}) + (K_M + \frac{K_L}{x}) \cdot (t_n + t_b + t_{vB}) \quad (1.36)$$

and the tool-related costs as:

$$K_3 = \frac{t_h}{T} (K_M + K_L) (t_w) + \frac{1}{m} K_W \quad (1.37)$$

The production cost can also be determined using [Kloc11, PHLT08]:

$$K_F = K_1 + K_2 + K_3 \quad (1.38)$$

The cutting speed has such a great influence on the tool life compared to the feed or the depth of cut that it greatly influences the overall economics of the machining process. For a given combination of work material and tool material, a 50% increase in speed results in a 90% decrease in tool life, while a 50% increase in feed results in a 60% decrease in tool life. A 50% increase in depth of cut produces only a 15% decrease in tool life. Therefore, in limited-horsepower situations, depth of cut and then feed should be maximized while speed is held constant and horsepower consumed is maintained within limits. As cutting speed is increased, the cutting time decreases but the tools wear out faster and must be changed more often. In terms of costs, the situation is as shown in Figure 1.16, which presents the effect of cutting speed on the cost per piece [BlKo13].

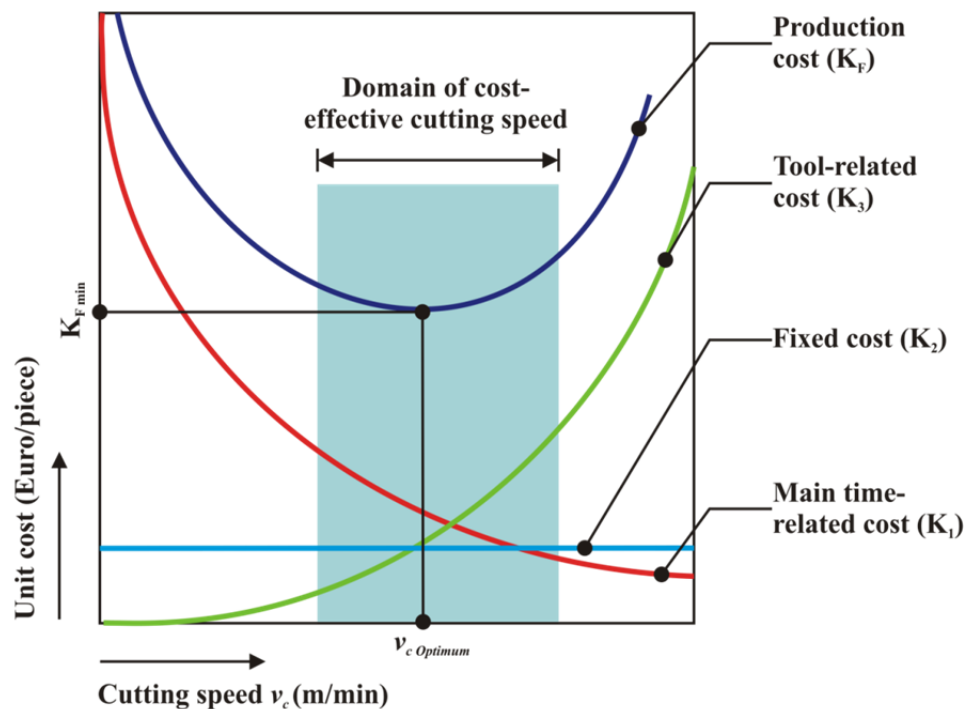


Figure 1.16: Cost per unit for a machining process versus cutting speed.

1.2 Background and aim

It is estimated that 15% of the value of all mechanical components manufactured worldwide is derived from machining operations. Despite this obvious economic and technical importance, it remains one of the least understood manufacturing operations due to the low predictive ability of the machining models [UsSh82a, Usui88].

In most of the textbooks on machining, a single shear plane model is described. This is based on the assumption that material removal takes place through shear over a very narrow zone. As argued by Astakhov [Asta05], this model suffers from a number of drawbacks, viz., infinite strain rate, unrealistically high shear strain, unrealistic behavior of the work material, improper accounting for the resistance of the work material to cut, unrealistic representation of the tool–workpiece contact, inapplicability for cutting brittle work materials, incorrect velocity diagram, incorrect force diagram and inability to explain chip curling. Actually the machining process is so complex that no existing physics-based model seems to describe the process properly. Other analytical modeling approaches such as the extended three dimensional shear plane model or oblique cutting slip-line field models are either poorly correlated with experimental results or quite complex, and for their application stress and strain data at the strain rates encountered in metal machining is needed. This is why other modeling approaches such as empirical, mechanistic, numerical and artificial intelligence are developed as alternatives to the metal cutting theory, because the latter did not prove its ability to solve even simple practical problems [Asta06].

Traditionally, mathematical programming techniques such as linear programming, method of feasible direction, dynamic programming and geometric programming had been used to solve optimization problems in machining. However, these traditional methods of optimization do not fare well over a broad spectrum of problem domains. Moreover, traditional techniques may not be robust. Numerous performances, constraints and multi-passes make machining optimization problems complicated, and hence these techniques are not ideal for solving such problems as they tend to obtain a local optimal solution [VePa10].

On the other hand, a search with the keywords ‘duplex stainless steel’ in popular databases, such as Science Citation Index-Expand or Scopus, would reveal tens of recent publications. This is a vivid testimony of the potential interest in DSSs as a key research topic by various researchers in the world. However, one can hardly find a scientific article which addresses the

computational and numerical modeling as well as the optimization of machining regarding such an important family of stainless steels.

Considering the respective drawbacks of metal cutting theory and traditional optimization techniques in the modeling and optimizing of machining processes as well as the scarcity of the work material's comprehensive machining investigations, the objective of the present dissertation is to address the machinability of DSSs through the systematic application of advanced modeling and optimization techniques in turning processes. The approaches proposed here could then be used to optimize the residual machining criteria, for example, towards a lower manufacturing cost or a more sustainable machining process or a more precise numerical simulation.

1.3 Research approach

Research in common parlance refers to a search for knowledge. One can also define research as a scientific and systematic search for pertinent information on a specific topic. In fact, research is an art of scientific investigation. The Advanced Learner's Dictionary of Current English lays down the meaning of research as "a careful investigation or inquiry especially through search for new facts in any branch of knowledge" [Hedb89]. The word itself is derived from the French word "rechercher", which means "to search closely", and "chercher" means "to search". Its literal meaning is "to investigate thoroughly" [Oful13].

Research is an academic activity and the term as such should be used in a technical sense. According to Clifford Woody, research comprises defining and redefining problems, formulating hypotheses or suggesting solutions, collecting, organizing and evaluating data, making deductions and reaching conclusions, and at last carefully testing the conclusions to determine whether they fit the formulated hypotheses [Koth04].

There are two basic approaches to research, viz., a quantitative approach and a qualitative approach. The former involves the generation of data in quantitative form, which can be subjected to rigorous quantitative analysis in a formal and rigid fashion. A qualitative approach to research is concerned with the subjective assessment of attitudes, opinions and behavior. Research in such a situation is a function of a researcher's insights and impressions. Such an approach to research generates results either in a non-quantitative form or in a form which is

not subjected to rigorous quantitative analysis. Generally, group interviews, projective techniques and depth interviews are used as the techniques of focus [Koth04].

The quantitative approach can be further sub-classified into inferential, experimental and simulation approaches to research. The inferential approach usually means survey research, in which a sample of the population is studied. Experimental approach is characterized by a much greater control over the research environment, and in this case some variables are manipulated to observe their effect on other variables. The simulation approach involves the construction of an artificial environment, within which relevant information and data can be generated. This permits an observation of the dynamic behavior of a system (or its sub-system) under controlled conditions [DaSa11].

The research approach adopted in the present dissertation is predominantly quantitative. Experimental and simulation approaches are applied to obtain quantitative results, through which the conclusions are based on the observations and experience (empiricism). However, since not all parts of the cutting process may be analyzed through a quantitative approach, additional qualitative observations have been collected, analyzed and converted into quantitative results. The estimation of chip volume ratio, based on the chip breaking chart, is an example of data interpretations from qualitative chip morphology format to quantitative chip volume ratio, based on the fuzzy set theory. On multiple occasions, a qualitative approach is also used as a complement to the quantitative approach.

1.4 Research hypothesis

- The application of statistical regression and computational optimization techniques in the multi-objective optimization of cutting can effectively obtain sets of non-dominated solutions.
- Fuzzy set theory principles can be proficiently applied to eliminate the discrepancy of the ranking system among the multiple attribute decision-making (MADM) methods, thus promoting the decision-making process.
- Coupling the Taguchi method with MADM and meta-heuristic optimization methods can suitably provide the decision maker and/or process planner with the skills essential for the mono- and multi-objective optimization of cutting processes.

- Multiple quality characteristics of the machining surface can be efficiently optimized when MADM methods are coupled with fuzzy set theory.
- The sustainability-based optimization of multi-pass cutting operations is possible if the hybridization of input-output modeling and optimization tools and MADM methods is systematically performed.
- The inverse identification of input parameters in numerical modeling of cutting can be effectively performed if coupled Java-based material properties (JMatPro) software, design of experiment (DOE), MADM, computational modeling and meta-heuristic algorithms are applied. The approach can also perform well for hypothetical, numerical optimization studies.

1.5 Research questions

In conjunction with the hypotheses, the following research questions are identified:

- Can the application of statistical regression and computational optimization techniques effectively obtain sets of non-dominated solutions in the multi-objective optimization of machining DSSs?
- Is the application of fuzzy set theory advantageous in eliminating the discrepancy of the ranking system among the MADM methods and can it achieve better results than other optimization approaches?
- Can the Taguchi-MADM-meta-heuristics concept be conveniently used for the mono- and multi-objective optimization of cutting stainless steels?
- Can multiple quality characteristics of the machining surface be efficiently optimized when MADM methods are coupled with fuzzy set theory?
- Would it be possible for multi-pass cutting operations to be sustainably optimized when the hybridization of input-output modeling and optimization tools and MADM methods is systematically performed?
- Is it possible to apply Java-based material properties (JMatPro) software, design of experiment (DOE), MADM, computational modeling and meta-heuristic approach to the inverse identification of the input parameters during the finite element simulation of cutting processes? If it is possible, can a hypothetical, numerical optimization study be performed as a case study?

1.6 Research delimitations

The important boundaries that have been set for the present dissertation are:

- The research is primarily focused on the machining of EN 1.4462 and EN 1.4410 DSSs. However, in some cases EN 1.4404 austenitic stainless steel grade has been used as a benchmark for comparison analyses of machinability.
- The research has primarily been limited to constant cutting speed facing and longitudinal turning operations. The latter was seen suitable for conducting multi-objective optimization and for numerical modeling.
- Coated and uncoated cemented carbide cutting inserts are employed in all experimental and numerical investigations as they are generally recommended for machining stainless steels by different manufacturers.
- The literature survey in this dissertation will not review non-traditional machining processes, unless they are the only processes through which the adaptability of modeling and optimization approaches is first examined.
- The optimization of the tool geometry and the orientation angles is restricted to the numerical modeling.

1.7 Outline of the dissertation

The present work is structured into ten Chapters. Chapter 2 proposes a review of the main techniques and tools enabling the modeling and the optimization of the cutting process. The basic concepts and the application potential of several modeling and optimization techniques in metal cutting processes, classified under several criteria, have been reviewed and critically appraised. A universal framework for parameter modeling and optimization in metal cutting processes is also proposed.

A detailed explanation of the experimental setup and the instruments is given in Chapter 3. Elements of the cutting measurement systems are characterized using illustrative, schematic diagrams. A brief description of the adopted experimental designs and the involved performance characteristics is presented. The chapter also contains an introduction into the temperature-dependent physical and mechanical properties of the work materials, which were generated using JMatPro software.

Chapter 4 presents the experimental investigations into longitudinal turning of duplex stainless steel grades with multi-layer coated inserts. The parametric influences of cutting and process conditions on the cutting performances are analyzed, and proper interim conclusion points are drawn. The chapter also presents the multi-objective optimization of machining duplex stainless steels, based on the nature-inspired Multi-Objective Bat Algorithm (MOBA).

Chapter 5 addresses a new methodology based on Mamdani fuzzy interference of classified chip shapes in chip breaking charts to predict the chip volume ratio. Several performance characteristics are considered and converted into four indices using four MADM methods. An expert system, based on the fuzzy rule modeling approach, is then adopted to combine the computed four indices into a single Universal Characteristics Index (UCI). First-ranking UCI values are analyzed and compared with the output of the Weighted Sum Method (WSM), using a constrained, Simulated Annealing algorithm.

Chapter 6 presents the multi-performance optimization of turning super duplex EN 1.4410, standard duplex EN 1.4462 and austenitic EN 1.4404 stainless steels, utilizing coupled Taguchi-based designs, MADM and meta-heuristic algorithms. Nature-inspired meta-heuristic algorithms such as the Firefly Algorithm (FA), Accelerated Particle Swarm Optimization (APSO) and Cuckoo Search (CS) are employed and their corresponding performances compared.

In Chapter 7, the Taguchi approach is coupled with fuzzy-multiple attribute decision-making methods for achieving better surface qualities in constant cutting speed face turning of austenitic and duplex stainless steels. Two typical multiple attribute decision-making techniques were simultaneously adopted to determine multi-surface quality characteristics indices. The differences in rankings among derived indices are solved through converting each crisp value into a trapezoidal fuzzy number and unifying them by using the fuzzy simple additive weight method.

In Chapter 8, a systematic approach, which employs different modeling and optimization tools under a three phase investigation scheme, is adopted. In phase I, the effect of design variables such as cutting parameters, cutting fluids and axial length of cuts are investigated using the D-Optimal method. In the phase II, comprehensive experiment-based production cost and production rate models are developed. In phase III, expert systems based on the fuzzy rule modeling approach are adopted to derive measures for machining operational sustainability, called Operational Sustainability Index (OSI). Finally, a new Cuckoo Search Neu-

ral Network System (CSNNS) is utilized to constrainedly optimize the cutting process per each cutting scenario.

Chapter 9 provides a novel methodology to inversely calculate the input parameters when simulating the machining of duplex stainless steels, based on Taguchi-VIKOR coupled with a Firefly Algorithm Neural Network System (FANNS). Thereafter, design of experiments, numerical simulations and fuzzy rule modeling approaches are employed to optimize types of cutting tool geometry, process conditions, cutting parameters and tool orientation angles based on many important performances.

While summaries of the research results obtained in chapters 4-9 can be found separately in the interim conclusion sections, Chapter 10 serves to provide a concise and overall summary of the main achievements of the study. Finally, a schematic illustration of the research methodology and the approximate location of the chapters included in this dissertation can be found in Figure 1.17.

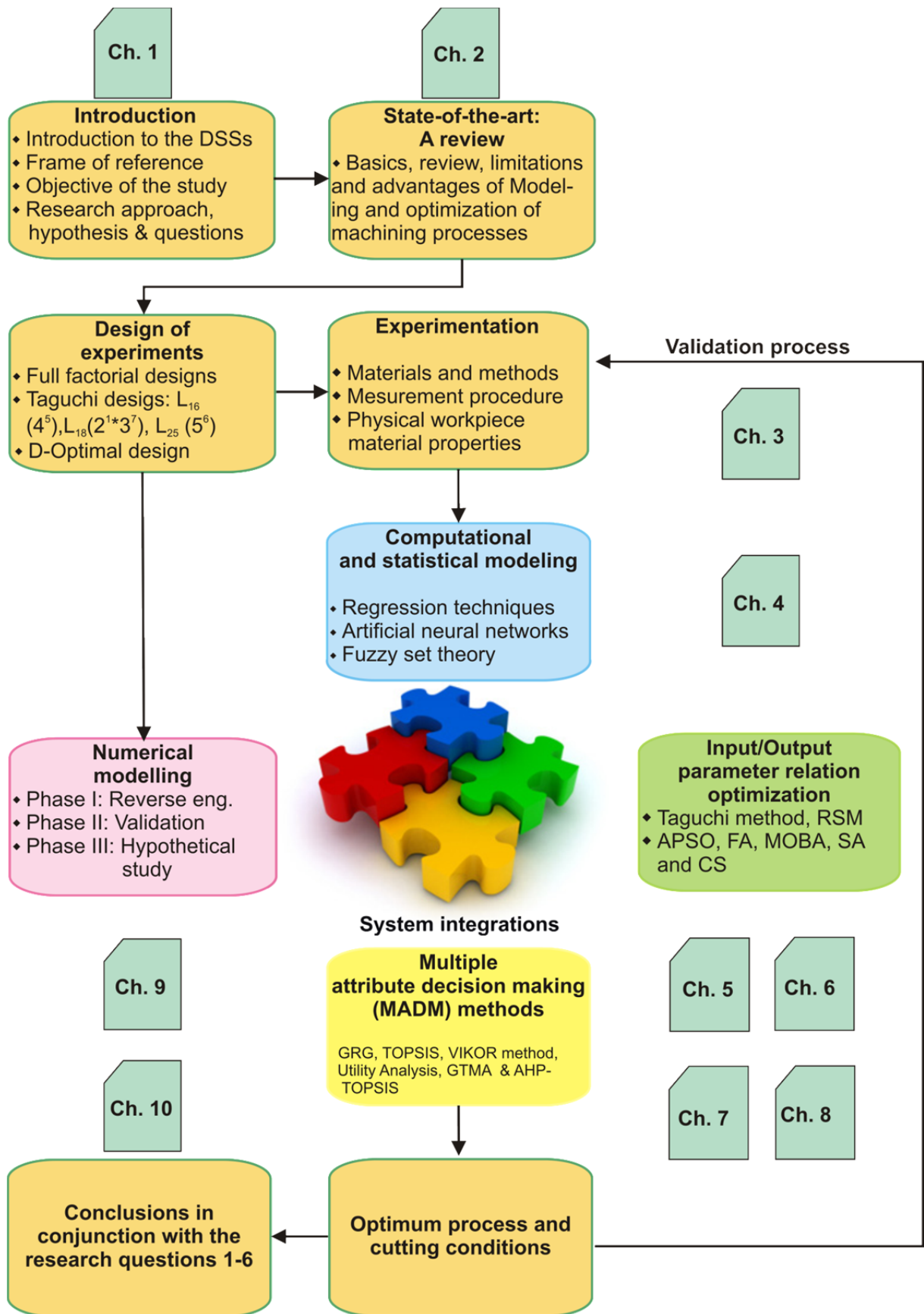


Figure 1.17: Research methodology and approximate locations of the dissertation’s chapters.

2 State of the art in machining modeling and optimization: A review

The history of research practice in metal cutting is well documented by Finnie [Finn56], who identified the work of Cocquilhat [Cocq51] in 1851 as the first research in the area of measuring the work required to remove a given material volume by drilling. However, the first who argued that the chip is created by shearing ahead of the tool was Time [3] in 1870, when he presented the results obtained from observing cutting. Astakhov confirmed in his book “Metal cutting mechanics” that this work is one of the first publications that suggests a shear plane theory [Asta98]. It has also been shown that there is no contradiction between Time’s work and Tresca’s work [Tres73]. In 1873 Tresca argued that the chip in metal cutting is produced by compression ahead of the tool. Also in 1873, Hartig published tabulations of the power and work required in cutting metal in his book ‘Versuche über Leistung und Arbeitsverbrauch der Werkzeugmaschine’, which seems to have been the authoritative work on the subject for several years [Hart73]. In 1896 Zvorykin [Zvor96] was the first to provide a physical explanation for this model; his work resulted in an equation predicting the shear angle. In 1881, Mallock established the basis of a shear plane model. In his turning experiments, Mallock made hand drawings of the chip formation process in the course of their formation by means of a microscope, mounted on the tool holder. He also emphasized the importance of friction in the tool-chip interface [Mall81]. Finnie also reports that a step backward in the understanding of metal cutting process was taken in 1900, when Reuleaux [Reul00] suggested that a crack occurred ahead of the tool and that this process could be linked to the splitting of wood. However, it was the work of Ernst and Merchant in 1941 that made the shear plane model popular. Most of the fundamental works on metal cutting mechanics refer to this paper, and many analytical models of orthogonal cutting still use the relations derived from this work [KnBo05, Mark13].

Many efforts have been made to refine Merchant’s model with the aim of improving the predictive capability [LeSc51, Oxle98, Zore63]. A modern analytical approach, known as the “unified or generalized mechanics approach”, has been pursued by Armarego and co-workers [ArHe00, Arma00] for years and then spread as the mechanistic approach in metal cutting [EnDK95]. However, due to the nature of the cutting process, which involves plastic deformation, heat transfer, diffusion, chemical reactions and other complex phenomena in machining, empirical models have been more successful than analytical ones. Hence, one has

not to be surprised when seeing that Taylor's empirical tool life model [Tayl07], which was developed in 1907, is still in action today and employed as the basis for many up-to-date studies of machining economics [QuDa09].

With the advent of powerful computers in the late 1970s and early 1980s, a number of important changes in machining modeling have been made. The most significant change to the cutting modeling was the introduction of artificial intelligence techniques. Techniques such as neural network, fuzzy logic, neuro-fuzzy system, support vector machines [BMUK12, ÇaEk12, RaRA09, ShGi06, WKFL13] and hidden Markov models [AtOB00, ErLO01, ScEH05, WaMK02, ZhWH09] have been widely applied in metal cutting performance predictions. On the other hand, in numerical modeling, the emergence of the finite element method (FEM) must be noted as a powerful numerical method to solve differential equations. In fact, efforts to apply the FEM of chip formation processes date back to the early 1970s [OkKa71, TaSD74, TSV076]. However, due to the extensive computational demands, it was not until the late 1990s that numerical methods became a useful and practical tool [AÖUD13, ArÖz09].

In addition, although it is quite important for planning efficient machining processes, the optimization of cutting parameters is a complicated target, challenged not only by the complex nature of the involved phenomena but also by the need for carefully defining realistic optimization objectives as well as developing and implementing powerful and versatile optimization techniques. In this sense, stochastic optimization techniques, mainly evolutionary algorithms, have been widely reported in recent literature [QuDa11]. The discussion here is mainly intended to provide a brief theoretical background to some important machining modeling and optimization techniques and review the recently used tools.

2.1 Input-output parameter relationship of modeling tools

The first necessary step for process parameter optimization is to understand the principles governing the manufacturing process by means of developing an explicit mathematical model, which may be of two types: mechanistic or empirical [BoDr87]. The model in which the functional relationship between input–output and in-process parameters is analytically determined is called mechanistic model. However, as there is lack of adequate and acceptable mechanistic models for manufacturing processes, empirical models are generally used in manufacturing processes. The modeling techniques of input–output and in-process parameter relationships

are mainly based on statistical regression, fuzzy set theory and artificial neural networks [LuSp95]. In terms of the computation methods, modeling based on physics is accomplished by the computational tools that may be called hard computing methods. On the other hand, modeling based on data is accomplished by soft computing tools, such as neural networks and fuzzy sets. Soft computing tools try to generate approximate solutions of the problem in the presence of uncertain or imprecise physics and/or the process variables. It differs from conventional (hard) computing in that, it is tolerant of imprecision, uncertainty, partial truth and approximation. A hybrid of hard and soft techniques may also be used [DeDi08].

The modeling techniques of input–output and in-process parameter relationships are mainly based on statistical regression, fuzzy set theory and artificial neural networks. Figure 2.1 provides a general classification of different modeling tools for input-output parameter relationships in metal cutting processes. In the following sections, some of these tools will be briefly explained.

2.1.1 Statistical regression

2.1.1.1 Theoretical background

The data collected through experiments usually exhibits a significant degree of errors or a “noise.” In such a case, there is no need to intersect every point as the individual data points may be incorrect. Rather, the curve is designed to follow the pattern of points taken in groups. This approach is known as statistical regression [MoPV12]. It utilizes experimental data on the related variables to develop a numerical relationship, showing the influence of the independent variables on a dependent variable of the system. If nothing is known from theory about the relationship between independent and dependent variables, a function may be assumed and fitted to the experimental data on the system. Usually a linear function is assumed. In other cases where a linear function does not properly fit the experimental data, the engineer might try a polynomial or exponential function [Lazi06]. Regression has been proved to be a conceptually simple technique for investigating functional relationships between output and input decision variables of a cutting process and may be useful for cutting process data description, parameter estimation and control [MuRa06].

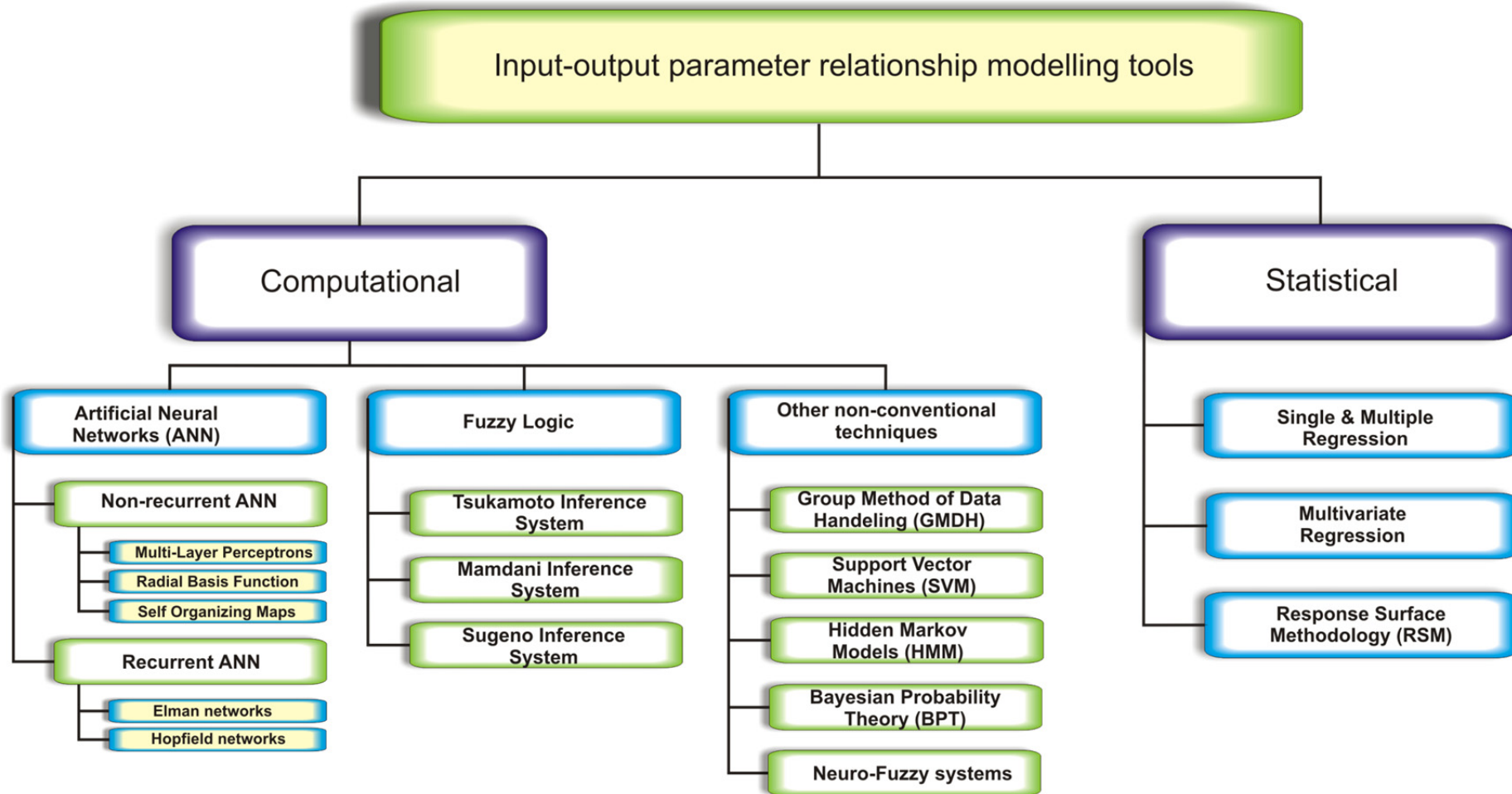


Figure 2.1: Classification of the modeling tools for input-output relationships in metal cutting process problems.

$$\begin{Bmatrix} y_1 \\ y_2 \\ \cdot \\ \cdot \\ y_m \end{Bmatrix} = \begin{bmatrix} 1 & x_{11} & x_{12} & \cdot & \cdot & x_{1n} \\ 1 & x_{21} & x_{22} & \cdot & \cdot & x_{2n} \\ \cdot & \cdot & \cdot & \cdot & \cdot & \cdot \\ \cdot & \cdot & \cdot & \cdot & \cdot & \cdot \\ 1 & x_{m1} & x_{m2} & \cdot & \cdot & x_{mn} \end{bmatrix} \begin{Bmatrix} c_0 \\ c_1 \\ \cdot \\ \cdot \\ c_n \end{Bmatrix} + \begin{Bmatrix} e_1 \\ e_2 \\ \cdot \\ \cdot \\ e_m \end{Bmatrix} \quad (2.3)$$

or

$$\mathbf{Y} = \mathbf{XC} + \mathbf{E} \quad (2.4)$$

Our attempt should be to minimize the error vector \mathbf{E} . If all the terms in the vector \mathbf{E} are zero, the model is perfect. Usually we minimize \mathbf{E} in least square sense. The sum-squared error is given by

$$\mathbf{E}'\mathbf{E} = (\mathbf{Y} - \mathbf{XC})'(\mathbf{Y} - \mathbf{XC}) = \mathbf{Y}'\mathbf{Y} - \mathbf{Y}'\mathbf{XC} - \mathbf{C}'\mathbf{X}'\mathbf{Y} + \mathbf{C}'\mathbf{X}'\mathbf{XC} \quad (2.5)$$

By making use of the property that the transpose of a scalar is equal to the scalar itself, we can write

$$\mathbf{Y}'\mathbf{XC} = \mathbf{C}'\mathbf{X}'\mathbf{Y} \quad (2.6)$$

Hence,

$$\mathbf{E}'\mathbf{E} = \mathbf{Y}'\mathbf{Y} - 2\mathbf{C}'\mathbf{X}'\mathbf{Y} + \mathbf{C}'\mathbf{X}'\mathbf{XC} \quad (2.7)$$

Minimizing this with respect to \mathbf{C} , we get

$$\frac{\partial(\mathbf{E}'\mathbf{E})}{\partial\mathbf{C}} = -2\mathbf{X}'\mathbf{Y} + 2\mathbf{X}'\mathbf{XC} = 0 \quad (2.8)$$

Thus, the error will be minimized if

$$\mathbf{X}'\mathbf{XC} = \mathbf{X}'\mathbf{Y} \quad (2.9)$$

or

$$\mathbf{C} = (\mathbf{X}'\mathbf{X})^{-1}\mathbf{X}'\mathbf{Y} \quad (2.10)$$

The coefficient vector can be found by solving for \mathbf{C} either from Eq. (2.9) by using any equation solver routine or from Eq. (2.10). The matrix $(\mathbf{X}'\mathbf{X})^{-1}\mathbf{X}'$ is called the pseudo-inverse of \mathbf{X} . The procedure described above for multiple linear regression can also be applied for non-

linear regression when y can be expressed as a polynomial function of the dependent variables [DiDi08].

2.1.1.2 Reviews of applications

Several applications of regression equation-based modeling in metal cutting processes are reported in literature [ChCh13, ErOz10, GoMG09, KaSR10, MaBh04, MaPa06, MaSa08, ÖKFD07, SiDM11, WaSK06]. For instance, Senthilkumar et al. have employed multiple regression analysis to determine the constants of Taylor's tool life equation in machining martensitic stainless steels. The tool life of alumina-based ceramic cutting tools is evaluated from these tool wear models, and the effect of various types of wear on tool life were analyzed [SeRS06]. Aslan et al. have investigated the machining of hardened steel using Al_2O_3 -based ceramic cutting tools and obtained relationships between the cutting parameters, namely cutting speed, feed and depth of cut, and performance measures such as flank wear and surface roughness using multiple linear regression [AsCB07]. Kaylan and Choudhury have developed regression equations for cutting force and flank wear both in dry and cryogenic turning of EN1.4373 austenitic stainless steel. It was concluded from this work that cryogenic cooling is a possible answer for high-speed, eco-friendly machining [KaCh08]. Ahmadi and Homami have developed multiple regression models for analyzing the effect of cutting parameters in tool wear when machining PH-hardened duplex stainless steels. The effective parameters of tool wear using ceramic cutting tools have been investigated, and the influence of different types of wear phenomena has been observed [AhHo12]. Krolczyk et al. examined the influence of cutting parameters on surface roughness in duplex stainless steel turning processes. The study included developing a second-order regression model to determine surface roughness. The established equations clearly showed that the feed rate was the main influencing factor of surface roughness. Surface roughness increased with growing feed rate [KrLG13].

2.1.1.1 Merits and drawbacks of the statistical regression method

Statistical regression may make a decent modeling technique [LiBK03]. However, this technique may not precisely describe the underlying non-linear complex relationship between the decision variables and responses. A prior assumption regarding functional relationships (such as linear, quadratic, higher order polynomial and exponential) between output and input decision variables is a prerequisite for regression equation-based modeling. Prediction of outputs for an unknown set of inputs, based on the regression technique, is valid only for the region of

the regression variables contained in the observed data. It is only an aid to confirm the cause–effect relationship and does not imply a cause and effect relationship. Moreover, error components of regression equation need to be mutually independent, normally distributed by having constant variance [MoPV12, MuRa06, Rao11a]. It has been proved that the use of the computational modeling techniques can further improve the accuracy of the prediction, particularly if the functional dependency is mostly nonlinear as in machining [AkAs11, AsÇu11, Çaha08, ErŞe09, KiPa05, ÖKFD07, ÖzCD09, ÖzKa05].

2.1.2 Neural network

2.1.2.1 Theoretical background

Neural networks are non-linear mapping systems that consist of simple processors, which are called neurons, linked by weighted connections. Each neuron has inputs and generates an output that is fed to other neurons as input signals via interconnections. The information is presented by the interconnection weights, which are adjusted during the training phase [Hayk99, QuDa11]. A multilayer neural network consists of at least three layers: input, hidden and output layer, where inputs p_i , are applied at the input layer, outputs, a_i , are obtained at the output layer and learning is achieved when the associations between a specified set of input–output (target) pairs $\{(p_1, t_1), (p_2, t_2), \dots, (p_Q, t_Q)\}$ are established, as illustrated in Figure 2.2.

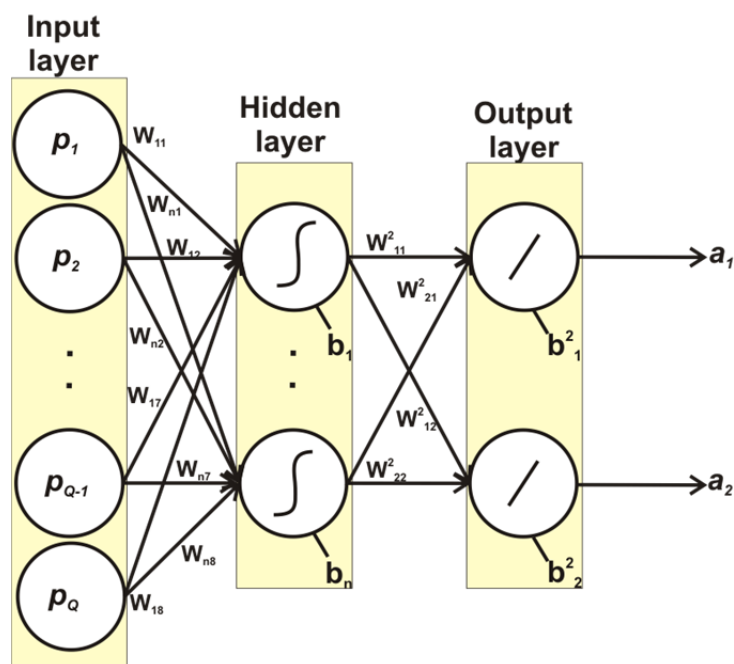


Figure 2.2: Components of a typical multi-layer feed forward neural network.

The learning or training is achieved by minimizing the sum of square error between the predicted output of the neural network and the actual output for a number of available training data, by continuously adjusting and finally determining the weights connecting neurons in adjacent layers. The most common learning algorithm is the back-propagation, used in the multi-layer perceptron (MLP), but it also includes most of the training methods for recurrent neural networks, time delay neural networks and radial basis networks. The back-propagation training methodology can be summarized as follows. Consider the multilayer feed-forward neural network given in Figure 2.2. The net input to unit i in layer $k + 1$ is

$$n_i^{k+1} = \sum_{j=1}^{S^k} w_{ij}^{k+1} a_j^k + b_i^{k+1} \quad (2.11)$$

The output of unit i will be

$$a_i^{k+1} = \psi^{k+1}(n_i^{k+1}) \quad (2.12)$$

where ψ is the activation function of neurons in $(k + 1)$ th layer. The performance index, which indicates all the aspects of this complex system, is selected as mean squared error.

$$V = \frac{1}{2} \sum_{q=1}^Q (t_q - a_q)^T (t_q - a_q) = \frac{1}{2} \sum_{q=1}^Q e_q^T e_q \quad (2.13)$$

In Eq. (2.13), a_q is the output of the network corresponding to q th input, t_q is the target, and $e_q = (t_q - a_q)$ is the error term. In back-propagation learning, weight update can be performed either after the presentation of all training data (batch training) or after each input–output pair (sequential training). The weight update for the steepest descent algorithm is:

$$\Delta w_{ij}^k = -\zeta \frac{\partial V}{\partial w_{ij}^k} \quad (2.14)$$

$$\Delta b_i^k = -\zeta \frac{\partial V}{\partial b_i^k} \quad (2.15)$$

where ζ is the learning rate, which should be selected small enough for true approximation and also at the same time large enough to speed up convergence. Gradient terms in Eqs. (2.13) and (2.14) can be computed by utilizing the chain rule of differentiation. Effects of changes in the net input of neuron i in layer k to the performance index are defined as the sensitivity shown with Eq. (2.16).

$$\delta_i^k = \frac{\partial V}{\partial n_i^k} \quad (2.16)$$

The back-propagation algorithm proceeds as follows: first, inputs are presented to the network and errors are calculated; second, sensitivities are propagated from the output layer to the first layer; then weights and biases (b) are updated by using Eqs. (2.14) and (2.15) [ÖKFD07, ÖzKa05]. A neural network is trained with a number of data and tested with other sets of data to arrive at an optimum topology and weight. Once trained, the neural networks can be used for prediction [DiDi08].

2.1.2.2 Reviews of applications

An early work for the prediction of machining performance using neural networks is reported by Rangwala and Dornfeld [RaDo89]. Thereafter, many researchers have used neural network for machining performance predictions. Teshima et al. proposed a system based on neural networks to estimate the life and wear type of cutting tools from their image data and cutting conditions. The validity of the system was confirmed by the examinations under various cutting conditions in turning [TSTY93]. Chien and Chou developed a predictive model for the machinability of AISI 304 stainless steel using the artificial neural network. The artificial neural network (ANN) theory was used to predict surface roughness of the workpiece, the cutting force and the tool life. Then the genetic algorithm and the ANN were coupled to find the optimum cutting conditions for the maximum metal removal rate under the constraints of the expected surface roughness and the expected surface roughness associated with the tool life [ChCh01]. Özel and Nadgir combined a predictive machining approach with neural network modeling of tool flank wear in order to estimate the performance of chamfered and honed cubic boron nitride (CBN) tools for various cutting conditions. The developed prediction system was found to be capable of accurate tool wear classification for the range it had been trained [ÖzNa02].

Chien and Tsai have utilized the back-propagation neural network to construct the predictive tool flank wear model in machining 17-4PH stainless steel. It has been shown that the predictive model was capable of predicting the tool flank wear in an agreement behavior. Furthermore, the systematic procedure to develop the models in this paper can be applied to the usage of the predictive or optimized problems in metal cutting [ChTs03]. Kohli and Dixit have proposed a neural network-based methodology for predicting the surface roughness in a turning

process by taking the acceleration of the radial vibration of the tool holder as feedback. The testing datasets were collected from experiments. It was observed that the methodology is able to make accurate predictions of surface roughness by utilizing small-sized training and testing datasets [KoDi05]. Heisel et al. introduced an algorithm that allows an automated development of machine tools in the phase of selecting the optimal structure's configuration by means of neural networks. The learning ability of the neural network guarantees high flexibility of the algorithm in solving new tasks and also in optimizing configurations of existing machine tool structures. No direct changes are required in the program or in its database if the extraction conditions are changed [HPSS11]. Finally, Venkata et al. have used ANN to predict surface roughness, tool wear and amplitude of workpiece vibration in the boring of EN 1.4404 steel with cemented carbide tool inserts. The predicted values were compared with the collected experimental data, and the percentage error was computed. The results have shown that neural networks can help with selecting the proper cutting parameters to reduce tool vibration as well as tool wear and can reduce surface roughness [VeMM14].

2.1.2.3 Merits and drawbacks of neural network modeling

Neural networks have many attractive properties for the modeling of complex production systems: (i) a universal function approximation capability resistance to noisy or missing data, (ii) the accommodation of multiple non-linear variables with unknown interactions, and a good generalization ability (iii) with no need to predefine a functional form to fit the data. A neural network-predictive model has the advantages listed above. However, there are drawbacks as well: (i) model parameters may be un-interpretable for non-linear relationships; (ii) it is dependent on voluminous data sets, as sparse data relative to the number of input and output variables may result in overfitting; (iii) identification of influential observations, outliers, and significance of various predictors may not be possible; (iv) there is always an uncertainty in finite convergence of algorithms used in ANN-based modeling techniques, and convergence criteria are generally set based on prior experiences gained from earlier applications; and (v) no universal rules exist regarding the choice of a particular ANN technique for any typical metal cutting process problem [CoJS98, Krus12, MuRa06, Rao11a].

2.1.3 Fuzzy set theory

2.1.3.1 Basic concepts of the fuzzy set theory

The elements of the universe are either a member or a non-member of a set. Such types of sets are called classical or crisp sets. On the other hand, there are sets which have imprecisely or vaguely defined boundaries. These sets were named fuzzy sets by Zadeh in his classic paper [Zade65]. A fuzzy set can be defined as a set in which its members are allowed to have any positive membership grade between 0 and 1. Mathematically, X denotes the universal set (a set containing all the possible elements of concern in some particular context). The process by which individuals from X are determined to be either members or non-members of a set can be defined by a characteristic (discrimination) function. For a given set A , this function assigns a value $\mu_A(x)$ to every $x \in X$ such that

$$\mu_A(x) = \begin{cases} 1 & \text{if and only if } x \in A, \\ 0 & \text{if and only if } x \notin A, \end{cases} \quad (2.17)$$

The application of fuzzy sets extends to logic. In the classical binary logic, a statement is either true or false. Quantitatively, we can say that the truth value of a statement is either 1 or 0. In fuzzy logic, it is possible for a statement to have any truth value in the closed interval $[0, 1]$. For example, membership functions for three subsets of the main cutting force F_c are shown in Figure 2.3. They are called low, moderate and high. Therefore, for a force of $F_c = 2500$ N, the following statements have the indicated degree of truth:

$$\begin{aligned} F_c \text{ is ``Low``} &= 0.2 \\ F_c \text{ is ``Moderate``} &= 0.8 \\ F_c \text{ is ``High``} &= 0 \end{aligned} \quad (2.18)$$

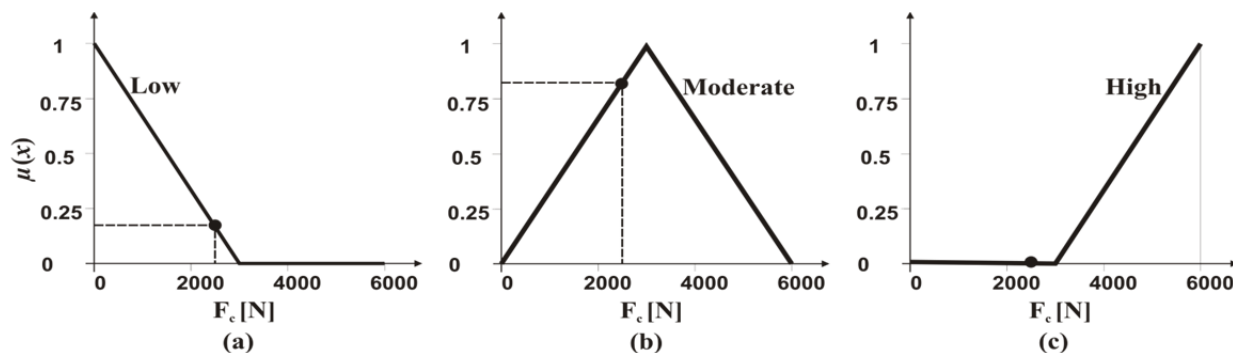


Figure 2.3: Samples of membership functions: (a) low, (b) moderate and (c) high [QuDa11].

Fuzzy set theory may be called a generalization of conventional crisp set theory. Various set-theoretic operations commonly used in crisp set theory have been defined for fuzzy set theory as well. These operations reduce their conventional forms for crisp sets. For example, the intersection of two fuzzy sets A and B , i.e., $A \cap B$, is defined as a set in which each element has a membership grade equal to the minimum of its membership grades in A and B . Similarly, the union of two fuzzy sets A and B , i.e., $A \cup B$, is defined as the set in which each element has a membership grade equal to the maximum of its membership grades in A and B . Another offshoot of fuzzy set theory is fuzzy arithmetic. Fuzzy arithmetic deals with operations on fuzzy numbers. A fuzzy number is defined as a convex and normalized fuzzy set defined on \mathbb{R} (set of real numbers), of which the membership function is piecewise continuous. If two fuzzy numbers are represented by (a_1^α, a_2^α) and (b_1^α, b_2^α) at an α -cut, then the four basic arithmetic operations are defined as follows:

$$\textit{Addition}: (a_1^\alpha, a_2^\alpha) + (b_1^\alpha, b_2^\alpha) = (a_1^\alpha + b_1^\alpha, a_2^\alpha + b_2^\alpha) \quad (2.19a)$$

$$\textit{Subtraction}: (a_1^\alpha, a_2^\alpha) - (b_1^\alpha, b_2^\alpha) = (a_1^\alpha - b_1^\alpha, a_2^\alpha - b_1^\alpha) \quad (2.19b)$$

$$\textit{Multiplication}: (a_1^\alpha, a_2^\alpha) \times (b_1^\alpha, b_2^\alpha) = (a_1^\alpha \times b_1^\alpha, a_2^\alpha \times b_2^\alpha) \quad (2.19c)$$

$$\textit{Division}: (a_1^\alpha, a_2^\alpha) \div (b_1^\alpha, b_2^\alpha) = (a_1^\alpha \div b_2^\alpha, a_2^\alpha \div b_1^\alpha) \quad (2.19d)$$

The fuzzy set theory can also be used to make predictions from the data by using fuzzy inference. A fuzzy inference can be defined as a process of mapping from a given input to an output using the theory of fuzzy sets [DiDi08]. The mapping from crisp inputs to crisp outputs is performed in fuzzy inference systems (FIS). A typical FIS architecture is shown in Figure 2.4. Three types of FISs have been widely used in engineering applications: Mamdani, Sugeno and Tsukamoto. Mamdani's fuzzy inference method is the most commonly seen fuzzy methodology. The Mamdani-style fuzzy inference process is performed in four steps: fuzzification of the input variables, rule evaluation, aggregation of the rule outputs and finally defuzzification.

To see how things fit together, suppose that the flank wear of the cutting tool is to be predicted for a particular cutting speed and feed in turning processes. The estimation of flank wear in this case consists of four steps. In the first step, the crisp values of cutting speed and feed rates are fuzzified, i.e., they are assigned to linguistic fuzzy sets. Once the independent variables are fuzzified, the rule evaluation is carried out. In this step, the strength of the various rules is

evaluated. Various rules are kept in a rule bank, which may be prepared by experts based on their experience or may be generated from data following systematic procedures. For the present example, let the two rules be:

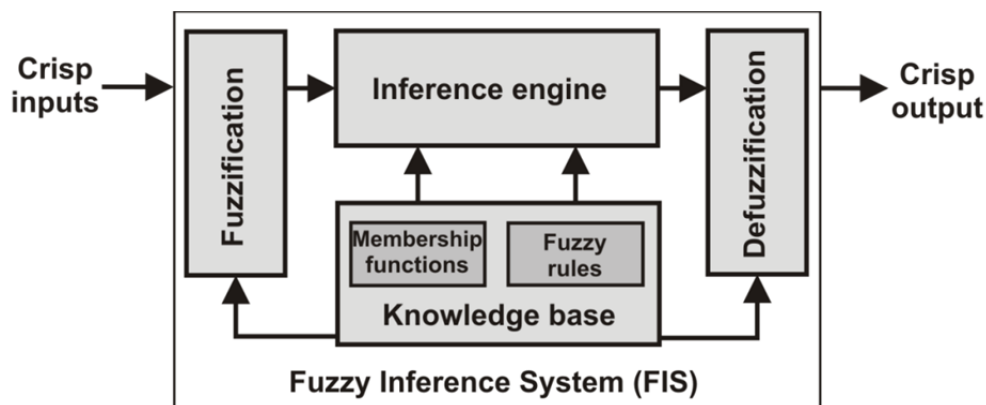


Figure 2.4: Structure of the fuzzy inference system (FIS).

Rule 1: If cutting speed is medium and feed rate is medium, then flank wear is high.

Rule 2: If cutting speed is high and feed rate is high, then flank wear is very high.

In each rule, the ‘if’-part is called the antecedent and the ‘then’-part is called the consequent. The strength of a rule is equal to the truth value of the antecedent. If the antecedent consists of the statements separated by ‘and’, which is equivalent to intersection operations, the truth value of the antecedent is equal to the minimum of the truth values for each of the statements. The third step is rule aggregation. The clipped rules are aggregated by applying union operation as shown in Figure 2.5. This provides the output, viz., flank wear in this case, in the form of a fuzzy variable. This needs to be defuzzified in the fourth step.

There are various methods of defuzzification. One method is finding out the centroid of the area covered by the membership function of the aggregated output. The defuzzified output corresponds to the horizontal coordinate of the centroid. Another simpler method is to take the output as the mean of the outputs at the maximum membership grade. In this way, the flank wear can be predicted for a given set of input variables.

2.1.3.2 Reviws of applications

Several applications of a fuzzy set theory-based modeling of metal cutting processes are reported in literature. Fang and Jawahir have introduced a fuzzy set method to quantify the effects of cutting parameters such as cutting speed, depth of cut, feed rate, normal rake angle, inclination angle, tool cutting edge angle, nose radius, work material chemical composition

and chip-breaker on the total machining performance, encompassing surface finish, tool wear rate, dimensional accuracy, cutting power and chip breakability [FaJa94]. Biglari and Fang developed a fuzzy logic controller based on the on-line diagnosis of drill conditions for automated small-diameter drilling operations. The methodology presented in this paper was expected to be applied to automated machining systems for improving the drilling process performance and reducing the production costs, by maximising the use of drill life and preventing drill failures [BiFa95].

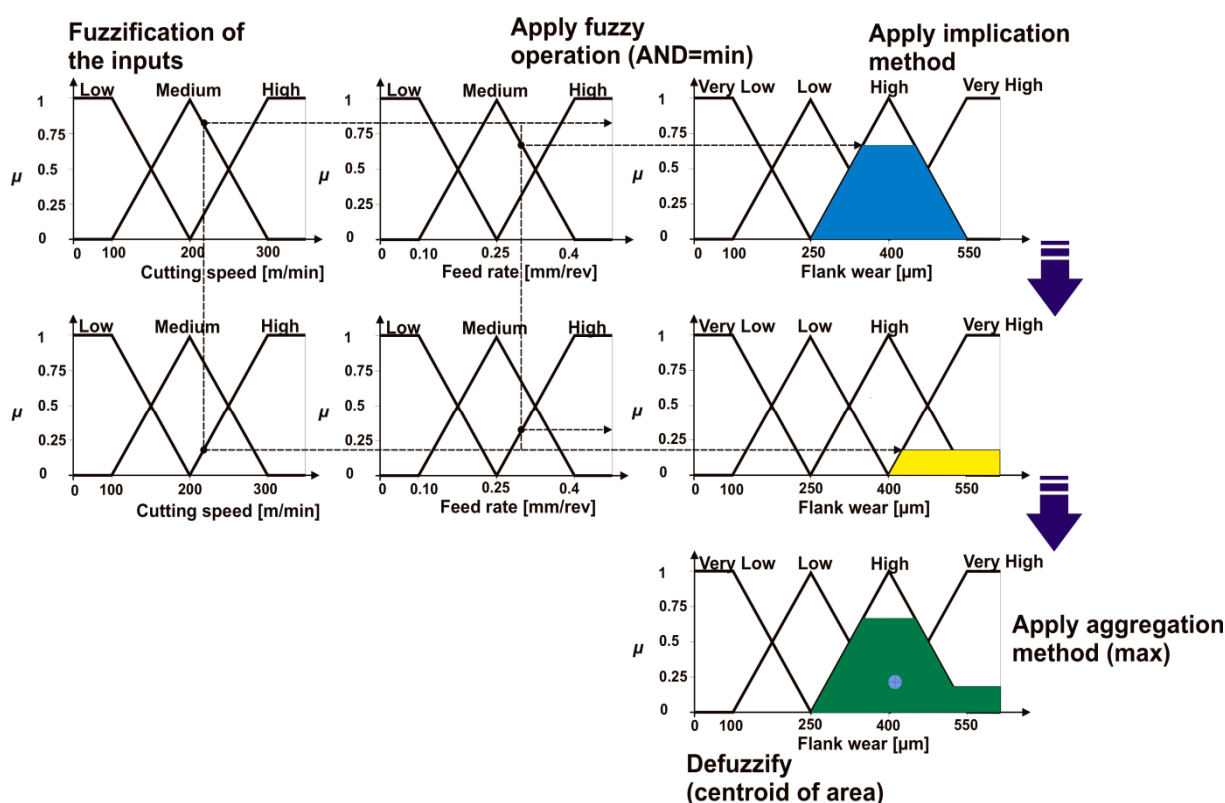


Figure 2.5: Aggregated fuzzy output for prescribed input parameters.

Hashmi et al. applied the fuzzy logic principles for selecting cutting conditions in machining operations. The approach was demonstrated to be an effective way to present a large volume of experimental data in a compressed form [HaBR99]. Chung and Tomizuka proposed a fuzzy logic model and control strategy to control the thrust force in order to reduce delamination when drilling composite laminates. The simulation results showed that the fuzzy model can well describe the nonlinear time-varying process [ChTo01]. Kwon et al. used a fuzzy adaptive modeling technique, which adapts the membership functions in accordance with the magnitude of the process variations to predict surface roughness. The test results showed good agreement between the actual process output and the predicted surface roughness [KwFT02].

Kirby and Chen developed a surface roughness prediction system for a turning operation, using a fuzzy-nets modeling technique. A series of validation runs indicate that this system has a mean accuracy of 95% [KiCh07]. Nandi and Davim studied the drilling performances with minimum quantity lubricant. Fuzzy logic rules, which were derived based on fuzzy set theory, were used to develop fuzzy rule-based models. A comparison of the model predictions with experimental results and those published in literature showed that fuzzy rule-based models with Tsukamoto-type fuzzy rules excellently describe the trade-off with experimental measurements [NaDa09].

Iqbal et al. presented an expert system, incorporating fuzzy reasoning mechanisms, for optimizing parameters and predicting performance measures in high-speed milling of hardened AISI D2. This expert system proved to be very effective and efficient for optimizing the hard-milling process and also for providing important predictions before the start of the actual process [IHLD07]. Latha and Senthilkumar predicted the surface roughness of drilled composite materials using fuzzy logic. The predicted fuzzy output values and measured values were fairly close to each other, which indicated that the fuzzy logic model can be effectively used to predict the surface roughness in the drilling of composite materials [LaSe10].

2.1.3.3 Merits and drawbacks of fuzzy-based modeling

Fuzzy set theory has been used to model systems that are hard to define precisely. It allows many variables to be considered, places no demands of linearity, is tolerant to noise and a suitable technique for manufacturing problems, if multiple quality characteristics exist and the hierarchy of importance of each objective is not clearly defined. However, fuzzy set theory suffers from some shortcomings: (i) the rules accrued from the experts or a priori experiments are not easily amenable to the dynamic change of the underlying process; (ii) an extensive amount of rules must be stored into a rule base, of which the management is not an easy task; and (iii) they do not provide the means of utilizing any existing analytical model [Sher94, ShVi96].

2.2 Finite element modeling of chip formation processes

The basic idea in the finite element method (FEM) is to find the solution of a complicated problem by replacing it with a simpler one. Since the actual problem is replaced with a simpler one in finding the solution, we will be able to find only an approximate solution rather

than the exact solution. The existing mathematical tools will not be sufficient to find the exact solution (and sometimes even an approximate solution) of most practical problems. Thus, in the absence of any other convenient method for even finding the approximate solution of a given problem, we have to prefer the finite element method. In the finite element method, the solution region is considered as built-up of many small, interconnected subregions called finite elements. In each piece or element, a convenient approximate solution is assumed and the conditions of overall equilibrium of the structure are derived. The satisfaction of these conditions will yield an approximate solution for the displacements and stresses [Rao11b].

The consideration of a process with the FEM is called finite element analysis (FEA). The following steps are taken in every FEA:

1. discretization of the continuum,
2. selection of interpolation functions,
3. determination of the element properties,
4. assembly of the element equations and
5. solution of the equation system.

The first step is to divide the structure or solution domains (e.g. the workpiece) into subdivisions or elements. Hence, the structure is to be modeled with suitable finite elements. The number, type, size, and arrangement of the elements are to be decided. Figure 2.6 shows some exemplary element types that are used for discretization. In the next step, interpolation functions, which serve to approximate the profile of state variables within an element, have to be selected. The selection of interpolation functions is in practice made simultaneously with the selection of the element type. In general, because of their differentiability or integrability, polynomials are frequently used as interpolation functions.

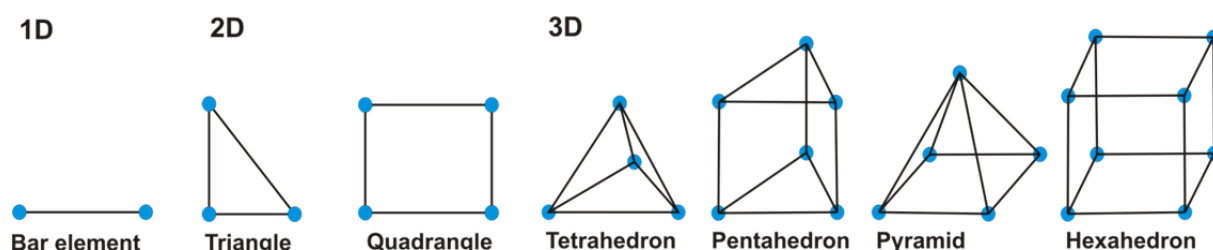


Figure 2.6: Types of elements for the discretization of continuum problems.

After element types and interpolation functions have been selected, the element equations (element matrices) are determined. These equations describe the relations between the prima-

ry unknowns (e.g. speed, displacement, temperature) and the secondary unknowns (e.g. stresses). To determine the unknowns, several approaches can be considered. Four possible schemes are reviewed below: i) the direct approach, ii) the variational approach, iii) the weighted residual approach, iv) the energy balance approach. Since the solution domain is composed of several finite elements, the individual element stiffness matrices and load vectors are to be combined (assembled) in the global matrix of the problem. Furthermore, before the system equations are ready for solution on the computer, they must incorporate the physics of the boundary conditions of the problem. For metal cutting they will include friction at the interface and the temperature conditions at the boundaries of the workpiece, tool holder and the free edge of the chip. In the final step, the assembly process of the preceding step gives a very large set of simultaneous equations, which can be solved on a computer to obtain the unknown nodal values of the field variable [Hueb01, Kloc11, Rao11b, TrWr00, ZiTZ13].

2.2.1 Basics of FEM formulations and remeshing techniques

How do the matrix equations get solved in a situation in which the tool and the work material are in relative motion? As summarized by Athavale and Strenkowski, the two basic approaches are the Lagrangian and the Eulerian formulations, together with an arbitrary Lagrangian-Eulerian formulation (see Figure 2.7) [AtSt98]. In a Lagrangian formulation, the mesh is attached to the workpiece. The tool or workpiece is advanced through predefined displacement increments, and the finite element solution is obtained. The displacement increment will be a function of the time step in explicit solution methods [LiLi92, MaOr95] and can be related to the material removal rate during cutting. In an implicit formulation, the time step has no physical significance, and the stability of the solution does not depend on the size of the time step [CaSt88, MaSO96, ObUs96]. The other major difference in the Lagrangian models stems from whether the material model is elastic-plastic, only plastic or viscoplastic. Lagrangian formulation brings the following advantages to machining simulation: the chip geometry is the result of the simulation and provides simpler schemes to simulate transient processes and discontinuous chip formation. However, element distortion has been a matter of concern and has restricted the analysis to incipient chip formation or machining ductile materials using larger rake angles and/or low-friction conditions pre-distorted meshes [GuDo00, HuB196, LiGS02, LiLo01, MaRi06, MHBM01, OhOb05, OSSU97, Shih96] or remeshing [BaRS02, BARS03, BCLS02, CeLA99, FaZe05, HuSh04, MaBM02, ÖzAl00a, Özel06, RhOh06] have been used to minimize the problem. In the case of remeshing, when the distortions of the

workpiece mesh are extremely high, a new mesh is generated. After the data from the distorted mesh is mapped to the new one, the calculation continues until the criterion that determines the regeneration of the mesh is reached again. The criterion that promotes the mesh renovation can be, for example, the plastic strain [ArÖz09, AtSt98, VOKL07].

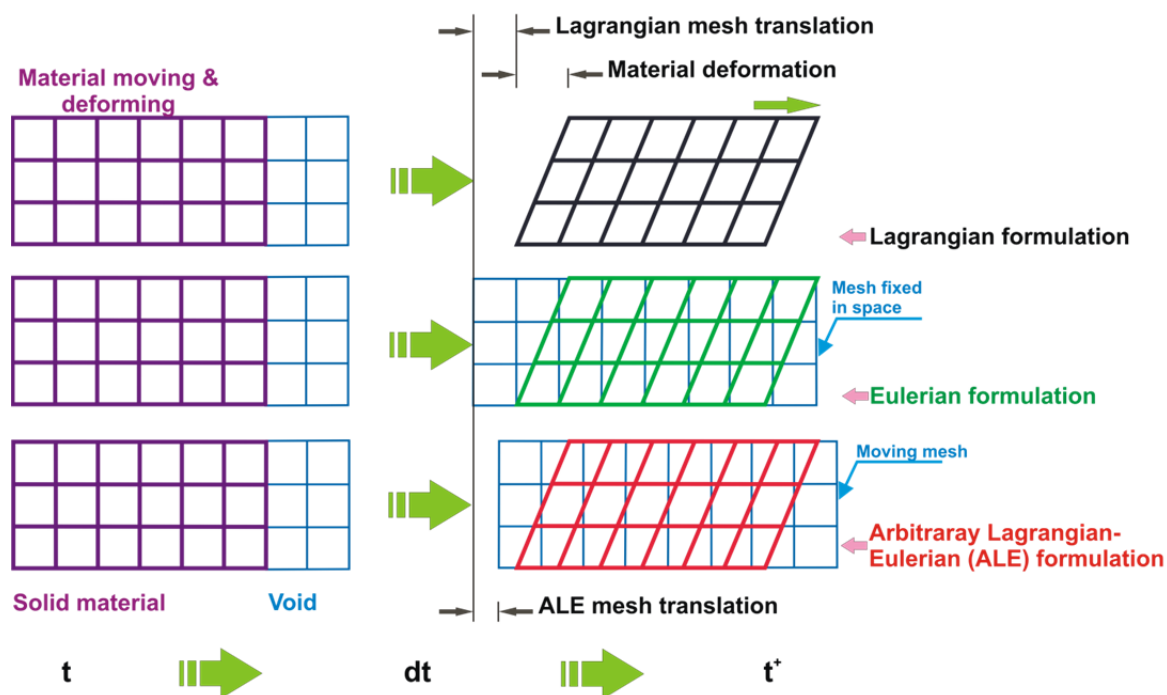


Figure 2.7: Finite element formulations.

In Eulerian formulations, the mesh is fixed in space and material flows through the element faces, allowing large strains without causing numerical problems. Moreover, this strategy is not affected by element distortion and allows steady state machining to be simulated. However, Eulerian approaches do not permit element separation or chip breakage and require a proper modeling of the convection terms associated with the material properties. In addition, such formulations also require the prior knowledge of the chip geometry and chip–tool contact length, thereby restricting the application range. In order to overcome this shortcoming, various authors have adopted iterative procedures to adjust the chip geometry and/or chip/tool contact length [AtSt98, CaSt88, IwOT84, JoDJ94, KiLS99a, KiLS99b, WuDL96].

On the other hand, in the arbitrary Lagrangian-Eulerian (ALE) method, the nodes can move but always remain inside the defined boundary region. In this way, the major disadvantages of the previous formulations are eliminated, conserving their advantages: easy application of the boundary conditions, easy treatment of the interfaces, shorter computation times and lower distortion of the mesh. Therefore, it is becoming more and more accepted among the re-

searchers [CMRM13, HaKR08, HoNg13, ÖzZe07, WuJF03]. Despite the above advantages, a careful numerical treatment of the advection terms is recommended [VOKL07]. More elaborate discussions about the use of ALE formulations in modeling metal machining are presented by Rakotomalala et al. [RaJT93], Olovsson et al. [OINS99], Movahhedy et al. [MoGA00], Benson and Okazawa [BeOk04], Pantalé [Pant04] and Madhavan and Adibi-Sedeh [MaAd05].

In metal cutting modeling, the common problem is related to the element distortion during the simulations due to severe plastic deformation. The distortion can cause a deterioration of the FE simulation in terms of convergence rate and numerical errors, or cause the Jacobian determinant to become negative, which makes further analysis impossible. It is often necessary to redefine the mesh after some stages of deformation. Several techniques are used to reduce the element distortion: re-meshing, smoothing and refinement. These techniques include the generation of a completely new finite element mesh out of the existing mesh, increasing the local element density by reducing the local element size (Figure 2.8(a)) and/or reallocating the individual nodes to improve the local quality of the elements (Figure 2.8(b)). The discussed techniques are used in the so-called adaptive mesh procedure. Adaptive mesh refers to a scheme for finite difference and finite element codes, dynamically changing the size and distribution of the mesh during the simulations. In the regions of strong gradients of variables involved, a higher mesh density is needed in order to diminish the solution errors. As these gradients are not known a priori, the adaptive mesh generation procedure starts with a relatively coarse primary mesh, and after the solution of this primary mesh has been obtained, the mesh density is increased for the strong gradients [AsOu08].

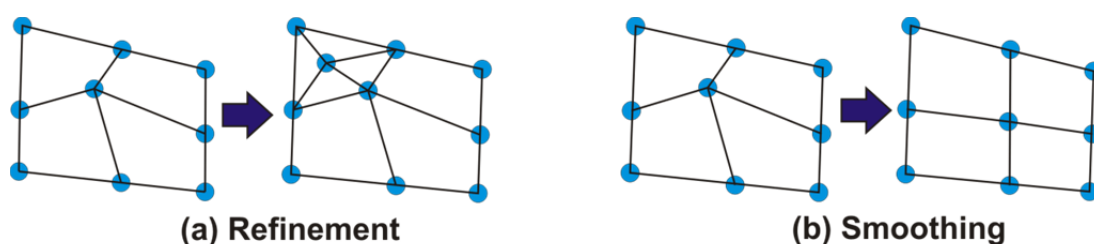


Figure 2.8: (a) Increase in local mesh density (refinement), (b) reallocation of the nodes (smoothing).

Finally, it should be noted here that many FE programs utilized to calculate large plastic deformations make use of “implicit” methods. For highly dynamic applications on the other hand, such as crash simulation, explicit time integration is prevalent in FE programs.

2.2.2 Historical perspective

For a historical perspective of how FEA is used in metal cutting research, the reader is first referred to the comprehensive reviews in the references [ChBl94, Mack03, Mack98]. These contain most of the significant citations up to the early 2000s. Second, the work undertaken by Vaz Jr. et al., in which a brief outline of the wide range of complex physical phenomena involved in chip formation, has been presented in a descriptive manner. Several numerical strategies used for simulation were also reviewed, and a short discussion of their relative merits and drawbacks was presented [VOKL07]. Third, an interesting reviewing contribution regarding the simulation of cutting and machining processes was reported by Lorong et al. The contributions provided by researchers from all over the world and published in the Proceedings of the European Scientific Association for material FORMing (ESAFORM) Conferences were highlighted [LoMT07]. Finally, the collection of papers edited by Arrazola et al. summarizes the state-of-the-art developments in the modeling of machining processes during the last 15 years, since the last CIRP keynote paper on the modeling of machining was produced in 1998. This includes a critical assessment of the relevant modeling techniques and their applicability and/or limitations for the prediction of the complex machining operations performed in industry. The paper includes contributions from academia and industry and serves as a comprehensive report of recent progress as well as a roadmap for future directions [AÖUD13].

2.2.3 Scales of the machining modeling

In order to effectively simulate a typical material removal process, all the input parameters that can have a remarkable influence on the attained results, such as machine tool, coolant, cutting tool, tool holder, tool clamping, workpiece, assembly, etc., should be considered. However, considering the whole machining system, it seems quite complex to solve one given problem. Therefore, in many cases the area or elements that are going to be analyzed in depth are isolated from the rest of the system. Depending on the problem to be studied, the FEM of machining processes can be focused on three scales, namely: (i) macroscale, (ii) mesoscale and (iii) microscale (see Figure 2.9). The first scale accounts for the interaction of the machine tool with the entire workpiece and tool engagement system [RaLB05, RLHB06]. In the second scale, only the area where the chip is formed is considered so that performances, such as cutting forces, residual stresses, tool temperature and stresses, etc., can be reasonably predicted [ACRU08, AuBi06, SoAD04, UhSZ07, DiCM01, GrBN05, GuLi02, HeSK13, KIKr05,

KoKS08, MHBM01, PiAS05]. In the microscale FEM, the influence of the microstructure, grain boundaries and crystalline plasticity are included [JIUA14, JNUM13, MoNE12, NoMa13, SHMS02, SiNE07, ZhSS14]. While in the meso- and microscales, the need for a fully coupled thermo-mechanical analysis is quite clear, a thermo-mechanical analysis (but not necessarily fully coupled) could be sufficient at the macroscale [ArÖz09].

The present thesis will focus on the modeling of cutting processes at mesoscale, i.e., what happens at the cutting edge.

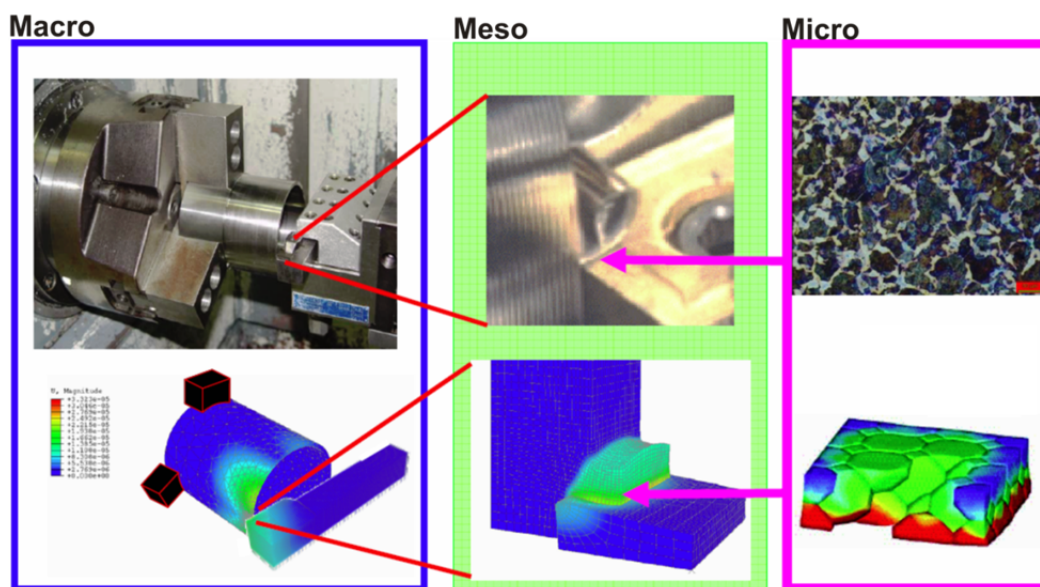


Figure 2.9: Scales of the FEM machining modeling [ArÖz09].

2.2.4 Simulation software & phases of metal cutting FEA

Commercial software products like DEFORMTM and THIRD WAVE/ADVANTEDGETM, and general purpose systems like ABAQUS or MSC/Marc or LS-DYNA are frequently used in cutting simulations. The software products in the first category are adapted to the requirements of machining technology, thus making it easier for the user to build and carry out simulations. On the other hand, general purpose systems are indeed highly flexible and can be used for a wide variety of applications, but they demand a large amount of experience for setting up the model as well as a larger amount of time.

Scientific Forming Technologies Corp., Columbus, OH registers DEFORMTM. The finite element code is based on the flow formulation approach and uses an updated Lagrangian procedure. It has an adaptive remeshing scheme to follow the modeling in steps of large or localized deformations. The software is specialized in modeling forming and machining operations

in 2D and 3D, based on an implicit integration method with fully coupled thermo-mechanical analysis [AsOu08, Kloc11].

From the standpoint of the users of the above software products, a typical finite element analysis takes place in three phases: (i) data preparation with the preprocessor (input), (ii) processing (calculation) and (ii) evaluation of the results with the postprocessor (output). Figure 2.10 summarizes the parameters that are involved in the FEA of metal cutting processes.

2.2.5 Advantages and problems associated with numerical cutting modeling

The finite element method can provide a comprehensive and in some cases complementary approach to experimental, mechanistic or analytical approaches to study machining process [ACRU08, KIBW05, ÖzKS08]. It provides some advantages, basically due to the following aspects: access to fields of values of thermo-mechanical variables, consideration of the non-linear effects of the friction at the tool–chip interface, ability to perform virtual machining tests that are difficult to justify experimentally (new tool geometries and materials or coatings) or to study cases that are difficult to carry out (zero friction coefficient, materials with ideal behavior, etc.) [AsOu08]. However, at this stage, it can be said that basically three kinds of problems can be found that relate to numerical cutting modeling, prior to becoming a reliable tool for industry (see Figure 2.10):

1. Identification of finite element model input parameters: material constitutive behavior, friction, thermal parameters, damage and wear. A sensitivity study showed the influence of input parameters on results. From this study, information about the uncertainty originated by input parameter identification can be estimated, and the remarkable difficulties in obtaining quantitative results can be pointed out. For instance, moving the yield stress (one of the best-known material coefficients) from 200 MPa to 900 MPa can lead to a temperature increase of 30% from an average value of 1240 K (i.e. of around 372 K). Thus it can be estimated that an uncertainty of 30 MPa can give an uncertainty in temperature of approximately 15 K [AsOu08].
2. Finite element model definition: boundary conditions, integration frame (explicit, implicit), formulations can lead to different quantitative results, calculation times, etc.

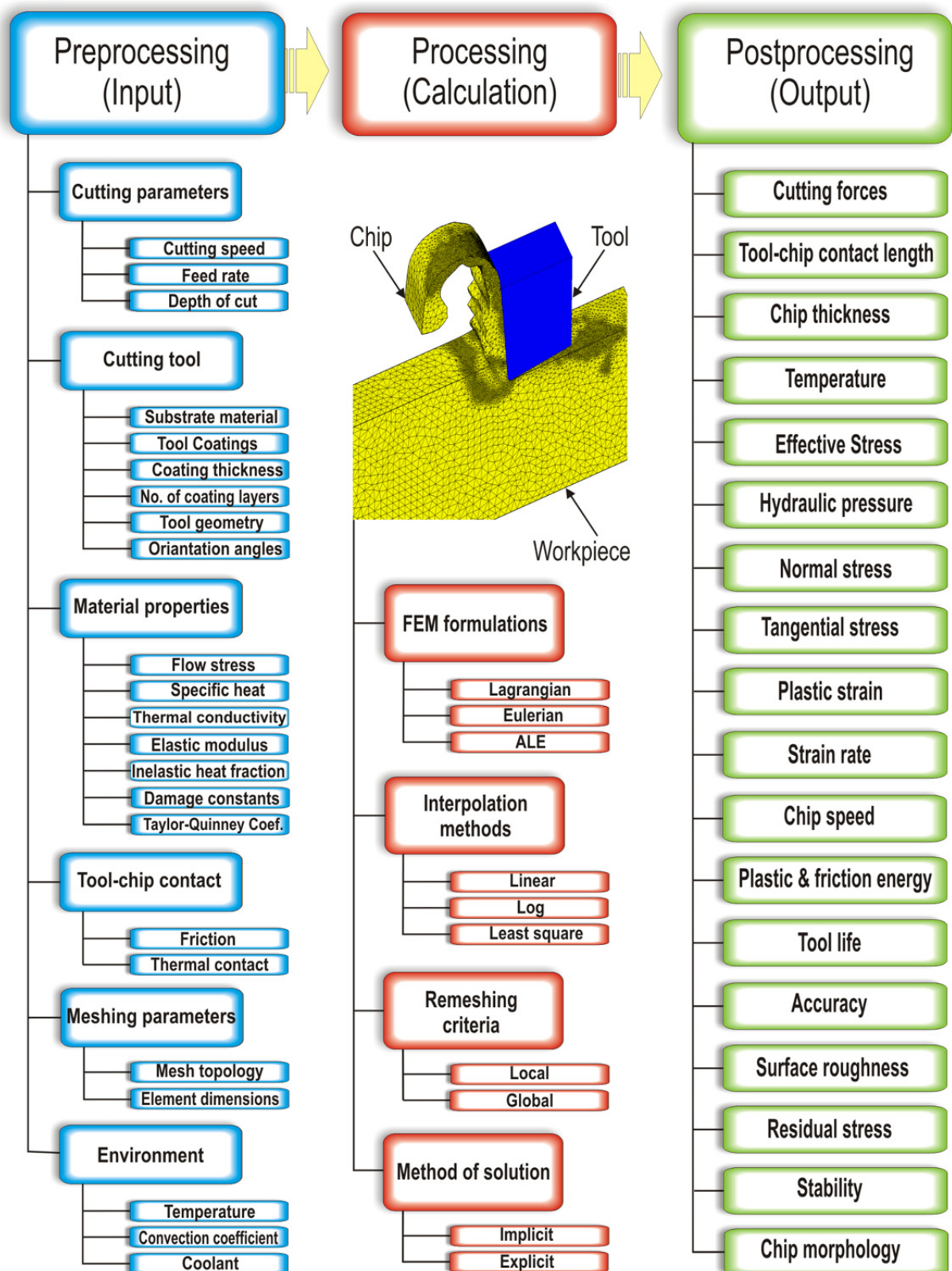


Figure 2.10: FEM of chip formation processes at mesoscale.

3. Finite element model validation: except for parameters like forces, chip thickness or tool-chip contact length, experimental measurement is quite complicated (e.g. temperature,

strain, strain rate) and in some cases quite difficult at this stage (strain rate, stresses, etc.). Thus model validation is quite difficult because experimental means are not available or they are not suitable enough [ArÖz09].

2.2.6 Input models and identification of input parameters

The success and reliability of modeling depends upon accurate mechanical data (elastic constants, flow stress, friction, fracture stress/ strain, etc.) and thermo-physical data (density, thermal conductivity, heat capacity, etc.) [ArÖz10, CaCG08, ÖzAl00b, Özel06, ÖzSS10, SaAG05, SiÖz10]. Thus, a characterization in the extreme conditions of machining is needed, i.e., for strains of 100–700%, strain-rates up to 10^6 s^{-1} , temperatures between 500 and 1400 °C, high heating rates close to 10^6 °C s^{-1} and high pressures near 2–3 GPa. A realistic material model should also include strain-hardening and thermal softening due to dynamic recovery or recrystallization. Therefore, other modeling approaches have been proposed, and flow stress data has been generated for machining a range of commonly known work materials [BWLM14, CaCG08, WaOh02, Chil06, GuWW06, Karp11, OHAS12, OzZe06, RhOh06, ShKA01, SLCM01].

2.2.6.1 Constitutive behavior of the work materials

The mechanical behavior of materials is an essential component of technology which has received considerable attention over many years. Of particular interest is the response of materials to mechanical and thermal loadings, the influence of environmental factors, and the conditions and mechanisms of failure. The terms “constitutive equations” and “material modeling” are usually applied to the analytical representation of the material response characteristics prior to total failure [Bodn02]. As the latter is the major and important module of any numerical code used for the simulation of the machining process, the accuracy of the simulation largely depends on the accuracy of the predictability of the material model. The need for the greater accuracy of the flow prediction has encouraged many researchers [LiCh11, LiKh99, Zeri04] to develop suitable constitutive models for different materials. In this context, many empirical, semi-empirical and physically-based constitutive equations have been proposed over the course of time. The list of these equations can be found in various review [LiCh11, LiKh99] and overview articles [SMBS10, VoAb05] on constitutive models [SPBA14].

Unfortunately, a universal material model suitable for all cutting simulations remains one of the important unaccomplished tasks. Due to the typical high strain, strain rate temperature and temperature gradient in machining, it is not always easy to determine the flow stress curves by experiment. Furthermore, experimental methods such as the Split-Hopkinson-Bar-Test are quite expensive and require a large number of experiments to be conducted. On the other hand, empirical material laws which describe the flow stress as a function of strain, strain rate and temperature contain specific material constants, which have to be determined by regression analyses or by the least squares method and verified experimentally. During the last three decades, a multitude of such models have been suggested [KaTU83, MaOk83, Oxle64]. The most notably are the engineering-based and physically-based models. In both fields, the earliest contributions were made by Johnson and Cook [JoCo83, JoCo85] and Zerilli and Armstrong in 1980s [ZeAr87, Zeri04] respectively. Additionally, JMatPro, an acronym for Java-based Materials Properties, can also be employed to calculate a wide range of material properties. These properties include thermo-physical, physical properties, time-temperature-transformation diagrams, stress/strain diagrams, proof and tensile stress, hardness, coarsening and creep. A feature of this program is that the calculations are based on sound physical principles rather than purely statistical methods. Thus, many of the shortcomings of methods such as the regression analysis can be overcome. With this program, a sensitivity to microstructures can be included for many of the properties and the true inter-relationship between properties can be developed, for example, in the modeling of creep and precipitation hardening [SGLM03]. Figure 2.11 shows an example of the predicted relationship between true stress and true strain for duplex stainless steel materials using JMatPro software.

It is worthwhile mentioning that in recent years, the inverse identification of the constitutive model parameters has been proposed as an alternative method for defining the constitutive equation coefficients, so that the models remain valid for large ranges of conditions during machining [KILB13, PAMC07, ShBä11, ShBä12].

2.2.6.2 Friction

Since the rate of tool wear heavily depends on the frictional conditions at the tool–chip interface, an accurate modeling is of critical practical importance [Özel06]. Friction under very extreme conditions is prevalent at the tool–chip interface (1-2 GPa, 500–100 °C) [ZMYP11]. In the earlier analyses of machining, frictional stresses (τ_f) on the tool rake face have been

considered proportional to the normal stresses (σ_n) with a coefficient of friction (μ) based on the Coulomb friction, as can be seen here.

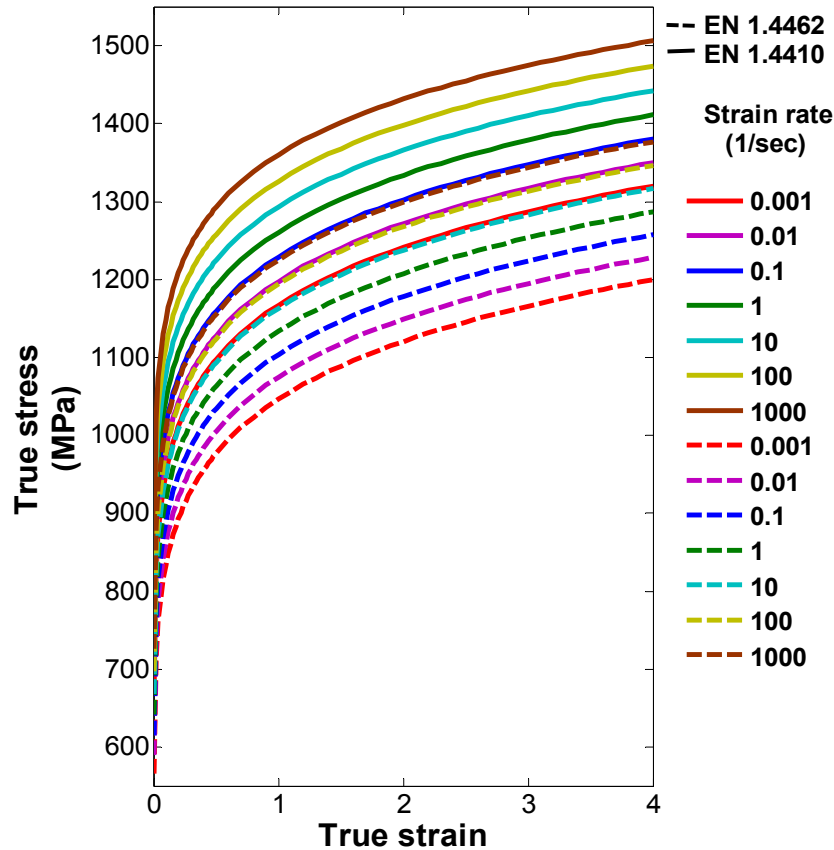


Figure 2.11: DSS flow stress curves at room temperature.

$$\tau_f = \mu\sigma_n \quad (2.20)$$

In conventional machining at low cutting speeds, the Coulomb model is found to be effective for describing the frictional conditions at the tool flank face but not at the rake face. Moreover, the contact conditions at the tool–chip and tool–workpiece interfaces are too complicated [Asta06] to be expressed in terms of the simple Coulomb friction condition. For instance, in FEM predictions of cutting characteristics by Özel [Özel06] and Arrazola et al. [ArUD08], an inadequate Coulomb's friction coefficient can generate more than 50% differences in cutting forces and the tool-chip contact length in comparison to the measured values. Zorev [Zore63] proposed a more realistic representation in a stick-slip friction law based on normal and shear stress distributions. According to this model, the normal stress is greatest at the tool tip and gradually decreases to zero at the point where the chip separates from the rake face, as shown in Figure 2.12.

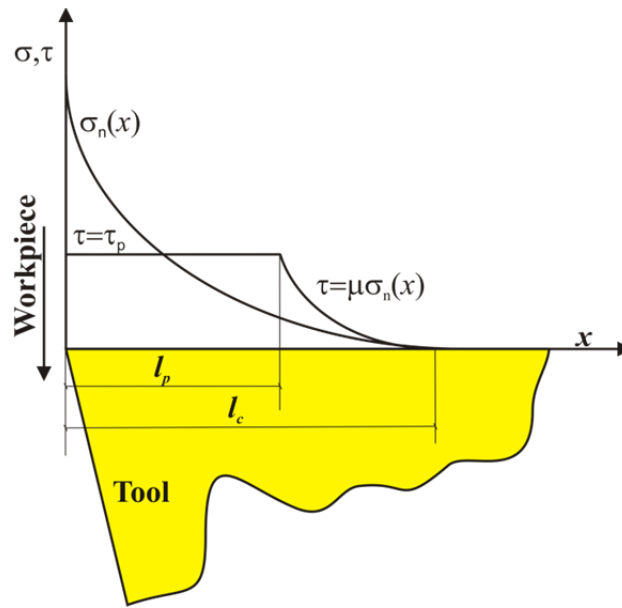


Figure 2.12: Curves representing normal and frictional stress distributions on the tool rake face, according to Zorev [Zore63].

This is represented mathematically as a sticking region, where the flow stress is equal to the plastic yield, and a sliding region, where a Coulomb model is adopted (Eq. (2.21)).

$$\tau_f(x) = \begin{cases} \tau_p : \mu\sigma_n \geq \tau_p, & (0 < x < l_p) \text{ Sticking region} \\ \mu\sigma_n : \mu\sigma_n < \tau_p, & (l_p < x < l_c) \text{ Sliding region} \end{cases} \quad (2.21)$$

Later on, more sophisticated friction models have been proposed by Usui and Shirakashi [UsSh82b], Dirikolu et al. [DiCM01] and Zemzemi et al. [ZRS09].

Despite over 100 years of effort, the controversy of the concept of friction in machining still exists. An extensive analysis of the inadequacy of the concept of the friction coefficient in metal cutting was presented by Kronenberg (pp. 18–25 in [Kron66]) who stated “I do not agree with the commonly accepted concept of coefficient of friction in metal cutting and I am using the term ‘apparent coefficient of friction’ wherever feasible until this problem has been resolved.” Unfortunately, it has never been resolved, although almost half a century have passed since Kronenberg made this statement [AsOu08].

2.2.6.3 Cockcroft-Latham damage criterion

In order to improve the physical comprehension of the chip formation during cutting of ductile metals, a proper fracture criterion is needed. In recent decades, several fracture models which employed FEA simulations have been proposed for ductile metals. These models have

been applied to various applications, including metal forming, high-velocity impact, forging, cutting, etc. The most commonly used models include Cockcroft-Latham [Cock68], McCintock [Mccl68], Brozzo [BrDR72] and Johnson-Cook [JoCo85] fracture criteria. The criterion proposed by Cockcroft and Latham in 1968 assumes that the maximum principal stress is the most relevant in the initiation of fracture. This criterion is therefore defined in terms of traction plastic work associated to the principal stress along the path of the equivalent plastic strain as:

$$D = \int_0^{\varepsilon_f} \sigma_1 d\varepsilon \quad (2.22)$$

where ε_f is the effective strain, σ_1 is the principal stress, and D is a material constant [ZhCP07]. Cockcroft and Latham's criterion states that when the integral of the largest tensile principal stress component over the plastic strain path in Eq. (2.22) reaches the critical value $D_{crit.}$, usually called damage value, fracture occurs or chip segmentation starts, the flow stress is reduced to a lower value $\%p_r$ (see Figure 2.13), which is expressed as percentage of the original flow stress. In many circumstances, the original Cockcroft-Latham fracture criterion and its various modifications have been applied to metal machining processes [AuBi06, BiKT04, KILB13, LoJJ09, UmMO07]. For example, Umbrello employed Cockcroft and Latham's criterion to predict the effect of tensile stress on the chip segmentation during orthogonal cutting of Ti-6Al-4V alloys [Umbr08]. Recently, Pu et al. have used Cockcroft and Latham's fracture criterion to predict the effect of the stress on the chip segmentation during cryogenic cutting of AZ31B Mg alloys [PUDJ14].

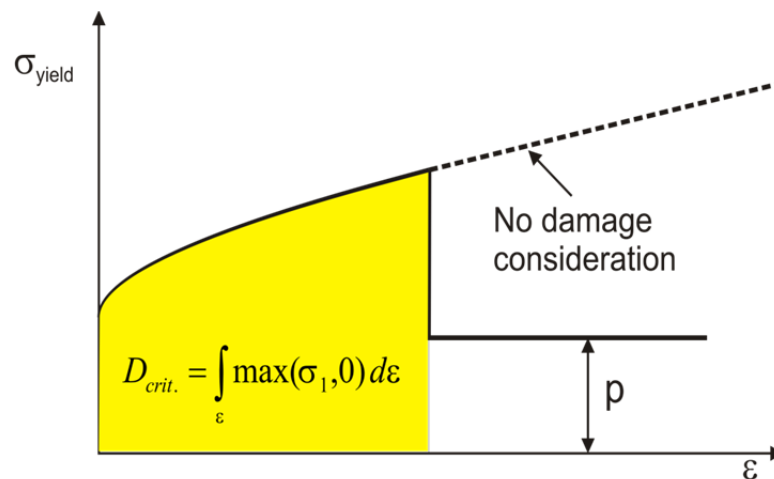


Figure 2.13: The Cockcroft & Latham damage criterion.

2.2.6.4 Thermal contact conductance

The thermal contact conductance h_{ic} , also known as the heat transfer coefficient, describes the heat flux of two solids in contact and is defined as follows:

$$h_{ic} = \frac{\phi}{\Delta T} \quad (2.23)$$

where ΔT is the temperature difference at the contacting surfaces, and the heat flux ϕ is defined as:

$$\phi = \frac{d}{dA} \left(\frac{d\Phi}{dt} \right) \quad (2.24)$$

where A is the area of contact surface, and Φ is the conducted heat in (J). It is recognized that thermal contact conductance is a function of several parameters, the dominant ones being the type of contacting materials, the macro- and micro-geometry of the contacting surfaces, the temperature, the interfacial pressure, the type of lubricant or contaminant and its thickness [RoBC03].

2.2.6.5 Taylor-Quinney coefficient

As the mechanical behavior is affected by temperature (softening effect), plastic deformation is accompanied by heat generation, which results in a temperature rise. The heat generation due to this phenomenon is described by the following relationship:

$$\dot{\phi}_p = \kappa_t \bar{\sigma} \dot{\bar{\epsilon}}_p \quad (2.25)$$

where $\dot{\phi}_p$ is the volumetric heat generation due to plastic work in (W/m^3), $\bar{\sigma}$ is the von Mises equivalent stress in (MPa), $\dot{\bar{\epsilon}}_p$ is the von Mises equivalent plastic strain, and κ_t is the Taylor-Quinney coefficient, which represents the proportion of plastic works converted into heat. Haddag and Nouari have shown a strong dependency of κ_t on both strain and strain rate for various engineering materials. Within the confines of their constitutive framework, the assumption that κ_t is constant was inconsistent with the rate independence of the stored energy of cold work, which was a fundamental consequence of thermodynamics. It would seem that the only justification for a priori assumptions on κ_t is a lack of information on the stored en-

ergy of cold work. Therefore, this coefficient is considered as an unknown input value, which has been specified in cutting simulations [HaNo13].

2.3 Determination of optimal or near-optimal cutting conditions

Machining optimization is the systematic and scientific approach for solving problems associated with engineering decision-making in selecting the best production method, process parameters or operational conditions. The ultimate goal of such problems is to either minimize the efforts required or maximize the desired benefits. Efforts required and benefits desired in a machining situation can be expressed according to the decision variables. Machining optimization can be defined as the process of finding such decision variables that give the maximum or minimum value of one or more objective functions subject to some resource, capacity or process constraint [Özel09].

With time, complexity in metal cutting process dynamics has increased, and as a consequence, problems related to the determination of optimal or near-optimal decision variables are faced with discrete and continuous parameter spaces with multi-modal, differentiable as well as non-differentiable objective functions or responses. The search for optimal or acceptable near-optimal solutions by a suitable optimization technique based on input–output and in-process parameter relationship or objective function formulated from models with or without constraints, is a critical and difficult task for researchers and practitioners [BAPS05, BASP06, CaGu00, ChTs96, HuLL01, VPAS03, Yild13a]. A large number of techniques has been developed by researchers to solve these types of parameter optimization problems and may be classified as conventional and nonconventional optimization techniques.

Whereas conventional techniques attempt to provide a local optimal solution, non-conventional techniques based on developed extrinsic models or objective functions are only an approximation and attempt to provide near-optimal cutting conditions. Conventional techniques may be broadly classified into two categories. In the first category, experimental techniques that include statistical design of experiment, such as the Taguchi method, and response surface design methodology (RSM) are referred to. In the second category, iterative mathematical search techniques, such as linear programming (LP), non-linear programming (NLP), and dynamic programming (DP) algorithms are included. Non-conventional, meta-heuristic search-based techniques, which are sufficiently general and extensively used by researchers in recent times, are based on biological, molecular or neurological phenomena that mimic the

metaphor of natural biological evolution and/or the social behavior of species. To mimic the efficient behavior of these species, various researchers have developed computational systems that seek fast and robust solutions to complex optimization problems [MuRa06, Rao11a]. Examples of these algorithms include Simulated Annealing (SA), Genetic Algorithm (GA), Particle Swarm Optimization (PSO), Firefly Algorithm (FA), Cuckoo Search (CS), Bat Algorithm (BA), etc.

2.3.1 Taguchi Method

2.3.1.1 Basic concepts in Taguchi's design and optimization procedure

The Taguchi method, named for Genechi Taguchi, the Japanese statistician who developed and advocated the method, is a powerful problem-solving tool which can improve the performance of the product quality, process, design and system with a great decrease in experiment time cost. This method, which contains the design of experiment theory and the quality loss function concept, can carry out the robust design of processes and products and solve several optimal problems in manufacture industries. Professor Genichi Taguchi used the term *robust* for the product or processes which perform consistently on target and are relatively insensitive to factors that are difficult to control. He referred to these uncontrollable factors as noise factors. He also developed a methodology for finding the optimum settings of control factors and making a product or process insensitive to noise factors [Mont09, Ross95]. Various steps of the Taguchi method are shown in Figure 2.14.

To design an experiment means to choose the optimal experiment design to be simultaneously used for varying all the analyzed factors. There are many different experimental designs that provide options for the investigator, who must perform experiments to address a variety of questions under a range of conditions and limitations. Several important considerations determine which experimental design is appropriate for a given investigation. As there are many parameters in machining, conducting a large number of experiments employing classical experimental design methods could be very costly, complex and not easy to use. This problem is overcome in the Taguchi method, which uses a special design of orthogonal arrays (OA) to study the entire major parameter space with only a small number of experiments. Commonly used orthogonal arrays include the L_4 , L_9 , L_{12} , L_{16} , L_{18} , L_{25} and L_{27} . A complete listing of OAs is presented by Phadke [Blan04, Phad89].

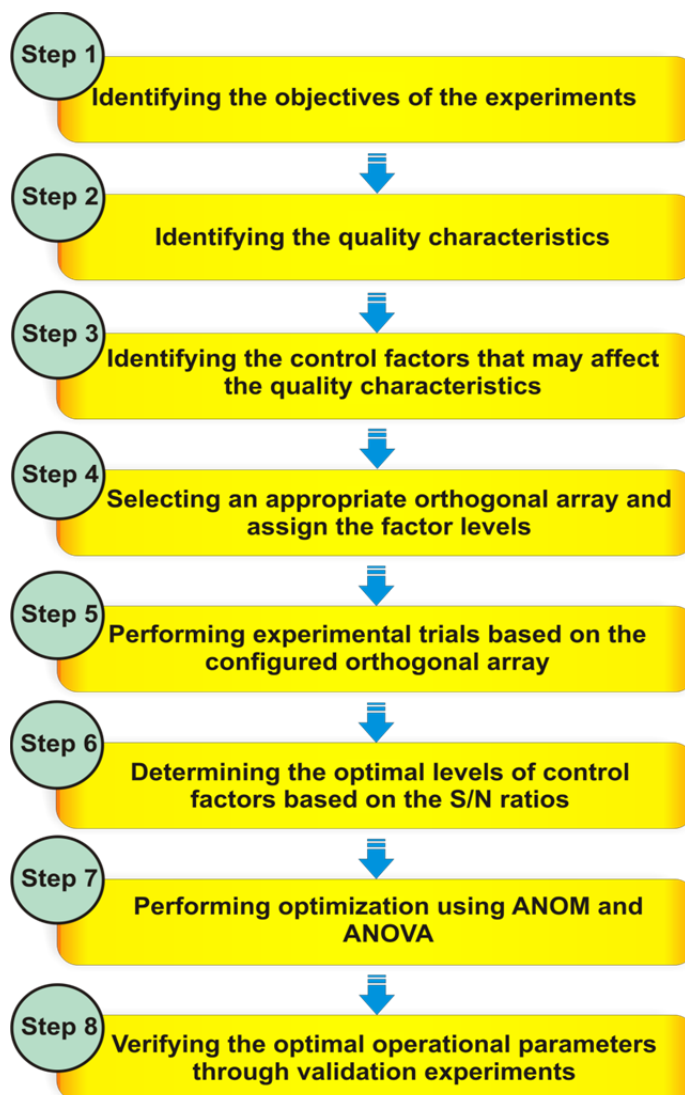


Figure 2.14: The outline for carrying out the Taguchi optimization procedure.

The selection of OAs begins with the distinct number of levels (L) defined for the number of control factors (K). The minimum number of trials in the OAs is

$$N_{t_{\min}} = (L - 1)K_n + 1 \quad (2.26)$$

In order to minimize the variations in the quality characteristic or response, Taguchi introduced a method to transform the repetition data to another value, which is a measure of variation present in the scattered response data. This transformation consists of the computation of signal-to-noise (S/N) ratio (η), which consolidates several repetitions into one performance measure reflecting the amount of variation present. The maximization of the S/N ratio simultaneously optimizes the response and minimizes the effect of noise factors. For each entry ' i ' in the OA, if the response (Ob) is repeated ' n ' times, the S/N ratio can be computed as follow:

- Smaller-the-better type:

$$\eta = -10 \log_{10} \left\{ \frac{1}{n} \sum_{i=1}^n Ob_i^2 \right\} \quad (2.27)$$

if Ob needs to be minimized;

- Larger-the-better type

$$\eta = -10 \log_{10} \left\{ \frac{1}{n} \sum_{i=1}^n Ob_i^{-2} \right\} \quad (2.28)$$

if Ob needs to be maximized.

The S/N ratios are further analyzed using statistical analysis of means (ANOM) and statistical analysis of variance (ANOVA). The first is used to identify the optimal factor level combinations and to estimate the main effects of each factor, while the second term is used to estimate the error variance for the effects and variance of the prediction error. The ANOM consists of the determination of the overall means by:

$$Mean = \frac{1}{L} \sum_{i=1}^L \eta_i \quad (2.29)$$

The effect of a factor level i for parameter j is defined as:

$$(Mean)_{i,j} = \frac{1}{L} \sum_{i=1}^L (\eta_i)_j \quad (2.30)$$

The optimum level for a factor is the level that gives the highest value of S/N ratio. The maximization of S/N ratio is determined by ANOM to give the optimum level associated with each factor and is given as:

$$j_{i,optimum} = \max \{ (Mean)_{i,j} \} \text{ for } j=1,2, \dots, K \quad (2.31)$$

After determining the optimal levels of control factors, the ANOVA is then performed to estimate the relative significance of each factor [GaKD09, Lazi06, Mont09, Phad89, Ross95].

Analysis of variance (ANOVA), often summarized in a table, is the statistical method used to interpret experimental data. ANOVA is used for detecting differences in the average performance of groups of items tested. It breaks total variation down into accountable sources. The main objective of ANOVA is to extract from the results how much variation each factor causes relative to the total variation observed in the result [Ruth01].

An ANOVA table contains the sources of variation, the degrees of freedom (DOF), the sum of squares (SS), the mean square (MS), the F-ratio, and sometimes the P-value. As per the ANOVA, the model developed is adequate within the specified confidence interval if F-ratio exceeds the standard tabulated value of *F-value*. Alternatively, one could use the P-value approach to testing. If a researcher finds the P-value to be less than a predetermined significance level, often 0.05 or 0.01, he/she will often decide to "reject the null hypothesis". Moreover, from ANOVA one can also determine the contribution of a particular control factor, for example *A*, in variance of a response using the ratio between the SS_A and the total sum of square SS_T . Finally, Table 2.1 shows a one way ANOVA table for an experimental design with L numbers of levels and N_i numbers of trials.

Source of variation	DOF	Sum of square (SS)	Mean square (MS)	F-ratio
Factor <i>A</i> (Between groups)	$L - 1$	$SS_A = \sum_{i=1}^L n_i (\bar{Y}_i - \bar{Y})^2$	$MS_A = SS_A / (L - 1)$	MS_A / MS_E
Error (<i>E</i>) (Within groups)	$N_i - L$	$SS_E = SS_T - SS_A$	$MS_E = SS_E / (N_i - L)$	
Total (<i>T</i>)	$N_i - 1$	$SS_T = \sum_{i=1}^L \sum_{j=1}^n (Y_{ij} - \bar{Y})^2$		

Table 2.1: The one way ANOVA table (using shortcut formulas).

2.3.1.2 Reviews of applications

Taguchi optimization is one of the most frequently applied procedures in metal cutting research. Over the past several years, numerous researchers have extensively applied this technique in order to improve and optimize the performance of cutting several engineering materials. Youssef et al. concluded that Taguchi designs appear to be reliable and more economical since they permit to reduce the amount of time and effort required to conduct the experimental design drastically without losing valuable information [YoBT94]. Yang and Tarn have used Taguchi method to find the optimal cutting parameters for turning operations. An orthogonal array, the signal-to-noise (S/N) ratio, and the analysis of variance (ANOVA) are employed to investigate the cutting characteristics of AISI 1045 steel bars using tungsten carbide cutting tools. Through this study, not only can the optimal cutting parameters for turning operations be obtained, but also the main cutting parameters that affect the cutting performance in turning operations can be found [YaTa98]. Ghani et al. applied Taguchi optimization methodology, to optimize cutting parameters in end milling when machining hardened steel AISI H13 with TiN coated P10 carbide insert tool under semi-finishing and finishing

conditions of high speed cutting. The study shows that the Taguchi method is suitable to solve the stated problem with minimum number of trials as compared with a full factorial design [GhCH04]. Gaitonde et al. presented the application of Taguchi optimization method for simultaneous minimization of burr height and burr thickness influenced by cutting conditions and drill geometry when drilling EN 1.4404 stainless steel. An approach of Taguchi design for multi-objective optimization problem is proposed. The effectiveness of proposed method is demonstrated through simulation results and experimental verifications [GKAS06]. Cetin et al. evaluated the performances of six cutting fluids for reducing of surface roughness, and cutting and feed forces during turning of AISI 304L austenitic stainless steel with carbide insert tool under Taguchi's L_{18} mixed level parameter design. Confirmation tests applied for Taguchi results and developed regression equations indicated reliable results [COKD11]. Philip et al. have successfully optimized the dry turning parameters of two different grades of nitrogen alloyed duplex stainless steel by using Taguchi method. The cutting parameters are optimized using signal to noise ratio and the analysis of variance. The effects of cutting speed and feed rate on surface roughness, cutting force and tool wear were analyzed. Through Taguchi's optimization procedure, feed rate has been identified as the more significant parameter influencing the surface roughness and cutting force and cutting speed as the more significant parameter influencing the tool wear [PhCM14].

2.3.1.3 Strength and limitations of Taguchi optimization procedure

Taguchi methods of experimental design were introduced into the western industries in the early 1980s. For instance, Taguchi's introduction of the method to several major American companies, including AT & T, Xerox and Ford, resulted in significant improvement of product and process quality [AnKa96]. It has proved to be successful in many manufacturing areas including plastics, automotive, metal fabrication, process and semi-conductors and today even the service industry is using this powerful technique for tackling service delivery time-related problems [RoAK00]. Maghsoodloo et al. have described the Taguchi's major contributions as:

- quantifying quality as deviation from the ideal target through quadratic loss function,
- introduction of OAs to simplify the use of DOE and
- definition and use of the S/N ratio, which combines the mean and standard deviation into one measure [MOJH04].

It is important to note that Taguchi's philosophy is inherently sound and his attempt to integrate statistical methods into the powerful engineering process is absolutely praiseworthy. However, his approach to experimental design and of course data analysis methods could be enhanced by integrating other alternative but powerful methods developed by researchers in the area. The following are the various technical issues which undermine Taguchi's approach to experimental design and optimization.

- Use of linear graphs which often lead to misleading conclusions.
- Disregarded modern graphical and analytical methods for rapid understanding [AnPr02].
- Taguchi rarely considers interactions among the control variables. In fact, many of the designs advocated by Taguchi do not allow estimation of these interactions [MyMA09].
- Taguchi proposes a short term, one-time improvement technique to reduce the number and cost of experimentations, which may eventually lead to sub-optimal solutions.
- Taguchi's method refers to optimization without intrinsic empirical or mechanistic modeling during experimentation. This type of technique closes the possibility for greater in-depth knowledge of the process [Box88, MyMA09].
- Alternative methods, claimed to be efficient for simultaneous optimization of multiple responses such as data transformation and using dual-response surface technique [MiPe63, UmSm59] and Lambda plot [Box88], are available in the literature where basic goals of Taguchi method are achieved by simultaneous optimization of mean and standard deviation without the use of controversial S/N ratio.
- Taguchi method for multiple objective optimization problems, as shown by Phadke [Phad89], is purely based on judgmental and subjective process knowledge [MuRa06].

2.3.2 Response surface methodology (RSM)

2.3.2.1 Basic concepts

The collective term "Response surface methodology" refers to a collection of statistical and mathematical techniques useful for developing, improving, and optimizing processes. It also has important applications in the design, development, and formulation of new products, as well as in the improvement of existing product designs. The separate term "response" refers to any characteristic, or variable, where variation has been observed, and this variation is the subject of a scientific or engineering research effort. As the word implies, a response is the

reaction of an investigated characteristic to the effects exercised on it by external factors. The term "surface" refers to the graphical perspective of the problem environment which is often used in graphical representation of the "Methodology". The latter refers to the systematic, theoretical analysis of the methods applied to a field of study [MyMA09, Shor11].

The application of RSM may be divided into the following major steps:

Step 1: The first step of performing RSM involves the design of a series of experiments that will provide adequate and reliable measurements from which information about how the different factors (independent variables) affect the response (dependent variable) can be gathered. Since the predictive capability of RSM is greatly influenced by the distribution of sampling points for fitting, the DOE techniques are applied. The following designs are more frequently used with RSM:

- Central composite designs: It can fit a full quadratic response surface model. These are often used when the design plan calls for sequential experimentation because these designs can incorporate information from a properly planned factorial experiment.
- Box-Behnken design: Typically it has fewer design points, thus, these are less expensive to run than central composite designs with the same number of factors. These allow efficient estimation of the first and second-order coefficients. However, these can't incorporate runs from a factorial experiment.
- Alphabetic optimality designs: optimal designs are a class of experimental designs that are optimal with respect to some statistical criterion. To differentiate between different criteria, each statistical criterion is assigned a letter, and thus commonly referred to as 'alphabetic' nomenclature for experimental designs. Building upon the initial work of Kiefer, the alphabetic criteria now includes A, D, E, G and I (also known as V or IV). These design methods use a single criterion in order to construct designs for RSM; this is especially relevant when fitting second-order models. For instance, D- and A-optimality criteria provide a measure of the variance of the model coefficients through the moment matrix, $\mathbf{M} = \mathbf{X}'\mathbf{X}/N$ where \mathbf{X} is the model matrix and N is the number of runs in the design. A D-optimal design is one that maximizes the determinant of \mathbf{M} , equivalently minimizing the volume of the confidence region on the model coefficients. An A-optimal design is one that maximizes the trace of the moment matrix, \mathbf{M} , and is directly related to minimizing the individual variances of the model coefficients [AnBM09, Monr09].

Step 2: The second step consists in finding the ‘best’ fit for the data by performing regression analysis (i.e. least square method) and the pertinent hypothesis tests on the model’s parameters. The most commonly used models are first and second order polynomials or also termed as linear and quadratic models respectively. A second-order model can significantly improve the optimization process when a first-order model suffers lack of fit due to interaction between variables and surface curvature. A general second-order model used in RSM designs is given in Eq. (2.32)

$$y = c_0 + \sum_{i=1}^k c_i x_i + \sum_{i=1}^k c_{ii} x_i^2 + \sum_{i=1}^k \sum_{j=1}^k c_{ij} x_i x_j \quad (2.32)$$

where y is actual response, x_i and x_j are the design variables (input factors), and c are the coefficients calculated based on least-square method (Eq. (2.10)). Next, ANOVA table and statistical measures such as root mean squared error (RMSE), the coefficient of determination (R^2) and the absolute average deviation ($AAD_{avg.}$) are used to check the model adequacy:

$$RMSE = \sqrt{\frac{1}{n} \sum_{i=1}^n [(y_{actual})_i - (y_{predicted})_i]^2} \quad (2.33)$$

$$R^2 = 1 - \frac{\sum_{i=1}^n [(y_{actual})_i - (y_{predicted})_i]^2}{\sum_{i=1}^n [(y_{actual})_i - (y_{mean})_i]^2} \quad (2.34)$$

$$AAD_{avg.} = \frac{1}{n} \left[\sum_{i=1}^n \left(\left| \frac{(y_{actual})_i - (y_{predicted})_i}{(y_{actual})_i} \right| \right) \right] \times 100 \quad (2.35)$$

where y_{actual} represents the actual, $y_{predicted}$ obtained by RSM and y_{mean} the mean of actual response values respectively, and n is the number of experimentation trials.

Step 3: The objective of the last step is to find the optimal settings of the experimental factors needed to obtain a desired response. Finally the flow chart of performing RSM is shown in Figure 2.15 below [AtMS14, GaKD09, Leon08].

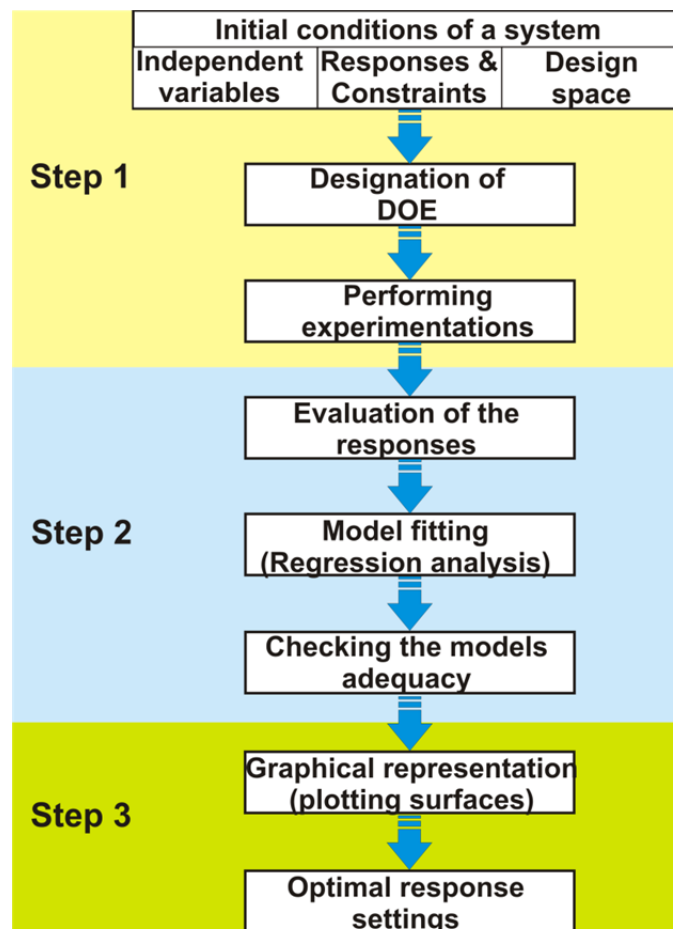


Figure 2.15: Response surface methodology.

2.3.2.2 Applications reviews

The first application of RSM in optimizing metal cutting parameters dates back to 1972, when Taraman and Lambert presented the use of RSM for analysis of material removal processes. Mathematical models of tool life, surface finish and cutting force are developed in terms of cutting speed, feed, and depth of cut. The models were then used to select the levels of the machining variables such that certain criteria could be achieved [TaLa72]. Taraman again used RSM to simultaneously optimize tool wear, surface finish, and tool force for finished turning operation. Mathematical models for such machining outputs were developed in terms of the cutting speed, feed and depth of cut. The developed models were utilized to obtain contours of the machining outputs in planes containing two of the independent variables. The methodology presented provided a large amount of information with a small amount of experimentation [Tara74]. Hassan and Suliman developed second-order mathematical models for some machining dependent variables, namely, surface roughness, tool vibration, power con-

sumption and cutting time when turning medium carbon steel using tungsten carbide tools under dry conditions. Theory of RSM optimization is then applied using the models developed as objective and constraint functions to find the optimal cutting conditions [HaSu90]. Thereafter, many other researchers have applied RSM in metal cutting optimization problem.

Recently, El-Tamimi and El-Hossainy investigated the machinability of austenitic EN 1.4310 stainless steel under oblique cutting. The parameters considered in the experiments were optimized to attain maximum tool life using a response graph and a response table [EIE108]. Aggrawal et al. presented the findings of an experimental investigation into the effects of cutting speed, feed rate, depth of cut, nose radius and cutting environment in CNC turning of AISI P-20 tool steel. DOE techniques, such as RSM and Taguchi, have been used to accomplish the objective of the experimental study. Though both the techniques predicted near similar results, RSM technique seems to have an edge over the Taguchi's technique [ASKS08]. Gaitonde et al. employed RSM-based models using central composite rotatable DOE to investigate the effects of process parameters on burr size during drilling of EN 1.4404 stainless steel [GKAS09]. Bouacha et al. achieved optimal values of cutting parameters in order to obtain the desired value of the machined surface roughness and the lowest cutting forces during the hard cubic boron nitride (CBN) turning of AISI 52100 bearing steel. Campatelli et al. applied RSM for minimizing power consumption in the milling of carbon steel. Results of their study have indicated that, through process parameters optimization using RSM, it could be possible to reduce the environmental impact of machining [CaLS14].

2.3.2.3 Benefits and drawbacks of RSM

Response surface methodology is a method for constructing global approximations of the objective and constraint functions based on functional evaluations at various points in the design space. The strength of the method is in applications where gradient based methods fail, i.e. when design sensitivities are difficult or impossible to evaluate. However, if the response dramatically changes, e.g. due to a change in buckling behavior, further iterations are needed to capture this with RSM [RFJM02]. Athisankar et al. have summarized the limitations of the method as:

- Large variations in the factors can be misleading the model fitment.
- Critical factors may not be correctly defined or specified.
- Range of levels of factors too narrow or too wide and optimum cannot be defined.

- Lack of use of good statistical principles, and
- Over-reliance on computer that make sure the results for good sense [AtMS14].

2.3.3 Nature-inspired meta-heuristic algorithms

Optimization techniques can be grouped into two broad categories: numeric and stochastic approaches. The first group comprises exact algorithmic methods, with a solid mathematical foundation, for obtaining the global optimum. Numeric approaches commonly use iterative algorithms. They include the gradient-based approaches, the descent method and the simplex algorithm. On the contrary, stochastic optimization tries to imitate some natural processes, which, although they do not guarantee the consecution of the global optimum, they allow good enough solutions to be obtained. These heuristics have a strong random component. Techniques such as evolutionary algorithms and simulated annealing are included in this group [QuDa11].

Heuristics is a solution strategy by trial-and-error to produce acceptable solutions to a complex problem in a reasonably practical time. The complexity of the problem of interest makes it impossible to search every possible solution or combination, the aim is to find good, feasible solutions in an acceptable timescale. There is no guarantee that the best solutions can be found, and we even do not know whether an algorithm will work and why if it does work. The idea is that an efficient but practical algorithm that will work most of the time and be able to produce good quality solutions. Among the found quality solutions, it is expected that some of them are nearly optimal, though there is no guarantee for such optimality [Yang10a].

Further development over the heuristic algorithms is the so-called meta-heuristic algorithms. Here *meta-* means ‘beyond’ or ‘higher level’ and they generally perform better than simple heuristics [Yang14a]. Meta-heuristics, in their original definition, are solution methods that orchestrate an interaction between local improvement procedures and higher level strategies to create a process capable of escaping from local optima and performing a robust search of a solution space. Over time, these methods have also come to include any procedures that employ strategies for overcoming the trap of local optimality in complex solution spaces, especially those procedures that utilize one or more neighborhood structures as a means of defining admissible moves to transition from one solution to another, or to build or destroy solutions in constructive and destructive processes [GePo10].

In the most generic term, the main source of inspiration for meta-heuristic algorithms is Nature. Therefore, almost all new algorithms can be referred to as nature-inspired. By far the majority of nature-inspired algorithms are based on some successful characteristics of biological system. Therefore, the largest fraction of nature-inspired algorithms is biology-inspired, or bio-inspired for short. Among bio-inspired algorithms, a special class of algorithms has been developed by drawing inspiration from swarm intelligence. Therefore, some of the bio-inspired algorithms can be called swarm-intelligence based. In fact, algorithms based on swarm intelligence are among the most popular. Good examples are Ant Colony Optimization [DoCa99], Particle Swarm Optimization [KeEb95], Cuckoo Search [YaDe09], Bat Algorithm [Yang10b], and Firefly Algorithm [FiYB13, FYBF13, Yang09].

Obviously, not all algorithms were based on biological systems. Many algorithms have been developed by using inspiration from physical and chemical systems. Some may even be based on music [Loga01]. Though not all of them are efficient, a few algorithms have proved to be very efficient and thus have become popular tools for solving real-world problems. Among these algorithms, many algorithms such as Particle Swarm Optimization, Cuckoo Search and Firefly Algorithm, have gained popularity due to their high efficiency. In the current literature, there are about 40 different algorithms. Fister et al. divided all existing algorithms into four major categories: swarm intelligence-based, bio-inspired (but not SI-based), physics/chemistry-based, and others [FYBF13]. For the sake of more convenience, five examples per each of the above categories are shown in Figure 2.16.

Mathematically speaking, it is possible to write an optimization problem in the generic form:

$$\underset{\mathbf{x} \in \mathfrak{R}^n}{\text{minimum}} \quad f_i(\mathbf{x}), \quad (i = 1, 2, \dots, M) \quad (2.36)$$

$$\text{subjected to} \quad \varphi_j(\mathbf{x}) = 0, \quad (j = 1, 2, \dots, J) \quad (2.37)$$

$$\psi_k(\mathbf{x}) \leq 0, \quad (k = 1, 2, \dots, K) \quad (2.38)$$

where $f_i(\mathbf{x})$, $\varphi_j(\mathbf{x})$ and $\psi_k(\mathbf{x})$ are functions of the design vector

$$\mathbf{x} = (x_1, x_2, \dots, x_n)^T \quad (2.39)$$

where the components x_i of \mathbf{x} ; are called design or decision variables, and they can be real continuous, discrete or a mixture of these two. The functions $f_i(\mathbf{x})$ where $(i = 1, 2, \dots, M)$ are called the objective functions, and in the case of $M = 1$, there is only a single objective. The

objective function is sometimes called the cost function or energy function in literature. The space spanned by the decision variables is called the search space \mathcal{R}^n , while the space formed by the objective function values is called the solution space [Yang10a].

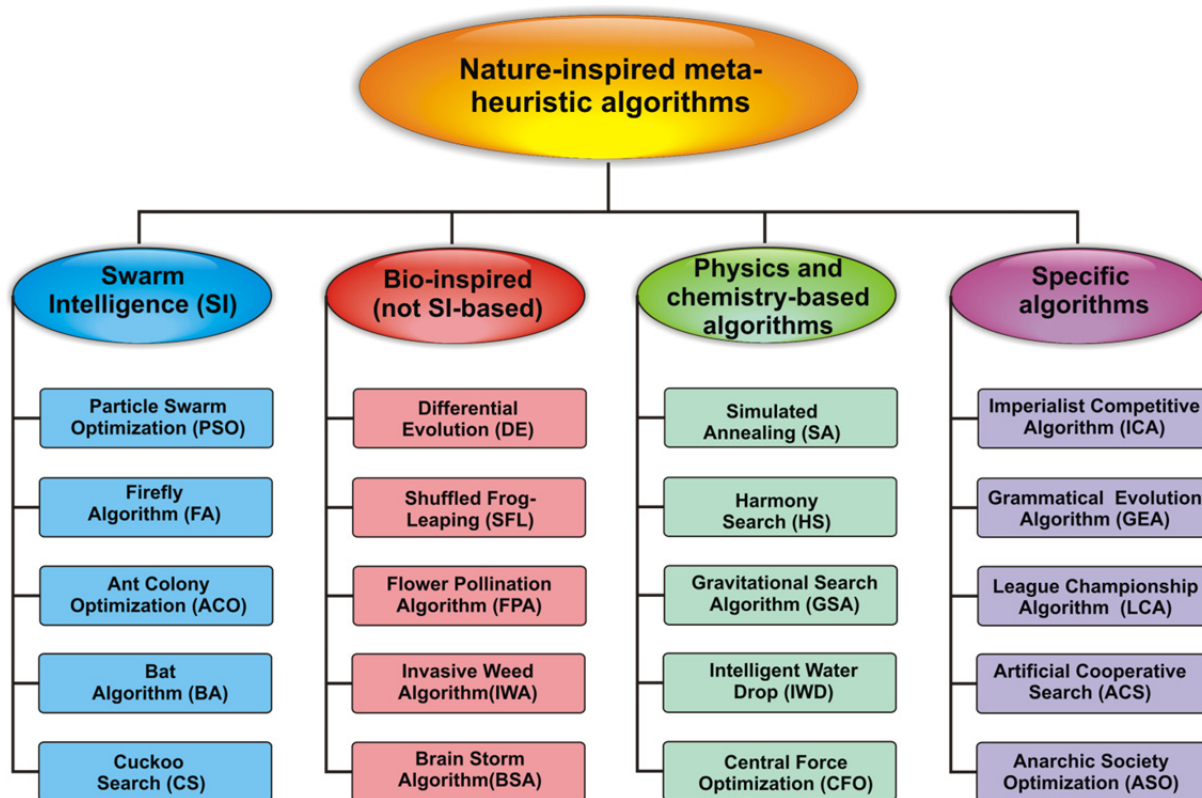


Figure 2.16: Classification of nature-inspired meta-heuristic algorithms.

In the next incoming subsections, a brief description of some of the efficient algorithms which have been adopted for machining processes optimization is provided.

2.3.3.1 Simulated Annealing (SA)

SA was proposed by Kirkpatrick, Gelatt, and Vecchi (1983) to find the optimal global cost function that may possess several local optima [KiGV83]. Unlike most heuristic optimization methods, Simulated Annealing process uses single-point search method. It mimics the annealing process in material processing when a metal cools and freezes into crystalline state with minimum energy and larger crystal size so as to reduce the defects in metallic structures. The SA procedure simulates this process of slow cooling of molten metal to achieve the minimum function value in a minimization problem. According to the Boltzmann probability distribution, a system in thermal equilibrium at a temperature T has its energy distributed probabilistically according to:

$$P(E) = \exp\left(\frac{-E}{k_b T}\right) \quad (2.40)$$

where k_b is the Boltzmann constant. Let us assume at any instant the current point $x^{(t)}$ and the function value at that point is $E(t) = f(x^{(t)})$. Using the Metropolis algorithm, we can say that the probability of the next point being at $x^{(t+1)}$ depends on the difference in the function values at these two points or on

$$\Delta(E) = E(t+1) - E(t) \quad (2.41)$$

and is calculated using the Boltzmann probability distribution:

$$P(E(t+1)) = \min\left(1, \exp\left(\frac{-\Delta E}{k_b T}\right)\right) \quad (2.42)$$

If $\Delta E \leq 0$, this probability is one and the point $x^{(t+1)}$ is always accepted. In the function minimization context, this makes sense because if the function value at $x^{(t+1)}$ is better than $x^{(t)}$, the point $x^{(t+1)}$ must be accepted. If $\Delta E > 0$, then the function value at $x^{(t+1)}$ is worse than at $x^{(t)}$. According to many traditional algorithms, the point $x^{(t+1)}$ must not be chosen in this situation. But according to the Metropolis algorithm, there is some finite probability of selecting the point $x^{(t+1)}$ even though it is worse than the point $x^{(t)}$. The algorithm terminates when a sufficiently small temperature is obtained or small enough change in function value is found [Deb09]. This can be summarized in the following steps:

Step 1: Choose an initial point $x^{(0)}$ and a termination criterion Θ . Set T a sufficiently high value, number of iterations to be performed at a particular temperature n , and set $t=0$.

Step 2: Calculate a neighboring point $x^{(t+1)} = N(x^t)$. Usually, a random point in the neighborhood is created.

Step 3: If $\Delta E = E(x^{(t+1)}) - E(x^{(t)}) < 0$, set $t = t + 1$;

Else create a random number (r) in the range (0,1). If $r \leq \exp(-\Delta E/T)$, set; $t = t + 1$

Else go to Step 2.

Step 4: If $|x^{(t+1)} - x^t| < \Theta$ and T is small, Terminate;

Else if $(t \bmod n) = 0$ then lower T according to a cooling schedule.

Go to Step 2;

Else go to Step 2.

Despite the numerous capabilities of SA, its application in optimization of cutting conditions for various machining performances was given less attention by researchers. Earlier, Chen and Tsai developed an optimization algorithm based on the SA algorithm and the Hooke-Jeeves pattern search (PS) for optimization of multi-pass turning operations. Experimental results indicate that the proposed nonlinear constrained optimization algorithm, named SA/PS, is effective for solving complex machining optimization problems [ChTs96]. Khan et al. have concluded that Genetic Algorithm (GA), SA and the continuous SA which are non-gradient based optimization techniques are reliable and accurate for solving machining optimization problems and offer certain advantages over gradient based methods [KhPS97]. Juan et al. applied SA to the polynomial network to determine the optimal cutting parameters for minimum production cost in high speed machining SKD61 tool steels [JuYL03]. Wnag et al. used Genetic Simulated Annealing (GSA), which is a hybrid of GA and SA, to determine optimal machining parameters for milling operations. For comparison, basic GA is also chosen as another optimization method. An application example that has previously been solved using geometric programming method is presented. The results indicate that GSA is more efficient than GA and geometric programming in the application of cutting optimization [WaWR04]. Zain et al. presented the estimation of the optimal effect of the radial rake angle of the tool, combined with cutting speed and feed in influencing the surface roughness result during end milling Ti-6Al-4V alloy. They concluded that SA is an effective tool for estimating the minimum surface roughness values as compared to the experimental and regression modeling results [ZaHS10].

2.3.3.2 Accelerated Particle Swarm Optimization (APSO)

Particle Swarm Optimization (PSO) was developed by Kennedy and Eberhard (1995) based on the swarm behavior such as fish and bird schooling in nature [KeEb95]. Since then, PSO has generated much wider interests and forms an exciting, ever expanding research subject called swarm intelligence. This algorithm searches the space of an objective function by adjusting the trajectories of individual agents, called particles, as the piecewise paths formed by positional vectors in a quasi-stochastic manner.

The PSO selects a number of particles to represent a swarm. Each particle in the swarm is a potential solution to the optimization problem under consideration. A particle explores the search domain by moving around. This move is decided by making use of its own experience and the collective experience of the swarm. Each particle has three main parameters: position,

velocity, and fitness. Position represents the decision variables of the optimization problem, velocity determines the rate of change of the position, and fitness is the value of the objective function at the particle's current position. The fitness value is a measure of how good is the solution it represents for the optimization problem [YaKa13].

The movement of a swarming particle consists of two major components: a stochastic component and a deterministic component. Each particle is attracted toward the position of the current global best g^* and its own best location x_i^* in history, while at the same time it has a tendency to move randomly. Let x_i and v_i be the position vector and velocity of particle i , respectively. The new velocity vector is determined by the following formula:

$$v_i^{t+1} = v_i^t + \zeta \ell_1 (x_i^* - x_i^t) + \Omega \ell_2 (g^* - x_i^t) \quad (2.43)$$

Where ℓ_1 and ℓ_2 are two random vectors drawn from a uniform distribution and ζ is the randomization factor. The parameters ζ and Ω are the learning parameters and acceleration constants, which can typically be taken as, say, $\zeta = \Omega = 2$. The initial locations of all particles should be distributed relatively uniformly so that they can sample over most regions, which is especially important for multimodal problems. The initial velocity of a particle can be taken as zero, i.e., $v_i^{t=0} = 0$ [YaKa13]. The new positions can then be updated by:

$$x_i^{t+1} = x_i^t + v_i^{t+1} \quad (2.44)$$

In Figure 2.17, a flowchart of the standard PSO algorithm is shown.

PSO is now widely used in solving tough optimization problems due to its low computational complexity, easy implementation and relatively few parameters. However, PSO also has several major shortcomings; it may suffer from premature convergence for highly multimodal problems. To overcome this, there are many PSO variants, which have been formed mainly by slight variations of certain terms and parameters in the PSO, especially by introducing inertia parameter and by hybridizing with other algorithms. Among many variants of PSO, the most noticeable improvement is possibly the use of inertia function $\Lambda(t)$ so that v_i^t is replaced by $\Lambda(t)v_i^t$:

$$v_i^{t+1} = \Lambda(t)v_i^t + \zeta \ell_1 (x_i^* - x_i^t) + \Omega \ell_2 (g^* - x_i^t) \quad (2.45)$$

where Λ takes the value between 0 and 1. In the simplest case, the inertia function can be taken as a constant, typically $\Lambda \approx 0.5 - 0.9$.

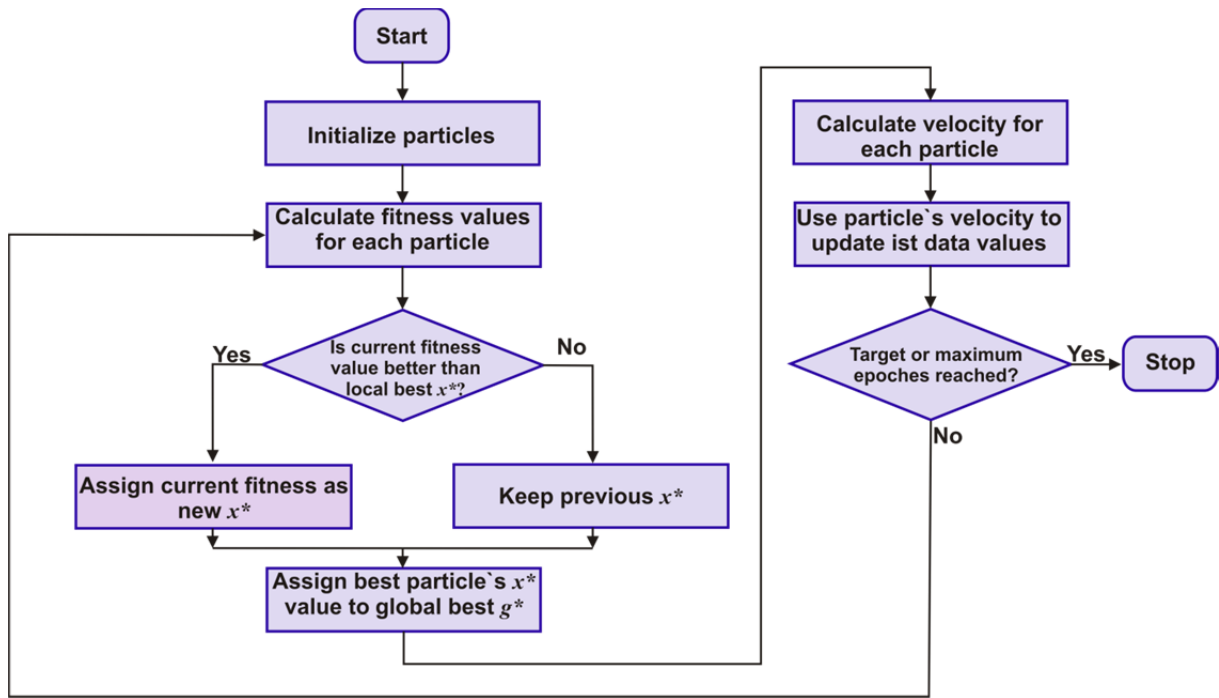


Figure 2.17: Flow chart of the PSO algorithm.

The standard PSO uses both the current global best g^* and the individual best x_i^* . The reason of using the individual best is primary to increase the diversity in the quality solutions. However, this diversity can be simulated using some randomness. Subsequently there is no compelling reason for using the individual best, unless the optimization problem of interest is highly nonlinear and multimodal. A simplified version which could accelerate the convergence of algorithm is to use the global best only. Thus, in the accelerated PSO, the velocity is generated by a simpler formula:

$$v_i^{t+1} = v_i^t + \zeta(\ell - 1/2) + \Omega(g^* - x_i^t) \quad (2.46)$$

where ℓ is a random variable with values from 0 to 1. Here the shift $1/2$ is purely out of convenience. We can also use a standard normal distribution $\zeta \ell_n$ where ℓ_n is drawn from $N(0,1)$ to replace the second term.

In order to increase the convergence even further, we can also write the update of the location in a single step as

$$x_i^{t+1} = (1 - \Omega)x_i^t + \Omega g^* + \zeta \ell_n \quad (2.47)$$

This simpler version will give the same order of convergence. It is worth pointing out that the velocity does not appear in the last equation, and thus there is no need to deal with the initiali-

zation of velocity vectors. Therefore, the accelerated PSO is much simpler to implement. Here the randomization term ζ^{ℓ_n} provides the ability for the system to escape any local optima if ζ is chosen to be consistent with the scales of the problem of interest [Yang14a].

Many researchers and practitioners used PSO in metal cutting process parameter optimization problems. Chandrasekaran et al. reviewed the application of major soft computing tools such as neural networks, fuzzy sets, GA, SA, ACO, and PSO to four traditional machining processes, namely turning, milling, drilling, and grinding. The paper highlights the progress made in this area and discusses the issues that need to be addressed [CMKD10]. Costa et al. addressed the machining economics problem concerning the multi-pass turning by a Hybrid Particle Swarm Optimization technique (HPSO). The significant outcomes of the research highlighted that HPSO can be taken into account as a useful and powerful technique for optimizing machining problems [CoCF11]. Yusup et al. gave an overview of PSO techniques to optimize machining process parameter of both traditional and modern machining from 2007 to 2011. From their review, the most machining process considered in PSO was multi-pass turning while the most considered machining performance was production costs [YuZH12]. Escamilla-Salazar et al. used PSO to optimize machining parameters in high speed milling processes where multiple conflicting objectives are presented. The relationships between machining parameters and the performance measures of interest are obtained by using experimental data and a hybrid system using a PSO and a neural network. Results showed that PSO is an effective method for solving multi-objective optimization problems and also that an integrated system of neural networks and swarm intelligence can be used to solve complex machining optimization problems [ETGZ13]. Recently, Marco et al. presented a proposal, how to successfully gain optimal cutting parameters for certain performances using PSO [MSTM14].

2.3.3.3 Firefly Algorithm (FA)

FA is one of the recent swarm intelligence methods developed by Yang in 2008 and is a kind of stochastic, nature-inspired, meta-heuristic algorithm that can be applied for solving the hardest optimization problems. The algorithm is inspired by the flashing lights of fireflies in nature. Such flashing light may serve as the primary courtship signals for mating. Besides attracting mating partners, the flashing light may also serve to warn off potential predators. The algorithm has been formulated by assuming:

- All fireflies are unisex so that one firefly will be attracted to other fireflies regardless of their sex.
- Attractiveness is proportional to their light intensities. The less bright will be moving towards the brighter one. It will move randomly if there is no brighter one.
- The brightness of a firefly is affected or determined by the landscape of the objective function.

The light intensity and attractiveness are in some way synonymous. While the intensity is referred to as an absolute measure of emitted light by the firefly, the attractiveness is a relative measure of the light that should be seen in the eyes of the beholders and judged by other fireflies. The attractiveness $\beta_a(\delta_r)$ and light intensities $I(\delta_r)$ of each firefly are considered to decrease monotonically depending on the distance δ_r as:

$$\beta_a(s) = \beta_{a_0} e^{-\gamma_a \delta_r^2} \quad (2.48)$$

$$I_t(s) = I_{t_0} e^{-\gamma_a \delta_r^2} \quad (2.49)$$

where β_{a_0} and I_{t_0} denote the maximum attractiveness and light intensities respectively (i.e. at $\delta_r = 0$), and γ_a is the light absorption coefficient, which controls the decrease of the light intensity. The light intensity I_t of a firefly representing the solution x_i and is proportional to the value of fitness function $I_t(x_i) \propto f(x_i)$. The distance between any two fireflies x_i and x_j is expressed as the Euclidean distance by the base Firefly Algorithm, as follows:

$$\delta_{r_{ij}} = \|x_i - x_j\| = \sqrt{\sum_{k=1}^{k=d_m} (x_{ik} - x_{jk})^2} \quad (2.50)$$

where d_m denotes the dimensionality of the problem. The movement of the i -th firefly is attracted to another more attractive firefly j . In this manner, the following equation is applied:

$$s_{i+1} = s_i + \beta_{a_0} e^{-\gamma_a \delta_{r_{ij}}^2} (x_j - x_i) + \alpha_{rand} \psi_g \quad (2.51)$$

where ψ_g is a random number drawn from Gaussian distribution and α_{rand} is the randomization parameter.

In summary, FA is controlled by three parameters: the attractiveness β_a , and the absorption coefficient γ_a and the randomization parameter α_{rand} [FiYB13]. The basic steps of the Firefly Algorithm (FA) can be summarized as the flow chart and shown in Figure 2.18.

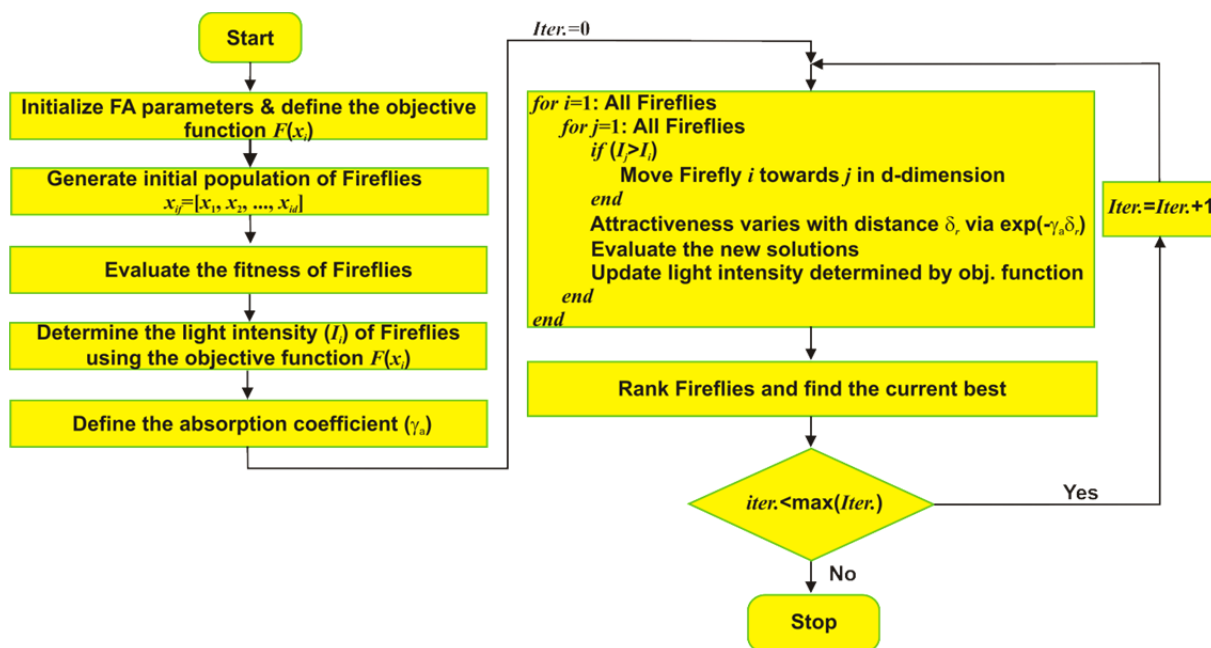


Figure 2.18: Flow chart of the Firefly Algorithm (FA).

Very few applications of FA in metal cutting process parameter optimization problems have been reported in the literature. Raja et al. implemented FA for selecting the optimal electric discharge machining parameters to achieve the desired performance measures. The predicted and actual machining performances revealed that FA was very much suitable for solving machining parameters optimization problems [BSVR13]. Belloufi et al. presented FA optimization for solving the multi-pass turning operations problem. The results obtained from comparing the Firefly Algorithm with those taken from recent literature proved its effectiveness [BeAR14].

2.3.3.4 Cuckoo Search (CS)

CS is one of the latest nature-inspired meta-heuristic algorithms, developed by Xin-She Yang and Suash Deb [YaDe09]. It is inspired by lifestyle of a bird family called cuckoo. Specific egg laying and breeding of cuckoos is the basis of this optimization algorithm. Like other evolutionary algorithms, the proposed algorithm starts with an initial population of cuckoos. These initial cuckoos have some eggs to lay in some host birds' nests. Some of these eggs which are more similar to the host bird's eggs have the opportunity to grow up and become a

mature cuckoo. Other eggs are detected by host birds and are killed. The grown eggs reveal the suitability of the nests in that area. The more eggs survive in an

- Each cuckoo lays one egg at a time, and dumps its egg in a randomly chosen nest;
- The best nest with high-quality eggs will be carried over to the next generation;
- The number of available host nests is fixed, and the egg laid by a cuckoo is discovered by the host bird with a probability p_a between 0 and 1. In this case, the host bird can either get rid of the egg, or simply abandon the nest and build a completely new nest.

The CS algorithm uses a balanced combination of a local random walk and the global explorative random walk, controlled by a switching parameter p_a . The local random walk can be written as

$$x_i^{t+1} = x_i^t + \alpha_z \otimes H(p_a - \nu) \otimes (x_j^t - x_k^t) \quad (2.52)$$

where x_j^t and x_k^t are two different solutions selected randomly by random permutation, $H(\nu)$ is a Heaviside function and ν is a random number drawn from a uniform distribution. On the other hand, the global random walk is carried out by using Lévy flights

$$x_i^{t+1} = x_i^t + \alpha_z L(s, \lambda), \quad (2.53)$$

where λ is the expectation of occurrence and s is the step length, and

$$L(s, \lambda) = \frac{\lambda \Gamma(\lambda) \sin(\pi\lambda/2)}{\pi} \frac{1}{s^{1+\lambda}} \quad (s \gg s_0 > 0) \quad (2.54)$$

Here $\alpha_z > 0$ is the step size scaling factor, which should be related to the scales of the problem of interest. The above equation is essentially the stochastic equation for a random walk. In general, a random walk is a Markov chain whose next state/location only depends on the current location (the first term in the above equation) and the transition probability (the second term). However, a substantial fraction of the new solutions should be generated by far field randomization and their locations should be far enough from the current best solution; this will make sure that the system will not be trapped in a local optimum [Yang14b]. Based on the previous descriptions, the basic steps of the CS algorithm can be summarized as flow chart and is shown in Figure 2.19.

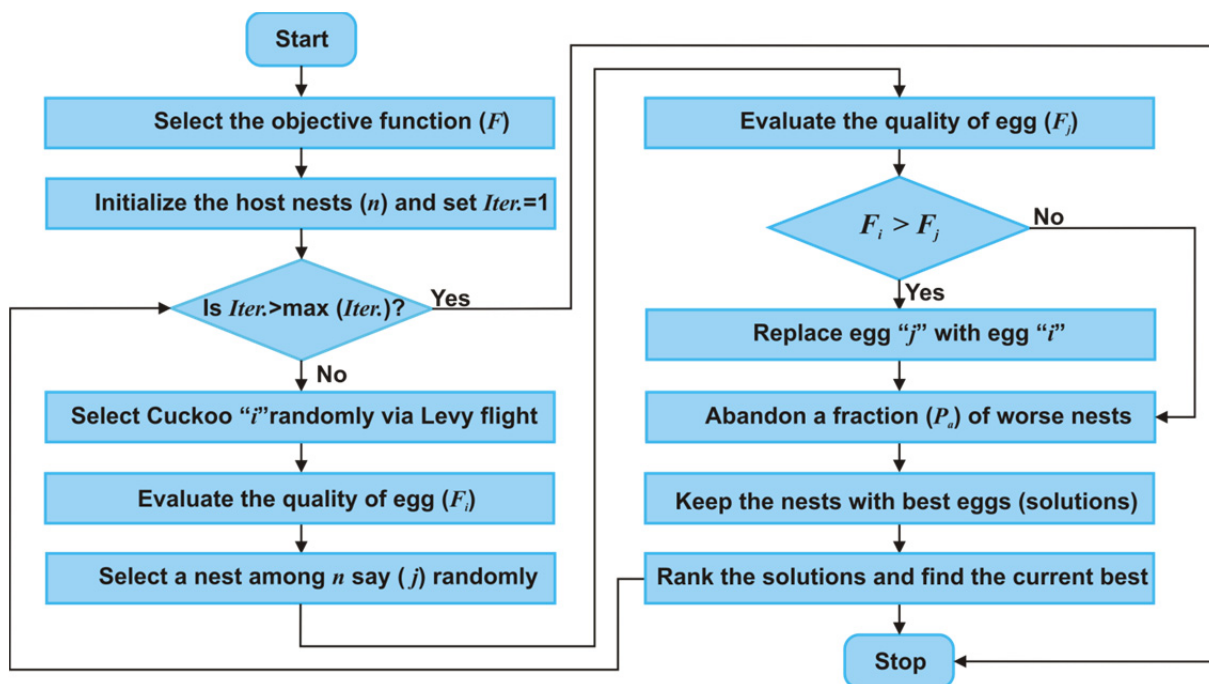


Figure 2.19: Flow chart of the Cuckoo Search (CS).

The algorithm is recently applied for solving manufacturing optimization problems. Yildiz successfully implemented CS to the optimization of machining parameters in milling operations. Significant improvement is obtained with the CS compared to the feasible direction method, Ant Colony Algorithm, Immune Algorithm, HPSO, Hybrid Immune Algorithm, Genetic Algorithm and handbook recommendations [Yild13b]. Mellal and Williams carried out multi-pass turning parameter optimization using CS. The obtained results are compared with previously published results available in the literature. It has been proven that the CS competes robustly with a wide range of optimization algorithms [MeWi14].

2.3.3.5 Bat Algorithm (BA)

Bat Algorithm (BA) is a population-based swarm intelligence algorithm which is inspired by the echolocation of microbats. Echolocation is an advanced hearing based navigation system used by bats and some other animals to detect objects in their surroundings by emitting a sound to the environment. In general echolocation calls are characterized by three features; namely pulse frequency, pulse emission rate and loudness (intensity). In general the frequency f_q in a range $[f_{q_{\min}}, f_{q_{\max}}]$ corresponds to a range of wavelengths $[\lambda_{w_{\min}}, \lambda_{w_{\max}}]$. For example a frequency range of [20kHz, 500kHz] corresponds to a range of wave-lengths from 0.7mm to 17mm in reality. Obviously, one can choose the ranges freely to suit different applications. In

order to develop a standard Bat Algorithm, the following approximate or idealized rules are applied:

- All bats use echolocation to sense distance, and they also ‘know’ the difference between food/prey and background barriers in some magical way;
- Bats fly randomly with velocity v_i at position x_i with a frequency $f_{q_{\min}}$, varying wavelength and loudness A_{i_0} to search for prey. They can automatically adjust the wavelength (or frequency) of their emitted pulses and adjust the rate of pulse emission $P_r \in [0, 1]$, depending on the proximity of their target;
- Although the loudness can vary in many ways, we assume that the loudness varies from a large (positive) A_{i_0} to a minimum constant value $A_{i_{\min}}$.

For the bats in simulations, we have to define the rules how their positions x_i and velocities v_i in a d-dimensional search space are updated. The new solutions x_i^t and velocities v_i^t at time step t are given by:

$$f_{q_i} = f_{q_{\min}} + (f_{q_{\max}} - f_{q_{\min}})\beta_r \quad (2.55)$$

$$v_i^{t+1} = v_i^t + (x_i^t - x^*)f_{q_i} \quad (2.56)$$

$$x_i^{t+1} = x_i^t + v_i^t \quad (2.57)$$

where $\beta_r \in [0, 1]$ is a random vector drawn from a uniform distribution. Here x^* is the current global best location (solution) which is located after comparing all the solutions among all the n bats at each iteration t . The loudness and pulse rate can vary with iteration t in the following way:

$$A_{i_i}^{t+1} = C_1 A_{i_i}^t \quad (2.58)$$

$$P_{r_i}^{t+1} = P_{r_i}^0 [1 - \exp(-C_2 t)] \quad (2.59)$$

Here C_1 and C_2 are constants. In fact, C_1 is similar to the cooling factor of a cooling schedule in the SA, which is discussed earlier. In the simplest case, we can use $C_1 = C_2$, and in fact $C_1 = C_2 = 0.9$ can be used in most simulations.

Bat Algorithm has been extended to Multi-Objective Bat Algorithm (MOBA) by Yang, and preliminary results suggested that it is very efficient [YaHo12, YaKa13, Yang10b, Yang11,

Yang14a]. Based on the above approximations and idealization, the basic steps of the BA can be summarized as the flow chart shown in Figure 2.20.

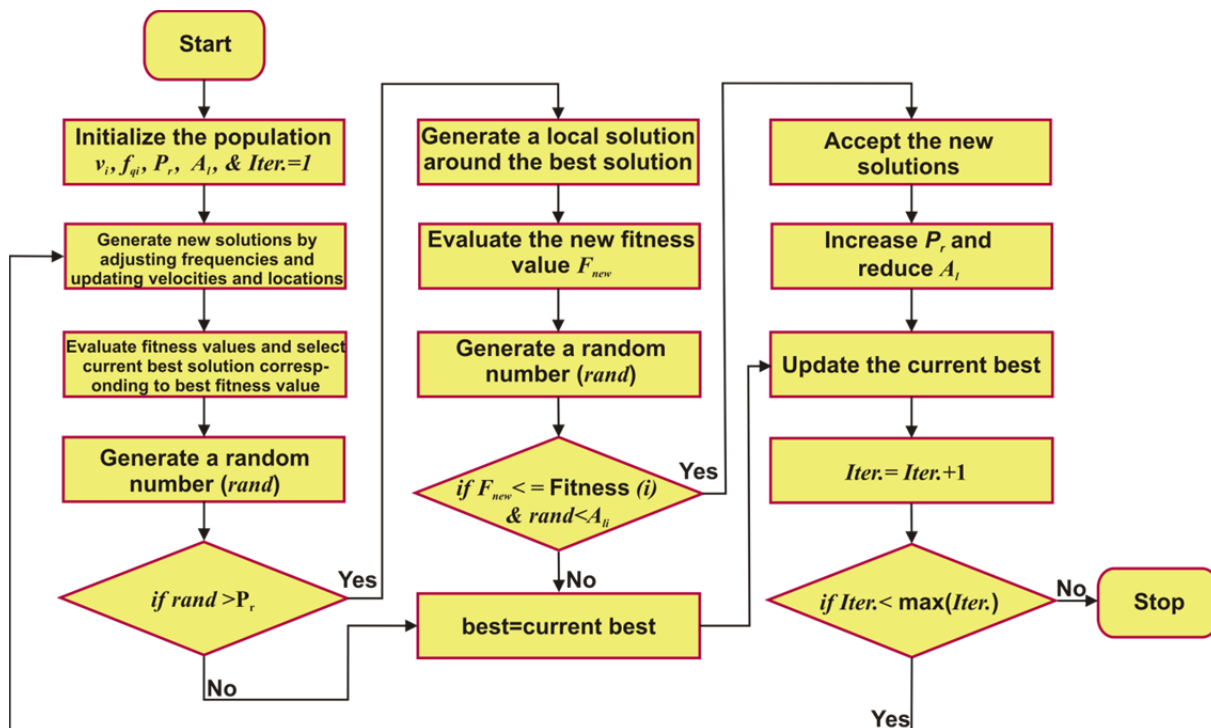


Figure 2.20: Flow chart of the Bat Algorithm (BA).

2.3.4 Multiple Attribute Decision Making (MADM) methods

Making decisions is a part of our daily lives. The major concern is that almost all decision problems have multiple, usually conflicting, criteria. Researches on how to solve such problems has been enormous. Methodologies, as well their applications, appear in professional journals of different disciplines. Diversifies as such problems may be, they are broadly classified into two categories: (1) Multiple Attribute Decision Making (MADM) and (2) Multiple Objective Decision Making. MADM is the most well-known branch of decision making. It is a branch of a general class of operations research models that deal with decision problems under the presence of a number of decision criteria. The MADM approach requires that the choice (selection) be made among decision alternatives described by their attributes. MADM problems are assumed to have a predetermined, limited number of decision alternatives. Solving a MADM problem often involves sorting and ranking. On the other hand, in the MODM approach, contrary to the MADM approach, the decision alternatives are not given. Instead, MODM provides a mathematical framework for designing a set of decision alternatives. Each alternative, once identified, is judged by how close it satisfies an objective or multiple objec-

tives. In the MODM approach, the number of potential decision alternatives may be very large [Kahr08, LaHw96].

In mathematical terms, that formulation of every MADM method starts with the construction of a decision matrix. A decision matrix (**DMA**) is a $(m \times n)$ matrix whose element (x_{ij}) indicates the performance rating of alternative i, A_i , with respect to attribute j, χ_j . Hence A_i , for $i=1, 2, \dots, m$ is denoted by:

$$A_i = (x_{i1}, x_{i2}, \dots, x_{in}) \quad (2.60)$$

and χ_j for $j=1, 2, 3, \dots, n$ is denoted by:

$$\chi_j = (x_{1j}, x_{2j}, \dots, x_{mj}) \quad (2.61)$$

In Eq. (2.62), an example of typical decision matrix elements is presented:

$$\mathbf{DMA} = \begin{matrix} & & \begin{bmatrix} \chi_1 & \chi_2 & \dots & \chi_j & \dots & \chi_n \end{bmatrix} \\ \begin{bmatrix} A_1 \\ A_2 \\ \dots \\ A_i \\ \dots \\ A_m \end{bmatrix} & \begin{bmatrix} x_{11} & x_{12} & \dots & x_{1j} & \dots & x_{1n} \\ x_{21} & x_{22} & \dots & x_{2j} & \dots & x_{2n} \\ \dots & \dots & \dots & \dots & \dots & \dots \\ x_{i1} & x_{i2} & \dots & x_{ij} & \dots & x_{in} \\ \dots & \dots & \dots & \dots & \dots & \dots \\ x_{m1} & x_{m2} & \dots & x_{mj} & \dots & x_{mn} \end{bmatrix} & \end{matrix} \quad (2.62)$$

It may be added here that in any MADM method, even though the weights of different attributes with respect to the objective, w_j (for $j=1, 2, \dots, m$), are decided by the decision maker rather arbitrarily, only few systematic methods can be used. Standard deviation, entropy-based methods analytical hierarchy process (AHP) are among the most commonly used systematic approaches to estimate the weight of the various attributes from the given payoff matrix. An advantage of utilizing the first two methods is that the estimation of the attribute weights is independent of the views of the decision maker. The systematic methods of deciding the weights of attributes are explained below.

- Standard deviation method

According to the standard deviation method, the larger the dispersion degree of the attribute j , the larger is the corresponding weight (w_j):

$$w_j = -\frac{STDV_j}{\sum_{j=1}^n STDV_j} \quad (2.63)$$

where $STDV_j$ represent the standard deviation of the j attribute.

- Entropy method

Shannon and Weaver [ShWe49] proposed the entropy concept and this concept has been highlighted by Zeleny [Zele98] for deciding the objective weights of attributes. Entropy is a measure of uncertainty in the information formulated using probability theory. It indicates that a broad distribution represents more uncertainty than does a sharply peaked one. The process of calculation of Entropy weights can be divided into the following steps:

Step1: For a given normalized **DMA**, r_{ij} , estimate entropy E_j of the set of alternatives for attribute j :

$$E_j = -\frac{1}{\ln(m)} \sum_{i=1}^m r_{ij} \ln(r_{ij}) \quad (2.64)$$

for $i=1, 2, \dots, m$ and $j=1, 2, \dots, n$.

Step 2: Compute degree of diversification DV_j of the information provided by the outcomes of attribute j :

$$DV_j = 1 - E_j \quad (2.65)$$

Step 3: Normalized weights of the criterion are

$$w_j = \frac{DV_j}{\sum_{j=1}^n DV_j} \quad (2.66)$$

If the entropy value is high, the uncertainty contained in the criterion vector is high (Step 1), diversification of the information is low (Step 2) and correspondingly the criterion is less important (Step 3).

- AHP

As mentioned before, both of the standard deviation method and entropy method calculate the objective weights of the attributes without giving any consideration to the preferences of the

decision maker [RaKu10]. However, if the preferences of the decision maker are to be addressed, the AHP weight assignment method should be employed. AHP, which is one of the most popular analytical techniques for complex decision-making problems, can be effectively applied to obtain the weights of non-tangible (i.e., subjective) attributes, especially where the subjective judgments of different individuals constitute an important part of the decision process. The main procedure of AHP's weight assignment method is as follows:

Step 1: Construct a pairwise comparison matrix using scale of relative importance. An attribute compared with itself is always assigned the value 1, so the main diagonal entries of the pair-wise comparison matrix are all 1. Assuming N attributes, the pair-wise comparison of attribute i with attribute j yields a square matrix $\mathbf{B} = N * N$. In the matrix, $b_{ij} = 1$ when $i = j$ and $b_{ij} = 1/b_{ji}$. Where b_{ij} denotes the comparative importance of attribute i with respect to attribute j .

$$\mathbf{B} = \begin{matrix} & \begin{matrix} \chi_1 & \chi_2 & \chi_3 & \cdot & \cdot & \chi_n \end{matrix} \\ \begin{matrix} \chi_1 \\ \chi_2 \\ \chi_3 \\ \cdot \\ \cdot \\ \chi_n \end{matrix} & \begin{bmatrix} 1 & b_{12} & b_{13} & \cdot & \cdot & b_{1n} \\ b_{21} & 1 & b_{23} & \cdot & \cdot & b_{2n} \\ b_{31} & b_{32} & 1 & \cdot & \cdot & b_{3n} \\ \cdot & \cdot & \cdot & 1 & \cdot & \cdot \\ \cdot & \cdot & \cdot & \cdot & 1 & \cdot \\ b_{n1} & \cdot & \cdot & \cdot & \cdot & 1 \end{bmatrix} \end{matrix} \quad (2.67)$$

Step 2: Find the relative normalized weight (w_j) of each attribute by calculating the geometric mean of the i -th row and normalizing the geometric means of rows in the comparison matrix. These can be represented as;

$$G_{M_j} = \left[\prod_{j=1}^n b_{ijl} \right]^{1/n} \quad (2.68)$$

$$w_j = \frac{G_{M_j}}{\sum_{j=1}^n G_{M_j}} \quad (2.69)$$

Step 3: Perform calculations to find the consistency ratio (CR). A CR of equal or less than 0.1 indicates that the consistency of individual judgment is acceptable. To determine the CR :

- a) Calculate matrices \mathbf{A}_3 and \mathbf{A}_4 such that $\mathbf{A}_3 = \mathbf{B} * \mathbf{A}_2$ and $\mathbf{A}_4 = \mathbf{A}_3 / \mathbf{A}_2$, where $\mathbf{A}_2 = [w_1, w_2, \dots, w_j]^T$.

- b) Determine the maximum Eigen value λ_{max} that is the average of matrix A_4 .
 c) Calculate the consistency index (CI) using:

$$CI = \frac{\lambda_{max} - n}{n - 1} \quad (2.70)$$

- d) Calculate the CR :

$$CR = \frac{CI}{RI} \quad (2.71)$$

where RI is the random index .

The next incoming subsections will focus on the MADM methods whose number of alternatives has been predetermined. Through which, the decision maker is guided to select/prioritize/rank a finite number of courses of action.

2.3.4.1 Technique for Order Preference by Similarity to Ideal Solution (TOPSIS)

Multiple attribute decision making methods such as Technique for Order Preference by Similarity to Ideal Solution (TOPSIS) is utilized to convert the multi-objective optimization of many objectives into a single objective optimization problem. The technique is based on the concept that the chosen alternative should have the shortest Euclidean distance from the ideal solution. The ideal solution is a hypothetical solution for which all attribute values correspond to the maximum attribute values in the database comprising the satisfying solutions; the negative-ideal solution is the hypothetical solution for which all attribute values correspond to the minimum attribute values in the above-mentioned database. TOPSIS, thus, gives a solution that is not only closest to the hypothetically best, but which is also farthest from the hypothetically worst. The steps involved for calculating the TOPSIS values are as follows:

Step 1: Formulate the multi-performance problem in DM format as per Eq. (2.62).

Step 2: Construct the normalized decision matrix, R_{ij} whose elements can be represented as:

$$r_{ij} = \frac{x_{ij}}{\sqrt{\sum_{i=1}^m x_{ij}^2}} \quad (2.72)$$

Step 3: Construct the weighted normalised decision matrix. This is obtained by the multiplication of each element of the column of the matrix R_{ij} with its associated weight w_j . Hence, the elements of the weighted normalized matrix are expressed as:

$$v_{ij} = w_j r_{ij} \quad (2.73)$$

Step 4: Determine the “ideal” (best) and “negative ideal” (worst) solutions. The ideal (best) and negative ideal (worst) solution can be expressed as:

$$A^* = \{ \max_i(v_{ij}) \text{ if } j \in J; \min_i(v_{ij}) \text{ if } j \in J', \text{ for } i = 1, 2, \dots, m \}$$

$$\text{Positive ideal solution} = \{v_1^*, v_2^*, \dots, v_j^*, \dots, v_n^*\} \quad (2.74)$$

$$A^- = \{ \min_i(v_{ij}) \text{ if } j \in J; \max_i(v_{ij}) \text{ if } j \in J', \text{ for } i = 1, 2, \dots, m \}$$

$$\text{Negative ideal solution} = \{v_1^-, v_2^-, \dots, v_j^-, \dots, v_n^-\} \quad (2.75)$$

Where, J is the set of cost type criteria and J' is the set of benefit type criteria.

Step 5: Obtain the separation measures. The separation of each alternative from the ideal one is given by Euclidean distance. Therefore, the separation from positive ideal alternative is:

$$S_i^* = \sqrt{\sum_{j=1}^n (v_{ij} - v_i^*)^2} \quad (2.76)$$

Similarly, the separation from the negative ideal alternative is:

$$S_i^- = \sqrt{\sum_{j=1}^n (v_{ij} - v_i^-)^2} \quad (2.77)$$

Step 6: The relative closeness of a particular alternative to the ideal solution C_i^* can be evaluated as:

$$C_i^* = \frac{S_i^-}{S_i^- + S_i^*} \quad (2.78)$$

$$i = 1, 2, \dots, m; 0 \leq C_i^* \leq 1$$

Step 7: Rank the preference order, so that the alternative that has the shortest distance to the ideal solution is ranked first [ChSr13, LaHw96, SiDM11].

TOPSIS has been used to solve MADM problem in various scenarios. Rao and Davim suggested a logical procedure based TOPSIS and AHP together to help in selection of a suitable material from among a large number of available alternative materials for a given engineering application [RaDa08]. Singh et al. adopted TOPSIS in combination with Taguchi’s robust design philosophy to optimize multiple surface roughness parameters of machined glass fiber reinforced polymer [SiDM11]. Sivapirakasam et al. developed a combination of Taguchi and

fuzzy TOPSIS methods to solve multi-response parameter optimization problems in green manufacturing. The model can be used as a systematic framework for parameter optimization in environmentally conscious manufacturing processes [SiMS11]. Thirumalai and Senthilku-
maar proposed TOPSIS for selecting a single solution from non-dominated solutions obtained by non-sorted genetic algorithm for multi-objective functions of high-speed machining of Inconel 718 [ThSe13].

TOPSIS is useful when dealing with a large number of alternatives and attributes, good for both qualitative and quantitative data, relatively easy and fast. The output can be a preferential ranking of the candidate materials [JaEd13a]. However, the method based on Euclidean distance does not consider correlation between indices, thus causing information overlap which, in turn, affects the decision results. Thus, the reduction of indicator correlation within the application often relies on qualitative analysis, the aim being to try to increase index independence during the process of index screening. These conditions make this approach strongly subjective [WaWa14].

2.3.4.2 VIKOR method

The VIKOR method was originally introduced in 1998 for multi-criteria optimization of complex systems. It determines the compromise ranking-list, the compromise solution, and the weight stability intervals for preference stability of the compromise solution obtained with the initial (given) weights. This method focuses on ranking and selecting from a set of alternatives in the presence of conflicting criteria. It introduces the multi-criteria ranking index based on the particular measure of “closeness” to the “ideal” solution. It is developed from the Lp-metric used as an aggregating function in a compromise programming method [Yu73, Zele98]. The method involves the following steps:

Step 1: Arrange the elements of the MADM problem in DMA format as per Eq. (2.62).

Step 2: Determine the best x_i^* and the worst x_i^- values of all attribute functions. If the i th function represents a benefit then:

$$x_i^* = \max_j x_{ij} \quad (2.79)$$

$$x_i^- = \min_j x_{ij} \quad (2.80)$$

Step 3: Compute the values of utility measure S_i and regret R_i measure by the relations:

$$S_i = \sum_{j=1}^n w_j \frac{(x_j^* - x_{ij})}{(x_j^* - x_j^-)} \quad (2.81)$$

$$R_i = \max_j \left[w_j \frac{(x_j^* - x_{ij})}{(x_j^* - x_j^-)} \right] \quad (2.82)$$

Step 4: Compute the VIKOR index (Q_V) values for attribute $j=1,2,\dots,n$, by the relation

$$Q_V = \xi \frac{(S_i - S^*)}{(S^- - S^*)} + (1 - \xi) \frac{(R_i - R^*)}{(R^- - R^*)} \quad (2.83)$$

where

$$S^* = \min_j S_j, \quad S^- = \max_j S_j,$$

$$R^* = \min_j R_j, \quad R^- = \max_j R_j.$$

ξ is introduced as weight of the strategy of “the majority of criteria” (or “the maximum group utility”), usually $\xi = 0.5$.

Step 5: Rank the alternatives, sorting by the values S , R and Q_V . The results are three ranking lists.

Step 6: For given attribute weights, propose a compromise solution, alternative A_{b_1} , which is the best ranked by Q_V , if the following two conditions are satisfied:

Condition 1: ‘Acceptable advantage $Q_V(A_{b_2}) - Q_V(A_{b_1}) \geq (1/(m-1))$ ’ where A_{b_1} and A_{b_2} are the first and second-best alternatives in the ranking order by Q_V .

Condition 2: ‘Acceptable stability in decision making’ alternative A_{b_1} must also be the best ranked by S and/or R . This compromise solution is stable within a decision-making process, which could be: ‘voting by majority rule’ (when $\xi > 0.5$ is needed) or ‘by consensus’ (when $\xi \approx 0.5$) or ‘with veto’ (when $\xi < 0.5$). If one of the conditions is not satisfied, then a set of compromise solutions is proposed, which consists of:

- Alternatives A_{b_1} and A_{b_2} if only condition 2 is not satisfied.
- Alternatives $A_{b_1}, A_{b_2}, \dots, A_{b_i}$ if condition 1 is not satisfied; A_p is determined by the relation $Q_V(A_{b_2}) - Q_V(A_{b_1}) \approx (1/(m-1))$ [OpTz04].

MADM using VIKOR method has attracted the attention of industrial decision makers recently. For example, Çalışkan et al. solved the material selection problem for the tool holder working under hard milling conditions utilizing a decision model. The model included PRO-

METHEE (Preference Ranking Organization METHod for Enrichment Evaluation), TOPSIS and VIKOR methods for the ranking of the alternative materials according to determined criteria [ÇKKG13]. Jahan and Edwards presented new VIKOR method for ranking materials with simultaneous availability of interval data and all types of criteria. It has been shown that the proposed method is able to address effectively mixed data, with precise and imprecise values, and with interval data [JaEd13b].

The VIKOR is an effective tool in the MADM, particularly in a situation where the decision maker is not able, or does not know how to describe his/her preference at the beginning of system design. The obtained compromise solution can be accepted by the decision maker's because it provides a maximum group utility of the majority represented by $\min S$ and a minimum of the individual regret of the opponent represented by $\min R$. The compromise solutions can be the basis for negotiations containing the decision maker's preference by criteria weights [OpTz04]. Although the VIKOR method is an effective tool for MADM problems, some errors would occur when some attributes have no difference among the alternatives, the utility measure has no difference among the alternatives and the regret measure has no difference among the alternatives [Chan10].

2.3.4.3 Grey relational analysis

A system that has none of information is defined as a black system, while a system that is full of information is called white. Systems between these extremes are described as being grey, hazy, or fuzzy. Therefore, a grey system means that a system in which a part of information is known and a part of information is unknown. Grey systems theory was initiated by Deng in 1982. The system has three approaches such as grey relational analysis (GRA), grey clustering, grey decision making [Julo82, Julo89].

GRA is an impact evaluation model that measures the degree of similarity or difference between the comparability sequence and the reference sequence based on the grade of relation known as grey relational grade (GRG) [ChTo07]. So that, if an alternative gets the highest gray relational grade with the reference sequence, it means that comparability sequence is most similar to the reference sequence and that alternative would be the best choice [Fung03]. In recent years, the grey relational analysis has become the powerful tool to analyse the processes with multiple performance characteristics. It has been widely applied in the last fifteen years in several research fields [Yin13]. It provides an efficient solution to multi-input and discrete data problems. In grey relational analysis, the complex multiple response optimiza-

tion problem can be simplified into an optimization of single response grey relational grade [Rao11a]. The procedure for determining the grey relational grade is discussed below:

Step 1: Perform grey relational generation

In GRA, when the range of sequences is large or the standard value is large, the function of factors is neglected. However, if the factors measured unit, goals and directions are different, the Grey Relational Analysis might produce incorrect results. Therefore, original experimental data must be pre-processed to avoid such effects. Data pre-processing is the process of transforming the original sequence to a comparable sequence. For this purpose, the experimental results are normalized in the range of zero and one, the process is called grey relational generation. The normalized values r_{ij} are determined by use of the Eq. (2.84), based on the response types which are for beneficial type (i.e. larger-the-better), target type (nominal-the-best) and non-beneficial type (i.e. smaller-the-better).

$$r_{ij} = \begin{cases} \text{Larger – the – better : } \left(\frac{\max(x_{ij}) - x_{ij}}{\max(x_{ij}) - \min(x_{ij})} \right) \\ \text{Nominal – the – best : } 1 - \left(\frac{|x_{ij} - x_j^*|}{\max(\max(x_{ij}) - x_j^*, x_j^* - \min(x_{ij}))} \right) \\ \text{Smaller – the – better : } \left(\frac{x_{ij} - \min(x_{ij})}{\max(x_{ij}) - \min(x_{ij})} \right) \end{cases} \quad (2.84)$$

where x_j^* is closer to the desired value of j th response.

Step 2: Generate references

In comparability sequence, all performance values are scaled to $[0, 1]$. For a response j of experiment i , if the value r_{ij} which has been processed by data pre-processing procedure is equal to 1 or nearer to 1 than the value for any other experiment, then the performance of experiment i is considered as best for the response j . The reference sequence R_0 is defined as $(r_{01}, r_{02}, \dots, r_{0j}, \dots, r_{0n}) = (1, 1, \dots, 1, \dots, 1)$, where r_{0j} is the reference value for j th response and it aims to find the experiment whose comparability sequence is the closest to the reference sequence.

Step 3: Find the deviation sequence (Δ_{ij}) , global minimum (Δ_{\min}) and maximum value (Δ_{\max}) in the difference series using the following Eqs.:

$$\Delta_{ij} = |r_{0j} - r_{ij}|, \quad (2.85)$$

$$\Delta_{\min} = \min\{\Delta_{ij}, i = 1, 2, \dots, m; j = 1, 2, \dots, n\}, \quad (2.86)$$

$$\Delta_{\max} = \max\{\Delta_{ij}, i = 1, 2, \dots, m; j = 1, 2, \dots, n\}, \quad (2.87)$$

Step 4: Gray relational coefficient (ζ_g):

Gray relational coefficient is used for determining how close r_{ij} is to r_{0j} . The larger the grey relational coefficient, the closer r_{ij} and r_{0j} are. The gray relational coefficient can be calculated by Eq.2.83 .

$$\zeta_g(r_{0j}, r_{ij}) = \frac{(\Delta_{\min} + \delta_d \Delta_{\max})}{(\Delta_{ij} + \delta_d \Delta_{\max})} \quad \text{for } i = 1, 2, \dots, m \text{ and } j = 1, 2, \dots, n \quad (2.88)$$

The factor δ_d is the distinguishing coefficient used to compensate for the effect of the data series and is defined as $\delta_d \in [0, 1]$. Generally, for equal weight performance characteristics, the value of δ_d can be set to 0.5.

Step 5: Grey relational grade (GRG): the measurement formula for quantification in gray relational space is called the gray relational grade. A gray relational grade (gray relational degree) is a weighted sum of the grey relational coefficients and it can be calculated using Eq. (2.84).

$$GRG = \sum_{j=1}^n w_j \zeta_g(r_{0j}, r_{ij}) \quad \text{for } i = 1, 2, \dots, m \quad (2.89)$$

where

$$\sum_{j=1}^n w_{jj} = 1 \quad (2.90)$$

Many papers have proposed GRA as aids in multi-performance optimization of machining processes. Kao and Hocheng applied the grey relational analysis for optimizing the electropolishing of EN 1.4404 stainless steel with multiple performance characteristics. The conducted validation experiments approved the effectiveness of the GRA [KaHo03]. Lin addressed an approach based on the Taguchi method with grey relational analysis for optimizing turning operations with multiple performance characteristics. It is shown that the performance characteristics of the turning operations such as tool life, cutting force, and surface roughness are improved together by using the method proposed by this study [Lin04]. Tosun used GRA for optimizing the drilling process parameters for the work piece surface roughness and the burr height is introduced. Experimental results have shown that both performances can be improved effectively through the new approach [Tosu06]. Ching and Lu employed orthogonal

array with grey-fuzzy logics to optimize the multiple performance characteristics of heavy cutting in side milling for EN 1.4301 stainless steel. The grey relational coefficients are used as indications to the relational degree of the multiple performance characteristics and Fuzzy logic to perform the fuzzy reasoning of the multiple performance characteristics. The results of confirmation experiments reveal that grey-fuzzy logics can effectively acquire an optimal combination of the cutting parameters [ChLu07]. Horng and Chiang focused on the development of a fast and effective algorithm to determine the optimum manufacturing conditions for turning Hadfield steel with $\text{Al}_2\text{O}_3/\text{TiC}$ mixed ceramic tool by coupling the grey relational analysis with the fuzzy logic [HoCh08]. Lu et al. presented the application of GRA coupled with principal component analysis for optimizing the cutting parameters of rough cutting process in high-speed end milling operation for SKD61 tool steel. The authors claimed that the proposed algorithm have greatly simplified the optimization design of cutting parameters with multiple performance characteristics [LCHC09]. Ranganathan and Senthivelan considered the multi-response optimization of machining parameters in hot turning of stainless steel EN 1.4404 based on a coupled Taguchi technique and GRA. Significant improvement in hot turning performances has been achieved using the coupled approach [RaSe11]. Yan and Li evaluated trade-offs between sustainability, production rate and cutting quality through a multi-objective optimization approach based on weighted GRA and RSM during milling AISI 1045 carbon steel. The optimization results confirmed the usefulness of the proposed optimization method in multi-objective optimization of cutting parameters [YaLi13]. Nayak et al. optimized the influence of machining parameters on material removal rate, cutting force and surface roughness during dry machining of EN 1.4301 austenitic stainless steel. The GRA was adopted to optimize the machining parameters in turning operation. A conducted confirmatory test observed an improvement of 88.78% in GRG in supporting the findings of the research [NPDG14].

Finally, GRA is a multi-factor analysis method with good and broad applicability. It can define system or factor boundary, analyze the influence of system and behavior, distinguish primary and secondary factors and so on [JiLi12]. However, GRA only presents the similarity between two curve collections. It cannot figure out the similar level of two curve collections' trend [ZhXi14].

2.3.4.4 Utility concept (UC)

Utility can be defined as the usefulness of a product in response to the expectations of the customers/users. It is the measure of the characteristic of a product to meet the customers' requirements. The overall usefulness of a process/product can be represented by a unified index termed as utility which is the sum of the individual utilities of various quality characteristics of the process/product. The methodological basis for the utility approach is to transform the estimated response of each quality characteristic into a common index. If x_j is the measure of performance of j th attribute and there are $i=1, 2, \dots, m$ alternatives in the entire selection space, then the joint utility function can be expressed as:

$$U(x_1, x_2, \dots, x_n) = f(U_1(x_1), U_2(x_2), \dots, U_n(x_n)) \quad (2.91)$$

where $U_1(x_1)$ is the utility of j th attribute and n is the total number of evaluation attributes. The overall utility function is the sum of individual utilities if the attributes are independent, and is given as follows:

$$U(x_1, x_2, \dots, x_n) = \sum_{j=1}^n U_j(x_j) \quad \text{for } j = 1, 2, \dots, n \quad (2.92)$$

Depending upon the requirements, the attributes may be given priorities and weights. Hence, the weighted form of Eq. 22 is:

$$U(x_1, x_2, \dots, x_n) = \sum_{j=1}^n w_j U_j(x_j) \quad (2.93)$$

where, w_j is the weight of j th attribute. To determine the utility values the following procedural steps are necessary:

Step 1: Assign best values of each attribute (x_j^*) based on the preference measure. For example, if the performance is of non-beneficiary type, then

$$x_j^* = \min(x_j) \quad (2.94)$$

Step 2: Calculate the utility constant (U_c). The value of U_c can be found using the expression:

$$U_{c_j} = \frac{9}{\log\left(\frac{x_j^*}{x'_j}\right)} \quad (2.95)$$

where x'_j is just acceptable value of quality characteristic for j th attribute. Hence, x'_j is equal to the $\min(x_j)$ for beneficial attribute and $\max(x_j)$ for non-beneficial attribute.

Step 3: Determine the preference number. Utility concept adopts an idea of preference number to show the performance measure of each alternative against each criterion, calculated on a logarithmic scale. A preference scale for each attribute is constructed for determining its utility value. The preference numbers vary from 0 (representing the lowest performance value) to 9 (denoting the highest performance value). Thus, a preference number of 0 represents the just acceptable attribute and the best value of the attribute is denoted by preference number 9 [GuMu80]. The preference number (PN) for j th attribute can be expressed on a logarithmic scale as follows:

$$PN_j = U_{C_j} * \log\left(\frac{x_j}{x'_j}\right) \quad (2.96)$$

Step 4: Calculate the overall utility value U_i .

The overall utility value can now be calculated as follows:

$$U_i = \sum_{j=1}^n w_j PN_j \quad (2.97)$$

Step 5: Rank the alternatives. The best alternative, ranked by U_i , is the one that will return maximum value of U_i [KaGC13].

In the proposed approach utility values of individual responses are accumulated to calculate overall utility index. Overall utility index serves as the single objective function for optimization.

A number of literature review papers showed the validity of coupled Taguchi-UC in multi-performance optimization of machining processes. Singh and Kumar introduced a simplified multi-characteristic model based on Taguchi's approach and UC to determine the optimal settings of EN 1.6582 steel turning process [SiKu06]. Gaitonde et al. employed the UC and multi-response Taguchi design to predict an optimum drilling process parameters setting for simultaneous minimization of delamination factor both at the entry and exit of the holes with minimum number of experiments [GaKD08a]. In their second contribution, Gaitonde et al. proposed Taguchi technique with the utility concept for simultaneous minimization of surface roughness and specific cutting force in determining the optimum amount of minimum quality

lubrication and the most appropriate cutting speed and feed rate during turning of brass using K10 carbide tool [GaKD08b]. Dubey presented a utility-based Taguchi loss function strategy for the multi-response optimization of electro-chemical honing process. The experimental results confirmed the validity of the approach for simultaneous optimization of multiple responses in electro-chemical honing [Dube09].

2.3.4.5 Graph Theory and Matrix Approach (GTMA)

Graph theory is a logical and systematic approach. The advanced theory of graphs and its applications are very well documented [DaYS09]. Graph/digraph model representations have proved to be useful for modeling and analyzing various kinds of systems and problems in numerous fields of science and technology. The matrix approach is useful in analyzing the graph/digraph models expeditiously to derive the system function and index to meet the objectives [Rao13]. The main procedure of GTMA methodology is as follows:

Step 1: Construct the normalized decision matrix, R_{ij} using Eq. (2.84).

Step 2: Assign the values of relative importance of normalized attributes r_{ij} . The number of nodes shall be equal to the number of attributes. This is represented by a binary matrix (I_{ij}), where I_{ij} represents the relative importance between attributes i and j . The relative importance between i, j and j, i is distributed on a scale 0 to L , so that if I_{ij} represents the relative importance of the i -th surface quality attribute over the j -th surface quality attribute, then the relative importance of the j -th surface quality attribute over the i -th surface quality attribute is evaluated using:

$$I_{ji} = L - I_{ij} \quad (2.98)$$

For example, let the decision maker select the following assignments (**DMA**):

$$\mathbf{DMA} = \begin{bmatrix} \chi_1 & \chi_1 & \chi_3 & \chi_4 & \cdot & \cdot & \cdot & \chi_n \\ \chi_1 & - & I_{12} & I_{13} & I_{14} & \cdot & \cdot & \cdot & I_{1n} \\ \chi_2 & I_{21} & - & I_{23} & I_{24} & \cdot & \cdot & \cdot & I_{2n} \\ \chi_3 & I_{31} & I_{32} & - & I_{34} & \cdot & \cdot & \cdot & I_{3n} \\ \chi_4 & I_{41} & I_{42} & I_{43} & - & \cdot & \cdot & \cdot & I_{4n} \\ \cdot & \cdot & \cdot & \cdot & \cdot & - & \cdot & \cdot & \cdot \\ \cdot & \cdot & \cdot & \cdot & \cdot & \cdot & - & \cdot & \cdot \\ \cdot & \cdot & \cdot & \cdot & \cdot & \cdot & \cdot & - & \cdot \\ \chi_n & I_{n1} & I_{n2} & \cdot & \cdot & \cdot & \cdot & \cdot & - \end{bmatrix} \quad (2.99)$$

Step 3: Develop the attributes matrix for the attributes digraph. This will be the $n*n$ matrix with diagonal elements as r_{ij} and off-diagonal elements as I_{ij} . Repeat the process for n -number of rows in normalized decision matrix. For example, for the first row of normalized decision matrix the attribute digraph can be represented by:

$$\mathbf{DMA} = \begin{matrix} & \begin{matrix} [\chi_1 & \chi_1 & \chi_3 & \chi_4 & \cdot & \cdot & \cdot & \chi_n] \end{matrix} \\ \begin{matrix} \chi_1 \\ \chi_2 \\ \chi_3 \\ \chi_4 \\ \cdot \\ \cdot \\ \cdot \\ \chi_n \end{matrix} & \begin{bmatrix} r_{11} & I_{12} & I_{13} & I_{14} & \cdot & \cdot & \cdot & I_{1n} \\ I_{21} & r_{12} & I_{23} & I_{24} & \cdot & \cdot & \cdot & I_{2n} \\ I_{31} & I_{32} & r_{13} & I_{34} & \cdot & \cdot & \cdot & I_{3n} \\ I_{41} & I_{42} & I_{43} & r_{14} & \cdot & \cdot & \cdot & I_{4n} \\ \cdot & \cdot & \cdot & \cdot & \cdot & - & \cdot & \cdot \\ \cdot & \cdot & \cdot & \cdot & \cdot & \cdot & - & \cdot \\ \cdot & \cdot & \cdot & \cdot & \cdot & \cdot & \cdot & - \\ I_{n1} & I_{n2} & \cdot & \cdot & \cdot & \cdot & \cdot & r_{1n} \end{bmatrix} \end{matrix} \quad (2.100)$$

Step 4: Obtain the permanent function $\text{Per}(\mathbf{DMA})$ for each generated attributes matrix.

Step 5: Rank the alternatives, sorting by the values of the corresponding $\text{Per}(\mathbf{DMA})$. The best alternative is the one with the maximum value of $\text{Per}(\mathbf{DMA})$.

GTMA techniques have already been applied by the past researchers in some industrial applications. The pioneer researcher in this field is R. Venkata Rao. He has demonstrated the application of GTMA in several different occasions. In 2001, he and Gandhi presented a methodology to select a cutting fluid for a given machining application using the digraph and matrix method. They concluded that the proposed graph theory and matrix approach is applicable to any type of metal-cutting operation [RaGa01]. Thereafter, he applied GTMA to evaluate the machinability of work materials for a given machining operation [VeGa02]. He also extended the application of GTMA to the material selection problem for engineering design [Rao06a] and the evaluation of flexible manufacturing systems [Rao06b].

GTMA can consider any number of quantitative and qualitative factors. However, it does not have a condition for checking the consistency made in the judgments of relative importance of the attributes. The method may be difficult to deal with if the number of attributes is more than 20 [JaEd13a].

2.4 A systematic methodology for modeling and optimization of cutting processes

Comprehensive schemes for modeling and optimizing turning process parameters are presented in Figure 2.21 and Figure 2.22, respectively. The schemes also suggest various approaches suitable for single and multi-objective problems. The detailed steps of the schemes are described below.

Step 1: Formulate the cutting process optimization problem spotlighting its significance in terms of the adopted criteria, such as production cost, quality characteristics and/or process performance measures.

Step 2: Designate the relevant process decision and response variables. Independent cutting variables such as cutting and process conditions, tool materials and coatings, tool shape, surface finish and sharpness, workpiece material and condition, characteristics of the machine tool and workpiece holding and fixturing can be potential decision variables. Meanwhile, dependent cutting variables such as type of chip produced, energy dissipated during cutting, temperature rise in the workpiece, the tool and the chip, tool wear and failure, surface finish and surface integrity are potential response variables.

Step 3: Plan and design of the cutting experiments using factorial designs, Taguchi designs, response surface designs,, etc. Selecting appropriate experimental layout will reduce the number of experiments, which in turn reduces the cost and time involved in the experimentation.

Step 4: Represent the collected technical data graphically employing histograms, contour maps, surface plots,, etc. This will provide a primary insight into the mean, the variability, and the control state of critical quality characteristics and identify the need for further improvement.

Step 5: In the case of Taguchi's robust design methodology, compute the S/N ratio to minimize the variations in the response. Otherwise, model the process through:

- Developing empirical models to express the complex relationship between decision and response variables based on prevailing constraints and assumptions need to be applied. The type of optimization modeling techniques used to express the objective function determines its accuracy and the possibility of reaching a global optimum solution. Therefore, a great attention has to be made to find a model expressing the case with simplest form

and highest possible precision. Statistical regression, neural networks and fuzzy set theory will be useful at this stage.

- Performing FEM analysis. FEM can provide a more comprehensive approach than the empirical ones as it can more flexibly cope with the introduction of new machining methods, fast introduction of new tool materials and new tool designs, and the introduction of an ever widening spectrum of work materials. It can also act as a complementary approach to the empirical models with an exclusive capability to predict what could happen during turning processes.

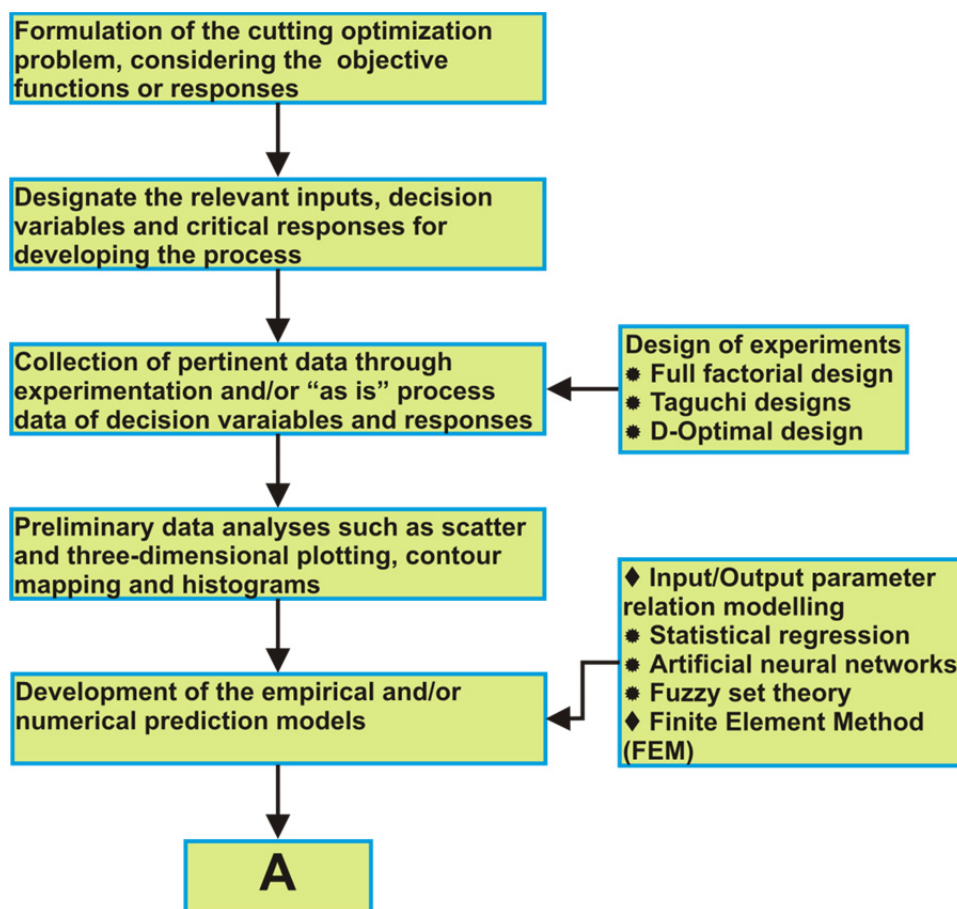


Figure 2.21: A systematic framework for modeling of cutting processes.

Following the selection of the suitable approach for modeling, the model(s) has to be verified and validated. Verification refers to the processes and techniques that the model developer uses to assure that his or her model is correct and matches any agreed-upon specifications and assumptions. While validation refers to the processes and techniques that the model developer, model customer and decision makers jointly use to assure that the model represents the real system (or proposed real system) to a sufficient level of accuracy. It should also be noted

that no model is ever 100% verified or validated. The latter is not an absolute. Any model is a representation of a system, and the model’s behavior is at best an approximation to the system’s behavior. When loosely saying that a model has been verified or validated, it means that a series of tasks have explicitly being carried out to verify and validate our model to the degree necessary for practical purposes [Cars02].

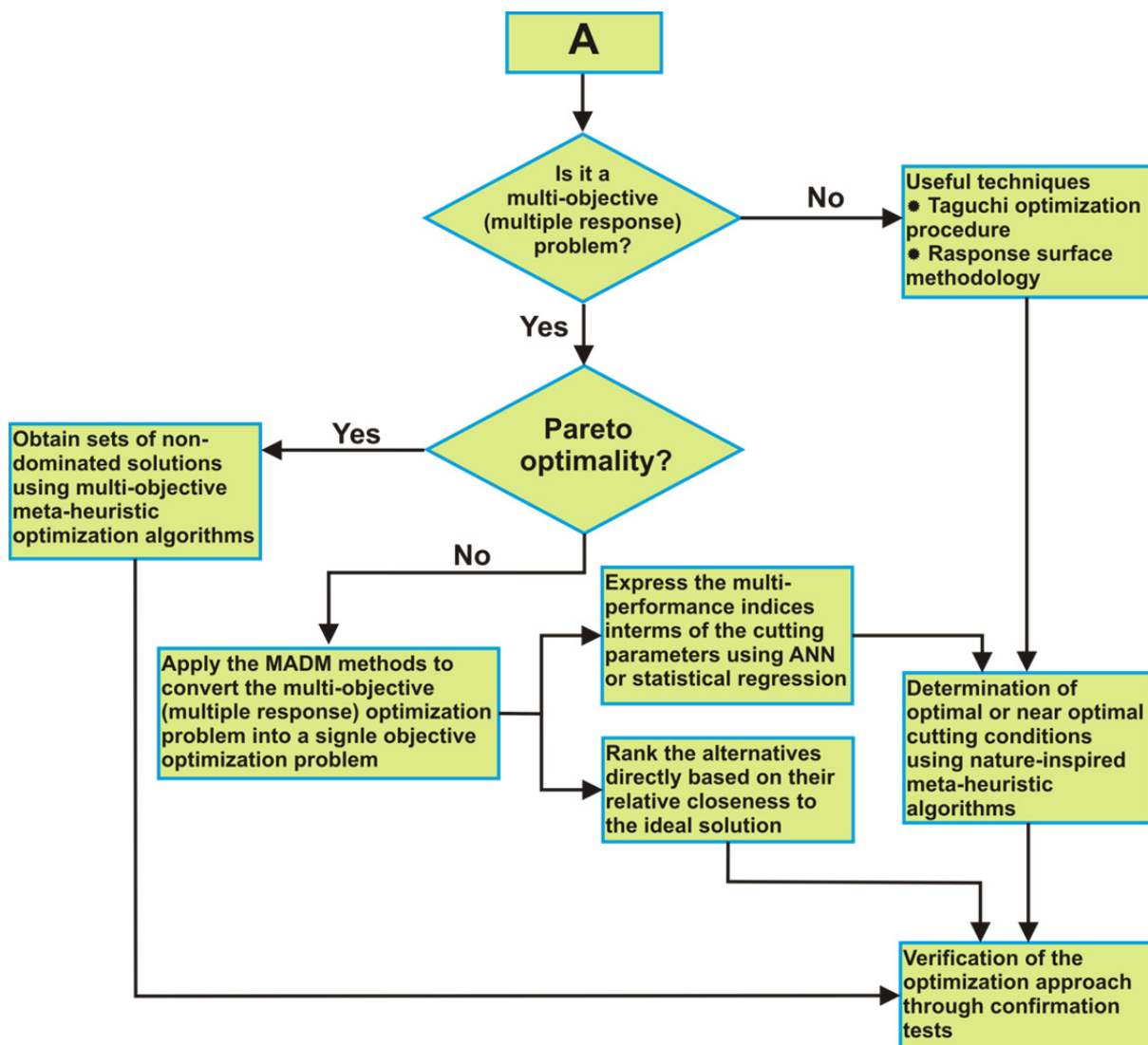


Figure 2.22: A systematic framework for optimization of cutting processes.

Step 6: Select the suitable optimization approach based on the form and number of objective function (response). Optimization can be broadly classified into mono and multiple objective optimization processes. Conventional optimization procedure such as Taguchi method and RSM or non-conventional optimization procedures such as meta-heuristic optimization algorithms can be dedicated to solving single objective optimization problems. However, when the objectives are more than one, multiple criteria decision analysis can be applied. Based on

the predetermination and limitations on the number of decision alternatives, the optimization problem can be solved employing a typical multi-objective optimization algorithm or a MADM method. When multiple near optimal solutions are necessary, nature inspired multi-objective optimization algorithms such as MOBA can be utilized. However, when the number of decision alternatives is pre-determined, MADM methods should be employed. The outcome of the MADM methods can be related to the decision variables using input/output process parameter relationship modeling techniques and further optimized as a mono-objective optimization problem using meta-heuristic or any other optimization algorithms.

Step 7: Conduct confirmation tests to verify the optimized process parameter(s).

3 Experimental details

The four major sections of this chapter describe the technical and experimental fundamentals of the present dissertation. In the first section, mechanical properties and chemical compositions of the adopted workpiece materials is briefly described. Additionally, results of JMatPro's software to predict temperature-dependent mechanical and physical behavior of the workpiece materials are presented. In the second section, a brief description of the involved cutting tools and machine tool is given. The utilized DOE techniques to plan the experiments are reported in the third section of the present chapter. The last section is dedicated to the experimental techniques employed to measure the machining performance characteristics.

3.1 Workpiece materials

3.1.1 Mechanical properties and chemical compositions

Altogether, three grades of stainless steels are used, namely austenitic EN 1.4404 (or AISI 316L), standard duplex EN 1.4462 (or SAF 2205) and super duplex EN 1.4410 (or SAF 2507). The first grade which is chosen as benchmark for machinability comparison analyses is an extra low carbon modification of type 1.4401. EN 1.4404 is a molybdenum-containing austenitic stainless steel intended to provide improved corrosion resistance relative to type 1.4307 in moderately corrosive process environments, particularly those containing chlorides or other halides. It has been used in handling many chemicals used by the process industries, including pulp and paper, textile, food, pharmaceutical, medical, and other chemical processing equipment. EN 1.4462 with equal amounts of ferrite and austenite is a duplex stainless steel that exhibits approximately two times higher mechanical strength, lower thermal expansion, better corrosion resistance and higher thermal conductivity than EN 1.4404. The material is suitable for use in production tubing and flow lines for the extraction of oil and gas from sour wells, in refineries and in process solutions contaminated with chlorides. The good mechanical and corrosion properties make EN 1.4462 an economical choice in many applications by reducing the life cycle cost of the equipment. Additionally, EN 1.4410 is also ferritic-austenitic stainless steel. It combines the most desirable properties of both ferritic and austenitic steels. The higher chromium and molybdenum contents provide higher mechanical strength, resistance to pitting, crevice, and corrosion resistance than type 1.4462. The duplex

microstructure results in good resistance to stress corrosion cracking. EN 1.4410 can be used in dilute hydrochloric acid. It is specially designed for service in aggressive chloride-containing environments. Typical applications fields are oil and gas industry, food industry, petrochemical industry and refineries, pulp and paper industry, chemical industry, seawater cooling, salt evaporation industry, desalination plants, geothermal wells and mechanical components requiring high strength [ArDe09, Fran08].

Finally, the chemical compositions and mechanical properties of workpiece materials are shown in Table 3.1 and Table 3.2, respectively. It is worth pointing out that the effect of different chemical elements, mechanical and physical properties on the machinability performance of stainless steels has been evaluated by Bertelli et al. [BCMC05].

Composition	EN 1.4404 % weight	EN 1.4462 % weight	EN 1.4410 % weight
Fe	68.893	67.583	62.703
C	0.008	0.018	0.015
Cr	16.74	22.42	24.92
Ni	10.19	5.44	6.91
Mo	2.02	3.12	4.06
Mn	1.75	0.84	0.75
Si	0.25	0.37	0.25
P	0.032	0.025	0.021
S	0.025	0.0033	0.0007
N	0.035	0.18	0.3
Cu	-	-	0.1
V	0.057	-	-

Table 3.1: Chemical composition of the workpiece materials.

Composition	Unit	EN 1.4404	EN 1.4462	EN 1.4410
Yield strength	MPa	264	514	579
Hardness	HB	148	212	236
% Elongation	-	58%	41%	40%

Table 3.2: Mechanical properties of the workpiece materials.

3.1.2 Temperature-dependent physical and mechanical properties of the workpiece materials

In the incoming subsections, the essential temperature-dependent physical and mechanical properties intended for numerical simulation of cutting DSSs is briefly described.

3.1.2.1 Temperature-dependent Young's modulus of elasticity

Young's modulus of elasticity is an elastic material property of solids. It strongly depends on temperature and directly influences the values of the element stiffness matrix. For the applied cutting materials the Young's modulus of elasticity decreases if the temperature is increased. The dependency relation of Young's modulus on the temperature for EN 1.4462 and EN 1.4410 DSS grades is generated by JMatPro software and shown in Figure 3.1(a).

Unfortunately, modulus of elasticity is inversely proportional to the temperature. This will lead to an extrapolation that could return negative modulus of elasticity, especially at high temperatures, and consequently causes the simulation to shut down. Therefore, it is recommended to prevent the simulation from uncontrolled extrapolation, so that higher temperatures do not lead to further decrease of the modulus.

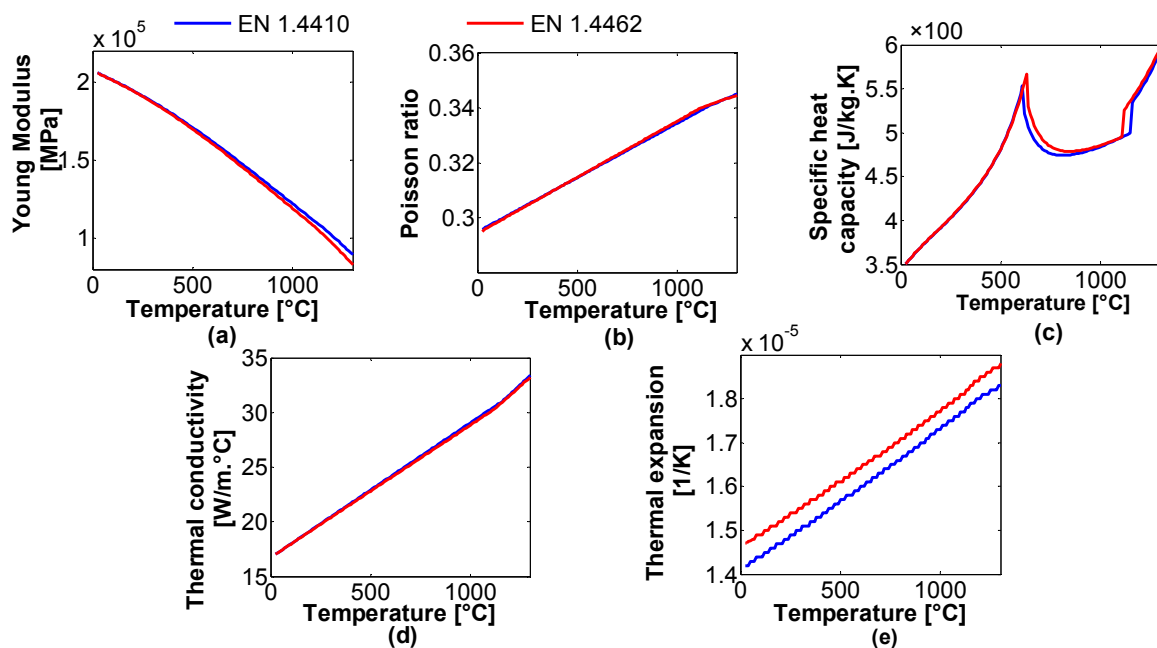


Figure 3.1: Dependence of the physical and mechanical properties of DSS on the temperature.

3.1.2.2 Temperature-dependent Poisson ratio

Poisson's ratio is one of the mechanical parameters which are required to fully describe the elastic property of the material. Poisson's ratio is defined as the ratio of the negative of transverse strain to the strain in the longitudinal direction. It is also a measure of material's relative resistance to dilatation and shearing. It has a value between 0 and 0.5 depending on the compressibility of the material [FAMS12]. The Poisson's ratio dependence on temperature for DSSs is shown in Figure 3.1(b).

3.1.2.3 Temperature-dependent specific heat capacity

In machining and forming, the lower the specific heat of a certain material, the higher the temperature will rise [YoEA11]. When different materials are machined with the same tool, cutting fluid and feed rate, the proportionality relation of temperature generated will be as per the following expression:

$$\bar{\theta}_T \sim k_c \left[\frac{v_c f_r}{k_{th} \rho_m C_p} \right] \quad (3.1)$$

where $\bar{\theta}_T$ is the mean tool face temperature; k_c is the specific cutting pressure; k_{th} is the thermal conductivity; ρ_m is the density and C_p is the specific heat capacity of the workmaterial [Shaw89]. In Figure 3.1(c), the specific heat capacities for the described DSSs as functions of temperature are visible.

3.1.2.4 Temperature-dependent thermal conductivity

When a material is deformed elastically, the energy required for the operation is stored in the material as strain energy, and no heat is generated. However, when a material is deformed plastically, most of the energy used is converted into heat. In metal cutting, the material is subjected to extremely high strains, and elastic deformation forms a very small proportion of the total deformation; therefore, it may be assumed that all the energy is converted into heat. Heat generation in metal cutting leads to temperature rise at the tool-chip interface. Among the factors that affect the cutting temperature, heat dispersion into the work and thickness of the tensile layer in the cutting process is thermal conductivity. Materials with higher thermal conductivity are responsible for production of lower temperature at cutting edge. Thermal conductivity (k_{th}) has a significant effect on the thickness of the tensile layer, where higher k_{th} results in thicker tensile layers [Jkau08]. As expected, the thermal conductivity is predicted to be mainly affected by the temperature. Figure 3.1(d) shows the effects of temperature on the thermal conductivity of DSSs.

3.1.2.5 Temperature-dependent coefficient of thermal expansion

DSSs have lower thermal expansion coefficients than austenitic stainless steels, similar to those of carbon steel and can therefore offer certain design advantages. Thermal expansion

coefficients have also shown dependence on the temperature as can be observed in Figure 3.1 (e).

In addition to the flow stress curves (shown in Figure 2.11), aforementioned physical and mechanical properties of the workpiece materials are expected to affect the outcome of the FEM simulations substantially. Therefore, a great deal of attention is needed to be paid when entering the data to the material module of the utilized FEM software.

3.2 Machine tool and cutting tool

A CNC lathe CTX 420 Linear V5 with maximum drive power 25kW and a speed range of 35-7000rpm is used to perform the experiments. In Figure 3.2, a brief description of the machine and its technical data are presented.

Recommended by SANDVIK Coromant, for medium-duty turning operations of stainless steels, negative 80° rhombic-shape coated carbide inserts with ISO codes of CNMG 120408-MM 2025 and CNMG 120408-QM 2025 are used throughout most of the empirical investigations. The basic difference between the two inserts lies in the employed chip breaker geometries. The MM designation has a sharp positive edge and open chip breaker which promotes low cutting force and more stable cutting operation. The QM designation has also a positive edge but $5-7^\circ$ less in sharpness. It can be considered as an alternative solution to the chip-breaker geometry MM when more machining stability is needed. Both inserts have a $5.5 \mu\text{m}$ thick multilayer chemical vapor deposition (CVD) coating ($\text{TiN}/\text{TiCN}/\text{Al}_2\text{O}_3$) on a cemented carbide substrate. The CVD coating consists of a thick, moderate temperature chemical vapor deposition of TiN for wear resistance and with low coefficient of friction, TiCN for wear resistance and thermal stability and Al_2O_3 for heat and crater wear resistance. The overall performance of the inserts is expected to show excellent resistance to both mechanical and thermal shock. On the other hand, in order to facilitate the optimization of insert shape and chip breaker geometry through numerical investigations, rhombic cemented carbide of ISO designation; CNMA 120412-IC20 is employed. IC20 is an uncoated carbide grade suitable for semi-finishing, finishing and semi-roughing of aluminum, cast iron and stainless steel. All the inserts were mounted on a right hand style PCLNL-2525M-12 ISO type tool holder with tool geometry as follows: including angle = 80° , back rake angle $\alpha_n = -6^\circ$, clearance angle $\gamma_c = 5^\circ$ and approach angle = 95° .



Manufacturer	Gildemeister
Model	CTX 420 Linear
Year of manufacturing	2003
Control	
Name	Sinumerik 840D power line
Manufacturer	Siemens
Kind	3D CNC control
Working area	
Swing diameter over guide ways	680 mm
Swing diameter over transverse guide ways	565 mm
Clamping chuck diameter max	250 mm
Main drive	
Type pf main drive	AC
Drive power (100% DC)	25 kW
Drive power (40% DC)	35 kW
Speed range	35-7000 rpm
Max torque (40%DC)	370 Nm
Slide	
Longitudinal stroke	635 mm
Transverse stroke	185 mm
Rapid transverse in X	60 m/min
Rapid transverse in Z	45 m/min
Tool holder	
Number of tool stations	12
Shank diameter according to DIN 69880	40 mm
Turning speed max	-4500 rpm
Power max	4.8 kW
Floor space and weight	
Dimensions (L*W*H)	4.9*2.5*2.1 mm
Weight approximately	6500 kg

Figure 3.2: Utilized machine tool to perform cutting operations.

3.3 Design of experiments (DOE)

An experiment takes a central place in science, particularly nowadays, due to the complexity of problems science deals with. The question of efficiency of using an experiment is therefore imposed. J. Bernal has made estimation that scientific research is organized and done fairly chaotically so that the coefficient of its usability is about 2%. To increase research efficiency, it is necessary to introduce something completely new into classical experimental research. One kind of innovation could be, to apply statistical mathematical methods or to develop design of experiments. DOE is a planned approach for determining cause and effect relationships [Lazi06].

In machining processes, when the objective is to find the correlation between the response(s) and the control factors included, it is possible to plan the experiments using DOE approach so as to reduce the number of experiments, which in turn reduces the time and cost involved in the experimentation. All the factors included in the DOE are varied simultaneously. The influence of unknown or non-included factors is minimized by properly randomizing the experiment. Mathematical methods are used not only at the final stage of the study, when the evaluation and analysis of the experimental data are conducted, but also throughout all the stages of DOE, i.e. from the formalization of a priori information till the decision-making stage. This allows answering of important questions: “What is the minimum number of tests that should be conducted? Which parameters should be taken into consideration? Which method(s) is (are) better to use in the evaluation and analysis of experimental data [Asta06, Mont09]?”

Based on the general purpose of experimentation, which essentially included the development of modeling and/or optimization of machining, the following DOE approaches have been applied in the present dissertation:

3.3.1 Full factorial design

A full factorial design (FFD) includes all possible combinations of the levels for all control factors. It allows the study of the effect of each control factor on the response variable, as well as the effects of interactions between control factors on the response variable. In the early stages of experimental work, FFD has been applied to

- determine the specific cutting pressure $k_{c1.1}$,
- define sets of non-dominated optimal straight turning solutions using MOBA,

- draw the chip breaking charts and
- estimate the UCI of constant cutting speed facing of duplex and austenitic stainless steels.

The experimental factors and their levels for the first two and last two applications are summarized in Table 3.3 and Table 3.4, respectively.

Control factors	Symbol	Unit	Level					
			1	2	3	4	5	6
Cutting speed	v_c	m/min	100	180				
Feed rate	f_r	mm/rev	0.15	0.2	0.25	0.3	0.35	0.4
Cutting depth	a_p	mm	1					
Cooling medium	CM	-	Dry	Wet				

Table 3.3: Control factors and levels selected in straight turning of DSSs.

Control factors	Symbol	Unit	Level						
			1	2	3	4	5	6	7
Feed rate	f_r	mm/rev	0.1	0.175	0.25	0.325	0.4		
Depth of cut	a_p	mm	0.5	1	1.5	2	2.5	3	3.5

Table 3.4: Control factors and levels selected in constant cutting speed facing of duplex and austenitic stainless steels at.

3.3.2 Taguchi designs

To estimate the effects of control factors on the response mean and variation, Taguchi designs use orthogonal arrays. The latter refers to a design which is balanced so that factor levels are weighted equally. Hence, each factor can be analyzed independently of all the other factors, so the effect of one factor does not affect the estimation of other factors. This can effectively reduce the time and cost associated with the experiment. Therefore, they have been extensively applied for conducting experiments. The applications of OAs include:

1. Optimization surface quality characteristics in constant cutting speed facing of austenitic and duplex stainless steels using $L_{16} (4^5)$ OA. Table 3.5 summarizes the control factors and levels planned for this objective

Control factors	Symbol	Unit	Level			
			1	2	3	4
Cutting speed	v_c	m/min	50	100	150	200
Feed rate	f_r	mm/rev	0.1	0.25	0.4	0.55
Depth of cut	a_p	mm	0.5	1.5	2.5	3.5

Table 3.5: Control factors and their levels chosen to optimize surface quality characteristics in constant cutting speed facing of duplex and austenitic stainless steels.

2. Multiple performance optimization in constant cutting speed facing of austenitic and duplex stainless steels using $L_{25} (5^5)$ OA using Taguchi-VIKOR-Meta-heuristic concept. It is worth mentioning here that the second column in the orthogonal array is dedicated to the interaction effects of cutting speed and feed rate as this interaction is expected to have substantial effects on some of the considered performances. Table 3.6 gives the control factors and their chosen levels designed for this purpose.

Control factors	Symbol	Unit	Level				
			1	2	3	4	5
Cutting speed	v_c	m/min	40	80	120	160	200
Feed rate	f_r	mm/rev	0.1	0.175	0.25	0.325	0.4
Depth of cut	a_p	mm	0.5	1	1.5	2	2.5

Table 3.6: Control factors and their levels chosen to apply Taguchi-VIKOR-Metaheuristic concept in optimizing the cutting of duplex and austenitic stainless steels.

3. Inverse identification of FEM input parameters and Taguchi-based FEM optimization of straight turning DSSs. In the first stage, $L_{18} (2^1 \times 3^7)$ is proposed to conduct the FEM simulations in order to inversely identify the FEM input parameters using the control factors and levels shown in Table 3.7.

Control factors	Symbol	Unit	Level		
			1	2	3
Thermal contact conductance	h_{tc}	N/(mm.sec.K)	100	1000	
Cutting speed	v_c	m/min	80	160	240
Feed rate	f_r	mm/rev	0.15	0.225	0.3
Coulomb friction coefficient	μ_c	-	0.5	0.75	1
Shear friction coefficient	μ_s	-	0.6	0.9	1.2
Taylor-Quinney coefficient	κ_t	-	0.8	0.9	1
Reduction in flow stress	$\%p_r$	-	10	30	50
Critical damage value	$\%D_{crit.}$	MPa	50	100	150

Table 3.7: Control factors and levels planned to be inversely identified during 3D-FEM of cutting DSSs.

In the second stage of the numerical analyses, the mixed Taguchi design $L_{18} (2^1 \times 3^7)$ once again is suggested to optimize many categorical and numerical parameters during straight turning of DSSs. The 3D-FEM simulations are planned to optimize types of chip breaker, insert shapes, process conditions, cutting parameters and tool orientation angles utilizing the control factors and levels given in Table 3.8.

Control factors	Symbol	Unit	Level		
			1	2	3
Chip-breaker type	CB	-	M3M	PP	
Insert shape	$Geo.$	-	DNMG	CNMG	WNMG
Cooling medium	CM	-	Still air	Water	Cryogenic
Cutting speed	v_c	m/min	75	150	225
Feed rate	f_r	mm/rev	0.1	0.175	0.25
Normal rake angle	α_n	degree	0	-6	-12
Inclination angle	λ_i	degree	0	6	12

Table 3.8: Control factors and their levels planned to numerically optimize the cutting of DSSs.

3.3.3 D-Optimal design

In order to estimate the operational sustainability performance of cutting DSSs, D-Optimal design is proposed for conducting the experiments. The design is especially suitable for conditions when categorical factors are desired to be included in experimentation plans, models, the full quadratic models have to be obtained and existing designs have to be augmented. As with completely randomized designs, computer generated designs are available to optimize based on various criteria. If interest lies primarily in estimating the machining parameters and generate flexible designs that meet the needs of particular experimental design situations then the D-optimal criterion can be well adapted to this objective. Based on the practical considerations, numerical parameters such as cutting speed v_c , feed rate f_r , depth of cut a_p and total length of cut L_c , and categorical parameter such as process conditions have been selected as input factors to the experimental design. Table 3.9 presents the low and high levels of the involved numerical and categorical factors.

It's worth pointing out that using of the D-optimal design is often involved with insufficient dispersion due to fewer degrees of freedom; therefore, the design has been bulked up to total 48 runs, i.e., 24 run for each category. Design-Expert V8 statistical package has been used to obtain the D-optimal plan. The program has identified 113 candidate points for each of the 2 the process conditions for a total of 226, from which 36 points have been selected as a minimum for the expected non-linear model. Eight more runs with unique factor combinations to test lack of fit. Finally, 4 of the 44 points already identified have been replicated.

Control factors	Symbol	Unit	Level	
			Low	High
Cutting speed	v_c	m/min	75	200
Feed rate	f_r	mm/rev	0.1	0.25
Depth of cut	a_p	mm	0.5	1.5
Length of cut	L_c	mm	3	12
Process conditions	CM	-	Wet	Dry

Table 3.9: Upper and lower bounds of control factors intended for D-Optimal design of experiments.

3.4 Measurement of the machining performance characteristics

Qualitative assessment of machinability of any material can be easily appreciated. However, the quantitative assessment seems to be far more complex as there is no unique and unambiguous methodology applicable to all the combinations of cutting operations, cutting materials, tooling and cutting conditions. Accordingly, in order to quantitatively assess the machinability of DSSs, certain criteria (performance characteristics) have to be specified, measured and analyzed beforehand. The measurement procedure of such performance characteristics are described as below.

3.4.1 Measurement of cutting forces and effective cutting power

During the turning tests, the main cutting force (F_c), feed force (F_f), and thrust force (F_t), are measured using Kistler type 9129A three component piezo-electric dynamometer, which was connected to a charged Kistler type 5070A amplifier and personal computer through an analog to digital converter card. To obtain and record the force softly, Windows software for data acquisition and evaluation DynoWare type 2825A was installed. Before conducting the experiments, the lathe tool dynamometer was calibrated for data accuracy. A standard force of 100N was applied on the tool dynamometer and the forces were measured. Then the force data were compared with the standard applied force. The result of this pretest found that the tool dynamometer had errors, but within the acceptable limit.

On the other hand, the power consumed by the motor of a machine tool is composed of an effective and an idle component. Because of its proportionality to the torque emitted by the motor, the effective power is often used as a signal within the control system for quantifying the motor load. External effective-power modules are installed in machine tools between the

frequency converter and the motor. To read the current, hall sensors are used that measure the current along with its phasing via the magnetic field surrounding the conductor in a circular shape. The effective power is obtained from these using the Eq. 3.2 below [Kloc11].

$$P_e = \sqrt{3} U_l I_c \cos \varphi_a \quad (3.2)$$

where U_l is the line voltage in volts, I_c is the line current in ampere and $\cos \varphi_a$ is the power factor. The experimental set up is shown in Figure 3.3.

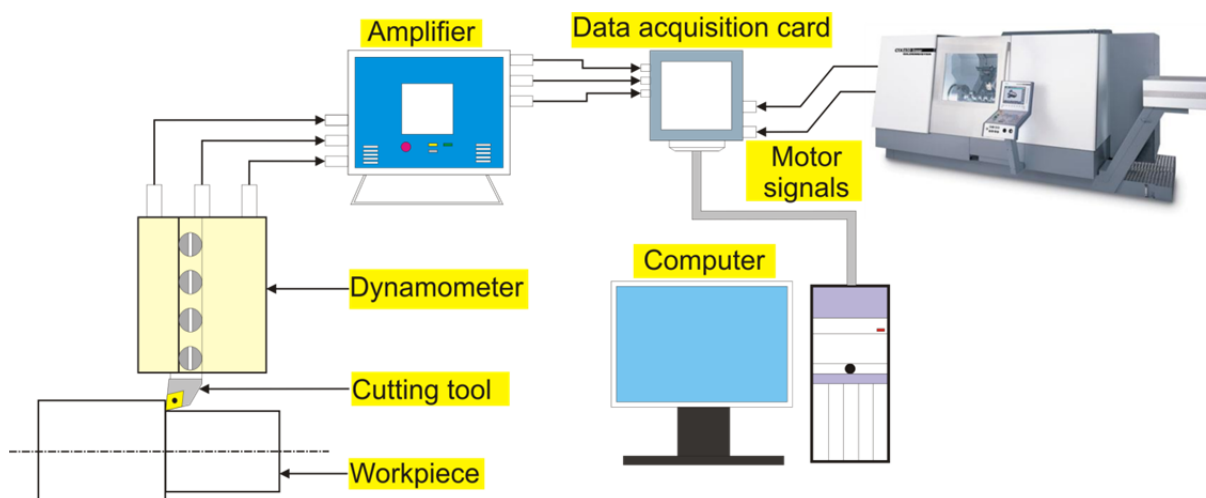


Figure 3.3: Experimental set-up for measuring cutting forces and cutting power.

3.4.2 Measurement of the chip volume ratio

During cutting tests, the metal chips posed great challenges to the machine tool and the workpiece. To deal with this problem, the chips are collected after each machining trial and later analyzed. Chip volume ratios (R) were then calculated by; a) measuring the mass of the sample chip, b) dividing the mass by density of the steels hence calculating the volume of the cut material prior to machining, c) gently placing the chips inside plastic bags, d) gently vacuum packaging which removed air from the package prior to sealing, e) measuring the volume of the gently packed chips using the water displacement procedure and f) dividing the volume of the gently packed chips by the volume of the cut material prior to machining, (refer to Eq. (1.10)). The ratio corresponds to the intended R .

3.4.3 Measurement of surface quality characteristics

The surface roughness values are measured immediately after the face turning process at three different locations on workpiece using Taylor-Hobson, Form Talysurf 120 Series 2 surface

roughness tester. The average of three Ra , Rz and Rt measurements according to the DIN EN ISO 3274 are recorded. The stylus tip angle and radius were 60° and $2\mu\text{m}$ respectively.

3.4.4 Measurement of the flank wear

The average VB and maximum VB_{max} width of flank wear (VB) are periodically measured during progressive tool-wear experiments using Leica MZ6 stereomicroscopes after every cutting pass of machining operation. The basic magnification range the microscope is 6.3x to 40x with a maximum magnification of 320x. It has been connected to a PC through Image Manager software for archiving and for post-processing the images. The adopted criterion for tool life on the coated carbide tools are $VB = 0.4\text{mm}$ or $VB_{\text{max}} = 0.6\text{mm}$ or catastrophic tool failure of the tool edge.

As an indirect tool wear monitoring technique, using measured signals of cutting forces offers many advantages like easy to measure and having a clear phenomenological relationship with tool wear. In terms of both magnitude and shape of the signals, the more the tool wears, the more the signals of worn tool differs from signals of sharp tool. As there is no agreement in which component of cutting force has the closest relationship with the tool wear, the resultant of cutting forces often adopted as an indirect wear signal. An example of indirect tool wear monitoring during wet constant cutting speed facing of EN 1.4404, EN 1.4462 and EN 1.4410 is depicted in Figure 3.4. Components of cutting forces have been measured and the resultant cutting forces are calculated employing Eq. (1.4). Tool life of coated carbide cutting tool with an ISO designation CNMG 120408-MM 2025 and cutting condition of $v_c = 300\text{m/min}$, $f_r = 0.1\text{mm/rev}$ and $a_p = 0.5\text{mm}$ has been estimated based on 0.4mm flank wear criteria. It can be obviously seen that the shapes of the R_c curves are similar to the typical wear curves of the cutting tools. Noteworthy, under similar cutting conditions, it can also be seen that the tool life when machining EN 1.4404 was almost triple that of EN 1.4410.

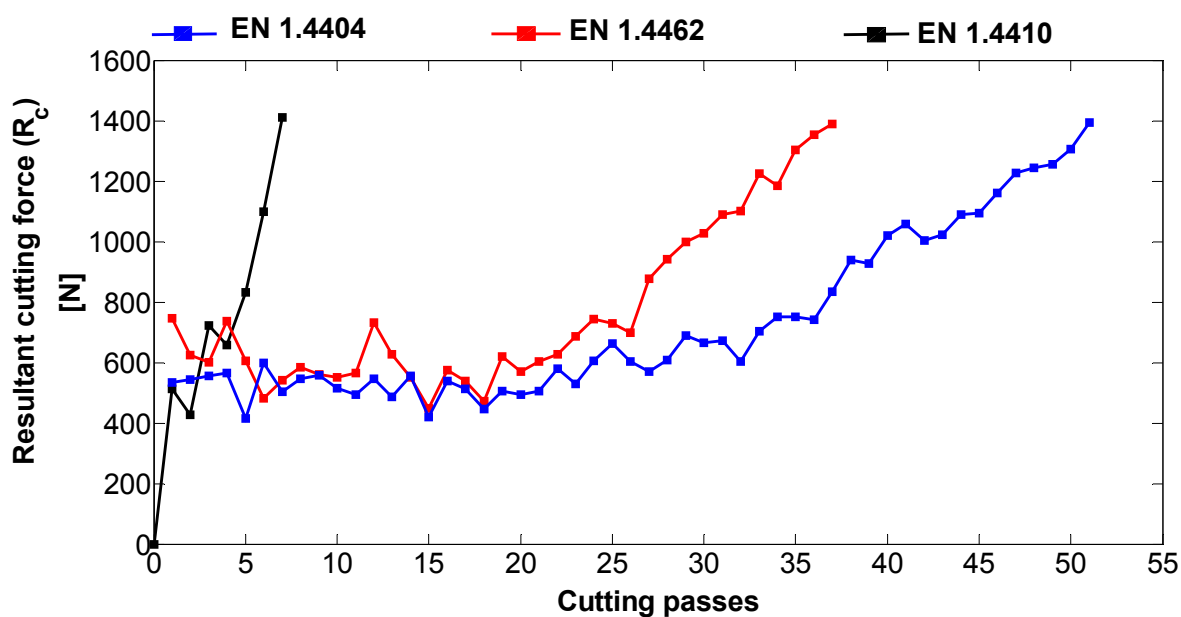


Figure 3.4: Progressive increase in resultant cutting force during face turning of stainless steels at 300m/min.

Owing to the dynamometer's relative high cost, negative impact on machining system rigidity, requirement of a wiring harness and extra space for installation, indirect tool wear monitoring systems such as acoustic emission, vibrations, cutting temperature, surface quality and signals from spindle or feed motors are used to monitor the tool wear. The latter have the advantage of simplicity in hardware implementation that does not interfere with the process and does not require high cost devices. Usually, spindle current signals correspond to torque, hence cutting force which is closely related to the cutting parameters. The signals can also be used for tool-breakage detection where the machining operation is interrupted after tool breakage. An example of adopting the consumed spindle motor current as an indirect tool wear monitoring technique is shown in Figure 3.5. Cutting tool, workmaterial, feed rate and depth of cut were all identical to the previous case except cutting speed which has been lowered to 50m/min. Results have shown that lowering cutting speed by six folds had remarkably increased the tool life of the mentioned workmaterials by almost 17, 19 and 40 folds, respectively.

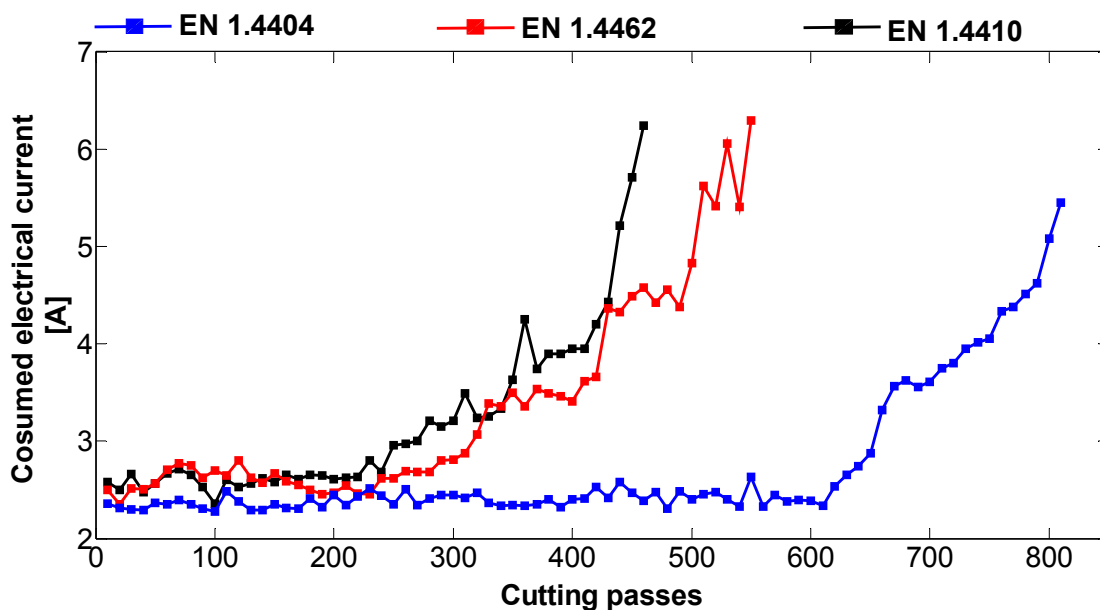


Figure 3.5: Progressive increase in electrical current consumption during face turning of stainless steels at 50m/min.

3.4.5 Infrared temperature measurement system

Although, infrared (IR) cameras are quite expensive, they remain one of the most promising solutions for temperature measurement since they allow for a non-contact, extensive measurement of temperature. Thus, the problem of perturbation of the heat flow in the tool and changes the results is avoided. The fast response of the IR camera lets high, cutting speeds to be used in machining experiments, since it can capture the transient changes and the stages of chip formation and entanglement around the workpiece, the tool holder and the tool post. In the present dissertation, high-resolution thermo-graphic camera of brand VarioCam head Hires 640 by InfraTec is used to film the chip formation and measure the chip temperature at a resolution of 640×480 pixels, spectral range of $7.5\text{-}14\ \mu\text{m}$, temperature measuring range $-40\text{-}1200^\circ\text{C}$, measurement accuracy of $\pm 2\%$ and an external data storage at 60 Hz on external computer via FireWire. The IR camera is placed straight above the rake face of the tool. The lens of the camera is protected against possible impacts of the chips flying about. The images in the films are examined and the mean of maximum temperature in the middle of the chips are recorded. A schematic diagram of the cutting temperature measurement system using IR camera is shown in Figure 3.6.

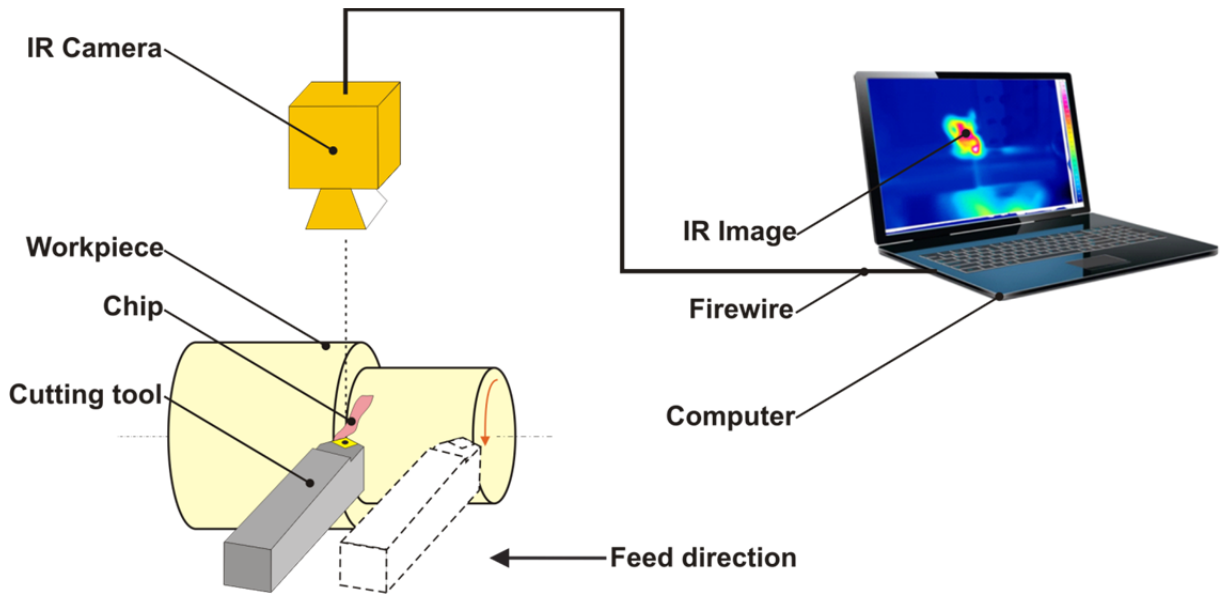


Figure 3.6: Experimental setup for temperature measurement in cutting.

3.4.6 Chip thickness and chip serration ratio

The serrated chip geometries, which were detected in some machining occasions, have to be correctly configured and measured. Among many chip-related measurements, maximum and minimum chip thickness and degree of serration are recorded using two different techniques. In the first, the collected chips are embedded in transparent epoxy, polished using increasingly finer diamond grit and etched in chemical solution. Despite the process time consuming nature and reduction of the 3D structures to 2D planes, this method enabled the ease tracings of the streamline of material flow and paths of the grains. In the second measurement technique, the chips are photographed and measured using a Leica MZ6 stereomicroscope. The average values of five consecutive chip thickness ratios (h_{\max_i} / h_{\min_i}) are measured and defined as the degree of serration:

$$H = \frac{1}{5} \sum_{i=1}^5 \frac{h_{\max_i}}{h_{\min_i}} \quad (3.3)$$

where h_{\max_i} and h_{\min_i} are the perpendicular distances measured from the bottom of the chip to the peaks and valleys respectively.

4 Experimental investigation and multi-objective optimization of turning DSSs: A case study

In this chapter, experimental investigations on turning EN 1.4462 and EN 1.4410 DSS grades with multi-layer coated carbide inserts are presented. Single-point wet and dry longitudinal turning tests of 55 mm diameter cylindrical bars are conducted as per Table 3.3. Performance characteristics such as cutting forces and tool wears are measured employing the measurement techniques described in the previous chapter. The parametric influences of cutting speed, feed rate and process conditions on the cutting performances such as resultant cutting forces and tool wear are analyzed and proper interim conclusions are drawn. Nature-inspired meta-heuristic Bat Algorithm is then employed to handle the multi-objective optimization of the conflicting performances. Finally, the optimum cutting condition for each process condition can be selected from calculated Pareto-optimal fronts by the user according to the planning requirements.

4.1 Pareto optimality

Multi-objective optimization problems are more complicated than single objective optimization as in many cases the decision maker has to find and/or approximate the Pareto optimality fronts. In addition, algorithms have to be modified to accommodate multi-objectives properly. The concept of Pareto optimum was formulated by Vilfredo Pareto in the 19th century, and constitutes by itself the origin of research in multi-objective optimization. A solution vector $u = (u_1, u_2, \dots, u_n)^T \in Y$ is said to dominate another vector $v = (v_1, v_2, \dots, v_n)^T$ if and only if $u_i \leq v_i$ for $\forall i \in \{1, 2, \dots, n\}$ and $\exists i \in \{1, 2, \dots, n\} : u_i < v_i$. In other words, no component of u is larger than the corresponding component of v , and at least one component is smaller. Similarly, we can define another dominance relationship \preceq by:

$$u \preceq v \Leftrightarrow u < v \vee u = v \quad (4.1)$$

It is worth pointing out that for maximization problems, the dominance can be defined by replacing $<$ with $>$. Therefore, a point $x^* \in Y$ is called a non-dominated solution if no solution can be found that dominates it [Coel99]. The Pareto front PF of a multi-objective can be defined as the set of non-dominated solutions so that

$$PF = \{ s \in S \mid \nexists s' \in S : s' \prec s \} \quad (4.2)$$

or in term of the Pareto optimal set in the search space

$$PF^* = \{ x \in Y \mid \nexists x' \in Y : \mathbf{G}(x') \prec \mathbf{G}(x) \} \quad (4.3)$$

where $\mathbf{G} = (G_1, G_2, \dots, G_K)^T$. To obtain a good approximation to Pareto front, a diverse range of solutions should be generated using efficient techniques [GuBa09, KoCS06].

In the present chapter, Bat Algorithm (BA) is extended to find and/or approximate Pareto fronts, hence solving multi-objective machining optimization problem.

4.2 Performance characteristics

4.2.1 Specific cutting pressures

The specific cutting pressure is often considered as an indication to the machinability of a given workmaterial. The higher the specific cutting pressure the lower is the machinability of the workmaterial. The specific cutting pressures for turning EN 1.4462 and EN 1.4410 were calculated from the cutting data employing Eqs. (1.6-8) and the results are shown in Figure 4.1. Based on a quick review of the results;

- No drastic difference between the cutting pressures of dry and wet conditions was observed. However, overall wet machining shows an improvement in the machining performance through lower cutting pressures.
- Generally, lower average values of the specific cutting pressures are noticed when cutting EN 1.4462 than EN 1.4410.
- The cutting pressures are generally showed a decreasing trend with increasing cutting speed and feed rate. The maximum values are located in low ranges of cutting speed and feed rate.
- Modified Kienzle's formula (Eq. (1.9)) can be applied to evaluate the parametric effects of cutting conditions on the cutting forces empirically. The model fitting has employed the least square method. Summary of models coefficients are listed in Table 4.1. It should be noted that the average at wet cutting is generally 5% lower than at dry cutting for both workmaterials and of turning EN 1.4410 is generally 25.281% higher than of turning EN 1.4462.

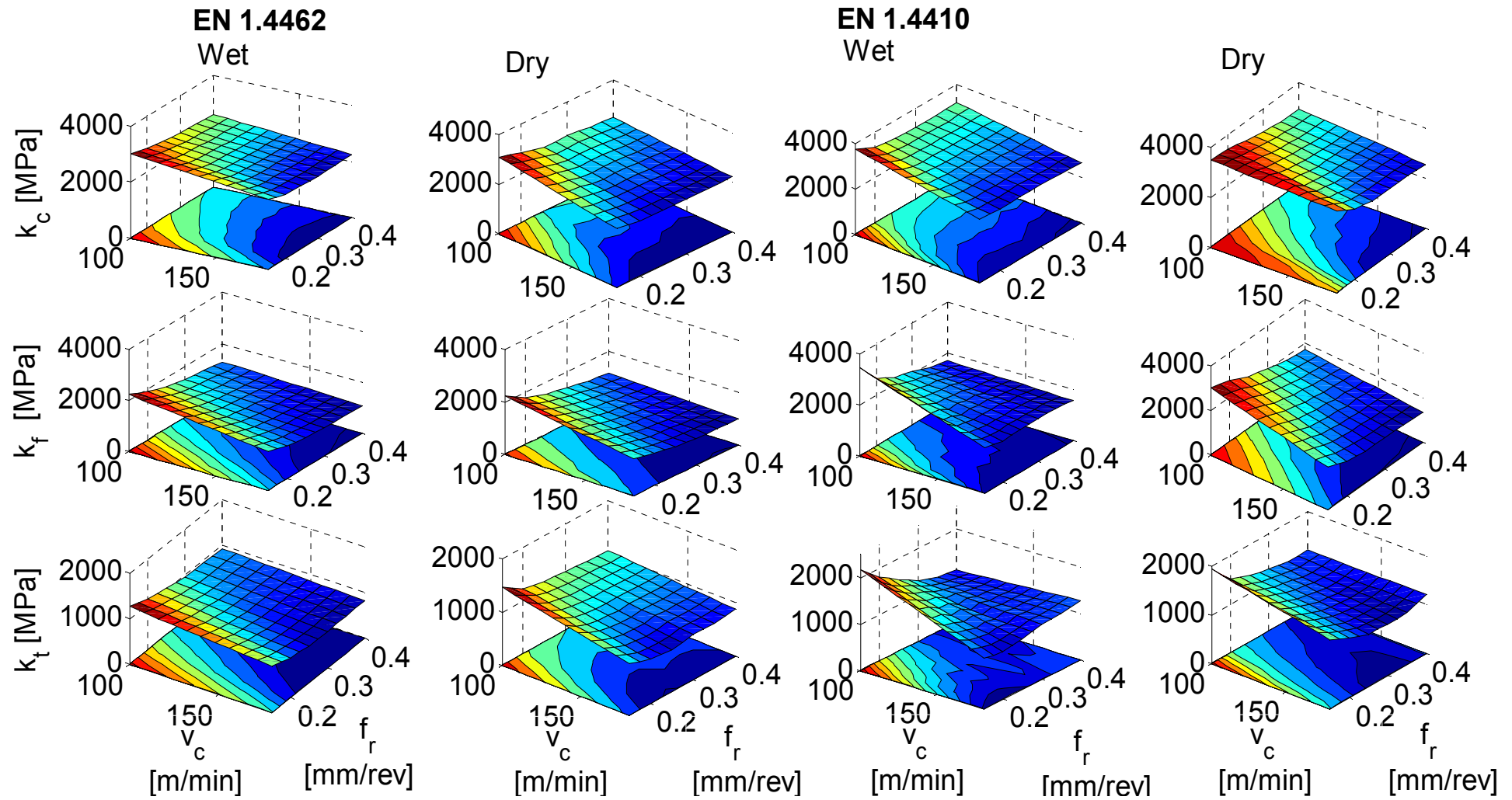


Figure 4.1: Computed specific cutting pressure.

Model	Process conditions	EN 1.4462			EN 1.4410		
		$k_{1,1}$ [MPa]	a	b	$k_{1,1}$ [MPa]	a	b
F_c	Dry	2366.8	-0.28495	0.10208	2920.01	-0.29361	0.07897
	Wet	2215.1	-0.26097	0.13359	2471.22	-0.26308	0.19012
F_f	Dry	851.82	-0.47921	0.47351	1182.12	-0.41215	0.46722
	Wet	737.12	-0.48811	0.53402	1126.13	-0.63874	0.50341
F_t	Dry	740.92	-0.27476	0.23299	920.84	-0.21903	0.31662
	Wet	899.16	-0.45785	0.18046	907.54	-0.22609	0.30137
R_c	Dry	2550.01	-0.32271	0.19634	3144.71	-0.31265	0.21344
	Wet	2431.4	-0.32448	0.21924	2811.09	-0.34563	0.28440

Table 4.1: Summary of the cutting force models coefficients.

To avoid misleading conclusions, the adequacy of the fitted models should be checked. Therefore, analysis of variance (ANOVA) for 95% a level of confidence was performed in order to estimate the predictive accuracy of the models and to determine the relative significances of the different factors. From the ANOVA shown in Table 4.2, it is apparent that almost all correlation coefficients are near from 1, showing that significant terms have been included in the model and that the model is capable of predicting the responses, P-value estimators are all close to zero (much lower than 0.05 corresponding to the confidence interval) which show the significant effect of factors on the corresponding response and F-values are much larger than one, which indicates that the factors have a significant effect on the response. Moreover, variations of the main, feed and thrust cutting forces towards cutting speed and feed rate are studied in each process conditions separately.

Model	Process Cond.	EN 1.4462				EN 1.4410			
		R^2	$R_{adj.}$	F - value	P - value	R^2	$R_{adj.}$	F - value	P - value
F_c	Dry	0.996	0.995	8.43e+03	7.83e-16	0.993	0.992	5.31e+03	6.25e-15
	Wet	0.991	0.988	4.01e+03	2.21e-14	0.994	0.993	7.90e+03	1.05e-15
F_f	Dry	0.964	0.955	1.66e+03	1.17e-12	0.842	0.807	3.50e+02	1.24e-09
	Wet	0.942	0.929	1.13e+03	6.58e-12	0.950	0.939	9.49e+02	1.43e-11
F_t	Dry	0.972	0.966	1.72e+03	9.91e-13	0.732	0.672	1.59e+02	4.14e-08
	Wet	0.965	0.958	1.06e+03	8.80e-12	0.884	0.858	4.57e+02	3.76e-10
R_c	Dry	0.989	0.986	3.87e+03	2.60e-14	0.962	0.953	1.12e+03	6.73e-12
	Wet	0.996	0.995	8.43e+03	7.83e-16	0.993	0.992	5.31e+03	6.25e-15

Table 4.2: Analysis of variance for cutting force models.

4.2.2 The width of maximum flank wear land (VB_{max})

The impacts of cutting parameters v_c and f_r , and process conditions on the VB_{max} are shown in Figure 4.2 and the summary of the findings are presented below.

- Based on the measurements of VB_{\max} with respect to the machining time, EN 1.4410 is considered more difficult-to-machine than EN 1.4462. For instance, in dry machining of EN 1.4410 at $v_c = 180$ m/min and $f_r = 0.35$ mm/rev, significantly higher wear rates thus shorter tool life, higher cutting temperature, higher cutting forces and higher energy consumption than machining EN 1.4462 was observed. Figure 4.3 presents the resulted wear patterns at different machining times. In Figure 4.4, the average value of recorded cutting forces in dry conditions after the first 60sec and 20sec and second 320sec and 40sec of machining EN 1.4462 and EN 1.4410 are illustrated, respectively.

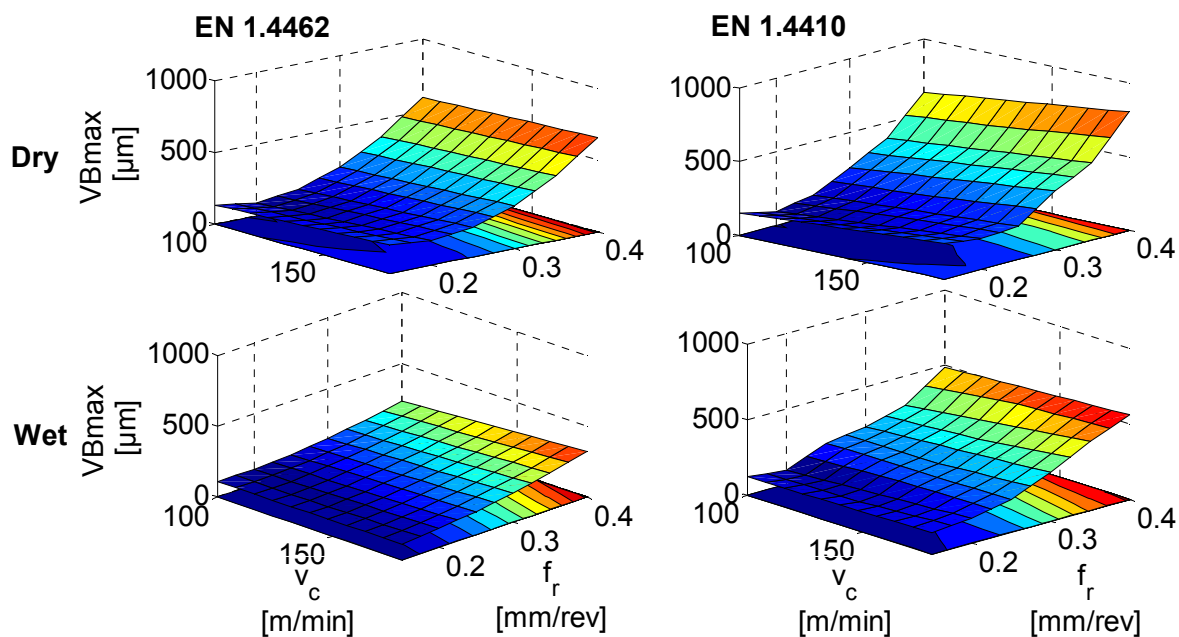


Figure 4.2: The width of maximum flank wear (VB_{\max}).

- The illustration of typical wear cases when machining DSSs are shown in Figure 4.5. It can be observed that in cases:
 1. Severe adhesion between the chip and the rake face of the tool (BUE) was visible throughout the worn crater area. High pressure and temperature encountered in machining ductile materials are the potential reasons behind this phenomenon. In Figure 4.5(a) examples of the BUE formation at dry cutting and cutting conditions of $v_c = 100$ m/min and $f_r = 0.30$ mm/rev, and cutting time of $t_c \approx 615$ sec for EN 1.4462 and $t_c \approx 406$ sec for EN 1.4410 are shown.

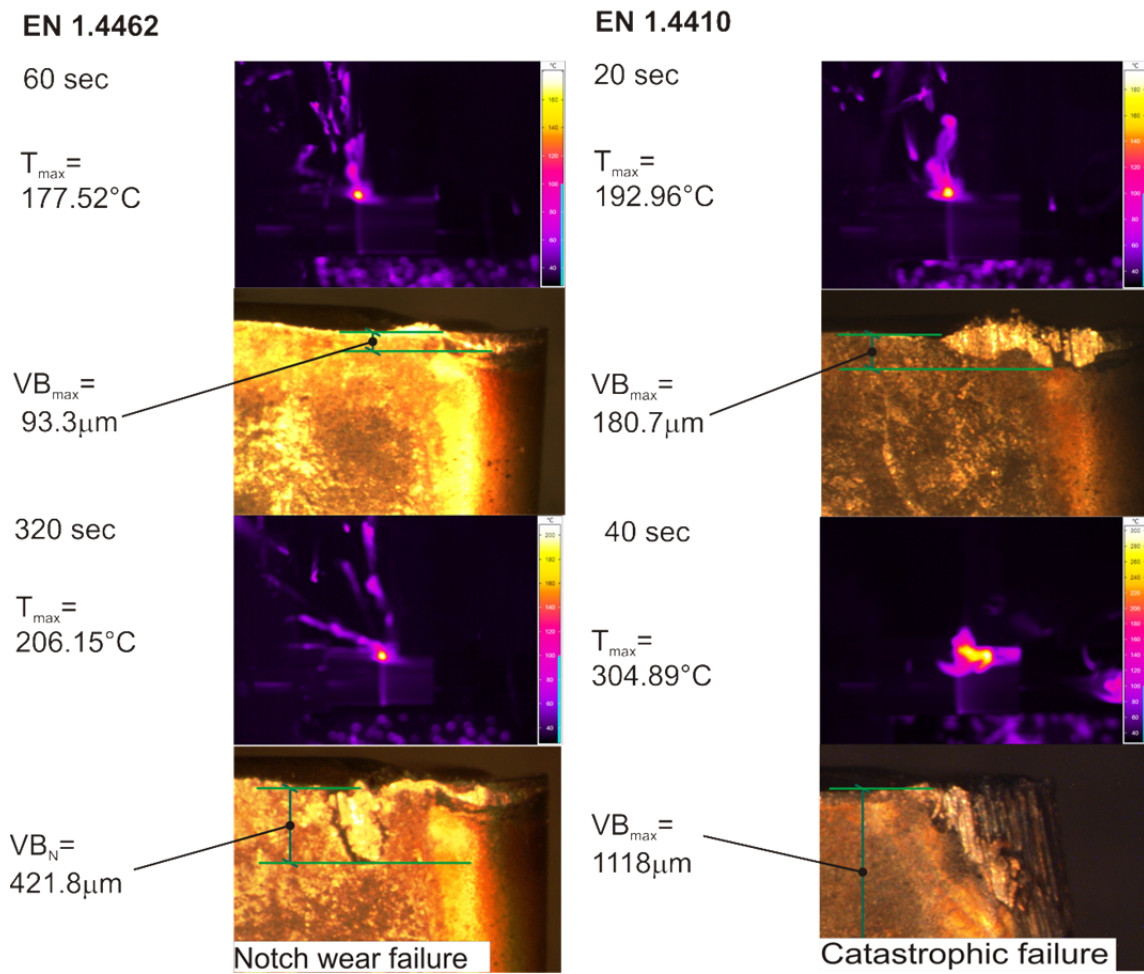


Figure 4.3: Progression of the maximum chip temperature and tool wear pattern with cutting time in dry cutting of DSSs using CNMG 120408-MM 2025 coated carbide tools at $v_c = 180 \text{ m/min}$ and $f_r = 0.35 \text{ mm/rev}$.

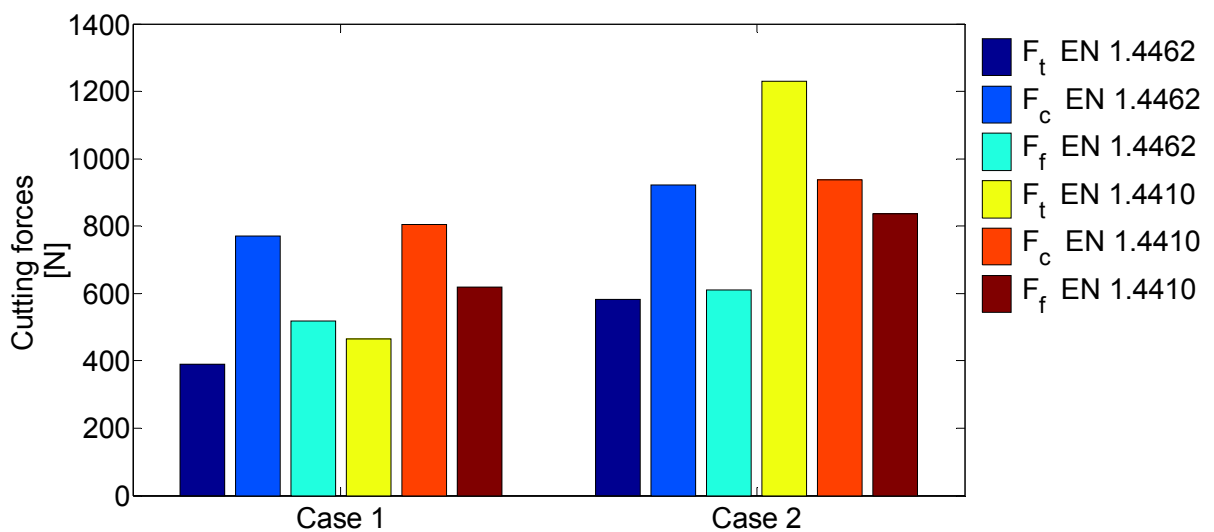


Figure 4.4: Variation of cutting forces with respect to the cutting time.

2. Regardless of the adopted process conditions, chipping of the cutting edge at high feed rate was often observed which has significantly contributed to the acceleration of tool failure. Heavy load and impact when the tool entered and/or extracted the workpiece are considered to be the basic cause of this type of tool failure. Figure 4.5(b) shows examples of the chip hammering at dry cutting of DSSs and cutting conditions of $v_c = 180$ m/min and $f_r = 0.30$ mm/rev, and cutting time of $t_c \approx 374$ sec for EN 1.4462 and $t_c \approx 103$ sec for EN 1.4410.

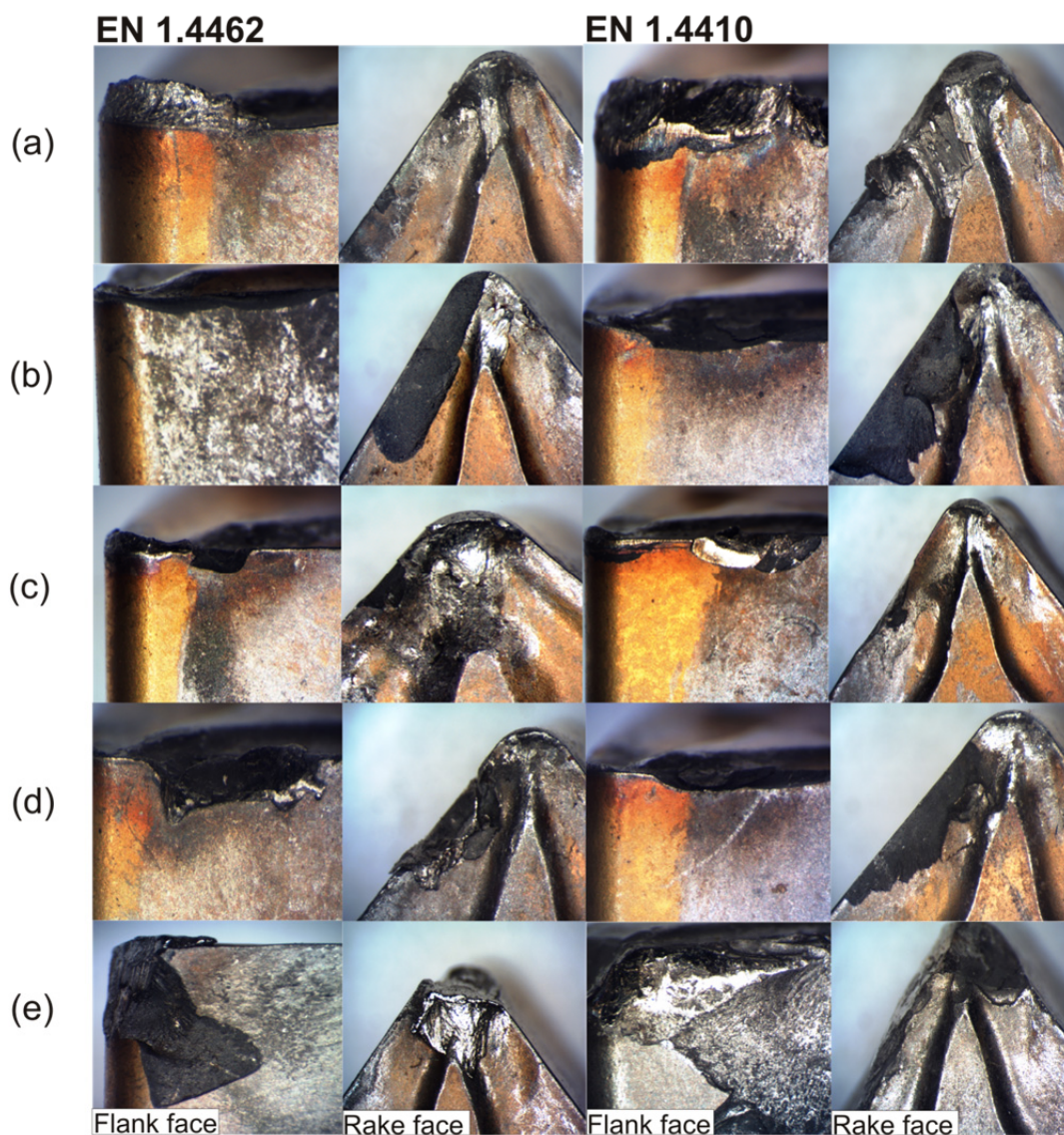


Figure 4.5: Wear patterns observed on the flank and rake face of cutting tools under dry and wet machining of DSSs using CNMG 120408-MM 2025 coated carbide tools.

3. The most dominant tool wear mode under low cutting speed conditions was the notch wear which was typically located near the depth of cut line. These notches acted as stress

and temperature raisers of the already high mechanical strength, strain hardening rate, fracture toughness and low conductivity DSSs chips. Flaking occurrence because of the concentrated thermal load is more possible there. Ultimately, the combination of notch wear and flaking caused the cutting edge to fail abruptly. Figure 4.5(c) illustrates examples of the notch wear at wet cutting of DSSs and cutting conditions of $v_c = 100 \text{ m/min}$ and $f_r = 0.20 \text{ mm/rev}$ and cutting time of ($t_c \approx 1141 \text{ sec}$ for EN 1.4462 and $t_c \approx 922 \text{ sec}$ for EN 1.4410).

4. Another form of the main cutting edge damage is caused by the unfavorable chip morphology and chip flow. Cutting DSSs at low cutting speed and feed rate has contributed in the formation of strong ribbon and snarled chips with dominant side-curl flow. The chips were entangled around the cutting tool, tool post and workpiece and damaged to the cutting edge and the workpiece surface. The damage is often propagated along the main cutting edge of the tool with cutting time and had exceeded 5mm length of damage especially in feed rate ranges of 0.15-0.20mm/rev. Figure 4.5(d) presents examples of the spalling of the cutting due to the continuous chip impact during dry cutting of DSSs and cutting conditions of $v_c = 100 \text{ m/min}$ and $f_r = 0.15 \text{ mm/rev}$ and cutting time of $t_c \approx 1020 \text{ sec}$ for EN 1.4462 and $t_c \approx 728 \text{ sec}$ for EN 1.4410.
 5. In addition to the combined notching and flaking effects, nearly equal proportions of soft ferrite and hard austenite grains in the DSS structure, makes the cutting tool alternate cutting between soft and hard grains, this leads to an automatic tendency to initiate chatter in the cutting system and promote the catastrophic failure of the cutting tools. Examples of the flaking layers beneath the flank wear land and plastic deformation of the nose is depicted in Figure 4.5(e) during wet cutting of DSSs and cutting conditions of $v_c = 180 \text{ m/min}$ and $f_r = 0.35 \text{ mm/rev}$ and cutting time of $t_c \approx 482 \text{ sec}$ for EN 1.4462 and $t_c \approx 186 \text{ sec}$ for EN 1.4410.
- To model VB_{\max} , an empirical formula described by the following equation is applied:

$$VB_{\max} = c_1 + c_2 v_c + c_3 f_r + c_4 f_r^2 + c_5 v_c f_r + c_6 f_r^3 + c_7 v_c f_r^2 \quad (4.4)$$

where c_{1-7} are model constants calculated using Eqs. 2.1-10. To check for the adequacy of derived models, ANOVA for 95% confidence interval has been applied. Table 4.3 summarizes the values of correlation coefficients and adequacy criterion. The R^2 of the mod-

els are in reasonable agreement with the R_{adj} . The large F – value and small P – value of the models imply that they are significant.

4.3 Bat Algorithm for multi-objective optimization of turning DSSs.

The objective is to simultaneously minimize the resultant cutting force, and the width of maximum flank wear. Thus, the mathematical formulation of the current optimization problem can be stated as follow:

$$\begin{aligned} \text{Min} : R_c(v_c, f_r) \\ \text{Min} : VB_{\max}(v_c, f_r) \end{aligned} \quad (4.5)$$

For the sake of simplicity, a weighted sum to combine above objectives into a G single objective is proposed as follow:

Process Conditions	EN 1.4462		EN 1.4410	
	Dry	Wet	Dry	Wet
c_1	628.46	304.86	655.08	558.46
c_2	0.33901	-0.88715	1.4101	-1.3256
c_3	-6266.4	-1948.1	-6873.2	-5051.6
c_4	16459	4507.9	19258	14408
c_5	4.6714	6.6947	-3.2372	12.517
c_6	-3703.7	-1851.9	-8666.7	-7777.8
c_7	-8.9286	-4.4643	11.964	-15.179
Check for models adequacy				
R^2	0.991	0.990	0.987	0.962
R_{adj}	0.985	0.975	0.966	0.943
F - value	7.42e+03	3.99e+03	1.42e+2	0.47e+2
P - value	1.05e-09	4.95e-09	2.04e-05	3.05e-4

Table 4.3: VB_{\max} models coefficients along with the model adequacy tests.

$$G = w_1 R_c + w_2 VB_{\max} \quad (4.6)$$

As the weights w_1 and w_2 are generated randomly from a uniform distribution, it is possible to vary the weight with sufficient diversity so that the Pareto front can be approximated correctly. The proposed MOO algorithm the optimization is implemented Matlab. The computing time was generally less than a minute on an Intel(R) Core™2 Quad CPU @2.66 GHz and

3.49 GB RAM. It was found that the best population size (n), loudness reduction (A_i), and pulse reduction rate (P_r) were 20, 0.8 and 0.8 respectively. Based on the previous approximations and idealizations, the basic steps of the MOBA can be summarized as the pseudo code shown in Figure 4.6.

```

Objective functions  $R_c$  and  $VB_{\max}$ ,  $x = (x_1, \dots, x_d)^T$ 
Initialize the bat population  $x_i$  ( $i = 1, 2, \dots, 20$ ) and  $v_i$ 
for  $j = 1$  to 20 (points on Pareto fronts)
    Generate two weights  $w_{1,2} \geq 0$  so that  $w_1 + w_2 = 1$ 
    Form a single objective  $G = w_1 R_c + (1 - w_1) VB_{\max}$ 
    while ( $t <$  Max number of iterations)
        Generate new solutions and update by Eqs. (2.55-57)
        if ( $\text{rand} > P_r$ )
            Random walk around a selected best solution
        end if
        Generate a new solution by flying randomly
        If ( $\text{rand} < A_i$  &  $f_q(x_i) < f_q(x^*)$ )
            Accept the new solutions,
            and increase  $P_r$  & reduce  $A_i$ 
        end if
        Rank the bats and find the current best  $x^*$ 
    end while
    Record  $x^*$  as a non-dominated solution
end
Postprocess results and visualization

```

Figure 4.6: Multi-objective Bat Algorithm (MOBA).

The optimum results should not violate the following:

1. Arithmetic average roughness (Ra)

$$Ra = \frac{0.032 f_r^2}{r_\varepsilon} \leq 2 \mu m \quad (4.7)$$

where r_ε is the tool nose radius for CNMG 120408-MM 2025 coated carbide cutting tools (i.e. $r_\varepsilon = 0.8\text{mm}$).

2. Cutting parameters upper and lower bounds as per Table 3.3.

Optimization results have shown that MOBA is very efficient and consistently converges to the sets of optimal solutions. Figure 4.7 shows the Pareto-optimal frontier points for different process conditions, at which the designers can determine the final solutions depending on

their preferences. The final optimum cutting parameters and performance characteristics are listed in Table A1. These process parameters are the Pareto-optimal process parameters that should be shown to the decision maker to simultaneously achieve the desired objectives in turning of the DSSs

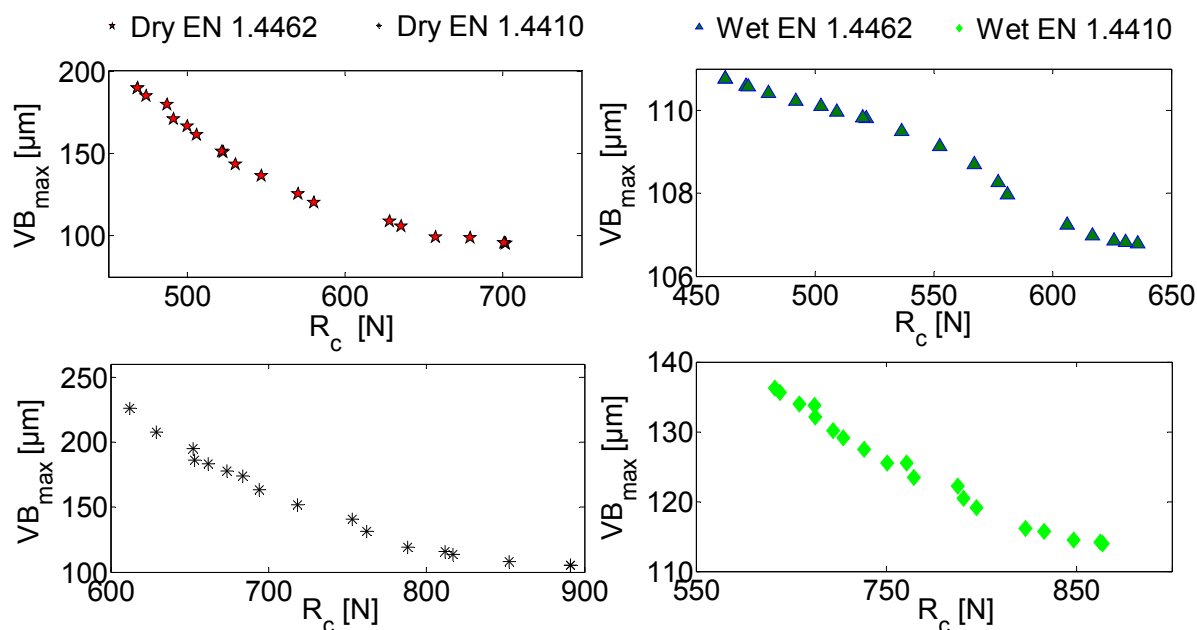


Figure 4.7: Pareto front points.

4.4 Interim conclusions

An experimental investigation on cutting of EN 1.4462 and EN 1.4410 DSSs is presented. Statistical regression modeling techniques are adopted to model the performance characteristics and ANOVA tests were performed to check the models adequacies. With the aid of three dimensional surface plots, the effects of workpiece materials, process and cutting conditions on the different cutting performances have been analyzed and proper conclusion points have been drawn. Results of the early analyses have shown that the values of no-beneficial performances during cutting EN 1.4410 were generally higher than those encountered during cutting EN 1.4462. Moreover, compared to the dry cutting, wet cutting has shown an improvement in the overall machining performance through lowering cutting forces and promoting tool life.

The chapter also presented multi-objective optimization of machining DSSs based on the nature-inspired Multi-Objective Bat Algorithm (MOBA). Two objectives are minimized simultaneously: resultant cutting force and maximum width of the flank wear. Arithmetic average roughness has been included in the formulation of the optimization problem as a constraint.

Results of optimization have shown that MOBA is very efficient and highly reliable. It has provided Pareto frontiers of non-dominated solution sets for optimum cutting conditions, enabling decision maker and/or process planner with a resourceful and efficient means of achieving the optimum cutting conditions.

5 Universal Characteristics Index

In this chapter, a comparative machining study of austenitic EN 1.4404, standard duplex EN 1.4462 and super duplex EN 1.4410 stainless steels through an extensive experimental study is introduced. A new methodology based on Mamdani fuzzy inference of classified chip shapes in chip breaking charts to predict the chip volume ratio is presented. Chip volume ratios, specific cutting pressures, cutting powers and resultant cutting forces are considered as performance characteristics and converted into single indices using TOPSIS, GRA, VIKOR and UC. An expert system based on fuzzy rule modeling approach is then adopted to combine the computed indices into a single Universal Characteristics Index (UCI). Constrained simulated annealing optimization algorithm is then employed to evaluate the optimal process parameters thereby satisfying conflicting requirements of each of performance factors. First ranking UCI values are analyzed and compared with the output of Multi-Objective Optimization (MOO) techniques using multiple regression and weighted sum method. The block diagram of the first phase is presented in Figure 5.1.

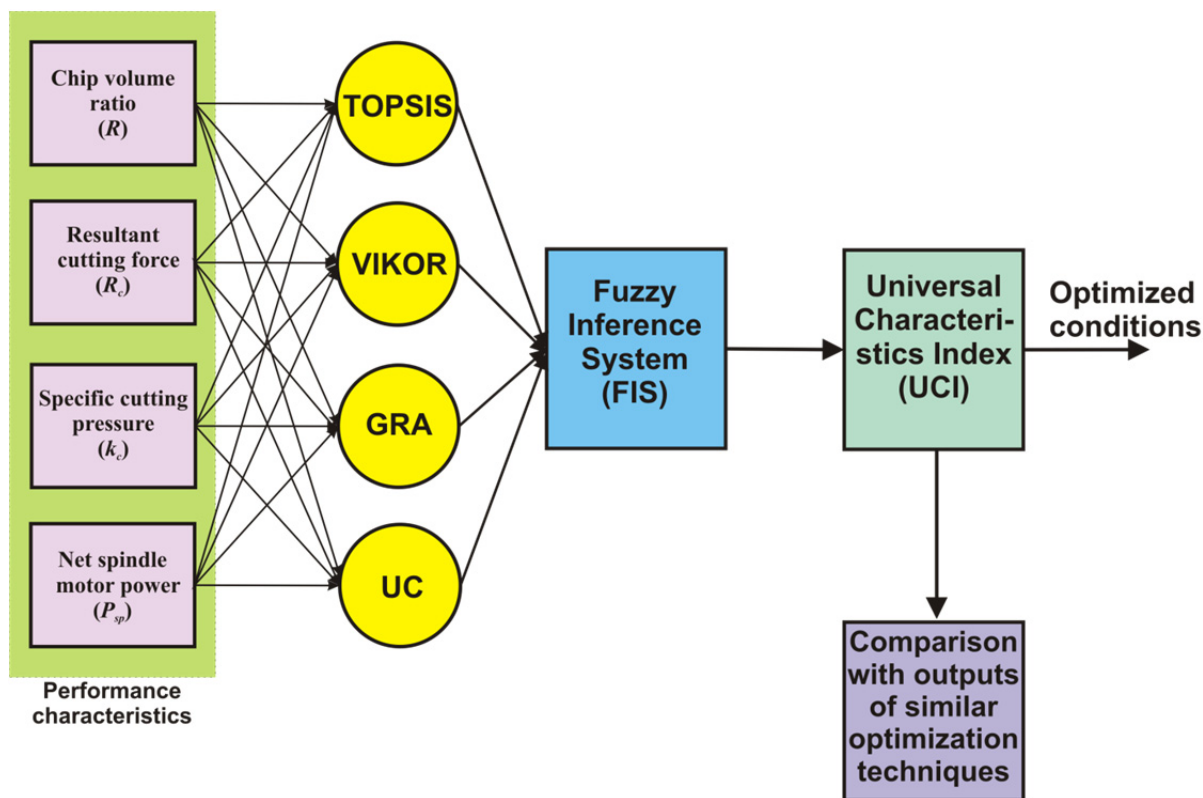


Figure 5.1: Framework for UCI determination and comparison.

5.1 Estimation of the chip volume ratio

One of the useful tools for investigating the machinability of materials is the chip breaking chart, which maps the sizes and shapes of chip forms across a feed rate \times depth of cut matrix. In order to draw the chart, a full factorial design as per Table 3.4 is adopted and the results are presented in Figure 5.2.

Detailed observations of the chip chart provide important visual information of the influence of cutting parameters and workpiece materials on the breakability of produced chips. Compared to the duplex grades, chips produced during cutting austenitic stainless steel EN 1.4404 were mainly in the form helical and spiral chips at higher feed ranges and less ribbon and snarled chip proportions at lower feed rates. On the other hand, in cutting DSS grades EN 1.4462 and EN 1.4410, snarled and ribbon chips were produced at low feed ranges and nearly all higher depth of cut ranges. At intermediate feed ranges, the produced chips were rather of flat-helical and cylindrical-helical forms. Helical and less spiral were the predominant form of chips when higher feed rates are used. Therefore, it can be roughly deduced that EN 1.4404 chips are expected to be less troublesome to the machine operator and friendlier to the machine tool.

In an attempt to quantify the information presented visually, fuzzy logic principles were nominated to loosely predict the chip volume ratio. A new chip classification system in conjunction with forms of chip and their loose chip volume ratio is proposed. The triangular membership function is applied for both input and output variables. Each level of input parameter is assigned with a corresponding fuzzy set. Accordingly, feed rate is classified into five fuzzy sets as: Very Low (VL), Low (L), Fair (F), High (H) and Very High (VH), and depth of cut into seven fuzzy sets as: Very Low (VL), Low (L), Moderately Low (ML), Moderate (M), Moderately High (MH), High (H) and Very High (VH). In order to increase the accuracy of prediction, chip forms in Figure 1.14 are further divided into shorter and longer subcategories. Hence, the output is divided into the following fuzzy sets as: Discontinuous chips (DC), Short Spiral Chips (SSC), Long Spiral Chips (LSC), Short Helical Chip Segments (SHCS), Long Helical Chip Segments (LHCS), Short Cylindrical and Flat helical Chips (SCFC), Long Cylindrical and Flat helical Chips (LCFC), Short Ribbon and Snarled Chips (SRSC) and Long Ribbon and Snarled Chips (LRSC). Figure 5.3 shows the proposed fuzzy membership functions which were employed to predict chip volume ratio (R).

	EN 1.4404					EN 1.4462					EN 1.4410				
3.5															
3															
2.5															
2															
1.5															
1															
0.50															
a_p [mm] f_r [mm/rev]	0.1	0.175	0.25	0.325	0.4	0.1	0.175	0.25	0.325	0.4	0.1	0.175	0.25	0.325	0.4

Figure 5.2: Chip breaking chart.

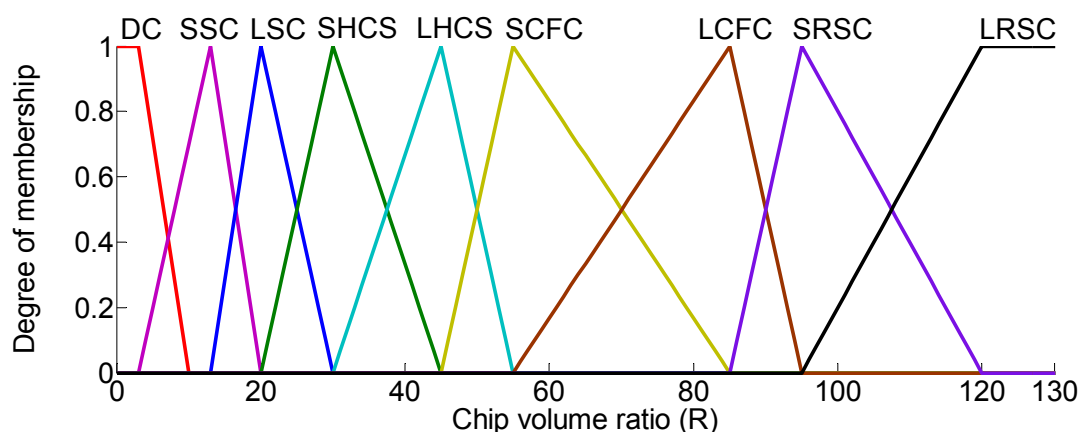


Figure 5.3: Chip volume ratio membership functions.

A set of 35 rules per each workmaterial case is written for activating the fuzzy inference system (FIS). For a fuzzy system involving two input parameters, rules can be described in a 5×7 matrix form. Table 5.1 presents the governing rules controlling the relations between feed rate and depth of cut on one hand and chip volume ratio on the other hand. Once the rules are formulated, center-of-gravity method is applied to defuzzify the rules and obtain the crisp chip volume ratio values.

Chip volume ratio along with other important performance characteristics are mapped as surface and contour plots and shown in Figure 5.4. The optimum and near optimum regions are filled with dark blue and light blue colors. This argument initially suggests that the optimum point should locate somewhere within shown dark blue regions. From these collective plots, one can easily depict the conflicting nature of the performances.

It is worth mentioning that P_{sp} is the net spindle power calculated through subtracting the average power fed to the spindle when freely spinning from the power fed to spindle when involved in cutting action. Resultant cutting forces R_c and specific cutting pressures k_c are computed using Eqs. (1.4) and (1.6) respectively.

5.2 Universal characteristics index

Since there is no single MADM method considered as the most suitable or the most acknowledged for multi-performance optimization in machining, therefore, adoption of more than one technique is recommended. In this section, MADM techniques such as TOPSIS, GRA, VIKOR and UA are separately applied to find the best alternative which can simultaneously minimize the described performance characteristics (attributes). Furthermore, through adopt-

ing the equal priority scenario, a weighting factor of 0.25 for each one of the four performances is employed.

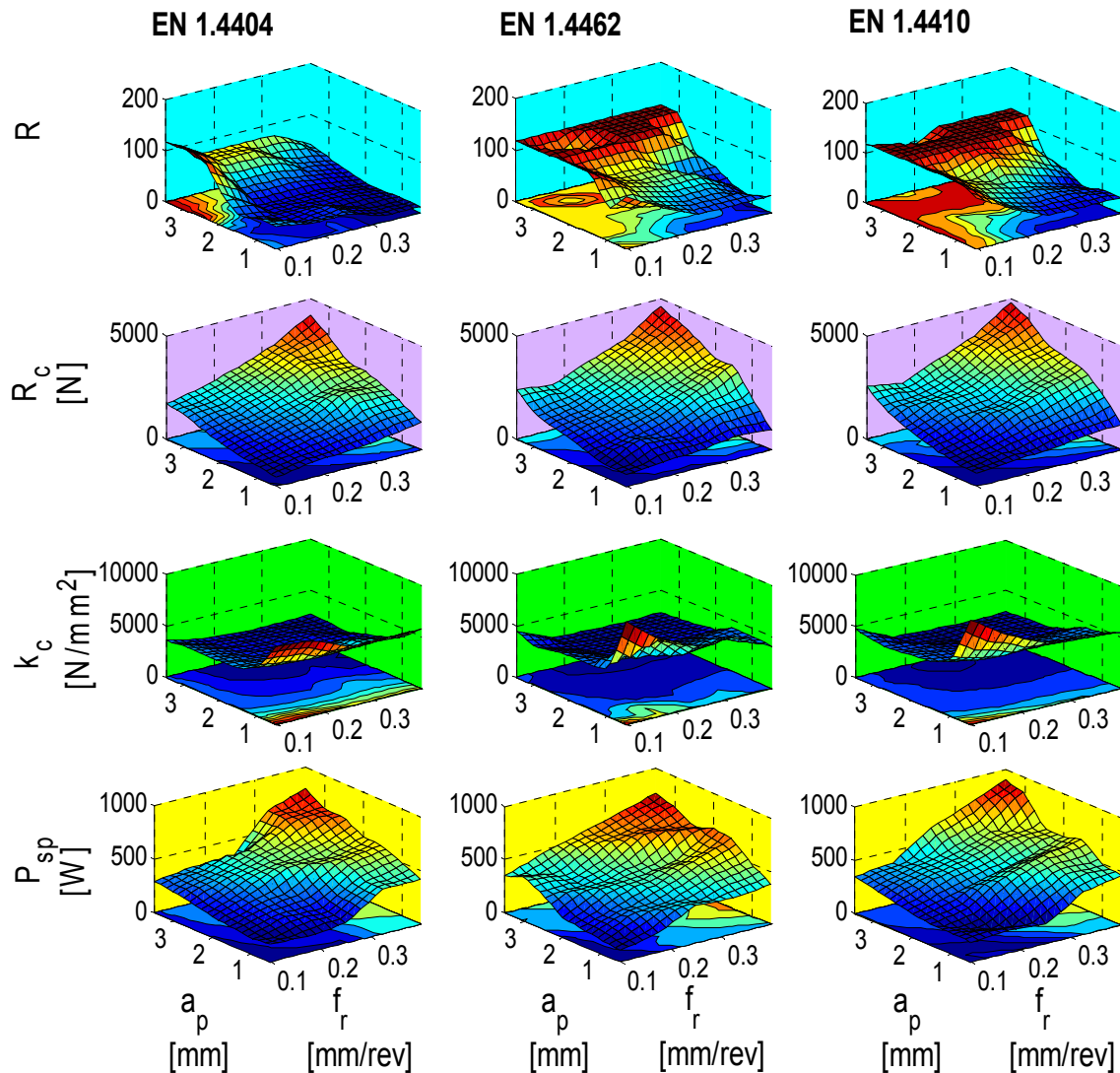


Figure 5.4: Surface plots and contour maps of machining performance characteristics.

5.2.1 TOPSIS

The first step in any MADM application is to represent all the information available of selected performance characteristics (attributes) in the form of a decision matrix. The performance characteristics are arranged as decision matrix $\mathbf{DMA}(35 \times 4)$ using Eq. 2.62. The attribute values are then normalized utilizing Eq. (2.72). Afterwards, Eq. (2.73) is employed to define weighted normalized matrix. Next, the ideal best A^* and ideal worst A^- values are determined through adopting Eqs. (2.74) and (2.75) respectively. The distances from the ideal best S_i^* and

ideal worst S_i^- solutions and the relative closeness to the ideal solution (C_i^*) are measured utilizing Eqs. (2.76-78). Finally, The results are ranked by the relative degree of approximation. The best alternative is the one which has the shortest Euclidean distance to the ideal solution.

5.2.2 VIKOR method

The best x_i^- and the worst x_i^* values of all criterion functions are computed using Eqs. (2.79) and (2.80) respectively. Thereafter, Eqs. (2.81-83) are utilized to compute the utility S_i and regret R_i measures, and VIKOR index Q_V . The alternatives are then ranked by the values S_i , R_i and Q_V . The results are three ranking lists with no difference in ranking order. The values of first rank alternative were in acceptable advantage range and both S_i and R_i by consensus proved the stability in decision making.

5.2.3 GRA

The adopted attributes are of non-beneficial kind where low values are always desired. Therefore, when using GRA as a MADM method, the ‘smaller-the-better’ option should be employed as a normalizing method using the last term in Eq. (2.84). The values of deviation sequence Δ_{ij} , which is the absolute difference between reference sequence r_{0j} , and the comparability sequence r_{ij} values, are computed using Eq. (2.85). The global minimum (Δ_{\min}) and maximum values (Δ_{\max}) are directly computed employing Eqs. (2.86) and (2.87) respectively. In all cases, Δ_{\min} and Δ_{\max} were equal to 0 and 1 respectively. Since, all the attributes have equal weighting, δ_d is assigned to be 0.5. Afterwards, Grey relational coefficients ζ_g and Grey relational grade GRG are evaluated using Eqs. (2.88) and (2.89) respectively. Finally, the alternatives are ranked based on the GRG values so that the largest has specified the best.

5.2.4 UC

Owing to the non-beneficial nature of performances, Eq. (2.94) is directly used to specify the best value of each attribute. Afterwards, Eqs. (2.95-97) are employed to determine the values the utility constant U_{C_j} , preference number PN_j and the overall utility value U_i , respectively. The best alternative is then ranked according to the U_i values.

5.2.5 Fuzzy-MADM

The output of the previous MADM methods showed different ranking outcomes, which will cause uncertainty and confusions to the decision maker and/or process planner. In order to eliminate the discrepancy of these methods and obtain a more general solution, fuzzy logic principles is proposed to solve the problem. The individual MADM-indices are combined into a single and comprehensive index called the Universal Characteristics Index (UCI).

Matlab software was used to construct the inference model of the UCI. The MADM-indices were first adjusted to a notionally common scale between null and one, using simple normalization methods. So that the digit ‘one’ represents the most desirable and ‘null’ is the least desirable alternative. The outputs of the previous MADM-methods are designated as input variables to the FIS and are assigned with the following fuzzy sets: Small (S), Medium (M) and Large (Lg). The output variable has the following nine levels: Extremely Low (EL), Very Low (VL), Low (L), Lower Medium (LM), Medium (M), Upper Medium (UM), High (H), Very High (VH) and Extremely High (EH). Mamdani implication method is employed for the fuzzy inference reasoning. The relationship between system input and output is expressed by an “If-Then” type. Totally 81 fuzzy rules per material were formulated. A sample of the formulated fuzzy rules is listed below.

Rule 1: TOPSIS is (S) and VIKOR is (S) and GRA is (S) and UA is (S) then UCI is (EL)

Rule 2: TOPSIS is (S) and VIKOR is (S) and GRA is (S) and UA is (M) then UCI is (VL)

Rule 3: TOPSIS is (S) and VIKOR is (S) and GRA is (S) and UA is (Lg) then UCI is (L)

Rule 80: TOPSIS is (Lg) and VIKOR is (Lg) and GRA is (Lg) and UA is (M) then UCI is (VH)

Rule 81: TOPSIS is (Lg) and VIKOR is (Lg) and GRA is (Lg) and UA is (Lg) then UCI is (EH)

The values of cutting performances and the developed UCIs are shown in Table A2. In order to evaluate the strength of the statistical relationship between the computed MADM-indices and the developed UCIs, Spearman’s rank-order correlation is applied, see Table 5.2. The near to one values of UCI coefficients are good indications of strong statistical relationship with other MADM-indices. The ranks of the estimated UCI values along with the ranks of the four MADM methods are shown in Figure 5.5. Noteworthy is the problem of MADM-methods rank differences which justifies the application of fuzzy logic to solve it.

Depth of cut	EN 1.4404					EN 1.4462					EN 1.4410				
	Feed rate					Feed rate					Feed rate				
	VL	L	F	H	VH	VL	L	F	H	VH	VL	L	F	H	VH
VL	LHCS	SHCS	SHCS	SSC	SSC	SRSC	SCFC	SHCS	LHCS	SHCS	SRSC	SCFC	SHCS	SHCS	SHCS
L	LHCS	LSC	SHCS	SSC	SSC	SCFC	SCFC	LHCS	LHCS	SSC	URSC	SCFC	LHCS	LHCS	SHCS
ML	SHCS	LSC	LSC	LSC	SSC	LRSC	LCFC	SCFC	SCFC	LSC	URSC	LCFC	SCFC	LHCS	LSC
M	SCFC	LSC	LSC	LSC	SSC	LRSC	LCFC	LCFC	LHCS	LHCS	URSC	LCFC	SRSC	LCFC	LHCS
MH	LRSC	LHCS	LHCS	LHCS	LSC	LRSC	LRSC	LRSC	LRSC	LHCS	URSC	LRSC	LRSC	LRSC	LHCS
H	LRSC	LCFC	LCFC	LHCS	SHCS	LRSC	LCFC	LRSC	LRSC	LRSC	URSC	LRSC	LRSC	LRSC	LRSC
VH	LRSC	LCFC	LCFC	LCFC	LHCS	LRSC	LRSC	LRSC	LRSC	LRSC	URSC	LCFC	LRSC	LRSC	LRSC

Table 5.1: Chip classification fuzzy-based rules.

	EN 1.4404					EN 1.4462					EN 1.4410				
	TOPSIS	VIKOR	GRA	UA	UCI	TOPSIS	VIKOR	GRA	UA	UCI	TOPSIS	VIKOR	GRA	UA	UCI
TOPSIS	1.000	0.925	0.9	0.936	0.986	1.000	0.819	0.895	0.918	0.906	1.000	0.815	0.825	0.872	0.918
VIKOR	0.925	1.000	0.738	0.808	0.914	0.819	1.000	0.78	0.798	0.877	0.815	1.000	0.735	0.824	0.922
GRA	0.90	0.738	1.000	0.983	0.929	0.895	0.78	1.000	0.996	0.911	0.825	0.735	1.000	0.98	0.914
UA	0.936	0.808	0.983	1.000	0.963	0.918	0.798	0.996	1.000	0.924	0.872	0.824	0.98	1.000	0.963
UCI	0.986	0.914	0.929	0.963	1.000	0.906	0.877	0.911	0.924	1.000	0.918	0.922	0.914	0.963	1.000

Table 5.2: Spearman's rank correlation coefficients.

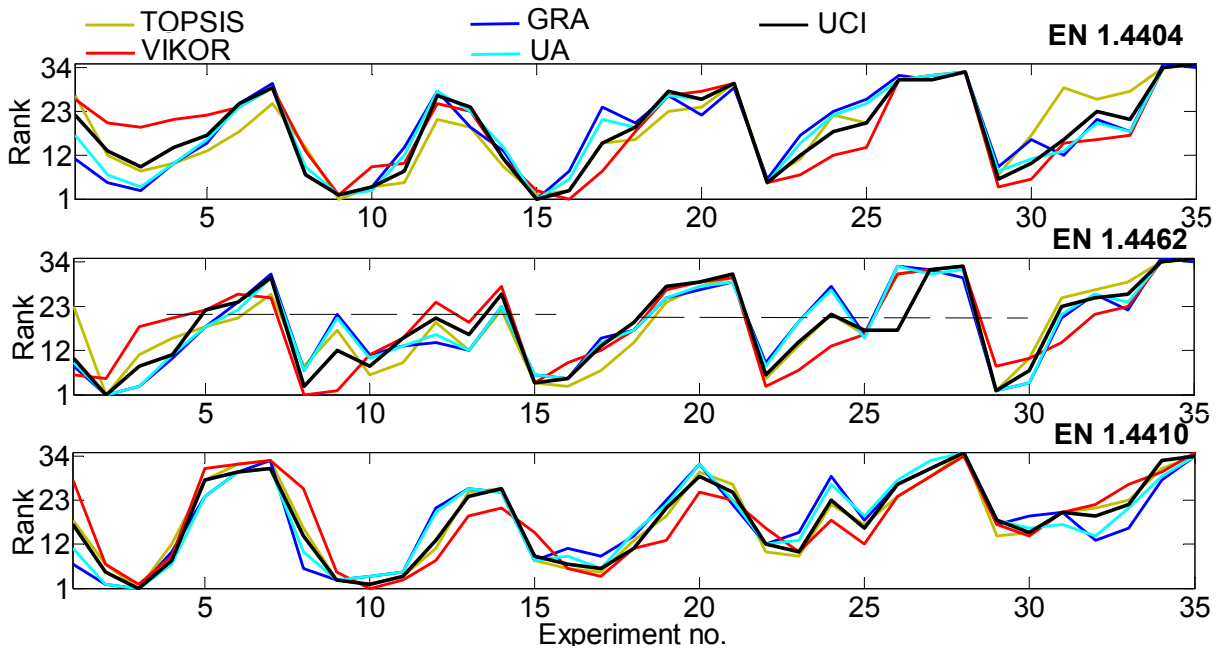


Figure 5.5: Ranking the output of MADA methods and UCI.

5.3 Optimization

After combining the MADM-indices into one universal index, the next step is to find the exact optimal settings of the process parameters using SA algorithm. Two approaches are simultaneously adopted to optimize the process: Weighted Sum Method (WSM) and UCI. The decision variables are feed rate and depth of cut. The following objective function is developed for Multi-Objective Optimization (MOO) of the performance characteristics based on the WSM:

$$Z = \frac{w_1}{\max(R)} Y(R) + \frac{w_2}{\max(R_c)} Y(R_c) + \frac{w_3}{\max(k_c)} Y(k_c) + \frac{w_4}{\max(P_{sp})} Y(P_{sp}) \quad (5.1)$$

where w_{1-4} are the weight values assigned to R , R_c , k_c and P_{sp} respectively. The weight values can be anything provided that $\sum w_i = 1$. Here, equal weights for all responses are considered, i.e. $w_1 = w_2 = w_3 = w_4 = 0.25$. Using multiple regressions, a second model based on computed UCI values has been developed. Since the possibility of determining a global optimum solution and its accuracy depends on the nature of the modeling used to express the objective function, hence, a great attention has been paid to select an accurate and reliable model. Consequently, the following objective function is employed for predicting UCI values:

$$\begin{aligned}
 UCI = & c_1 + c_2 f_r + c_3 a_p + c_4 f_r^2 + c_5 f_r a_p + c_6 a_p^2 + c_7 f_r^3 + c_8 f_r^2 a_p + \\
 & c_9 f_r a_p^2 + c_{10} a_p^3 + c_{11} f_r^3 a_p + c_{12} f_r^2 a_p^2 + c_{13} f_r a_p^3 + c_{14} a_p^4
 \end{aligned}
 \tag{5.2}$$

where c_{1-14} are model coefficients calculated using Eqs. 2.1-10. Performance characteristics are formulated using multiple nonlinear regression analysis, and applied as constraints on both objective functions separately. Simplest forms of constraints are suggested and tabulated in Table 5.3. The constraint models are considered adequate to represent the system based on the adjusted correlation factor R_{adj} . The boundaries of the decision variables are expressed as:

$$\begin{aligned}
 0.1 \leq f_r \leq 0.4 \text{ mm/rev} \\
 0.5 \leq a_p \leq 3.5 \text{ mm}
 \end{aligned}
 \tag{5.3}$$

Constraints	EN 1.4404	EN 1.4462	EN 1.4410
R	$5.776 f_r^{-0.767} a_p^{1.077} \leq R_{\max}$	$37 f_r^{-0.29} a_p^{0.549} \leq R_{\max}$	$39.74 f_r^{-0.318} a_p^{0.445} \leq R_{\max}$
R_c	$3641 f_r^{0.752} a_p^{0.606} \leq R_{c_{\max}}$	$4368 f_r^{0.808} a_p^{0.615} \leq R_{c_{\max}}$	$4196 f_r^{0.746} a_p^{0.614} \leq R_{c_{\max}}$
k_c	$3474 f_r^{-0.185} a_p^{-0.445} \leq k_{c_{\max}}$	$3163 f_r^{-0.291} a_p^{-0.429} \leq k_{c_{\max}}$	$3412 f_r^{-0.278} a_p^{-0.435} \leq k_{c_{\max}}$
P_{sp}	$1094 f_r^{0.867} a_p^{0.346} \leq P_{sp_{\max}}$	$915.4 f_r^{0.694} a_p^{0.367} \leq P_{sp_{\max}}$	$1071 f_r^{0.797} a_p^{0.375} \leq P_{sp_{\max}}$
R models :	EN 1.4404 : $R_{adj} = 0.609$,	EN 1.4462 : $R_{adj} = 0.605$	EN 1.4410 : $R_{adj} = 0.612$
R_c models :	EN 1.4404 : $R_{adj} = 0.961$,	EN 1.4462 : $R_{adj} = 0.939$	EN 1.4410 : $R_{adj} = 0.941$
k_c models :	EN 1.4404 : $R_{adj} = 0.943$,	EN 1.4462 : $R_{adj} = 0.791$	EN 1.4410 : $R_{adj} = 0.883$
P_{sp} models :	EN 1.4404 : $R_{adj} = 0.902$,	EN 1.4462 : $R_{adj} = 0.913$	EN 1.4410 : $R_{adj} = 0.891$

Table 5.3: Performance characteristic models as constraints with 95% confidence interval.

The initializing optimization parameters for simulated annealing algorithms were: initial $T=1.0$, final stopping temperature = 1×10^{-10} , maximum number of rejection = 2500, maximum number of runs = 500, maximum number of accept = 250, Boltzmann constant $k_b=1$ and energy norm $\Delta E = 1 \times 10^{-5}$. The obtained optimization results showed that SA is highly reliable and converges consistently to the optimum solution. Following the application of SA, optimum results of optimizations using the above objective and constraint models are compared with the first ranking alternatives given in Table A2. Table 5.4 presents the results of optimization, UCI and performance values at optimal level.

Factors	Objective function						Per-Table A2 first rank UCI, cutting parameters and performance values			Average improvement	
	Model I (Eq. 5.1)			Model II (Eq. 5.2)			EN 1. 4404	EN 1. 4462	EN 1. 4410	Model I (%)	Model II (%)
	EN 1. 4404	EN 1. 4462	EN 1. 4410	EN 1. 4404	EN 1. 4462	EN 1. 4410					
R	20.8	36.55	48.69	37.9	70.3	46	31.7	61.7	31.7	-28.7	19.89
R_c [N]	617.5	1021	824.0	959.8	660.1	938.3	717.6	560.3	896.7	6.700	14.92
k_c [MPa]	5891	6174	7227	4401	6315	6885	3905	4614	6207	24.36	16.01
P_{sp} [W]	157.8	293.6	228.7	146.5	181.7	262.8	172.2	130.9	182.5	22.14	13.63
f_r [mm/rev]	0.121	0.28	0.20	0.132	0.101	0.238	0.102	0.101	0.25		
a_p [mm]	0.732	0.50	0.50	1.365	0.959	0.501	1.502	101	0.5		
Results	0.323	0.329	0.384	0.898	0.743	0.828	0.959	0.887	0.886		

Table 5.4: Process optimization results.

It should be noted here that ranking the alternatives according to UCI values offers many advantages like, simplicity, accuracy, generally lower non-beneficial performance values and the reducing the necessity of performing optimization process. At optimum UCI values, when simple ranking UCI results is used and compared to the optimum results obtained in model I (Eq. 5.1), the average improvement in cutting power consumption is 22.147%, specific cutting pressure is 24.364% and resultant cutting force is 6.7%. In contrast, optimization with model I could reach lower chip volume ratio with an average rate of deterioration of -28.77%. This relative large percentage is attributed to the inaccurate models used to predict chip volume ratio with margins of errors to up to 23.54, 23.08 and 14.622 for EN 1.4410, EN 1.4462 and EN 1.4404 respectively. To compensate for this inconvenience, all root mean square of errors are added to the models and optimization process ran again. Results has shown that the average improve in cutting power consumption would raise to a new level of 41.433%, specific cutting pressure of 30.961%, resultant cutting forces of 30.081% and the chip volume ratio could raise of 14.675%. This confirms the viability of derived UCI values when compared with conventional multi-objective optimization algorithms. Although an accurate and relatively complex objective function which could best model UCI is used as a model for a second optimization process and the optimizations were ran under the same set of constraints, no traces of any improvement is reported.

5.4 Interim conclusions

- For the studied range of process parameters, the resulting chip form was strongly influenced by the workpiece material and cutting conditions. When machining super duplex EN 1.4410 and standard duplex EN 1.4462 stainless steels, snarled and ribbon chips were the dominant at lower feed ranges and nearly all higher depth of cut ranges. Meanwhile, flat helical and cylindrical helical chips at medium feed ranges and helical and less spiral chips at higher feed ranges were the dominant. Chips obtained when machining austenitic EN 1.4404 stainless steel are friendlier to the machine and generally produce lower ribbon, snarled and flat helical chips. Fuzzy logic principles were applied to quantify the information presented in chip breaking chart and could successfully predicts the chip volume ratio.
- In the present chapter, the objective was to simultaneously minimize performance characteristics such as chip volume ratio, resultant cutting forces, specific cutting pressures and net spindle powers. Because the values of above non-beneficial performance characteristics when machining austenitic EN 1.4404 were generally lower than standard duplex EN 1.4462 and super duplex EN 1.4410 grades, therefore, one can roughly conclude that the machinability of EN 1.4404 is better than EN 1.4462 and EN 1.4410.
- The multiple performance characteristics were successfully converted into single MADM-indices using TOPSIS, VIKOR, GRA and UA. Due to the differences among MADM preferences and rankings, and the absence of a reference defining a 'super method', fuzzy rule modeling approach was proposed to eliminate the discrepancy among the MADM methods and derive a single characterization index called UCI. Spearman's rank correlation coefficients have confirmed that the proposed index had a very good correlation with the output of other MPCCI methods. Predicted UCI values have been analyzed and compared with output of other optimization techniques. A remarkable improvement in reduction of cutting power consumption, specific cutting pressure and resultant cutting forces has been reported when direct ranking system of predicted UCI indices are set as optimum.

6 Taguchi-MADM-Meta-heuristic concept

The main objective of this chapter is to examine the machinability of different grades of stainless steels in seeking simultaneous improvement in performance characteristics (or response factors) using different statistical and mathematical tools. Accordingly, multi-performance optimization of turning austenitic EN 1.4404, standard duplex EN 1.4462 and super duplex EN 1.4410 stainless steels utilizing coupled Taguchi-based designs, multiple attribute decision making (MADM) and meta-heuristic algorithms is experimentally addressed. The flow chart of the methodology presented in this chapter is shown in Figure 6.1. Surface roughness, specific cutting energy, cutting power and resultant cutting forces are optimized per each material under Taguchi optimization procedure and combined as a single, cutting parameter dependent Multi-Performance Characteristics Index (MPCI) using VIKOR method. Analysis of means (ANOM) and Analysis of variance (ANOVA) are employed to designate the optimum level of cutting parameters and to investigate the influence of cutting parameters and their interactions on the computed index, respectively. Nature-inspired meta-heuristic algorithms such as; Firefly Algorithm (FA), Accelerated Particle Swarm Optimization (APSO) and Cuckoo Search (CS) are used to constrainedly optimize the developed MPCIs and find the exact setting of optimum cutting parameter. Finally, a comparison analysis is conducted in order to designate the algorithm which has shown the best performance in quickly and consistently converge to the global optimum point.

6.1 Taguchi method

In order to systematically approach the variance in controllable input factors and to observe the effect of these factors and their interactions on the output performance parameters, an L_{25} (5^6) orthogonal array proposed by Taguchi is used in the experimental procedure per each workpiece material (see Table 3.6) using coated carbide cutting tool of ISO designation CNMG 120408-MM 2025. The control factors are the three known cutting parameters which are cutting speed (v_c), feed rate (f_r) and depth of cut (a_p). Under a full factorial run and in the case of three factors with five levels, $5^3=125$ experiments should be conducted. In accordance with Taguchi's method the standard orthogonal array L_{25} with only one fifth of that number of experiments could be used. However, the selection of L_{25} orthogonal array, that

can have six control factors for a saturated design of three factors leaves unassigned column in the matrix which can be used to investigate first order interactions among the cutting parameters. Therefore, the first, the second and the fourth columns of the matrix represent different levels of the cutting parameters and the third column is employed for studying the interaction between the first two (i.e. cutting speed and feed rate interaction).

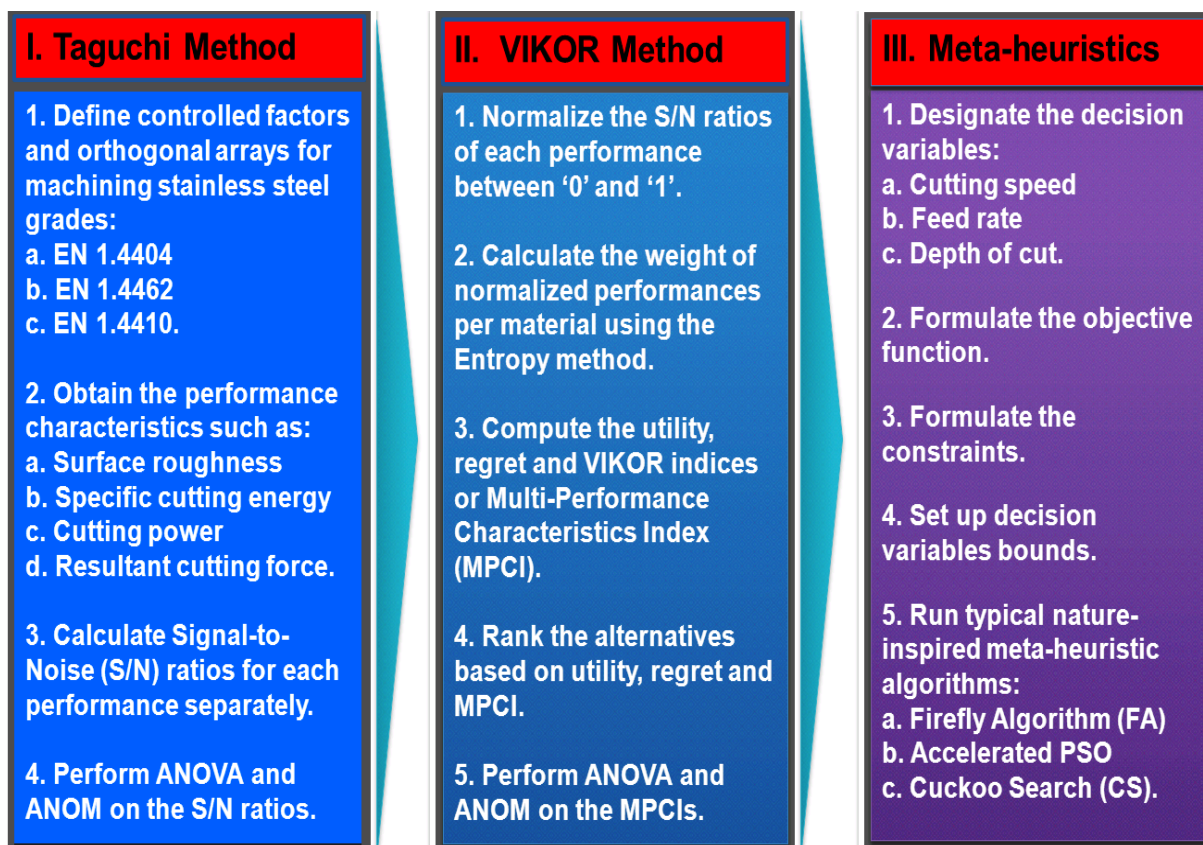


Figure 6.1: The flow chart of the Taguchi-VIKOR-Meta-heuristic methodology.

In order to minimize the variations in the performance characteristics, Taguchi introduced a method to transform the repetition data to another value, which is a measure of variation present in the scattered response data. This transformation consists of the computation of signal-to-noise (S/N) ratio (η) that consolidates several repetitions into one performance measure which reflects the amount of variation present. Since, all the adopted performance characteristics are of non-beneficial kind, thus Eq. 2.27 must be adopted to calculate the S/N ratios. They are further analyzed using statistical analysis of means (ANOM) employing Eqs. 2.29 & 2.30. Furthermore, in order to simultaneously optimize the performance characteristics and minimize the effect of noise factors, Eq. 2.31 is applied to maximize the mean S/N ratio. The op-

timum level for a performance characteristic is the level that gives the highest value of the mean S/N ratio.

Figure 6.2 presents the results of applying ANOM on the computed S/N ratios. Accordingly, the optimum control $factor^{level}$ combinations during turning EN 1.4404 were: $v_c^5 f_r^1 a_p^2$ for surface roughness, $v_c^4 f_r^5 a_p^5$ for specific cutting energy, $v_c^1 f_r^1 a_p^1$ for cutting power and $v_c^4 f_r^1 a_p^1$ for resultant cutting forces. In turning EN 1.4462, the following optimum $factor^{level}$ combinations were optimum: $v_c^5 f_r^1 a_p^2$ for surface roughness, $v_c^3 f_r^3 a_p^5$ for specific cutting energy, $v_c^1 f_r^1 a_p^1$ for cutting power and $v_c^3 f_r^1 a_p^1$ for resultant cutting forces. Finally, for turning EN 1.4410 the optimum $factor^{level}$ combinations were: $v_c^4 f_r^1 a_p^2$ for surface roughness, $v_c^4 f_r^3 a_p^5$ for specific cutting energy, $v_c^1 f_r^1 a_p^1$ for cutting power and $v_c^4 f_r^1 a_p^1$ for resultant cutting forces.

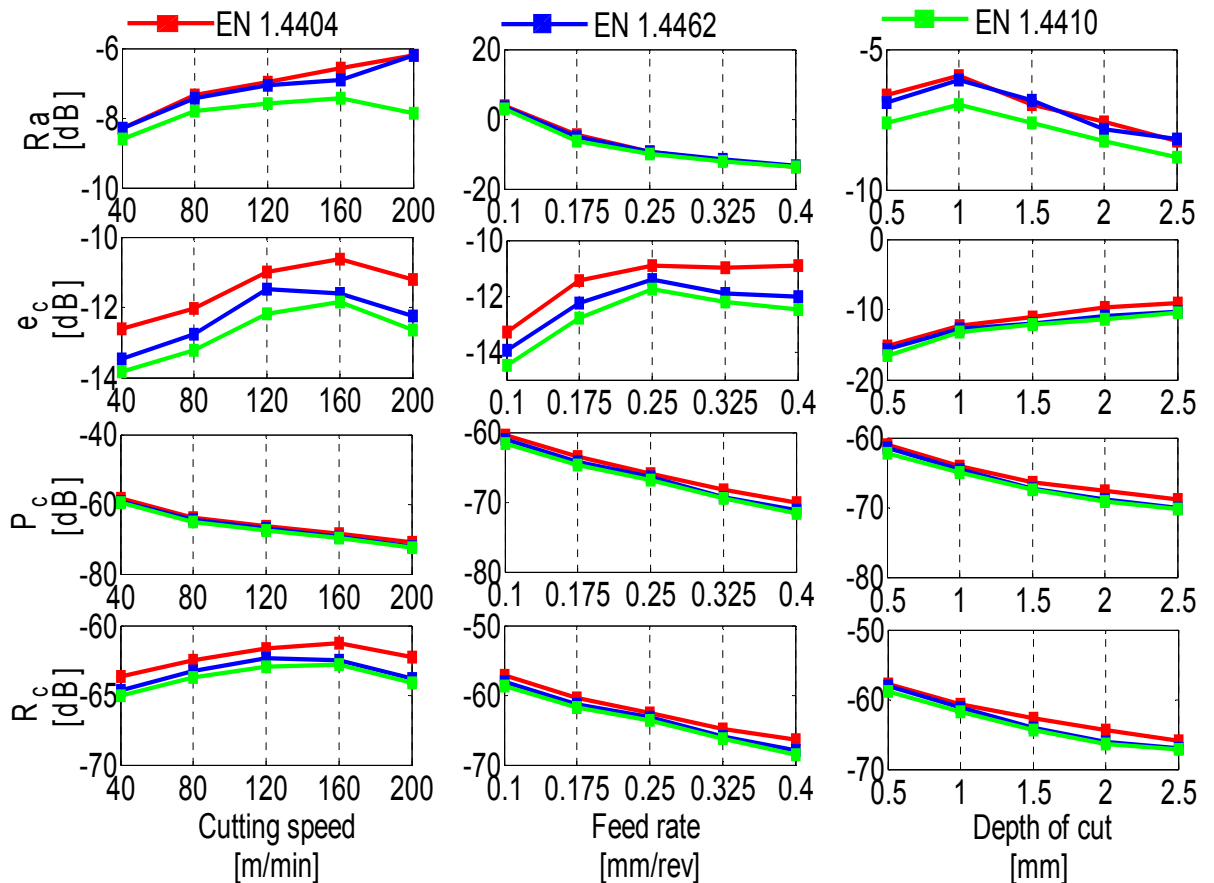


Figure 6.2: Main effect plot of SN ratio in machining stainless steels.

Following the determination the optimal levels of control factors, ANOVA of S/N ratios of all performance characteristics are performed to estimate the relative significance of each factor.

Table 6.1 shows the result of ANOVA on SN ratios for 95% level of confidence. The P-values of cutting speed, feed rate and depth of cut smaller than 0.05 are marked in bold revealing the statistical and physical impact of control factors. The last three column of the table presents the percent contribution (%Contribution) which indicates the contribution of the control factors in total variation of performance characteristics.

Factors	DOF	SS			F-value			P-value			%Contribution		
		EN 1. 4404	EN 1. 4462	EN 1. 4410	EN 1. 4404	EN 1. 4462	EN 1. 4410	EN 1. 4404	EN 1. 4462	EN 1. 4410	EN 1. 4404	EN 1. 4462	EN 1. 4410
Surface roughness (R_a)													
v_c	4	13.13	11.54	4.152	5.51	2.91	1.63	0.02*	0.093	0.257	1.291	1.219	0.469
f_r	4	977.4	907.3	862.7	410.1	228.7	339.6	0.000	0.000	0.000	96.05	95.84	97.63
$v_c f_r$	4	5.506	5.506	1.535	2.41	1.39	0.6	0.135	0.32	0.671	0.564	0.581	0.173
a_p	4	14.31	14.31	10.12	6.82	3.61	3.98	0.011	0.058	0.046	1.624	1.512	1.145
Error	8	7.932	7.932	5.080	F-table _(4,16,0.05) =3.0069						0.84	0.84	0.469
Total	24	946.6	946.6	883.5							100	100	100
Specific cutting energy (e_c)													
v_c	4	13.08	13.67	12.80	1.97	1.78	1.32	0.192	0.226	0.341	7.749	9.875	7.734
f_r	4	20.90	18.91	22.13	3.15	2.46	2.28	0.079	0.129	0.149	12.38	13.66	13.36
$v_c f_r$	4	4.044	3.176	2.559	0.61	0.41	0.26	0.668	0.795	0.893	2.394	2.293	1.545
a_p	4	117.5	87.32	108.6	17.69	11.36	11.19	0.000	0.002	0.002	69.60	63.06	65.62
Error	8	13.29	15.36	19.41	F-table _(4,16,0.05) =3.0069						7.871	11.10	7.871
Total	24	168.8	138.4	165.5							100	100	100
Cutting power (P_c)													
v_c	4	463.2	475.8	473.3	69.69	61.93	48.77	0.171	0.000	0.000	47.79	45.12	46.66
f_r	4	295.8	320.7	311.2	44.52	41.74	32.06	0.000	0.000	0.000	30.52	30.41	30.68
$v_c f_r$	4	4.044	3.176	2.559	0.61	0.41	0.26	0.771	0.795	0.893	0.417	0.301	0.252
a_p	4	192.7	239.5	207.7	29.00	31.17	21.4	0.000	0.000	0.000	19.88	22.70	20.48
Error	8	13.29	15.36	19.41	F-table _(4,16,0.05) =3.0069						1.374	1.456	1.374
Total	24	969.1	1054.	1014.							100	100	100
Resultant cutting force (R_c)													
v_c	4	16.72	19.01	16.81	2.11	2.31	1.4	0.171	0.146	0.317	3.313	3.541	2.978
f_r	4	226.1	229.2	290.5	33.56	36.35	24.19	0.000	0.000	0.000	52.71	42.7	51.46
$v_c f_r$	4	3.557	3.126	2.349	0.45	0.38	0.2	0.771	0.817	0.934	0.704	0.582	0.416
a_p	4	202.6	269.0	230.8	25.55	32.68	19.21	0.000	0.000	0.000	40.13	50.11	40.88
Error	8	15.86	16.46	24.02	F-table _(4,16,0.05) =3.0069						3.141	3.066	3.141
Total	24	504.9	536.9	564.5							100	100	100
*Bold P-values are less than 0.05													

Table 6.1: ANOVA of S/N ratios.

According to above table, the most influential cutting parameters affecting the performance characteristics: (a) Ra is f_r with average contribution percentage of 96.512%, (b) e_c is a_p with an average contribution percentage of 66.098%, (c) P_c are v_c and f_r with average contribution percentages of 46.528% and 30.54% respectively, and (d) R_c are f_r and a_p with contribution percentages of 48.959% and 43.707% respectively. In all of the above conditions, the contribution percentage of $v_c f_r$ interaction did not exceed 3%. Therefore, it can be neglected.

6.2 VIKOR method

Taguchi method is seen suitable only for single objective optimization, in order to perform multi-objective optimization of the problem, VIKOR method is utilized. S/N ratios of the performance characteristics are first normalized between '0' and '1' and the weights are determined using the entropy method which makes the weight designation process independent of the views of the decision maker. Eqs (2.64-68) are employed to define the weights of performance characteristics and the weights are tabulated in Table 6.2. Thereafter, utility and regret measures, and MPCIs are computed utilizing Eqs. (2.81-83), respectively.

Performance characteristics	Entropy weights (w_j)		
	EN 1.4404	EN 1.4462	EN 1.4410
Surface roughness (Ra)	0.269	0.265	0.275
Specific cutting energy (e_c)	0.205	0.215	0.214
Cutting power (P_c)	0.284	0.279	0.286
Resultant cutting force (R_c)	0.242	0.241	0.225

Table 6.2: Entropy weights.

The values of first rank alternatives are in acceptable advantage range (i.e. $MPCI(A_{b_2}) - MPCI(A_{b_1})$) is always greater than $(1/(25 - 1))$. Both regret and utility measure values by consensus have proved the stability in decision making. Therefore, the values of MPCIs are directly used in the next analyses.

In order to indicate the sensitivity of calculated MPCIs to changing cutting parameters, contour plots for newly computed MPCIs are mapped as shown in Figure 6.3. The optimum and near optimum regions are filled with dark blue and light blue colors. This argument initially suggests that the optimum point should locate somewhere within shown dark blue regions.

Performing ANOM on the computed MPCIs, an optimum global level for any control factor is a level that returns minimum value of the mean MPCI. Figure 6.4 presents the main effect plot of cutting parameters on the computed MPCIs. The global optimum $factor^{level}$ combinations while turning EN 1.4410 and both of EN 1.4404 and EN 1.4462 were: $v_c^2 f_r^1 a_p^2$ and $v_c^3 f_r^1 a_p^2$, respectively.

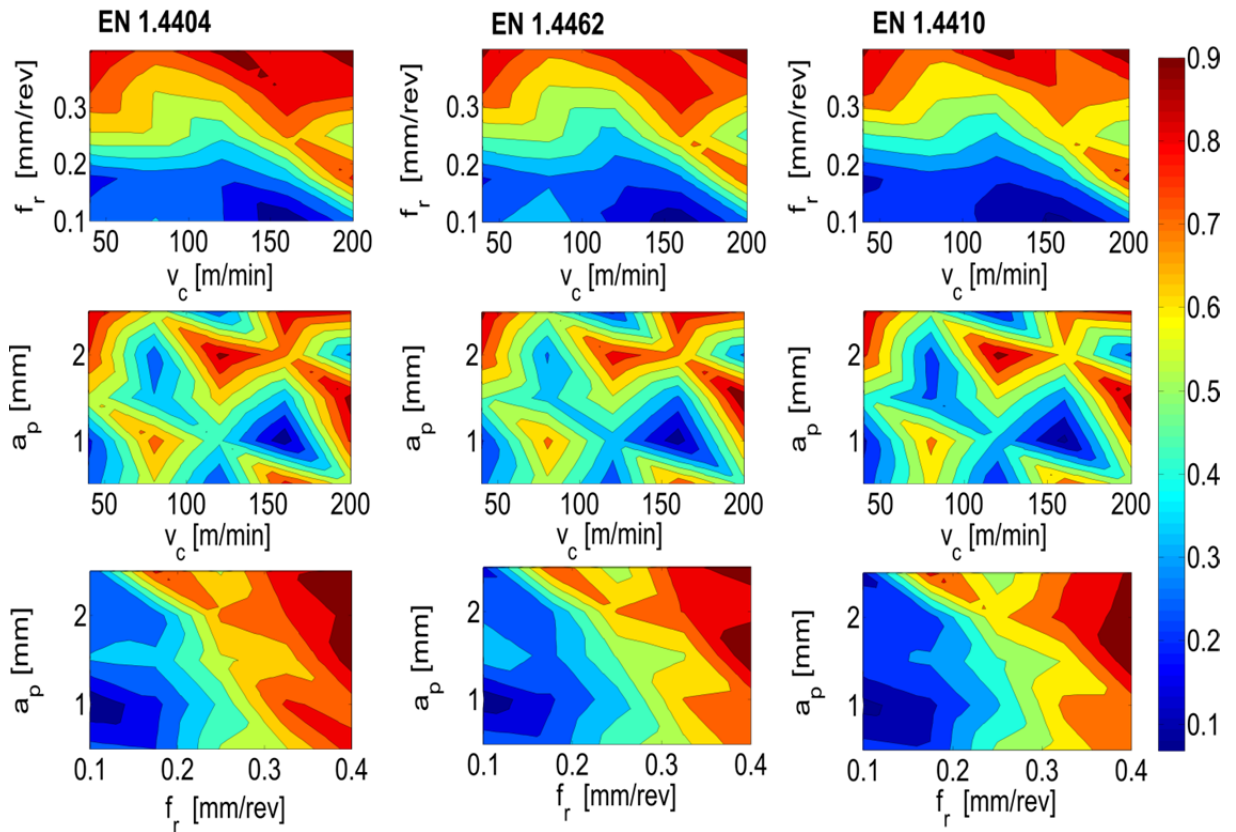


Figure 6.3: Topography of computed MPCI.

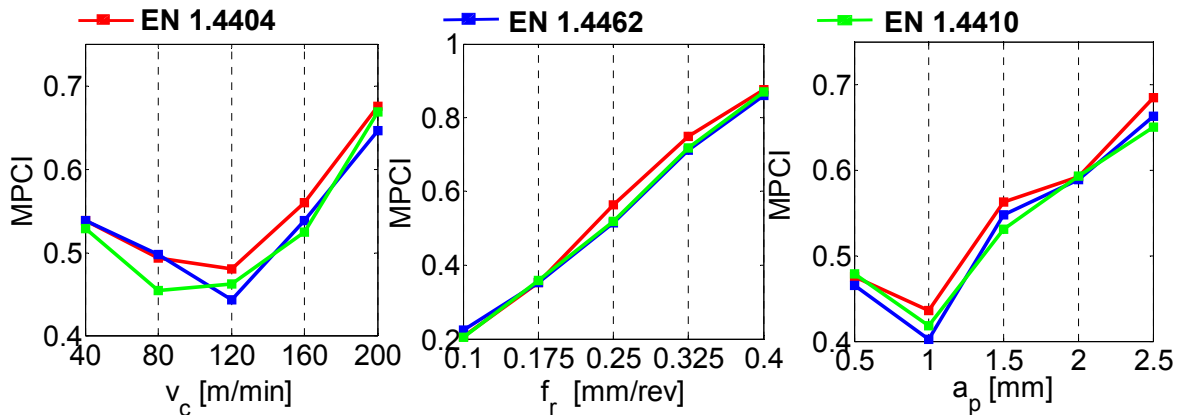


Figure 6.4: Main effect plot of MPCI values in machining stainless steels.

Table 6.3 presents the results of applying ANOVA to the MPCIs so as to define the global significant control factor. Compared to cutting speed and depth of cut, results have shown that the feed rate has the most significant effect of the MPCIs. This contribution is partly attributed to the weights that were assigned to the performances on which feed rate has the impact. Furthermore, the interaction effect of cutting speed and feed rate was insignificant.

Factors	DOF	SS			F-value			P-value			%Contribution		
		EN 1. 4404	EN 1. 4462	EN 1. 4410	EN 1. 4404	EN 1. 4462	EN 1. 4410	EN 1. 4404	EN 1. 4462	EN 1. 4410	EN 1. 4404	EN 1. 4462	EN 1. 4410
v_c	4	0.119	0.110	0.128	2.05	1.94	2.33	0.179	0.198	0.143	5.969	6.031	6.783
f_r	4	1.518	1.335	1.431	26.05	23.42	25.97	0.00*	0.000	0.000	75.72	72.90	75.58
$v_c f_r$	4	0.056	0.062	0.056	0.98	1.09	1.02	0.471	0.424	0.453	2.837	3.389	2.961
a_p	4	0.193	0.209	0.167	3.32	3.68	3.04	0.070	0.055	0.085	9.654	11.45	8.853
Error	8	0.116	0.114	0.117	F-table _(4,16,0.05) =3.0069						5.811	6.229	5.823
Total	24	2.005	1.832	1.894							100	100	100

*Bold P-values are less than 0.05

Table 6.3: ANOVA of the computed MPCIs.

6.3 Meta-heuristic optimization

In the two previous sections, the conflicting responses are converted into one single dimensionless index called MPCIs (VIKOR index). Through this approach, the exact values of the control factors at which the performance characteristics are simultaneously minimum without exceeding certain design limits was not possible. Therefore, the need for employing a more comprehensive approach arises. For this purpose, the application of nature-inspired meta-heuristic algorithms is one of the most versatile options.

In this section, recently developed nature-inspired meta-heuristic algorithms such as FA, AP-SO and CS are systematically applied to the problem and the performances are compared. The systematic optimization procedure involves the following basic steps:

Step 1. Designation of decision variables: The adopted decision variables in present work are v_c , f_r and a_p .

Step 2. Formulation of objective functions: Formulation of optimization model is one of the most important tasks in optimization process. The type of optimization modeling techniques used to express the objective function determines its accuracy and the possibility of reaching a global optimum solution. Therefore, a great attention is made to find a model expressing the

case with simplest form and highest possible precision. Many linear and nonlinear models are examined using NonLinearModel.fit function in Matlab. Finally, the most realistic, reliable, and easier to solve (from optimization point of view) model selected is in the format of:

$$\text{MPCI} = c_1 + c_2 v_c + c_3 f_r + c_4 a_p + c_5 v_c^2 + c_6 f_r^2 + c_7 a_p^2 + c_8 v_c f_r + c_9 v_c a_p \quad (6.1)$$

where c_{1-9} are coefficients of the model, calculated using Eqs. 2.1-10 and are presented in Table 6.4 below.

Workmaterial	c_1	c_2	c_3	c_4	c_5	c_6	c_7	c_8	c_9
EN 1.4404	0.177	-0.006	2.566	-0.149	18e-6	-1.076	0.051	0.003	0.001
EN 1.4462	0.365	-0.007	1.427	-0.158	19e-6	0.685	0.053	0.004	0.001
EN 1.4410	0.233	-0.005	2.197	-0.181	20e-6	0.163	0.053	98e-5	0.001

Table 6.4: Objective function coefficients.

Step 3. Formulation of constraints: For the process of effective optimization, nonlinear constraint models need to be derived and incorporated in optimization model. The mathematical model for the prediction of constraint variables in terms of the decision variables can be expressed as:

$$\ln|C_{ij}| = \ln K_{ij} + \alpha_{ij} \ln v_c + \beta_{ij} \ln f_r + \gamma_{ij} \ln a_p \quad (6.2)$$

where C_{ij} is the predicted constraint for i th material and j th number of performances. K_{ij} , α_{ij} , β_{ij} , and γ_{ij} , are the model constant parameters. Exponentiate both sides of above equation using e , transform it into a power regression Eq.:

$$C_{ij} = K_{ij} \times v_c^{\alpha_{ij}} \times f_r^{\beta_{ij}} \times a_p^{\gamma_{ij}} \quad (6.3)$$

In other words, minimization of each VIKOR index model is imposed by different nonlinear constraints namely:

$$\begin{aligned} \text{Surface roughness constraint: } Ra_{\min} &\leq K_{i1} \times v_c^{\alpha_{i1}} \times f_r^{\beta_{i1}} \times a_p^{\gamma_{i1}} \leq Ra_{\text{average}} \\ \text{Spec. Cutt. energy constraint: } e_{c_{\min}} &\leq K_{i2} \times v_c^{\alpha_{i2}} \times f_r^{\beta_{i2}} \times a_p^{\gamma_{i2}} \leq e_{c_{\text{average}}} \\ \text{Cutting power constraint: } P_{c_{\min}} &\leq K_{i3} \times v_c^{\alpha_{i3}} \times f_r^{\beta_{i3}} \times a_p^{\gamma_{i3}} \leq P_{c_{\text{average}}} \\ \text{Rslt. cutt. force constraint: } R_{c_{\min}} &\leq K_{i4} \times v_c^{\alpha_{i4}} \times f_r^{\beta_{i4}} \times a_p^{\gamma_{i4}} \leq R_{c_{\text{average}}} \end{aligned} \quad (6.4)$$

Table 6.5: presents the estimates of the proposed constraint models and the corresponding numerical bounds. It should be noted that the minimum and maximum adjusted correlation coefficients for the models were 0.762 and 0.967 respectively.

Performance	Material	K_{i1}	α_{i1}	β_{i1}	γ_{i1}	Min	Average
Ra [μm]	EN 1.4404	22.405	-0.091	1.241	0.1444	0.25	2.808
	EN 1.4462	18.166	-0.058	1.202	0.1746	0.25	2.801
	EN 1.4410	16.432	-0.043	1.12	0.131	0.25	2.977
Performance	Material	K_{i2}	α_{i2}	β_{i2}	γ_{i2}	Min	Average
e_c [J/mm^3]	EN 1.4404	5.7772	-0.130	-0.198	-0.427	2	3.938
	EN 1.4462	6.262	0.119	-0.163	-0.369	2	4.284
	EN 1.4410	6.5016	-0.114	-0.164	-0.416	2	4.538
Performance	Material	K_{i3}	α_{i3}	β_{i3}	γ_{i3}	Min	Average
P_c [W]	EN 1.4404	73.51	0.9254	0.802	0.5655	200	2379.93
	EN 1.4462	59.564	0.9995	0.8645	0.662	200	2667.39
	EN 1.4410	85.078	0.9305	0.8226	0.590	200	2775.13
Performance	Material	K_{i4}	α_{i4}	β_{i4}	γ_{i4}	Min	Average
R_c [N]	EN 1.4404	7660.2	-0.163	0.777	0.5761	200	1479.08
	EN 1.4462	8076	-0.127	0.8671	0.665	200	1710.35
	EN 1.4410	9597.9	-0.149	0.8711	0.609	200	1778.42

Table 6.5: Constraint models coefficients and bounds.

Step 4. Setting up decision variables bounds: The bounds of decision variables were selected based on their maximum and minimum values in Table 3.5, i.e.:

$$40 \leq v_c \leq 200[\text{m}/\text{min}]$$

$$0.1 \leq f_r \leq 0.4[\text{mm}/\text{rev}] \quad (6.5)$$

$$0.5 \leq a_p \leq 2.5[\text{mm}]$$

Step 5. Running typical nature-inspired meta-heuristic algorithms: Nature inspired meta-heuristic algorithms are among the most powerful algorithms for engineering optimizations nowadays. Out of many meta-heuristic optimization algorithms, the present chapter compares the performances of three different algorithms namely: FA, APSO and CS. The algorithms are recently developed and simultaneously employed for comparison purposes. For more details, the reader is recommended to refer to the Chapter 2 of the present dissertation. Table 6.6 summarizes the typical initializing optimization parameters for each algorithm.

FA	APSO	CS
Population size = 20	Randomness ampl. (ζ) = 0.2	Number of nests = 20
Number of iterations = 4000	Speed of converg. (Ω) = 0.5	Probability (p_a) = 0.25
Randomization (α_{rand}) = 0.5	Number of particles = 25	Number of iterations = 4000
Attractiveness (β_a) = 0.2	Number of iterations = 4000	
Attractiveness variat. (γ_a) = 1	Randomness = 0.95	

Table 6.6: Initializing parameters.

The obtained optimization results showed that all three methods are highly reliable and converge consistently to the optimum solution. Table 6.7 presents the result of optimization for each workmaterial case. Results have showed that higher values of depth of cuts were needed to get the optimum conditions when machining austenitic stainless steel compared to standard and super duplex stainless steels. The optimization of the latter has required lower cutting speed and higher depth of cut than standard duplex steels.

Optimum Parameter	FA			APSO			CS		
	EN 1.4404	EN 1.4462	EN 1.4410	EN 1.4404	EN 1.4462	EN 1.4410	EN 1.4404	EN 1.4462	EN 1.4410
v_c [m/min]	123.88	129.62	112.57	123.47	134.7	112.07	139.35	148.55	130.18
f_r [mm/rev]	0.101	0.1000	0.1000	0.1000	0.1040	0.1000	0.1000	0.1000	0.1000
a_p [mm]	1.642	1.6063	1.6144	1.6437	1.5863	1.6163	0.5000	0.5000	0.5000
$MPCI_{opt.}$	0.106	0.1201	0.09241	0.10633	0.1198	0.09244	0.0031	0.00945	0.0286
Iter.no.	3811	3989	3844	2515	2416	2494	1189	1286	1092

Table 6.7: Summary of optimization results and meta-heuristic algorithms performances.

The efficiency of algorithms is measured in terms of the required iteration numbers per each algorithm to reach the global optimum or near global optimum and in terms of the extent of minimization. Based on this statement along with running optimization algorithms on an Intel® Xeon® CPU 3.47 GHz and 24GB RAM computer, CS was seen the most efficient followed by APSO and the least efficient FA. Figure 6.5 shows the performance of each algorithm in converging to the global optimum solutions.

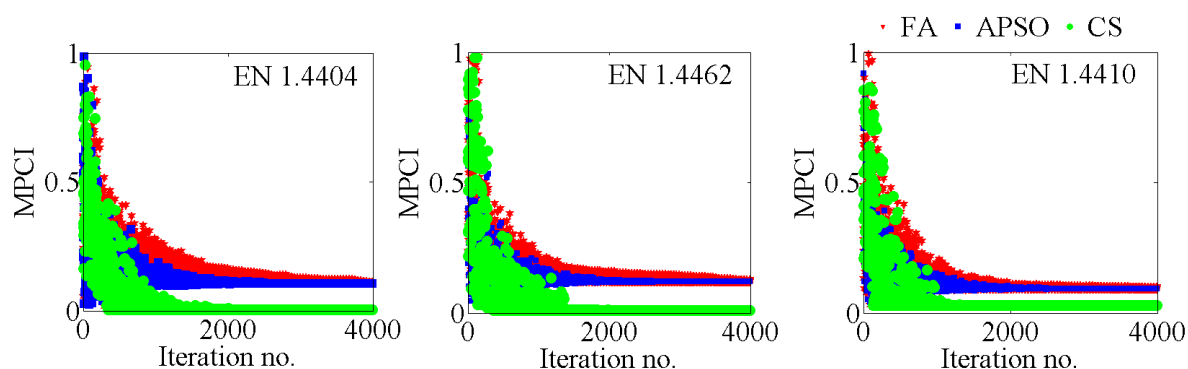


Figure 6.5: Performance of meta-heuristic algorithms in optimization of cutting process.

6.4 Interim conclusions

The present chapter has experimentally addressed the multi-performance optimization of turning of austenitic EN 1.4404, standard duplex EN 1.4462 and super duplex EN 1.4410 stainless

steels utilizing Taguchi-VIKOR-Meta-heuristic concept. Surface roughness, specific cutting energy, cutting power and resultant cutting forces are optimized per each material employing Taguchi optimization procedure and combined as a single, cutting parameter dependent multi-performance characteristics index (MPCI) using VIKOR method. In order to select a meta-heuristics algorithm which could fit the problem the best and determine the optimum global cutting parameter setting, constrained meta-heuristic algorithms such as FA, APSO and CS are simultaneously adopted.

- Under Taguchi optimization procedure, the optimum control $factor^{level}$ combinations for optimizing Ra , e_c , P_c and R_c during turning EN 1.4404 were: $v_c^5 f_r^1 a_p^2$, $v_c^4 f_r^5 a_p^5$, $v_c^1 f_r^1 a_p^1$ and $v_c^4 f_r^1 a_p^1$, respectively. In the same respective manner, the optimum $factor^{level}$ for turning EN 1.4462 were: $v_c^5 f_r^1 a_p^2$, $v_c^3 f_r^3 a_p^5$, $v_c^1 f_r^1 a_p^1$ and $v_c^3 f_r^1 a_p^1$, and for turning EN 1.4410 were: $v_c^4 f_r^1 a_p^2$, $v_c^4 f_r^3 a_p^5$, $v_c^1 f_r^1 a_p^1$ and $v_c^4 f_r^1 a_p^1$.
- Under the utilization of VIKOR as a multi-performance optimization method, the global optimum $factor^{level}$ combinations while turning EN 1.4410, and both of EN 1.4404 and EN 1.4462 were: $v_c^2 f_r^1 a_p^2$, and $v_c^3 f_r^1 a_p^2$, respectively.
- Under the application of meta-heuristic algorithms, constrained optimizations of the developed MPCIs are performed, performances of FA, APSO and CS are compared, and the exact settings of optimum cutting parameters are determined. The obtained optimization results showed that the algorithms are highly reliable and converge consistently to the optimum solution. However, when it comes to comparisons based on the iteration numbers required for convergence and computation results, APSO outperformed the FA and CS was seen far more efficient than both.

7 Application of Fuzzy–MADM approach in optimizing surface quality of stainless steels

In this chapter, Taguchi approach is coupled with fuzzy-MADM methods for achieving better surface quality in constant cutting speed face turning of EN 1.4404 austenitic, EN 1.4462 standard duplex and EN 1.4410 super duplex stainless steels. MADM methods such as GTMA and AHP-TOPSIS are simultaneously adopted to combine well-known surface quality characteristics like arithmetic average (Ra), average distance between the highest peak and lowest valley (Rz) and maximum height of the profile (Rt) into a single index called multi-surface quality characteristics index (MSQCI). The differences in rankings between derived indices are solved through converting each crisp values into trapezoidal fuzzy number and unifying them using fuzzy simple additive weight method. The fuzzy numbers are then defuzzified into crisp values employing techniques like; the spread, mode and area between centroid of centroids. The results are further analyzed using analysis of means (ANOM) and analysis of variance (ANOVA). Finally, confirmation tests are conducted to verify the obtained optimal results.

7.1 Proposed methodology

The novel approach proposed in this chapter can be summarized into five stages as shown in Figure 7.1. Following the determination of MSQCI crisp values for each alternative using described MADM approaches, they are converted into fuzzy numbers. The reason behind the conversion into fuzzy refers to the fact that none of MADM methods can be considered as the ‘super method’ appropriate to all decision making situations. This implies that it is critical to select the most appropriate method to solve the problem under consideration, since the use of unsuitable method always leads to misleading decisions. Therefore, to avoid risking, a level of uncertainty in each computed MSQCI is accounted for, so that the decision maker is uncertain or partially certain based on the values of adopted membership functions.

The fuzzification process of crisp MSQCI values (CV) into fuzzy number MSQCI (a_1, a_2, a_3, a_4) is governed by the following expressions:

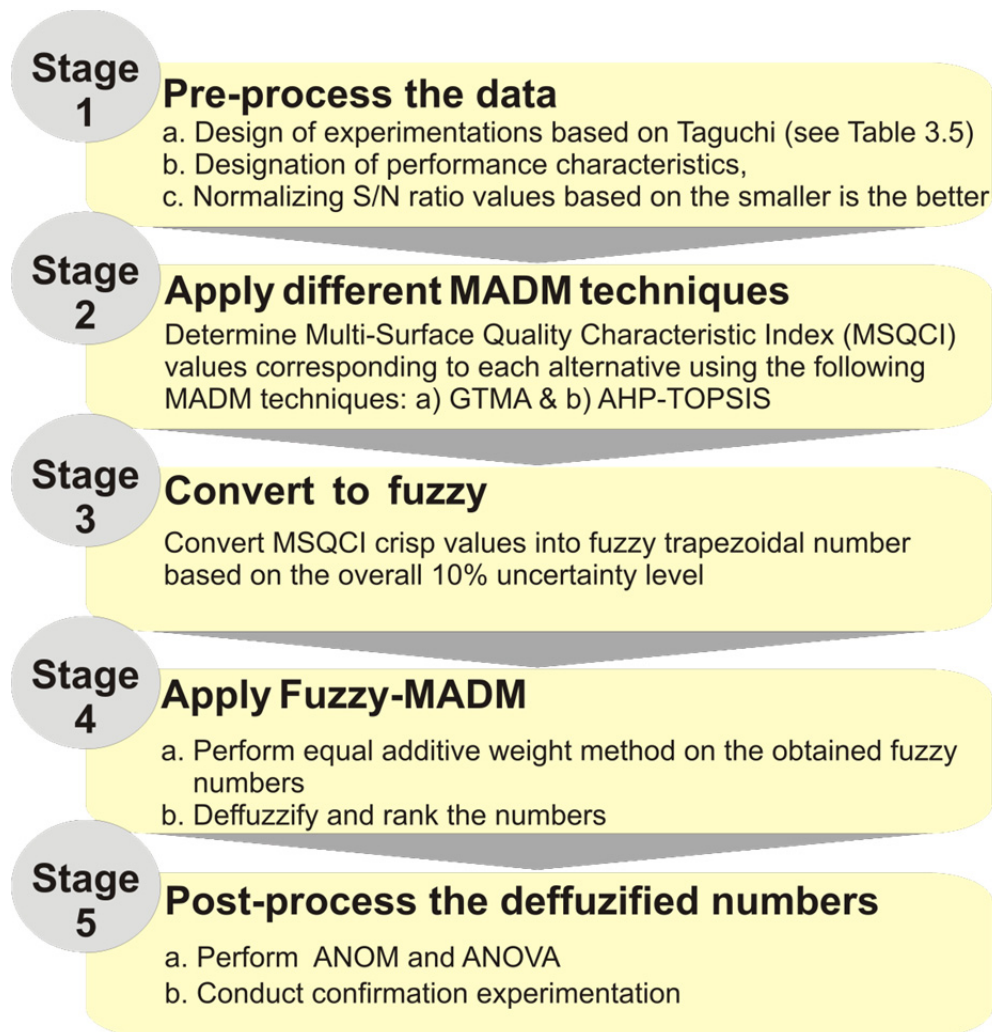


Figure 7.1: Framework of the research.

$$a_1 = \left(1 - \frac{\rho}{2}\right) CV$$

$$a_2 = \left(1 - \frac{\rho}{4}\right) CV$$

$$a_3 = \left(1 + \frac{\rho}{2}\right) CV$$

$$a_4 = \left(1 + \frac{\rho}{2}\right) CV$$

(7.1)

The value of ρ which defines the degree of uncertainty among the crisp MSQCI ranks has to be assumed by decision maker. Typical 10% value of ρ is supposed to give satisfactory results. Consider the generalized trapezoidal function shown in Figure 7.2, the centroids of the

three planes are G_1 , G_2 and G_3 respectively. These centroids are taken as the point of reference to define the ranking of generalized trapezoidal fuzzy numbers. The reason for selecting this point as a point of reference is that each centroid point represents balancing points of each individual plane figure and the centroid of these centroid points i.e. G_0 is a much more balancing point for a generalized trapezoidal fuzzy number. Thus, the ranking function of the generalized trapezoidal fuzzy number $MSQCI(a_1, a_2, a_3, a_4)$ is expressed in terms of its centroid (\tilde{R}), Mode and Spread as follow:

$$\tilde{R}(MSQCI) = \left(\frac{2a_1 + 7a_2 + 7a_3 + 2a_4}{18} \right) \left(\frac{7V}{18} \right) \quad (7.2)$$

$$\text{Mode} = \left(\frac{V}{2} \right) (a_2 + a_3) \quad (7.3)$$

$$\text{Spread} = (V)(a_4 - a_1) \quad (7.4)$$

$$\text{Left spread} = (V)(a_2 - a_1) \quad (7.5)$$

$$\text{Right spread} = (V)(a_4 - a_3) \quad (7.6)$$

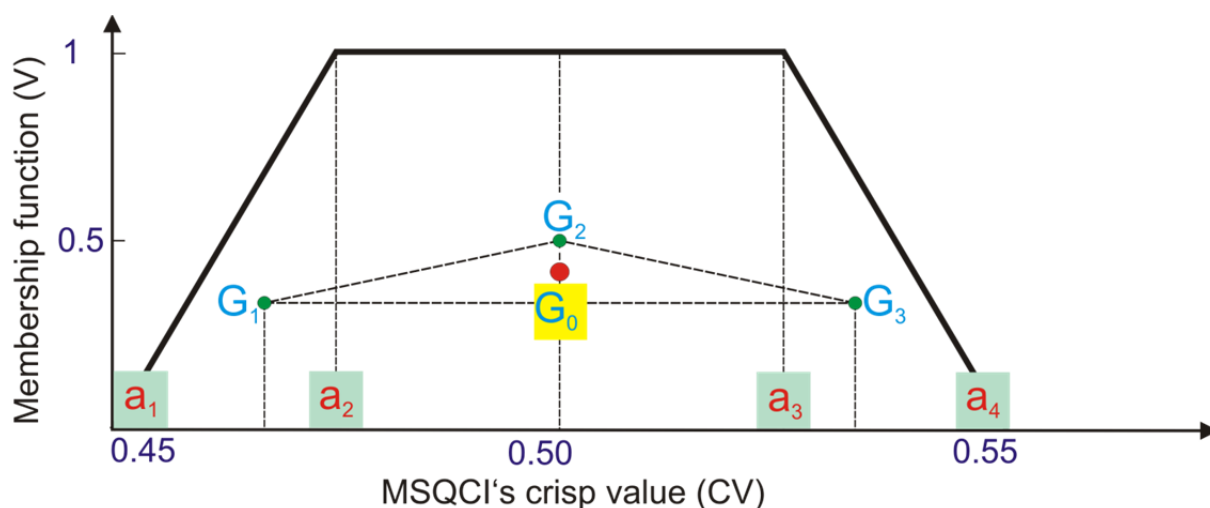


Figure 7.2: Typical fuzzification process of MSQCI's crisp value of 0.5 and $\rho = 0.1$.

Using the above definitions, the ranking procedure of two generalized trapezoidal fuzzy numbers, say $MSQCI_i(a_{1i}, a_{2i}, a_{3i}, a_{4i})$ and $MSQCI_j(a_{1j}, a_{2j}, a_{3j}, a_{4j})$ as follow:

Step 1: Find $\tilde{R}(MSQCI)_i$ and $\tilde{R}(MSQCI)_j$:

- If $\tilde{R}(\text{MSQCI})_i > \tilde{R}(\text{MSQCI})_j$ then $(\text{MSQCI})_i$ outperforms $(\text{MSQCI})_j$.
- If $\tilde{R}(\text{MSQCI})_i < \tilde{R}(\text{MSQCI})_j$ then $(\text{MSQCI})_j$ outperforms $(\text{MSQCI})_i$.

Otherwise, comparisons are not possible and proceed to the next step.

Step 2: Find $\text{Mode}(\text{MSQCI})_i$ and $\text{Mode}(\text{MSQCI})_j$:

- If $\text{Mode}(\text{MSQCI})_i > \text{Mode}(\text{MSQCI})_j$ then $(\text{MSQCI})_i$ outperforms $(\text{MSQCI})_j$.
- If $\text{Mode}(\text{MSQCI})_i < \text{Mode}(\text{MSQCI})_j$ then $(\text{MSQCI})_j$ outperforms $(\text{MSQCI})_i$.

Otherwise, comparisons are not possible and proceed to the next step.

Step 3: Find $\text{Spread}(\text{MSQCI})_i$ and $\text{Spread}(\text{MSQCI})_j$:

- If $\text{Spread}(\text{MSQCI})_i > \text{Spread}(\text{MSQCI})_j$ then $(\text{MSQCI})_j$ outperforms $(\text{MSQCI})_i$.
- If $\text{Spread}(\text{MSQCI})_i < \text{Spread}(\text{MSQCI})_j$ then $(\text{MSQCI})_i$ outperforms $(\text{MSQCI})_j$.

Otherwise, comparisons are not possible and proceed to the next step.

Step 4: Find $\text{Left spread}(\text{MSQCI})_i$ and $\text{Left spread}(\text{MSQCI})_j$:

- If $\text{Left spread}(\text{MSQCI})_i > \text{Left spread}(\text{MSQCI})_j$ then $(\text{MSQCI})_i$ outperforms $(\text{MSQCI})_j$.
- If $\text{Left spread}(\text{MSQCI})_i < \text{Left spread}(\text{MSQCI})_j$ then $(\text{MSQCI})_j$ outperforms $(\text{MSQCI})_i$.

Otherwise, comparisons are not possible and proceed to the next step.

Step 5: Find $\text{Right spread}(\text{MSQCI})_i$ and $\text{Right spread}(\text{MSQCI})_j$:

- If $\text{Right spread}(\text{MSQCI})_i > \text{Right spread}(\text{MSQCI})_j$ then $(\text{MSQCI})_j$ outperforms $(\text{MSQCI})_i$.
- If $\text{Right spread}(\text{MSQCI})_i < \text{Right spread}(\text{MSQCI})_j$ then $(\text{MSQCI})_i$ outperforms $(\text{MSQCI})_j$.

Otherwise, comparisons are not possible and proceed to the next step.

7.2 Results and discussions

7.2.1 Computation of the MSQCI

The experimental layout plan and result as per Taguchi orthogonal array for the current investigation is illustrated in Table A3. From this layout, one can easily conclude that the mean

values of non-beneficial surface quality characteristics during turning super DSS EN 1.4410 are higher than of standard DSS EN 1.4462 and austenitic stainless steel EN 1.4404. The latter has the least mean values of non-beneficial surface quality characteristics.

MADM methods are coupled with Taguchi design to overcome the problem of finding the best alternative for situations where there is more than one performance. Because the selected quality characteristics are of non-beneficial nature, the smaller-the-better criterion is adopted in this study. Therefore, Eq. (2.27) is utilized to transform the real roughness values into S/N ratio values. The following sections briefly describe the procedure of MSQCI calculations.

7.2.1.1 Computation of MSQCI using GTMA

The decision problem is formulated in matrix format using Eq. (2.60-62). Then, larger-the-better term of Eq. (2.84) is used to normalize the S/N ratio to minimize the scale effect. In order to assign the weight to each normalized performance, the superiority of one performance over another has to be considered. In industry, the arithmetic average roughness (Ra) is more pronounced when it comes to the evaluation of surface quality. Therefore, the following relative importance scheme is adopted (refer to Eq. (2.99)):

$$DMA_{GTMA} = \begin{matrix} & \begin{matrix} [Rt & Rz & Ra] \end{matrix} \\ \begin{matrix} [Rt \\ Rz \\ Ra] \end{matrix} & \begin{bmatrix} - & 0.475 & 0.475 \\ 0.225 & - & 0.5 \\ 0.225 & 0.5 & - \end{bmatrix} \end{matrix} \quad (7.7)$$

Then attributes matrix can be written based on Eq. (2.100). It is similar to matrix equation above but also with presence of diagonal elements. To estimate the permanent of matrices, a Matlab code has been programmed. The determined permanent values represent MSQCI using GTMA. From the values of MSQCI it is understood that alternatives A_5 , A_{13} and A_1 are the best choices among the considered sixteen alternatives when surface qualities of EN 1.4404, EN 1.4462 and EN 1.4410 are needed to be optimized respectively.

7.2.1.2 Computation of MSQCI using AHP-TOPSIS

To determine the MSQCI values using AHP-TOPSIS method, Eq. (2.72) is employed first to normalize the computed S/N ratios. The comparison process requires that the relative normalized weights used in AHP-TOPSIS to be equal to those used in the GTMA method. Following

the described procedure for AHP weight calculations, the relative normalized weights of above DMA_{GTMA} matrix are calculated using Eqs. (2.67-69) and the outcomes were; $w_{Ra} = 0.45$ and $w_{Rz} = w_{Rt} = 0.275$. However, using the same decision maker assignment matrix as a pairwise comparison matrix will not give satisfactory CR values which are essential to assess the consistency in the judgment made by AHP and also do not conform to the rule of pairwise comparison. Therefore, the following pairwise matrix is adopted:

$$B_{AHP-TOPSIS} = \begin{matrix} & \begin{matrix} Rt & Rz & Ra \end{matrix} \\ \begin{matrix} Rt \\ Rz \\ Ra \end{matrix} & \begin{bmatrix} 1 & 0.945 & 0.645 \\ 1.058 & 1 & 0.577 \\ 1.55 & 1.733 & 1 \end{bmatrix} \end{matrix} \quad (7.8)$$

With above matrix configuration, the relative normalized weights are the same as those adopted by GTMA. The values of λ_{max} and CR are 3.003 and 0.0031 respectively. The latter is calculated using Eq. (2.71). There is a good consistency in the judgments made, as the calculated value of CR is less than the allowed CR value of 0.1. Weighted normalized matrix is then calculated using Eq. (2.73). The positive ideal A^* and negative ideal A^- values are determined by Eqs. (2.74) and (2.75). The distances from the positive ideal S_i^* , negative ideal solutions S_i^- and the relative closeness to the ideal solution C_i^* are measured using Eqs. (2.76-78). The AHP-TOPSIS method revealed different ranking structure from that of GTMA although the two methods have the same weight values (see Figure 7.3). The ranking suggests optimal alternatives to be A_{13} , A_9 and A_1 for each of EN 1.4404, EN 1.4462 and EN 1.4410 respectively.

The above calculation results showed that, while a specified alternative is the best choice according to a specified MADM method, the same specified alternative is not necessarily regarded as optimum when another MADM method is adopted. To avoid inconsistency in the decision process, the fuzzy logic concept is advised to deal with the problem.

7.2.2 Fuzzy-MADM method

In order to eliminate the scale effect, MSQCI numbers are first normalized between ‘0’ the worst and ‘1’ the best using the normalization technique expressed in Eq. (2.84). Figure 7.4 depicts the effect of cutting speed, feed rate and depth of cut on the MSQCI values. The predominant effect of feed rate can be clearly observed from the slopes of the MSQCI surfaces.

Further, at a medium feed rate value, the interaction of cutting speed and depth of cut reveals that surface quality is optimum when both cutting speed and depth of cut are simultaneously low or high.

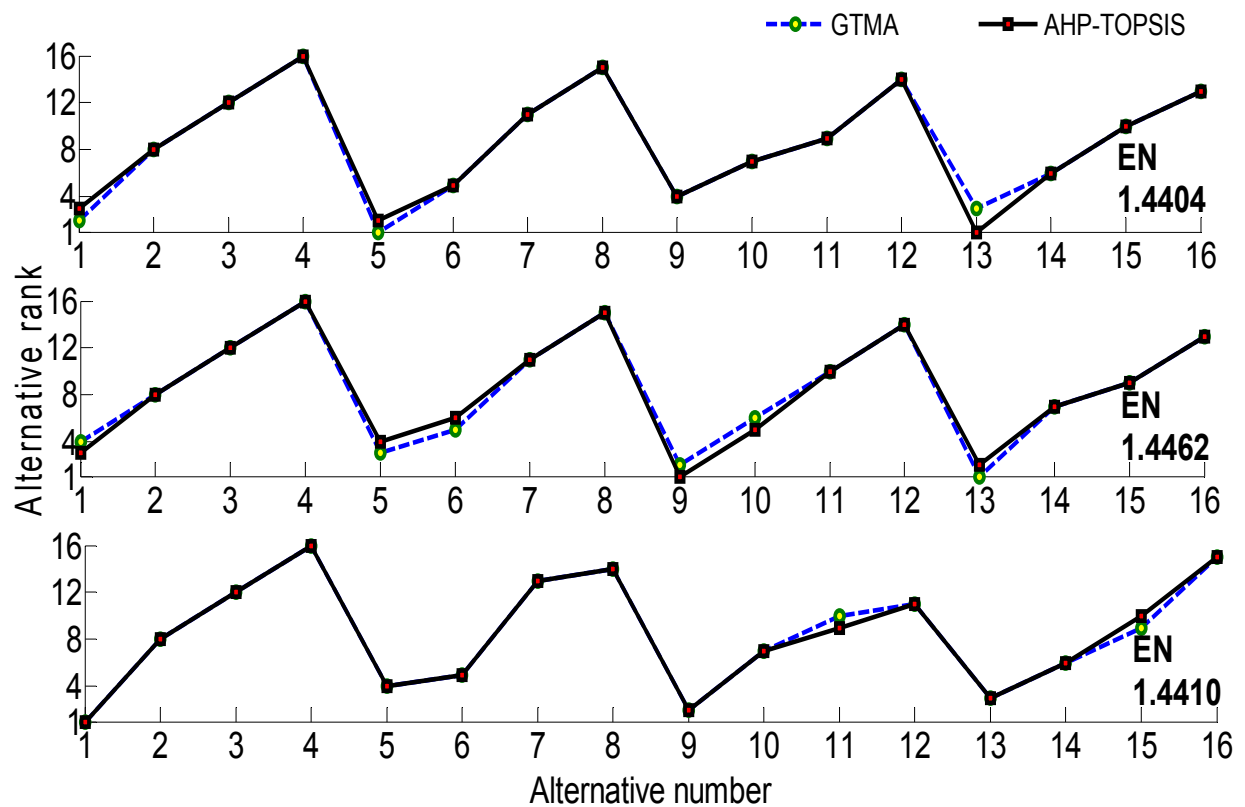


Figure 7.3: Ranking of the MSQCI.

MSQCI crisp values are then converted into fuzzy trapezoidal number based on the overall 10% uncertainty level using terms in Eq. (7.1). For example, for the normalized crisp value (CV) of A_1 when face turning EN 1.4404, the fuzzification process is accomplished as follow:

$$a_1 = \left(1 - \frac{0.1}{2}\right) \times 0.965 = 0.917$$

$$a_2 = \left(1 - \frac{0.1}{4}\right) \times 0.965 = 0.941$$

$$a_3 = \left(1 + \frac{0.1}{4}\right) \times 0.965 = 0.989$$

$$a_4 = \left(1 + \frac{0.1}{2}\right) \times 0.965 = 1.013$$

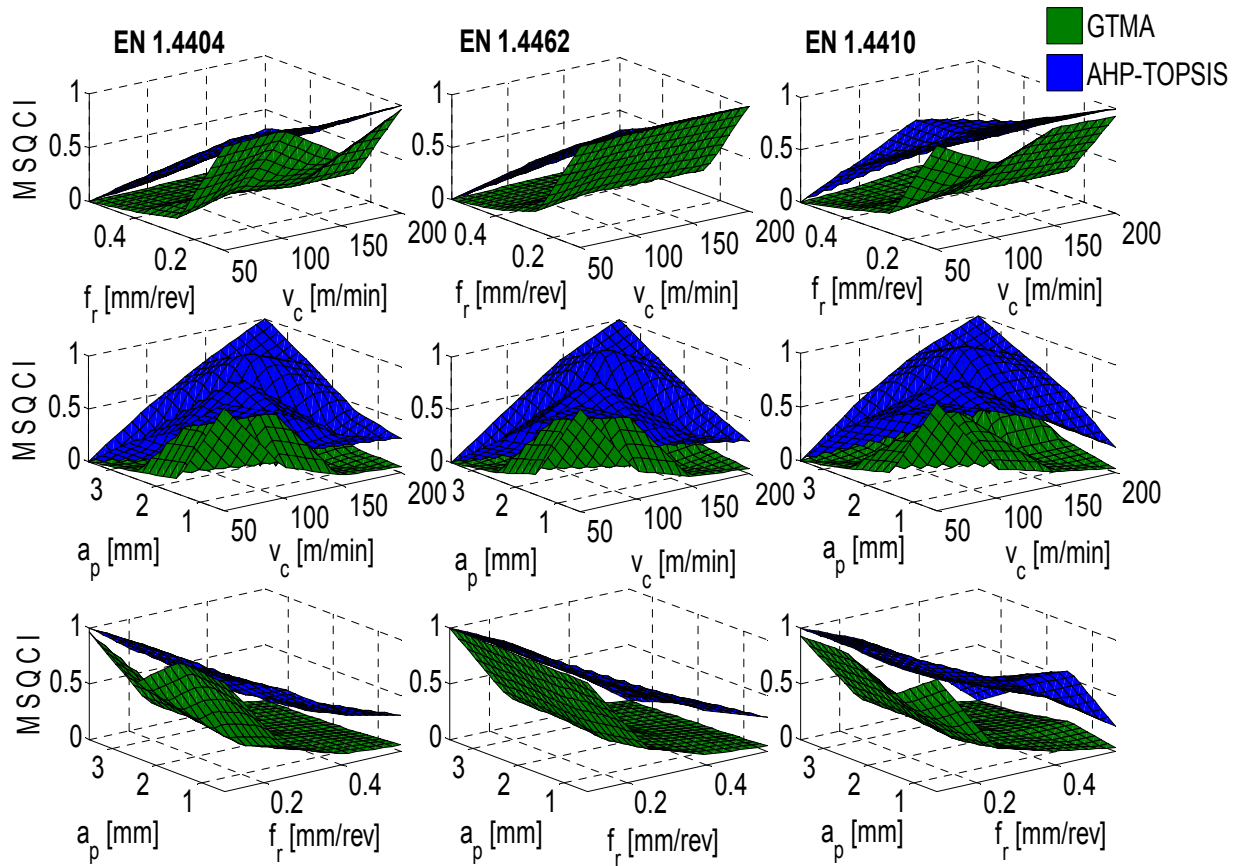


Figure 7.4: Surface plots of the normalized MSQCI values.

Thus, the newly generated number is expressed as fuzzy number (0.917, 0.941, 0.989, 1.013) instead of the crisp value of $CV_{GTMA}=0.965$. Similarly, the fuzzy conversion of A_1 calculated by the AHP-TOPSIS ($CV_{AHP-TOPSIS}=0.998$) is (0.95, 0.973, 1.023, 1.048). The weight vector for each MADM process is kept constant to (0.2, 0.4, 0.6, 0.8). The fuzzy simple additive weighting approach is then applied to the problem. The final score for above numbers is calculated using the arithmetic process described in Eq. (2.19):

$$\begin{aligned} \tilde{A}_1 &= (0.92, 0.94, 0.99, 1.013) \times (0.2, 0.4, 0.6, 0.8) + (0.95, 0.973, 1.023, 1.048) \times \\ &\quad (0.2, 0.4, 0.6, 0.8) = (0.373, 0.766, 1.207, 1.649) \end{aligned}$$

Thereafter, Eqs.(7.2-6) are consecutively applied to calculate the area between centroid of centroids, mode and spreads of each alter alternative. For example, alternative A_1 will have the following fuzzy measures:

$$\tilde{R}_1 = \left(\frac{2 \times 0.373 + 7 \times (0.766 + 1.207) + 2 \times 1.649}{18} \right) \times \left(\frac{7 \times 1}{18} \right) = 0.38576$$

$$\text{Mode}_1 = \frac{1}{2} \times (0.766 + 1.207) = 0.987$$

$$\text{Spread}_1 = 1 \times (1.649 - 0.373) = 1.276$$

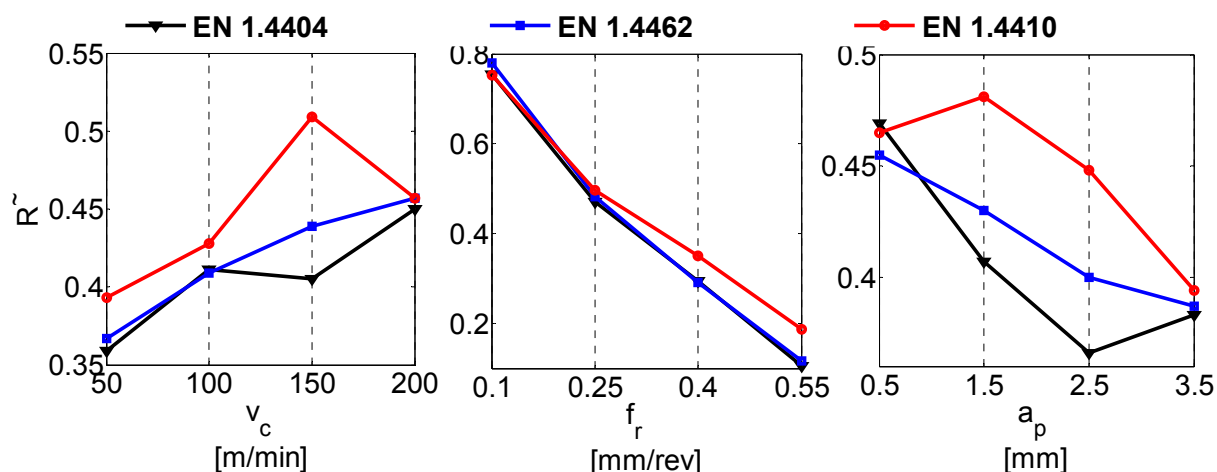
$$\text{Left spread}_1 = 1 \times (0.766 - 0.373) = 0.393$$

$$\text{Right spread}_1 = 1 \times (1.649 - 1.207) = 0.442$$

The same procedure is repeated for the reminder of alternatives. These parameters have shown much less sensitivity toward change in weights than their MSQCI counterparts. For example changing the weight vector to (0.25, 0.5, 0.75, 1) will not cause any change in ranking order. The optimum alternative is defined as an alternative which gives maximum (\tilde{R}), Mode and Spread values. Since the values of these criterions do not present any conflict numbers and no difference in ranking order is noticed among \tilde{R} , mode and spread values, therefore, the alternatives could be ranked directly depending on \tilde{R} . Table A4 lists the computed \tilde{R} , mode, spread values. It also shows the ranking of the alternatives according to the \tilde{R} values.

Performing analysis of means on computed \tilde{R} values, the levels of optimum cutting condition which corresponds to the levels of maximum \tilde{R} value could be determined as shown in Figure 7.5. The reason behind the preference of higher optimum depth of cut in cutting EN1.4410 workmaterial refers to the more breakable, less entangled and better morphology of the chips which often tended to accumulate around the cutting area.

Analysis of variance is then conducted on the computed \tilde{R} values suggesting linear models as per Table 7.1. Statistically significant relationship between cutting variables and performance characteristics at the 95% confidence level were proved based on relatively big differences between $F_{\text{table}(3,12,0.05)} = 3.49$ and individual model F_{ratio} values. The adjusted correlation factor ($R_{\text{adj.}}$) is in very good agreement with predicted correlation factor ($R_{\text{pred.}}$) which supports the prediction power of the model. P-value of terms which are less than 0.05 are designated as significant terms and marked bold. The last three column of the table shows the percent contribution (%Contribution) of each factor. Notably, the contribution of feed rate in determining the surface quality is in average over 90%. However, one has to expect less pronouncing effect when the feed domain is covering smaller ranges.

Figure 7.5: Main effect of cutting parameters on \tilde{R} values.

Parameter	DOF	Sum of squares			P-Value			% Contribution		
		EN 1.4404	EN 1.4462	EN 1.4410	EN 1.4404	EN 1.4462	EN 1.4410	EN 1.4404	EN 1.4462	EN 1.4410
v_c	1	0.0015	0.0026	0.0023	0.378	0.237	0.293	0.558	0.905	1.014
f_r	1	0.2424	0.2631	0.1999	0.000	0.000	0.000	90.17	91.61	88.18
a_p	1	0.0026	0.0012	0.0016	0.260	0.415	0.374	0.967	0.417	0.705
Error	12	0.0223	0.0203	0.0229				8.305	7.068	10.10
Total	15	0.2688	0.2872	0.2267				100	100	100

EN 1.4404 model: $R_{adj.} = 0.8960$, $R_{pred.} = 0.8367$, $F_{ratio} = 44.060 \gg F_{table(3,12,0.05)} = 3.49$
EN 1.4462 model: $R_{adj.} = 0.9117$, $R_{pred.} = 0.8702$, $F_{ratio} = 52.655 \gg F_{table(3,12,0.05)} = 3.49$
EN 1.4410 model: $R_{adj.} = 0.8987$, $R_{pred.} = 0.8152$, $F_{ratio} = 35.489 \gg F_{table(3,12,0.05)} = 3.49$

Table 7.1: ANOVA of \tilde{R} values.

7.3 Confirmation tests

The final step after determining the optimal level of the process parameters is to verify the improvement of the overall performance using the optimal setting of the process parameters. As per Figure 7.5, the optimum $factor^{level}$ combinations for machining both EN 1.4404 and EN 1.4462 were $v_c^4 f_r^1 a_p^1$ and for machining EN 1.4410 were $v_c^3 f_r^1 a_p^1$. The averages of three confirmation run experiments (see Table 7.2) at optimum factor-level combinations are compared with the minimum roughness measured as per Table A3. The positive percentage confirms the advantage of fuzzy application in improving the surface qualities while machining austenitic and duplex stainless steels. The average percentage improvement in surface quality during facing EN 1.4404, EN 1.4462 and EN 1.4410 were: 26.302%, 10.62% and 12.679%

respectively. Thus, the optimal cutting parameters were obtained successfully and the proposed methodology has proved its efficiency.

Facing at optimum cutting conditions	EN 1.4404			EN 1.4462			EN 1.4410		
	<i>Ra</i> [μm]	<i>Rz</i> [μm]	<i>Rt</i> [μm]	<i>Ra</i> [μm]	<i>Rz</i> [μm]	<i>Rt</i> [μm]	<i>Ra</i> [μm]	<i>Rz</i> [μm]	<i>Rt</i> [μm]
Sample 1	0.340	1.640	1.702	0.500	2.010	2.090	0.390	2.120	2.270
Sample 2	0.360	1.730	1.870	0.510	2.160	2.440	0.380	2.030	2.150
Sample 3	0.350	1.870	1.890	0.570	2.420	2.450	0.410	2.340	2.350
Average	0.350	1.746	1.821	0.526	2.196	2.326	0.393	2.163	2.256
Minimum measured roughness in Table A3.	0.453	2.355	2.613	0.558	2.506	2.697	0.482	2.461	2.438
% Improvement	22.737	25.859	30.31	5.734	12.37	13.756	18.465	12.108	7.465

Table 7.2: Confirmation tests results.

7.4 Interim conclusions

Machining of stainless steel grades such as; EN 1.4404, EN 1.4462 and EN 1.4410 have been systematically investigated under a constant cutting speed facing operation. Taguchi method applied on an L_{16} (4^3) orthogonal array. As a result, 16 experiments per material were conducted instead of the full factorial 64 experiments. S/N ratios of quality characteristics like arithmetic average roughness (*Ra*), average distance between the highest peak and lowest valley (*Rz*) and maximum height of the profile (*Rt*) were analyzed using ‘the smaller the better’ criteria. For each performance and material, the optimum cutting parameter level which corresponds to the level of maximum S/N ratio was determined. In this investigation, the following conclusion points are drawn:

- The mean values of non-beneficial surface quality characteristics during turning super duplex stainless steel EN 1.4410 were found to be higher than of standard duplex stainless steel EN 1.4462 and austenitic stainless steel EN 1.4404.
- Through ANOVA and from the percentages of contribution to the stainless steel’s final surface quality, the feed rate was proved to be the predominant controlled factor.
- The ranking conflict among the outputs of different MADM methods has been solved using the Fuzzy approach. The outcomes proved to be far less sensitive to the change of weights with no difference in ranks among the adopted defuzzification techniques.

- The optimum $factor^{level}$ combinations while turning EN 1.4404, EN 1.4462 and EN 1.4410 were: $v_c^4 f_r^1 a_p^1$, $v_c^4 f_r^1 a_p^1$ and $v_c^3 f_r^1 a_p^1$ respectively.
- Utilizing the optimum $factor^{level}$ combinations for confirmation test, the average percentage improvement in surface quality during facing EN 1.4404, EN 1.4462 and EN 1.4410 were: 26.302 %, 10.62% and 12.679% respectively.

8 Sustainability-based multi-pass optimization of cutting DSSs

More recently there has been an increased interest in achieving sustainable manufacturing through implementation of sustainability principles in machining practices. Sustainability principles are considering: machining costs, energy consumption, waste management, environmental impact, operational safety and personal health. In order to address this concern, the present chapter adopts a systematic approach which employs different modeling and optimization tools under a three phase investigation scheme. In phase I, the effect of control factors such as cutting parameters, cutting fluids and axial length of cuts are investigated using the D-Optimal method. The mathematical models for performance characteristics such as; percentage increase in thrust cutting force ($\%F_t$), effective cutting power (P_e), maximum tool flank wear (VB_{\max}) and chip volume ratio (R) are developed using response surface methodology (RSM). The adequacy of derived models for each cutting scenario is checked using analysis of variance (ANOVA). Parametric meta-heuristic optimization using Cuckoo Search (CS) algorithm is then performed to determine the optimum design variable set for each performance.

In the phase II, comprehensive experiment-based production cost and production rate models are analyzed. To overcome the conflict between the desire of minimizing the production cost and maximizing the production rate, compromise solutions are suggested using Technique for Order Preference by Similarity to Ideal Solution (TOPSIS). The alternatives are ranked according to their relative closeness to the ideal solution. In the phase III, expert systems based on fuzzy rule modeling approach are adopted to derive measures of machining operational sustainability called operational sustainability index (OSI). ANN-based models are developed to study the effect of control factors on computed OSIs. Cuckoo Search neural network systems (CSNNS) are finally utilized to constrainedly optimize the cutting process per each cutting scenario. The most appropriate cutting setup to ensure successful turning of standard EN 1.4462 and super EN 1.4410 for each scenario is selected in accordance with conditions which give the maximum OSI. The flowchart of the study is shown in Figure 8.1.

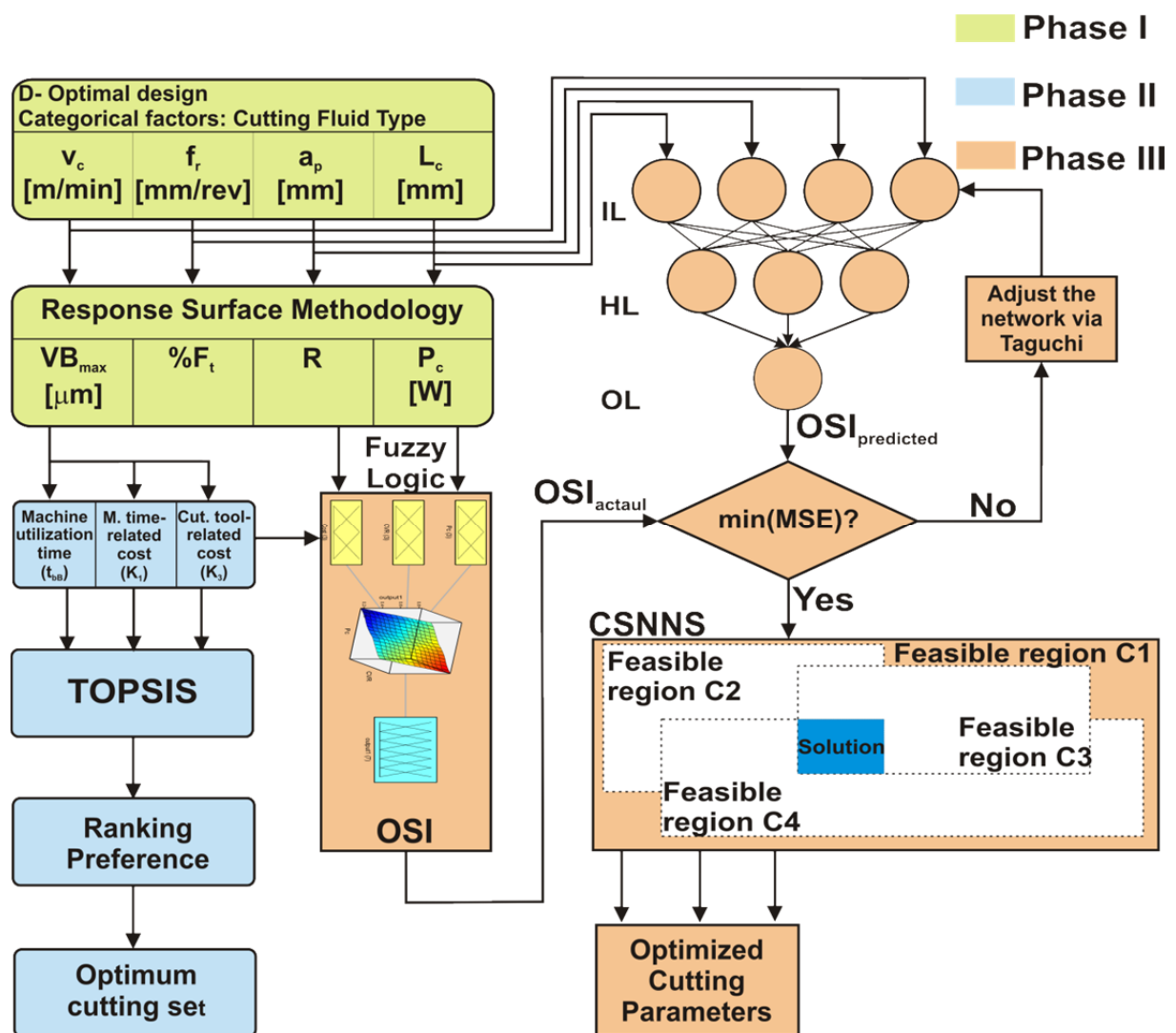


Figure 8.1: Flow chart of the study.

8.1 Performance characteristics

D-optimal designs are used to design the experiments as per Table 3.9. Facing at constant cutting speed of EN 1.4462 and EN 1.4410 DSSs were performed using coated carbide cutting tools with ISO designation CNMG 120408MQ 2025. The workpieces were cut with rotational speed limit of 3500 rpm. An example of the performed cutting operation including the control factors is shown in Figure 8.2. The force signals were analyzed to determine the most sensitive force component to the cutting time. Cutting force in thrust direction was seen more sensitive than the other two components in axial and tangential directions. Therefore, a new parameter which accounts for percentage increase in thrust cutting force has been calculated using the formula:

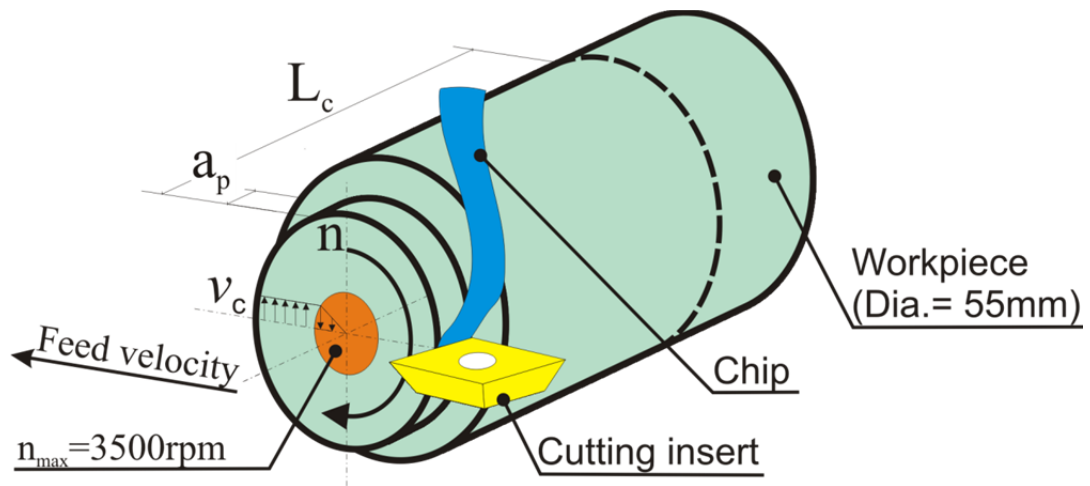


Figure 8.2: Constant cutting speed facing operation.

$$\%F_t = \frac{F_{t_{\max}} - F_{t_{\text{initial}}}}{F_{t_{\text{initial}}}} \quad (8.1)$$

where $F_{t_{\max}}$ is the maximum and $F_{t_{\text{initial}}}$ is the initial thrust cutting forces in each experimental run. In Figure 8.3, a typical thrust force signal of wet cutting EN 1.4462 at $v_c = 200 \text{ m/min}$, $f_r = 0.25 \text{ mm/rev}$, $a_p = 1.5 \text{ mm}$ and $L_c = 12 \text{ mm}$ is shown, indicative of the increasing trend when the total length of cut has been reached. The average thrust cutting force in constant cutting speed area in every cutting pass per cutting run is calculated and the cutting pass with maximum value is designated. In order to compute all increasing percentages in the study, a total of 236 cutting passes per category and 472 cutting passes per material have to be similarly analyzed.

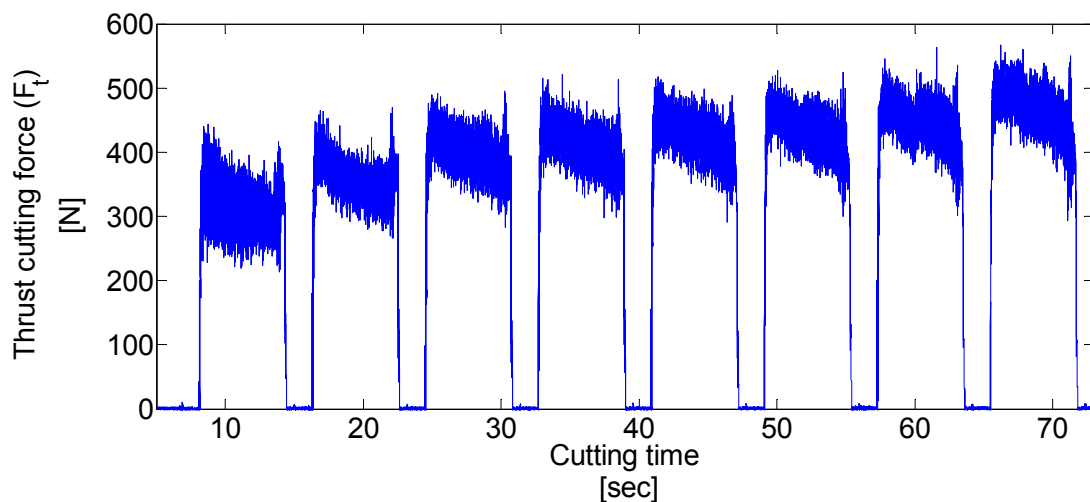


Figure 8.3: Typical increasing trend in thrust cutting force.

One of the most important items related to cleaner production consists in reducing energy consumption in order to cut down carbon emissions associated to energy generation. Therefore, the association of environmental footprint in view of minimization of motor power per each experimental run was considered. The power consumed by the motor of a machine tool is composed of an effective and an idle component. Because of its proportionality to the torque emitted by the motor, the effective power is often used as a signal within the control system for quantifying the motor load. The effective power is obtained from this using Eq. (3.2).

On the other hand, at the end of each experimental run the tool wear was measured and the tool life was estimated based on flank wear criterion of $VB_{\max} = 600\mu m$ on the major cutting edge. Furthermore, during cutting tests the metal chips posed great challenges to the machine tool and the workpiece. To deal with this problem, the chips were collected after each machining trial and later analyzed. Chip volume ratios (R) were then calculated using the procedure described in Chapter 3 of the present dissertation. The experimental results are shown Table A5.

8.2 Phase I: Parametric cutting investigations

Response surface methodology (RSM) has important applications in the design, development, and formulation of new products, as well as in the improvement of existing product designs. Successful use of RSM is critically dependent upon the experimenter's ability to develop a suitable approximation for response function. Usually, a low-order polynomial in some relatively small region of the independent variable space is appropriate. In many cases, either a first-order or a second-order model is used. Often the curvature in the true response surface in machining experimentations is strong enough that the first-order model (even with the interaction term included) is inadequate. A second-order model will likely be required in these situations. The second-order model is widely used in response surface methodology for their flexibility, easiness in estimating the constant parameters, and indications of considerable practical experiences which confirm that second-order models work well in solving real response surface problems [MyMA09]. However, when the entire design space is used to develop the models, then, second-order models, modified second order models, cubic models, modified cubic models, response transformations and model design reductions were seen not satisfactory to capture accurately the highly non-linear relations between the cutting variables and per-

formance characteristics. Therefore, an intermediate and reasonable solution was found for all the cases when second-order non-linear mathematical models in terms of natural variables are selected to predict the performance characteristics (Y) for each condition category in separate, which were of the following form:

$$Y = c_0 + c_1v_c + c_2f_r + c_3a_p + c_4L_c + c_{11}v_c^2 + c_{22}f_r^2 + c_{33}a_p^2 + c_{44}L_c^2 + c_{12}v_c f_r + c_{13}v_c a_p + c_{14}v_c L_c + c_{23}f_r a_p + c_{24}f_r L_c + c_{34}a_p L_c \quad (8.2)$$

The values of the regression coefficients as defined above are determined using the Eqs. (2.1-10). The reader is advised to review the basic concepts of the RSM presented in Chapter 2 of the present study.

8.2.1 Effect of control factors on performance characteristics

The values of regression coefficients in natural form and various statistics about the statistical validity of the developed models at a 95% confidence interval are given in Table A5. The statistical correlation factors such as R^2 and R_{adj} indicates that the models fit the data well. As per analysis of variance (ANOVA) technique, since the calculated value of F-value of all developed second-order models are greater than the standard tabulated value of $F_{table(14,9,0.05)} = 3.03$, then the models are considered adequate within the confidence limit. The adequate precision (A_{prec}), for all models are greater than 4, which indicate an adequate signal to noise ratio, thus the models can be used to navigate the design space.

8.2.1.1 Effect of control factors on the percentage increase in thrust cutting force ($\%F_t$)

In phase I, the developed RSM models were utilized to study the interaction effects of selected independent variables on $\%F_t$. To analyze the interaction effects, three dimensional plots were generated considering two parameter at a time while the other parameters are held constant at their respective center levels. These interaction plots are presented in Figure 8.4a. From which, the following observations can be made:

- For a given depth and length of cut, $\%F_t$ approaches its minimum value as cutting speed and feed rate increase to certain specified limit. Beyond that limit it starts to increase again. When the materials are cut dry, lower cutting speed and feed rates are preferred to minimize $\%F_t$. The values of obtained $\%F_t$ when EN 1.4410 are cut were higher than EN

1.4462 due to the generally higher mechanical strength of EN 1.4410 and fewer weight percentage of assisting machinability elements such as sulfur and phosphorus, see Table 3.1.

- For a specified cutting speed and feed rate, depth of cut values of (1.25-1.5mm) were seen to give the minimum $\%F_t$, as they reduce the ploughing effect, produce friendlier-to-machine chips and exert a more stable cutting process. Generally, lower values of depths of cuts are recommended when process conditions are dry and/or super DSS EN 1.4410 is machined. Values lower than tool nose radius of 0.8mm have to be avoided.
- When cutting speed, feed rate and depth of cut are set at a specified value, $\%F_t$ is expected to increase with the increase of total length of cut. However, the slopes of $\%F_t$ versus total length of cut were seen steeper at higher levels of cutting speeds.

8.2.1.2 Effect of control factors on the effective cutting power (P_e)

Effective power measurement systems are characterized by the fact that they do not affect the mechanical properties of the machine tool. The machining torque can be measured during the operation without the integration of external sensors into the electric flux of the machine. The primary area of application is the recognition of tool fractures and collisions in the workspace. Sufficiently large force changes are necessary for efficient wear monitoring. When monitoring cutting processes, usually external effective-power measurement tools are used, often with associated evaluation software and visualization unit [Kloc11].

Figure 8.4b. illustrates the interaction effects of the independent variables on the effective cutting power. It is seen from this collective figure that:

- Effective cutting power is most sensitive to cutting speed variations when other parameters are kept constant. Maximum and minimum consumptions in effective cutting power are seen at wet cutting of EN 1.4462 and dry cutting of EN 1.4410 respectively.
- Effective cutting power is less sensitive to the length of cut variations as far as the cutting tool does not suffer the catastrophic chipping in the cutting edges.
- Minimum consumption in effective cutting power results when the feed rate is in the range 0.125-0.175 mm/rev of dry cutting and 0.1-0.15mm/rev of wet cutting.
- Two-factor interaction models were seen accurate enough to explain the interaction effects of cutting parameters on the effective cutting power.

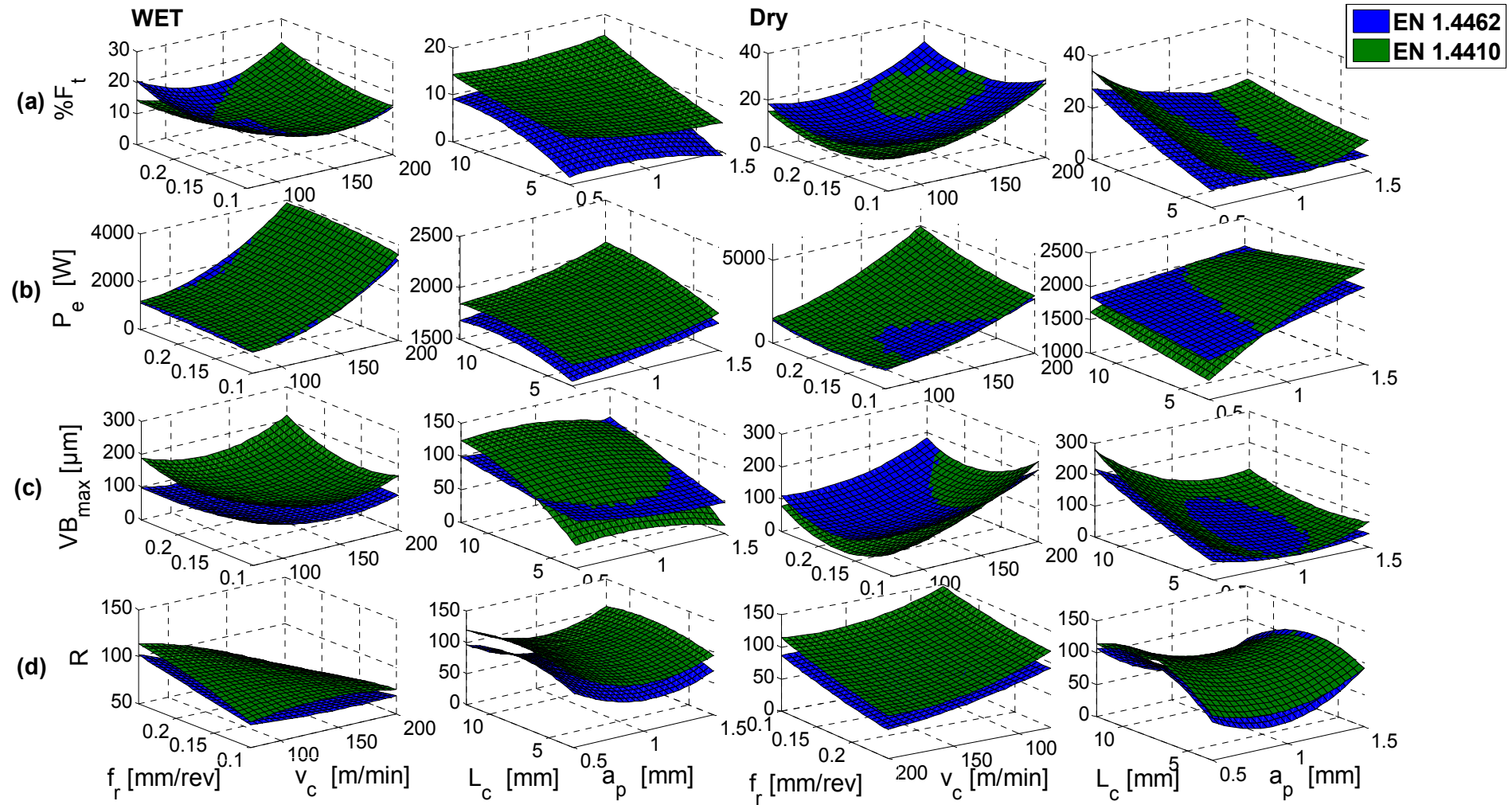


Figure 8.4: Interaction effects of design cutting variables on the performance characteristics.

8.2.1.3 Effect of control factors on the maximum width of tool flank wear (VB_{\max})

Tool wear has a remarkable influence in tool life, cutting forces, vibration, quality of the machined surface and its dimensional accuracy, and consequently, the economics of cutting operations. In this study off-line modeling of the maximum flank wear lands (VB_{\max}) are described as functions of independent cutting variables. Figure 8.4c depicts the interaction contour plots of VB_{\max} as per RSM models tabulated in Table A6. It can be found that:

- During the course of the dry cutting of DSSs, an increased built up edge formation on the tool, obvious inferior chip morphologies, more aggressive notch wear on the major and minor cutting edges and inferior surface qualities were noticed. Therefore, when cutting DSSs, generous amount of cutting fluid is always recommended.
- Wet cutting at cutting parameter ranges of $v_c \approx 100-160$ m/min, $f_r \approx 0.15-0.25$ mm/rev, $a_p \approx 0.75-1.0$ mm for machining EN 1.4462 and $v_c \approx 120-160$ m/min, $f_r \approx 0.15-0.20$ mm/rev, $a_p \approx 1.25-1.5$ mm for machining EN 1.4410 were seen optimum in minimizing the tool flank wear.
- Dry machining is possible when cutting parameters are set appropriately. The settings include; machining of EN 1.4462 at $v_c \approx 75-110$ m/min, $f_r \approx 0.15-0.2$ mm/rev, $a_p \approx 1-1.5$ mm and maximum $L_c/a_p \leq 6$, and machining of EN 1.4410 at $v_c \approx 75-90$ m/min, $f_r \approx 0.125-0.175$ mm/rev, $a_p \approx 0.8-1.35$ mm and maximum $L_c/a_p \leq 4$.
- Direct linear correlations between $\%F_t$ and $\%VB_{\max}$ with reasonable coefficients of determinations (R^2) were noticed:

Cutting of DSS EN 1.4462

Wet: $R^2 = 0.7$

$$VB_{\max} = 5.4198(\%F_t) + 35.149 \quad (8.3)$$

Dry: $R^2 = 0.92$

$$VB_{\max} = 7.7696(\%F_t) - 18.549 \quad (8.4)$$

Cutting of DSS EN 1.4410

Wet: $R^2 = 0.71$

$$VB_{\max} = 6.5767(\%F_r) - 16.793 \quad (8.5)$$

Dry: $R^2 = 0.93$

$$VB_{\max} = 9.918(\%F_r) - 63.494 \quad (8.6)$$

8.2.1.4 Effect of control factors on the on the chip volume ratio (R)

The chip shapes are assessed according to two criteria: transportability and danger for the machine operator. It is no problem to move short, broken chips, such as fragmented spiral chips, in containers. By contrast, this is impossible for ribbon chips, since they always demand special treatment (breaking in the chip breaker or briquetting) in order to make them ready for transport. In a plant with automated manufacturing equipment, where many chips occur, these treatment procedures are very expensive. Consequently, as an alternative, always the aim is to produce chip forms that can be handled easily. Since long ribbon chips and entangled chips, whose edges are very sharp, could possibly endanger the machine operator and cause safety risks [TsRe09]. At this stage, utilizing the chip volume ratio R , the spatial requirement for the chips is considered. Each chip form is assigned to a chip volume ratio R , which defines by what factor the transport volume needed for the specific chip form exceeds the intrinsic material volume of the chip. According to the assignments presented in Figure 1.14, $R \geq 90$ for snarled and ribbon chips, $50 \leq R \leq 90$ for coiled, flat helical and cylindrical helical chips, $25 \leq R \leq 50$ for short coiled chips, $8 \leq R \leq 25$ for spiral chips and $3 \leq R \leq 8$ for short chip particles. It is clear from Figure 8.4d that;

- Higher values of cutting speeds and feed rates are necessary to minimize the chip volume ratio.
- In wet cutting of DSSs, friendlier-to-machine chip forms were produced because of the less encountered friction in the contact area between the chip and rake face.
- Ribbon and snarled chip forms were common when the metals are machined at feed rate and depth of cuts lower than 0.15 mm/rev and 1mm respectively. At intermediate feed ranges, the produced chips were rather of flat-helical and cylindrical-helical forms. The chip forms were rather short coiled chips at higher feed ranges.

- Under the same machining conditions which might produce continuous chips, different chip forms were possible due to continuous entanglement of chips especially when $L_c / a_p \geq 6$.
- Due to the higher proof and tensile strength, and, lower sulfur and phosphor constituents to assist chip breaking, R values of cutting EN 1.4410 were generally higher than of cutting EN 1.4462.
- The tendency to enhance chip segmentation is expected to rise when the chip curl radius is reduced, the coolant pressure is increased and the coolant restricted to smaller area of the chip.

8.2.2 Parametric optimization of performance characteristics

The first optimization process in this investigation is formulated as follow:

- *Objective function*

Formulation of optimization model is one of the most important tasks in optimization process. The type of optimization modeling techniques used to express the objective function determines its accuracy and the possibility of reaching a global optimum solution. The developed response surface models, expressed by Eq. (8.2) and presented previously in Table A6 are used as both objective and constraint functions.

- *Decision variables*

Process parameters considered in the optimization problem were cutting speed, feed rate, depth of cut and length of cut. The length of cut and depth of cuts were set constant at their maximum values to account for the maximum production rates and ensure an integer L_c / a_p ratio due to the imposed practical considerations. Therefore, the parameter bounds for the decision parameters were set as described below:

$$\begin{aligned}
 75 &\leq v_c \leq 200 \text{ m/min} \\
 0.1 &\leq f_r \leq 0.25 \text{ mm/rev} \\
 a_p &= 1.5 \text{ mm} \\
 L_c &= 12 \text{ mm}
 \end{aligned}
 \tag{8.7}$$

- *Constraints*

To ensure that the result of minimization of a performance will not cause an excessive increase in the other three performances, once a performance is selected as a primary objective the others are selected as implicit constraints . This is mathematically expressed as below:

$$LB_j \leq C_j \leq UB_j \quad j = 1:3 \quad (8.8)$$

where: LB_j and UB_j are lower and upper bounds of the implicit constraints which are selected based on practical considerations. At this stage, it would be appropriate if $\%F_t \leq \%F_{t\max}$, $P_e \leq P_{e\max}$, $VB_{\max} \leq VB_{\max(\max)}$ and $R \leq R_{\max}$.

- *Optimization algorithm*

For the purpose of finding minimum of constrained nonlinear multivariable functions described before, Cuckoo Search (CS) algorithm was seen powerful enough to perform the task. The initializing optimization parameters for CS algorithms were: number of nests $n = 20$ and probability $p_a = 0.25$. The obtained optimization results showed that CS is highly reliable and converge consistently to the optimum solution. In Table 8.1, the presented results indicate a conflicting influence of the process parameter on the performance characteristics in conjunction with the different process conditions. As a summary, the following conclusion points can be depicted from the table:

- To optimize $\%F_t$ and VB_{\max} in dry cutting, lower cutting speeds should be considered.
- Unsatisfactory chip forms are expected when the other performances are optimized. For example, when optimizing the maximum tool flank wear, all performances show major decreases, while chip volume ratios show a major increase and the reverse is also true.
- Dry cutting of DSSs can outperform wet cutting of DSS in terms of total progressive tool wear, when appropriate cutting parameters are selected.
- Generally, better chip forms, lower effective cutting power consumption, percentage increase in thrust cutting force and lower wear rates are expected when varying depth of cuts at wet cutting than dry cutting is considered.
- When varying the cutting speed, the effective cutting power consumption, percentage increase in thrust cutting force and maximum tool flank wear show the identical behavior in terms of increase or decrease.

Material	Process condition	v_c [m/min]	f_r [mm/rev]	a_p [mm]	L_c [mm]	$\%F_t$	P_e [W]	VB_{\max} [μm]	R
Minimization of percentage increase in thrust cutting force									
EN 1.4462	Wet	144.83	0.1582	1.500	12.00	6.058*	2027.4	104.36	73.493
	Dry	107.18	0.1833	1.500	12.00	9.498	1578.7	51.648	92.637
EN 1.4410	Wet	140.73	0.1238	1.500	12.00	14.80	1904.1	108.00	99.232
	Dry	80.806	0.1678	1.500	12.00	11.98	1142.4	53.707	114.14
Minimization of effective cutting power									
EN 1.4462	Wet	75.000	0.1000	1.500	12.00	19.18	824.87	146.14	102.56
	Dry	75.000	0.1372	1.500	12.00	14.17	1022.9	69.718	124.58
EN 1.4410	Wet	75.000	0.1000	1.500	12.00	22.47	953.47	184.99	113.13
	Dry	75.000	0.1163	1.500	12.00	14.77	964.92	84.545	141.09
Minimization of maximum cutting tool flank wear									
EN 1.4462	Wet	122.74	0.2388	1.500	12.00	12.27	1861.6	124.96	88.106
	Dry	85.129	0.1802	1.500	12.00	10.48	1240.8	47.443	111.85
EN 1.4410	Wet	134.54	0.1600	1.500	12.00	15.19	1965.8	98.418	105.78
	Dry	75.000	0.1732	1.500	12.00	12.07	1136.9	49.986	118.43
Minimization of chip volume ratio									
EN 1.4462	Wet	200.00	0.2500	1.500	12.00	21.11	4151.2	195.95	35.143
	Dry	200.00	0.2500	1.500	12.00	32.15	4533.9	210.01	19.651
EN 1.4410	Wet	200.00	0.2432	1.500	12.00	29.58	4299.4	225.96	45.862
	Dry	200.00	0.2500	1.500	12.00	40.24	5344.2	259.32	8.9413

*Objectives are written in bold letter.

Table 8.1: Optimization results.

8.3 Phase II: Economics of cutting DSSs

The effective optimization of machining process affects dramatically the cost and production time of machined components as well as the quality of the final product. This section presents the details of multi-objective optimization of multi-pass constant speed facing operation. MADM optimization approach is proposed to determine the optimal cutting parameter which simultaneously minimizes multiple machining economic objectives. Since, the machining parameters that giving maximum production rate would not be identical to those giving minimum production cost, therefore, machine utilization time, main time and cutting tool related costs are considered as potential objectives, in order to optimize the economics of the cutting process.

- *Case study*

To demonstrate the application of the basic concepts of turning process economics practically, productions of 12,000 identical components were considered as a case study. The machining

of each unit has to be accomplished through removing a total cutting length of 12mm under constant cutting speed facing operation. Eqs. (1.11-37) were employed to define each machining economics terms presented in this study. The objective is to simultaneously minimize the conflicting objectives such as machine utilization time t_{bb} , main time-related costs K_1 and the tool related costs K_3 using a multiple attribute decision making (MADM) method called TOPSIS. In conjunction with experimentations and utilizing the feature of simulation on the CNC- controller, the main cutting times of the trials were accurately recorded. The data considered for the case study are given below:

$k_{bb} = 100,000\text{€}$	$Q_m = 40\text{m}^2$	$K_{WSP} = 6\text{€}$
$m = 12,000 \text{ unit}$	$A_a = 30\text{€/m}^2 \cdot \text{Month}$	$x = 1$
$t_n = 1.5 \text{ min}$	$E_c = 0.13\text{€/kWh}$	$P_M = 25\text{kW}$
$t_{vm} = 30 \text{ min}$	$k_k = 0.9\text{€/hrs.}$	$\%C_2 = 30$
$t_{wz} = 0.5 \text{ min}$	$L_m = 34\text{€/hrs.}$	$\text{hrs./week} = 40$
$t_l = 2 \text{ years}$	$r_n = 2.5$	$\text{working shift/day} = 1.9$
$d = 55 \text{ mm}$	$k_{WH} = 80\text{€}$	$\text{week/annum} = 40$
$l_r = 6.875 \text{ mm}$	$z_s = 4$	
$p_p = 10$	$q_i = 10.5$	

The problem can be defined in the context of multi-objective optimization. TOPSIS is proposed to convert the multi-objective optimization of three objectives into a single objective optimization problem. The technique is based on the concept that the chosen alternative should have the shortest Euclidean distance from the ideal solution. The ideal solution is a hypothetical solution for which all attribute values correspond to the maximum attribute values in the database comprising the satisfying solutions; the negative-ideal solution is the hypothetical solution for which all attribute values correspond to the minimum attribute values in the above-mentioned database. TOPSIS, thus, gives a solution that is not only closest to the hypothetically best, but which is also farthest from the hypothetically worst.

The data given in Table A5 are represented as decision matrix (48×4) for each material case. The matrix is not shown here as it is nothing but the repetition of data given in that table, which is represented in a matrix form. The attribute weights of t_{bb} , K_1 and K_3 were 0.45, 0.3, 0.25, respectively. The normalized decision matrix and the weighted normalized matrix are determined by using Eqs (2.72) and (2.73), respectively. The positive ideal solution (A^*) and the negative ideal solution (A^-) were found utilizing Eqs (2.74) and (2.75), respectively. Eqs

(2.76) and (2.77) are used to determine the separation measures. Finally, Eq. (2.78) is adopted to calculate the relative closeness to the ideal solution C_i^* . The results of performing TOPSIS are summarized in Table A7.

The rankings of alternatives by their corresponding TOPSIS indices (see Figure 8.5) revealed the favorability of adapting wet cutting for a simultaneous minimization approach. This is mainly attributed to the fact that when the components are dry machined the cost of increasingly tool wear rate and power consumption overtakes the advantage of not employing cutting fluids. It is also seen that the order of ranking of both materials is almost identical. Because of the higher effective power consumption and tool wears rate at higher cutting speed and higher feed rate ranges and the worst chip morphology at lower ranges, an intermediate range has given the preference over both ranges. It is also noticed that the lower cutting speed when dry cutting EN 1.4410 and the higher cutting speed when wet cutting EN 1.4462 has given higher preference than the similar dry cutting EN 1.4462 and wet cutting EN 1.4410 respectively.

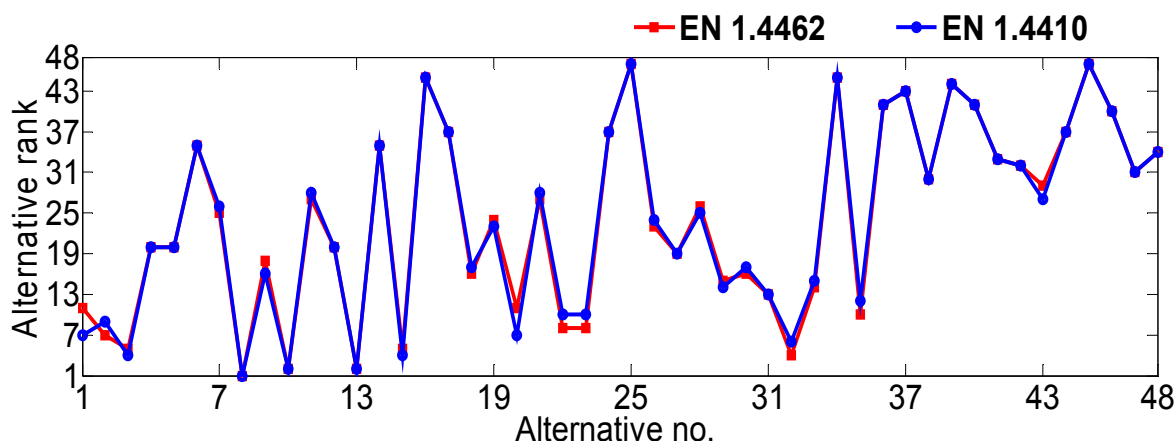


Figure 8.5: Alternatives ranks.

8.4 Phase III: Operational sustainability index

Originally, sustainability relates to forestry. In a very broad and fuzzy definition, forestry is called sustainable, if just as much timber is cut down as can replenish to maintain the basis of life for future generations [KuHM10]. A more widely accepted general definition of sustainable development is provided by the United Nations' Brundtland Commission in 1987: '*development that meets the needs of the present without compromising the ability of future generations to meet their own needs*' [Unng87]. Based on this view, the United Nations 2005 World Summit Outcome document refers to the independent and mutually reinforcing pillars

of sustainable development as economic development, social development and environmental protection (see Figure 8.6) [ChMi11].

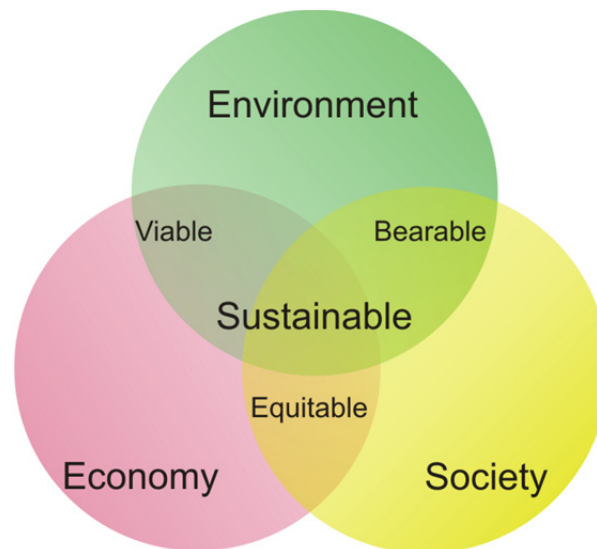


Figure 8.6: The overlapping circles model of sustainable development.

In the context of manufacturing, sustainability means the ability to produce specific product operations and the circulation of resources at the rate of production. Although improving sustainability through manufacturing process optimization is far from simple, it is appealing because manageable number of variables and as relatively low uncertainty can be achieved by measurement of local manufacturing operations [Nahk13]. In this study, the applications of sustainability principles in manufacturing processes are presented using machining as an example. With the implementation of sustainability principles in machining technologies, end-users have the potential to reduce the cost, enhance operational safety and reduce power consumption.

Operational sustainability in machining can be defined in terms of the cost of machining, power consumption and chip volume ratio which greatly affect the waste management. Based on these three interacting and contradicting elements, a compromise solution has to be introduced for a comprehensive evaluation of machining operational sustainability. To obtain this sustainability measure, fuzzy logic system (see Figure 8.7) is employed to combine the total production cost per unit K_F , effective cutting power P_e and chip volume ratios R of each experimental trial into a single sustainability characteristics index called Operational Sustainability Index (OSI). Eqs. (1.11-38) and constants presented in the case study of phase II were respectively employed to calculate the total production cost per unit K_F . Matlab software was

used to construct the inference model of the OSI. The three performance values were first adjusted to a notionally common scale between null and one, using simple normalization methods, so that the digit ‘one’ represents the most desirable and ‘null’ is the least desirable alternative. Small (S), Medium (M) and Large (Lg) fuzzy sets are assigned to the performances. The sustainability index has the following seven levels: Very Low (VL), Low (L), Lower Medium (LM), Medium (M), Upper Medium (UM), High (H), Very High (VH). Mamdani implication method is employed for the fuzzy inference reasoning. The relationship between system input and output is expressed by an “If-Then” type. Totally 27 fuzzy rules per material were formulated.

The predicted values of OSI are presented in Figure 8.8 and the following conclusions are extracted:

- Generally, higher OSI values were noticed when cutting EN 1.4462 is performed.

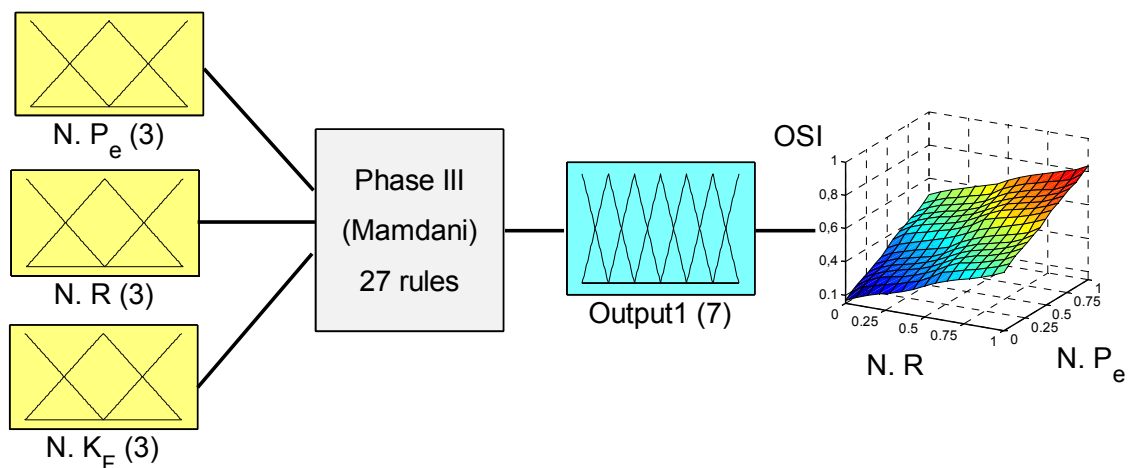


Figure 8.7: Fuzzy Inference System prediction of OSI.

- The average wet cutting OSI is 10% higher than dry cutting due to the fact that the production cost, the effective cutting power and the chip volume ratios were lower in the wet cutting.
- Lower cutting speed, intermediate feed rate and depth of cut ranges, and higher cutting speed, intermediate feed rate and lower depth of cut ranges tend to maximize OSI in dry and wet cutting respectively.
- OSI deteriorates with increasing number cutting passes (L_c / a_p), since all non-beneficial performances are expected to increase as L_c / a_p increases.

- For the equal cutting length scenario of facing EN 1.4462 and EN 1.4410, the maximum OSIs are obtained when alternatives number 8 are selected.

8.4.1 Optimization of OSI using CSNNS

Due to the highly complex relation between cutting parameters and OSI, the RSM was seen no longer efficient to accurately predict the values of OSI. Serious divergences were noticed between experimental data and predicted values for several points. Therefore, a multilayer perceptron (MLP) ANN which can describe the relationships with more precision was integrated with Cuckoo Search meta-heuristic algorithm to perform the task of modeling and optimization of OSIs. The neural networks have two layers: one hidden layer and one output layer. The hidden layer uses a sigmoid-type transference function:

$$f(x) = \frac{1}{1 + \exp[-(b + \sum w_i x_i)]} \quad (8.9)$$

while the output layer uses a linear function:

$$Output_{predicted} = b + \sum w_i x_i \quad (8.10)$$

where w_i and b are the weights and biases of the network respectively. To facilitate the neural network training process, all the inputs were normalized using the following equation:

$$x_i = \frac{2(x - x_{min})}{(x_{max} - x_{min})} - 1 \quad (8.11)$$

This normalization maps all the inputs and OSI between -1 and +1. The ANN architecture consists of 4 neurons in the input layer, 1 neuron in the output layer. The weights and biases of the network are initialized to small random values to avoid immediate saturation in the respective functions. The network was trained by using gradient descent with momentum back propagation algorithm. In this algorithm four parameters must be tuned: learning rate L_R , momentum constant M_c , training epochs E_p and number of hidden neurons H_n . For this tuning the Taguchi design $L_9(3^4)$ was used to find the most convenient values for achieving not only lower root mean square, but also good generalization capability, giving the following values: $L_R = 0.0705$, $M_c = 0.5895$, $E_p = 5000$ and $H_n = 7$. Basic concepts of ANN and Taguchi optimization procedure have been previously described in Chapter 2 of the present

dissertation. Therefore, the reader is advised to review it, in order to facilitate a better understanding of the adopted modeling and optimization techniques.

The performance of the ANNs was statistically measured by the root mean squared error (RMSE), the coefficient of determination (R^2) and the absolute average deviation ($AAD_{avg.}$) obtained using Eqs. (2.33-35). It must be remarked that number of hidden neurons guarantee that there are more training samples than the total amount of free parameters, thus the training process is mathematically determined. The R-squared statistics of the models were generally greater than 0.99, which indicate that the models as fitted explain over 99% of the variability in OSI. The trained networks achieved RSME and $AAD_{avg.}$ values below target (0.0001) and (1%) respectively. It must be mentioned that the relationships between variables are complex, which prove the application of artificial neural networks very advantageous.

Neural network models are then integrated with the Cuckoo Search optimization algorithm, so that solutions which will provide useful information to the user during the selection of machining parameters are obtained. The architecture of the Cuckoo Search Neural Network System (CSNNS) is shown in Figure 8.9. CS outperforms many existing algorithms such as genetic algorithm and Particle Swarm Optimization. This superiority can be attributed to the fact that CS uses a combination of vectorized mutation, crossover by permutation and Le'vy flights and selective elitism among the best solutions. In addition, the not-so-good solutions can be replaced systematically by new solutions, and new solutions are often generated by preferring quality solutions in the solution sets. Thus, the mechanism of the overall search moves is more subtle and balanced, compared with the simple mechanism used in PSO [Yang14b]. The number of host nests (or the population size n) and the probabilities (p_a) were tuned using trial and error method. The population size of (25) and probability of (0.25) were found sufficient in this case.

The selected decision variables were cutting parameters for each process condition. They were defined for the ranges between the minimum and maximum experimental levels presented in Table 2. OSIs were selected as the objective functions to maximize:

$$OSI_i = \psi_i(v_c, f_r, a_p, L_c) \quad (8.12)$$

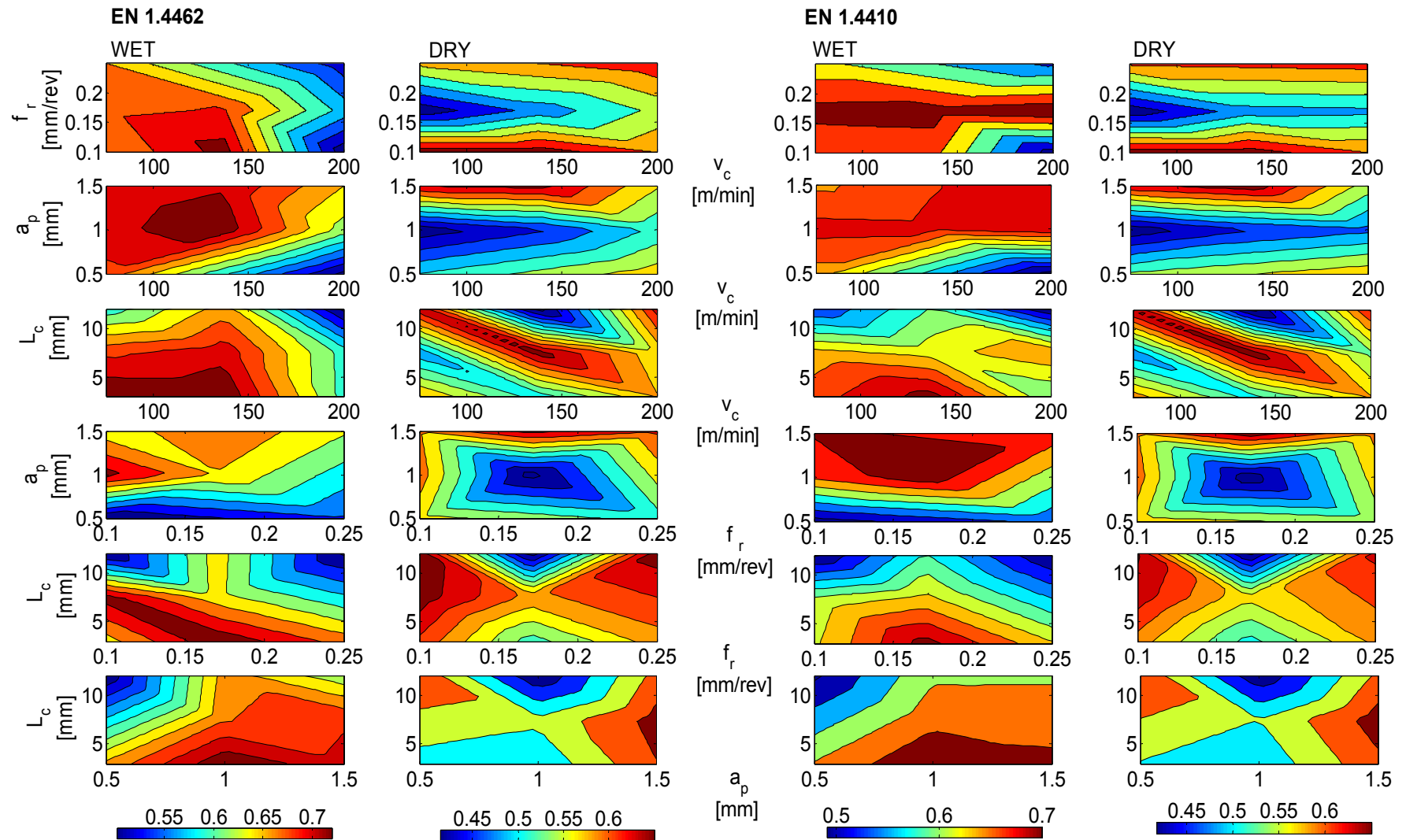


Figure 8.8: Process parameters interaction effects on OSI.

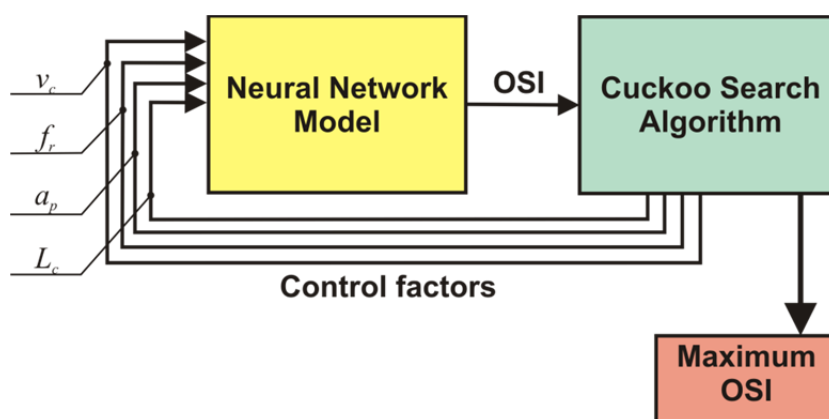


Figure 8.9: Cuckoo Search Neural Network System (CSNNS).

where ψ_i are the neural-network-based models. The considered constraints are the percentage increase in thrust cutting force ($\%F_t$), maximum width of flank wear land (VB_{\max}) and the arithmetic average roughness (Ra). The latter is determined employing Eq. (4.7). In this case, the constrain formulation is preferably defined as

$$\begin{aligned} \%0 &\leq \%F_t \leq \%15 \\ 0 &\leq VB_{\max} \leq 150\mu\text{m} \\ 0 &\leq Ra \leq 2\mu\text{m} \end{aligned} \quad (8.13)$$

CSNNS optimization of OSI has to yield minimum production cost, minimum effective cutting power and the best chip morphology, while considering technological constraints. Figure 8.10 shows the performance of proposed CSNNS. Total computation time were less than 3 minutes with an Intel® Xeon® CPU 3.47 GHz and 24GB RAM computer. Less than 2000 iterations were sufficient to reach to the global optimums in each case. It is evident that the developed CSNNS is very efficient and highly reliable approach for the selection of optimum control parameters.

The obtained optimization results are listed in Table 8.2. Generally, the following conclusion point can be depicted:

- Higher optimum cutting speeds were more often to observe in wet cutting process than in dry cutting process which promotes higher production rates.
- Based on the estimated optimum OSIs, the machinability of EN 1.4462 is higher than the machinability of EN 1.4410.
- Wet cutting of EN 1.4462 and EN 1.4410 outperforms their respective dry cutting in operational sustainability by 9.768% and 12.383% respectively.

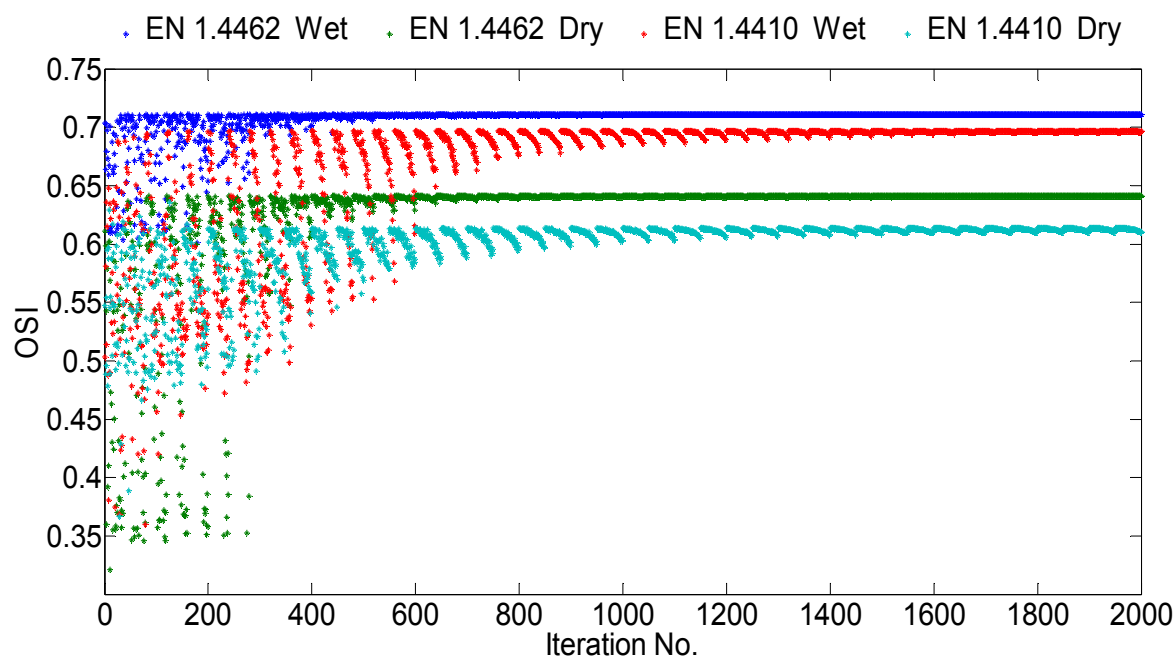


Figure 8.10: Maximization of OSI with CSNNS.

- While wet cutting generally gives lower non-beneficial performance values, this conclusion is hard to notice due to the different adopted optimum cutting speeds and feed rates.
- The magnitudes of surface roughness and chip volume ratio have shown similar trends.
- The coincidence between optimum cutting conditions of the first rank TOPSIS and those of the optimized OSI is observed.

Material	Process condition	v_c [m/min]	f_r [mm/rev]	a_p [mm]	L_c [mm]	$\%F_t$	P_e [W]	VB_{\max} [μm]	R	OSI
EN 1.4462	Wet	156.283	0.1359	1.500	12.00	6.6477	2218.1	104.19	69.073	0.7105
	Dry	91.793	0.1848	1.500	12.00	9.9772	1354.6	48.049	105.60	0.6411
EN 1.4410	Wet	146.30	0.1286	1.500	12.00	14.878	2066.7	106.401	97.052	0.6969
	Dry	82.3259	0.2019	1.500	12.00	13.204	1.4175	62.135	100.7	0.6106

Table 8.2. Results of CSNNS.

8.5 Interim conclusions

Machining of duplex stainless steel grades such as EN 1.4462 and EN 1.4410 has been systematically investigated under a multi-pass constant cutting speed facing operation. In the first phase of the investigation, D-optimal experimental design is used extensively to investigate the effect of process variables on performance characteristics such as percentage increase in thrust cutting force, effective cutting power, maximum tool flank wear and chip volume ratio.

Based on RSM, effective empirical relationships to predict performance characteristics at 95% confidence level were developed. ANOVA used to check the adequacy of the models. The models were then analyzed using 3D surface graphs and used to study the interaction effects of process parameters. At the end of the first phase, constrained Cuckoo Search algorithm is selected to perform optimization of the performance characteristics thereby defining the optimum process conditions. The following general conclusions can be drawn from the first phase of the investigation:

- The values of obtained $\%F_t$ when EN 1.4410 steels are cut were higher than EN 1.4462 steels. They have shown direct linear correlations with maximum tool flank wear and proportional dependency on L_c/a_p ratio, and approached their minimum values as cutting speed and feed rate increased to certain specified limit. However, when the materials are cut dry, lower cutting speed and feed rates than wet cutting are preferred to minimize $\%F_t$.
- Generally, the two-factor interaction models were seen accurate enough to explain the dependency relation between effective cutting power and independent variables. Their minimum consumption were seen when the feed rate is in the range 0.125-0.175 mm/rev of dry cutting and 0.1-0.15mm/rev of wet cutting and the rest of the remained independent variables are kept at their lowest levels.
- Wet cutting at cutting parameter ranges of $v_c \approx 100-160$ m/min, $f_r \approx 0.15-0.25$ mm/rev, $a_p \approx 0.75-1.0$ mm for machining EN 1.4462 and $v_c \approx 120-160$ m/min, $f_r \approx 0.15-0.20$ mm/rev, $a_p \approx 1.25-1.5$ mm for machining EN 1.4410 were seen optimum in minimizing the tool flank wear. Dry machining is possible when cutting parameters are set appropriately. The settings include; machining of EN 1.4462 at $v_c \approx 75-110$ m/min, $f_r \approx 0.15-0.20$ mm/rev, $a_p \approx 1-1.5$ mm and maximum $L_c/a_p \leq 6$, and machining of EN 1.4410 at $v_c \approx 75-90$ m/min, $f_r \approx 0.125-0.175$ mm/rev, $a_p \approx 0.8-1.35$ mm and maximum $L_c/a_p \leq 4$.
- Ribbon and snarled chip forms were common when the DSSs are machined at feed rate and depth of cuts lower than 0.15 mm/rev and 1mm respectively. In wet cutting, friendlier-to-machine chip forms were produced and the R values of cutting EN 1.4410 were generally seen higher than of cutting EN 1.4462. Under the same machining conditions

which might produce continuous chips, different chip forms were also possible, especially when $L_c/a_p \geq 6$.

In the second phase of the study, the measurements were used to develop a comprehensive machining economics model. A case study of producing 12000 units of per each experimental run is considered and the corresponding machining costs and production rates were determined. Summarizing the conclusion points depicted at this stage:

- The optimization conflict between machining economics attributes, such as simultaneous minimization of machine utilization time t_{bb} , main time-related costs K_1 and the tool related costs K_3 could be effectively solved employing TOPSIS.
- The alternatives were ranked based on their computed relative closeness to the ideal solution C^* . The ranking of the alternatives has revealed that the intermediate range of cutting speed, feed rates at wet cutting produce the optimum choice to minimize the considered attributes simultaneously.
- The order of ranking of both materials is almost identical. However, under the same cutting condition, lower cutting speed when dry cutting EN 1.4410 and higher cutting speed when wet cutting EN 1.4462 has shown higher preference than similar dry cutting EN 1.4462 and wet cutting EN 1.4410 respectively.

In the third phase of the study, the computed performances in the first and second phases were utilized to derive a new index of measuring machining sustainability called operational sustainability index (OSI). Based on the Mamdani implication method for the fuzzy inference reasoning, normalized production cost per unit to consider the economics of the machining process, normalized effective cutting power to assess the energy demand of the machining process and normalized chip volume ratio to consider the chip morphology were successfully employed to define the OSI. The optimal machining parameters were tabulated and many conclusion points were extracted:

- To accurately model and constrainedly optimize the highly nonlinear OSIs, neural network models could be integrated with Cuckoo Search algorithm and form Cuckoo Search Neural Network System which is abbreviated as CSNNS. Results have indicated the efficiency of the proposed approach for solving the optimization problem effectively.

-
- Generally, higher OSI values were noticed when wet cutting of DSSs are performed. For instance, in this study, wet cutting of EN 1.4462 and EN 1.4410 outperforms their respective dry cutting in operational sustainability by 9.768% and 12.383% respectively.
 - Based on the predicted OSIs values, the machinability of EN 1.4462 is higher than the machinability of EN 1.4410.
 - Lower cutting speed, intermediate feed rate depth of cut ranges, and higher cutting speed, intermediate feed rate and lower depth of cut ranges tend to maximize OSI in dry and wet cutting respectively.
 - Results also showed coincidence between optimum cutting conditions in second and third phases.

9 Numerical modeling and optimization of turning DSSs

A vividly testimony to the potential interest on duplex stainless steels as a key research topic by various researches in the world is obvious when a search with the keywords ‘duplex stainless steel’ in popular database such us Science Citation Index-Expand or Scopus returns tens of recent publication. However, one can hardly find a study that addresses the FEM simulation of machining duplex grades. Furthermore, despite significant recent advances, FEM itself remains a “plug and play” technique for predicting some process output, depending on the assumed boundary conditions, including the friction.

To address the FEM simulation of machining DSSs correctly, the plug and play technique must be limited first. For this purpose, the present chapter introduces a new method of inverse identification through converting the overall differences between FEM simulation results and experimentation ones into a single measure using Taguchi-VIKOR method. FEM modeling under mixed Taguchi design $L_{18}(2^1 \times 3^7)$ is performed to tune input parameters. Thermal contact conductance (h_{tc}), cutting speed (v_c), feed rate (f_r), cutting tool-workpiece interface hybrid Coulomb (μ_c) and shear (μ_s) friction coefficients, Taylor-Quinney coefficient (κ_t), percentage reduction of original flow stress ($\%p_r$) and Cockcroft-Latham critical damage criterion ($D_{crit.}$) are considered as controllable input parameters. On the other hand, cutting experimentations are conducted and different performances are measured, recorded and analyzed. The percentage difference between numerically and experimentally obtained performances such as thrust cutting force ($\%E_t$), feed cutting force ($\%E_f$), main cutting force ($\%E_c$), chip thickness ($\%E_h$) and tool nose temperature ($\%E_T$) are considered as performance characteristics and are unified into a single index using VIKOR method. The derived indices are then optimized globally to determine the optimum set of input parameter using an effective hybrid neural network-based nature inspired meta-heuristic algorithm known as Firefly Algorithm Neural Network System (FANNS). The optimum sets are next validated through experimentations. In the next stage of the research work, Taguchi optimization procedure (see Figure 2.14) is employed to numerically optimize the chip breaker types (CB), insert geometries ($Geo.$), cooling medium (CM) such as still air, water based and cryogenic

coolants, cutting conditions such as v_c and f_r , and tool orientation angles such as normal rake (α_n) and inclination angle (λ_i). Resultant cutting forces (R_c), effective plastic stresses, chip-tool interface cutting temperatures and tool wear rate are designated as performance characteristics. An expert system based on fuzzy rule modeling approach is adopted to derive a new index called Numerical Machining Performance Measure (NMPM). Finally, analysis of means (ANOM) is applied on the computed NMPMs to define the optimum levels of control factors. A schematic diagram summarizing the methodological framework developed in this study is shown in Figure 9.1.

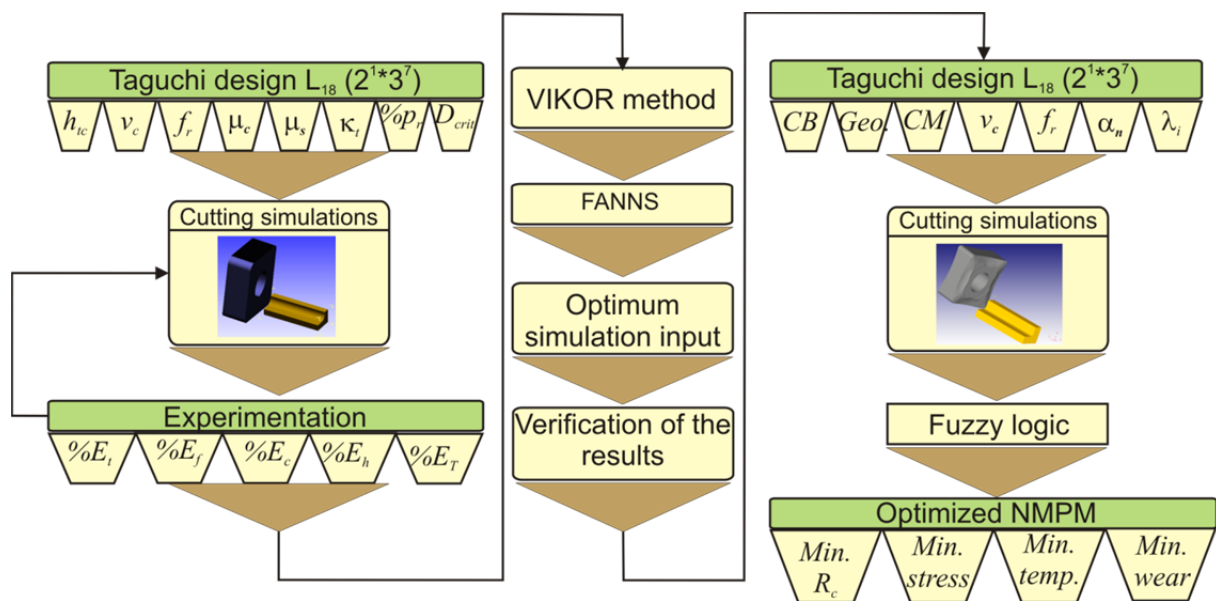


Figure 9.1: Framework of the research.

9.1 3D FEM prediction of the chip serration

EN 1.4462 and EN 1.4410 rods of circular cross-section (diameter 55mm, length 200mm) were machined on a CNC lathe using uncoated rhombic cemented carbide of ISO designation; CNMA 120412-IC20 under Table 3.7's experimental design. The cutting tests are conducted at constant cutting depth of 1.5mm owing to the parameter's less pronouncing effect, and at dry process condition owing to the complications in cutting temperature measurements.

The effect of feed rate and cutting speed on the components of cutting force are shown in Figure 9.2. For instance, increasing the cutting speed from $v_c = 80$ to 240m/min at constant $f_r = 0.225$ mm/rev during turning EN 1.4462 had reduced F_c , F_f and F_t by 6.594%, 40.613% and 19.8% respectively. On the other hand, increasing feed rate from $f_r = 0.15$ to 0.3mm/rev

at constant $v_c = 160$ m/min during turning EN 1.4410 had increased F_c , F_f and F_t by 47.39%, 22.076%, and 52.82% respectively.

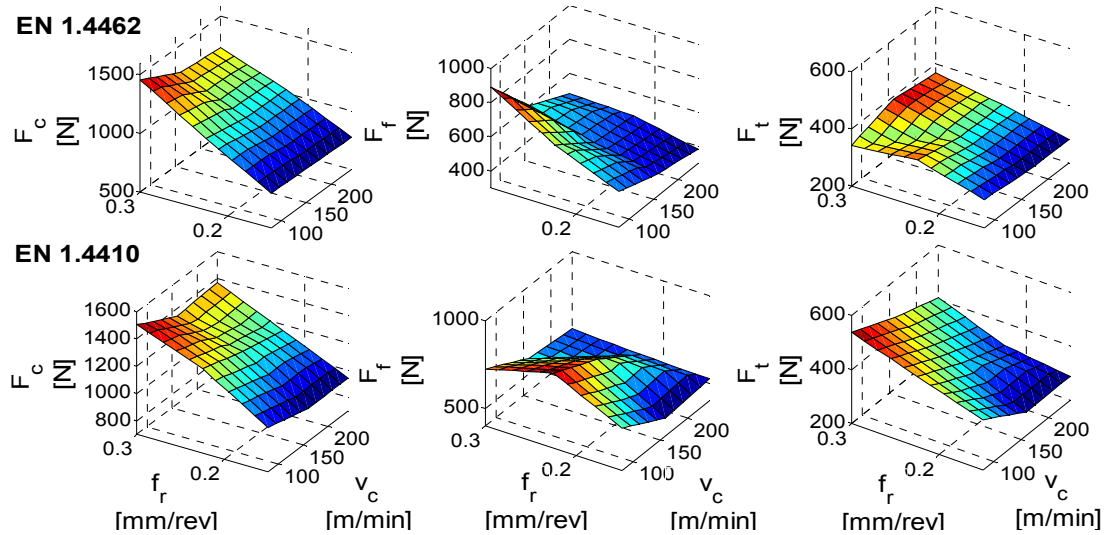


Figure 9.2: Dependency of the components of cutting force on the cutting conditions.

On the other hand, the dependency of maximum chip temperature on the cutting condition and the machined material can be seen in Figure 9.3. Examining the mean maximum chip temperature values, the average maximum chip temperature when machining EN 1.4410 was higher than EN 1.4462 by 3-5%. Experimental results have shown that high cutting speed and feed rates will not always lead to high chip temperatures. This seems in contradiction with the known proportional relations between cutting conditions and cutting temperature. The most likely explanation to this is that when the cutting speed and feed rate is increased, higher rate of removed volume is expected. In this case, the higher heat flux entering the chip resulting from the higher interface temperature is divided over a larger volume, hence lower intensity.

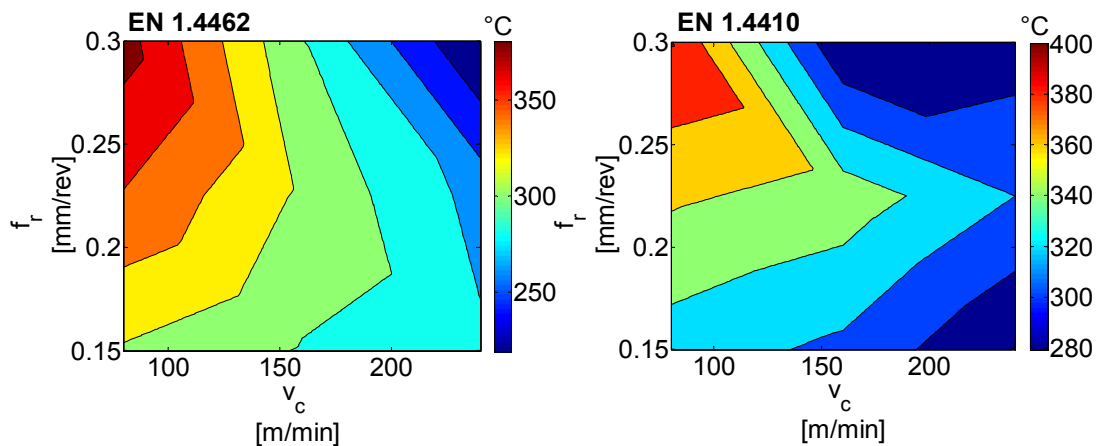


Figure 9.3: Dependency of maximum chip face temperature on the cutting conditions.

Due to the continuous entanglement of the DSS chips around the cutting tool and workpiece surface, the chip surface was not always available for direct observation by the IR camera. Furthermore, due to the concave surface of the scanned workpiece, highly reflective nature of DSS surface and difficulties in accurately measuring surface emissivity, the erroneous temperature reading of tool-chip interface was inevitable (see Figure 9.4). During the early efforts to compare the maximum chip temperatures, similar problems of measuring maximum chip temperature due to the obstructed chip's free face have also been encountered. Therefore, the application of the obtained maximum chip temperature results is restricted only to the experimentation phase. Instead, the calibrated IR images of the black tool tip with emissivity value of 0.93 were obtained very shortly (0.25sec) after the feed was halted and the temperature of the cutter at the end of steady cutting is recorded. The experimentally measured temperature data is then utilized to validate the results obtained in the simulation phase.

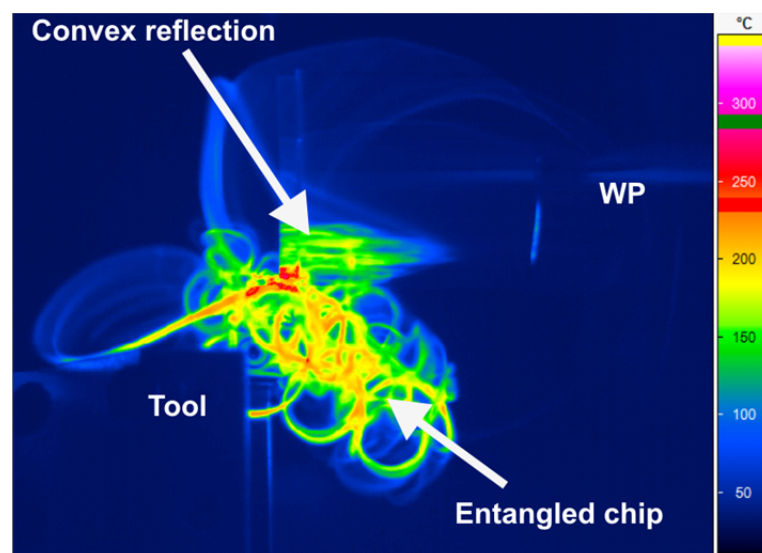


Figure 9.4: Problems associated with IR Camera temperature measurement during machining DSSs.

Figure 9.5 maps the experimentally measured maximum tool surface temperatures at location of $0.5\text{mm} < 45^\circ$ from the origin of the nose curvature. It can be seen that the maximum temperature on the tool face increases with cutting speed. With the increase in feed rate, the cross-section of chip and tool-chip contact length increases and consequently friction rises. This is also involves the increase of temperature.

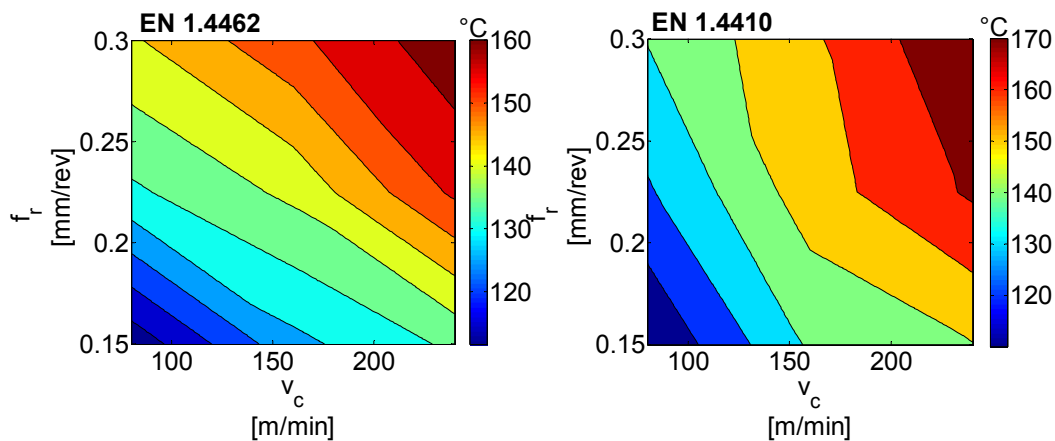


Figure 9.5: Dependency of tool tip temperature on the cutting conditions.

Moreover, the variation of plastic deformation during a chip formation cycle can be depicted using the chip measurement techniques described in Chapter 3 (see Figure 9.6 (a)). Higher plastic deformation during the loading stage and lower plastic deformation during the unloading stage of the chip formation cycle have influenced the grain shapes, so that in the zone of high plastic deformation the grains are severely deformed and in the zone of low plastic deformation the grains are moderately deformed. The tips of the cracks can be clearly observed at the boundary between the zones. The chip structure shown in Figure 9.6 (b) is an example of saw-tooth continuous transitional chips obtained when DSSs are machined. The presence of fragments is also revealed by showing the image of free side of the chip.

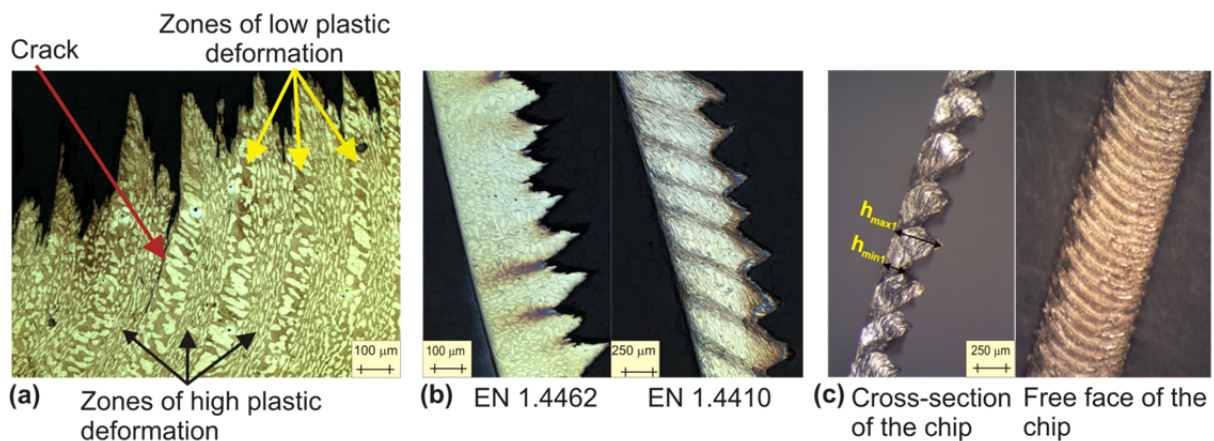


Figure 9.6: Examples of formed chips when machining DSS (a) EN 1.4462 test 2 (b) Left, EN 1.4462 test 1, right, EN 1.4410 test 3 (c) EN 1.4410 Test 6.

Additionally, the average values of five consecutive chip thickness ratios (h_{max_i} / h_{min_i}) are measured to determine the degree of serration (see Figure 9.6(c)). In general, as cutting speed

and feed rate are increased, there are increases in the degree of serration (H) as observed in the Figure 9.7. It is also observed that cutting speed, which adversely affected the h_{\max} , has contributed positively in the chip thinning process through reducing the consecutive distance between the peaks.

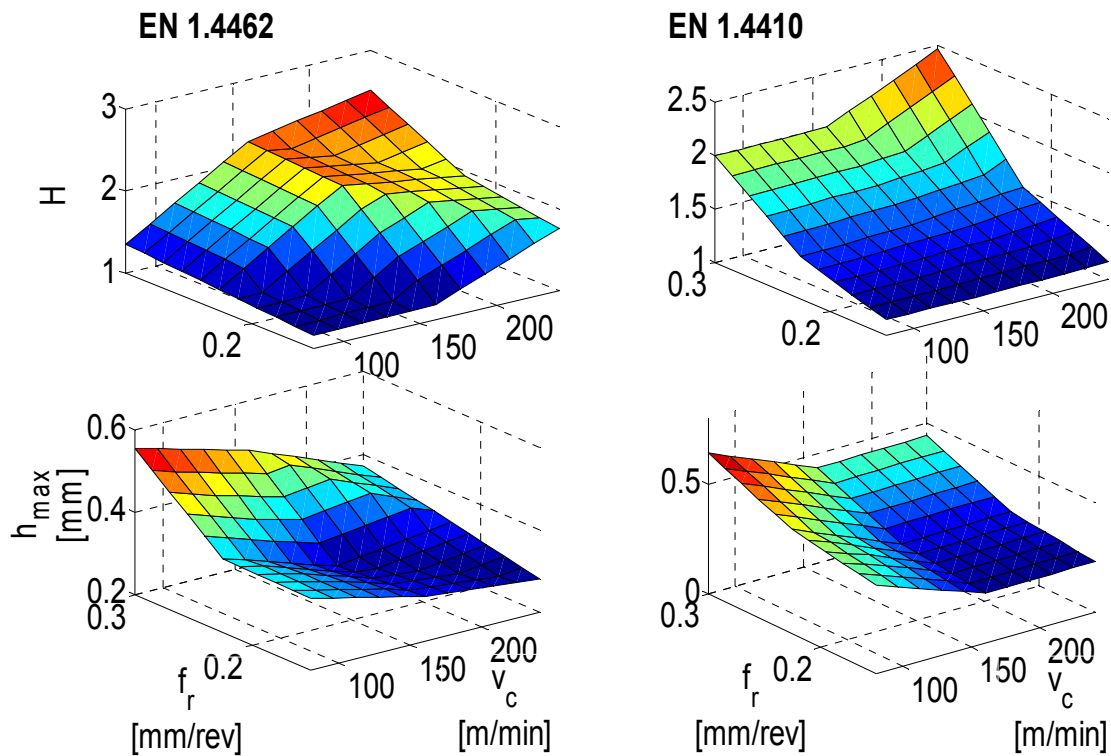


Figure 9.7: Dependency of the chip characteristics on the cutting conditions.

9.2 3D FEM prediction of the chip serration

Serrated chips (also called segmented or nonhomogeneous chips, see Figure 9.6(c)) are semi-continuous with large zones of low shear strain and small zones of high shear strain, hence the latter zone is called shear localization. Metals with low thermal conductivity and strength that decreases sharply with temperature (thermal softening) exhibit this behavior [KaSc06]. Adiabatic shear bands have been observed in the serrated chip during high strain rate metal cutting process of titanium [CaCG08, DuRF14, KaSc06, SiÖz10], carbon steel [RhOh06], nickel-based alloys [LoJJ09] and stainless steels [CBBM13]. Adiabatic shear bands are narrow zones with thickness of the order of few micro-meters where shear deformation is highly localized. Each material has a different susceptibility to adiabatic shear because it depends on properties like heat capacity, heat conductivity, strength level, microstructure, geometry, defects and

strain rates. It is also known that adiabatic shear banding precedes material failures at high strain rates. Adiabatic shear banding is usually accompanied by a loss in stress capacity owing to intense thermal softening in the shear bands and, in many cases, shear bands serve as sites for crack initiation and growth during subsequent dynamic fracture [OdAB05]. Localized adiabatic shearing can be considered a unique consequence of severe plastic deformation at high strain rates. As both thermal and strain softening lead to rapid deformation localization, a shear band forms via a nearly adiabatic process. Also of note is that grain refinement can occur within shear bands and severe plastic strain (which can reach 5–20) can also appear within these shear bands [XLZG05].

In order capture the formation of chip serrations numerically, a material model which accounts for thermal and strain softening should be employed. In last several years, numerous attempts have been made to predict serrated chip formation by finite element method. However, it was found to be difficult to predict the shear band and the serrated chip formation by the FEM technique, especially in three dimension configuration. In addition to the improper meshing size and strategy, the application of conventional flow stress models is one of the main reasons.

As previously mentioned, a universal material model suitable for all cutting simulations remains one of the main unaccomplished tasks. Due to the typical machining high strain, strain rate temperature and temperature gradient, it is not always easy to determine the flow stress curves experimentally. For example, in order to compare the performance of conventional JC and JMatPro in prediction of the chip serration and morphology, the following conditions were considered in 3D-FEM and extruded 2D-FEM modeling approaches:

- Tool: $\alpha_n = -5^\circ$, $\gamma_c = 7^\circ$, $\lambda_i = 0^\circ$, radius of the cutting edge = 0.03mm and tool material is tungsten carbide (WC).
- Workmaterial: EN 1.4462
- Workmaterial models: (a) JMatPro and (b) JC model. The JC constitutive model is given by equation:

$$\sigma = \left(A + B \varepsilon^n \right) \left(1 + C \ln \left(\frac{\dot{\varepsilon}}{\dot{\varepsilon}_0} \right) \right) \left(1 - \left(\frac{T - T_r}{T_m - T_r} \right)^m \right) \quad (9.1)$$

where:

σ is current von Mises flow stress

A is initial yield strength

B is strain hardening coefficient

ε is equivalent plastic strain

n is strain hardening exponent

C is strain rate coefficient

$\dot{\varepsilon}$ is equivalent plastic strain rate

$\dot{\varepsilon}_0$ is reference plastic strain rate = 1 sec^{-1}

m is thermal softening exponent

T is current temperature

T_m is melting temperature = 1440°C

T_r is reference temperature at which material constants are determined [NaNE07].

The elastic-plastic, viscosity and thermal softening terms are represented by the first, second and third brackets of the above equation, respectively. The procedure of computing the constants of Johnson-Cook model from JMatPro stress flow curves involved the following steps:

- The value of A is calculated from the yield stress of the metal given in Table 3.2, i.e. $A = 514 \text{ MPa}$.
- At $T = T_r$ and $\dot{\varepsilon} = \dot{\varepsilon}_0$ the curve $\ln(\sigma - A)$ vs. $\ln(\varepsilon)$ is plotted. The values of B and n are extracted from the intercept and slope of this plot respectively.
- Substituting the values of A , B and n in Eq. (9.1) and assuming $T = T_r$ which eliminates the thermal softening term, the strain rate coefficient (C) is obtained from the slope of the graph $\{\sigma / (A + B\varepsilon^n)\}$ vs. $\ln(\dot{\varepsilon})$.
- At $\dot{\varepsilon} = \dot{\varepsilon}_0$ the viscosity term is eliminated. The exponent (m) is obtained from the slope of the graph $\ln[1 - \{\sigma / (A + B\varepsilon^n)\}]$ vs. $\ln\{(T - T_r) / (T_m - T_r)\}$. Finally, the overall correlation coefficient was found satisfactory at $R^2 = 0.85567$.
- The JC parameters of the EN 1.4462 DSS are given in Table 9.1 and the flow stress curves predicted by JMatPro and the approximated JC model are shown in Figure 9.8.

Parameter	A [MPa]	B [MPa]	n	C	m	$\dot{\varepsilon}_0$ [sec^{-1}]
Value	514	612.96	0.1801	0.01194	0.9765	1

Table 9.1: Parameters of the Johnson-Cook model for EN 1.4462.

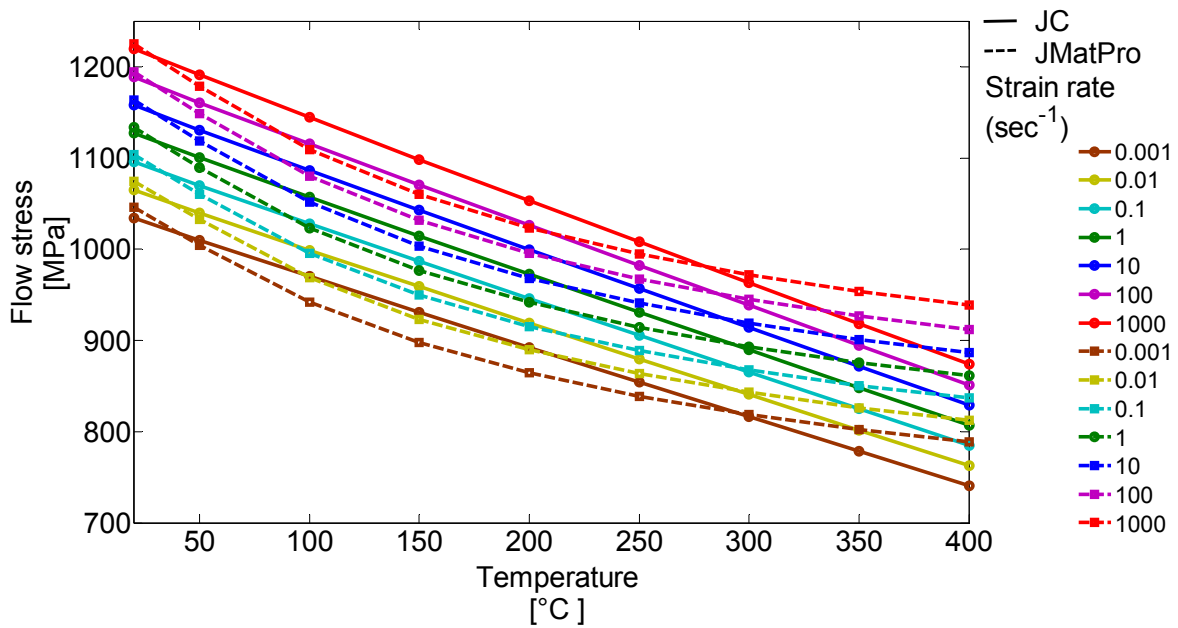


Figure 9.8: EN 1.4462 JC and JMatPro flow stress curves at $\varepsilon = 1$.

- Cutting regime: $v_c = 100\text{m/min}$ and $f_r = 0.25\text{mm/rev}$.
- Damage criteria: $D_{crit.} = 50\text{MPa}$ and $\%p_r = 20$.
- Shear coefficient: $\mu_s = 0.4$ and $h_{tc} = 45\text{N}/(\text{mm}\cdot\text{sec}\cdot\text{K})$.
- Mesh size = $20\mu\text{m}$, aspect ratio = 7 and $\kappa_t = 0.9$.

The left and right sides of the Figure 9.9 presents the states of the deformation zones for JMatPro and JC models, respectively. For instance, Figure 9.9 (b) illustrates the plastic strain distribution in the deformation zone, while Figure 9.9 (c) depicts the temperature distribution in the deformation zones. As clearly seen from the figures, the formation of transitional or saw-tooth chip types are hardly predicted in the chips correspond to the JC model. Furthermore, the morphologies of the chips when cutting stainless steel materials are often related with chip up-curling and side-curling are also hardly noticed in JC material model cases. On the other hand, FEM results employed JMatPro flow stress curves seem to perform better in terms of the prediction of chip curling and formation adiabatic shear bands phenomenon. Therefore, the option of implementing flow stress data generated by JMatPro software is adopted. A text file was first generated for each workpiece material with chemical composition and mechanical properties shown in Table 3.1 and copied into the keyword file of the actual simulation. The software is also used to model the thermo-physical behavior of the work material (see Figure 3.1).

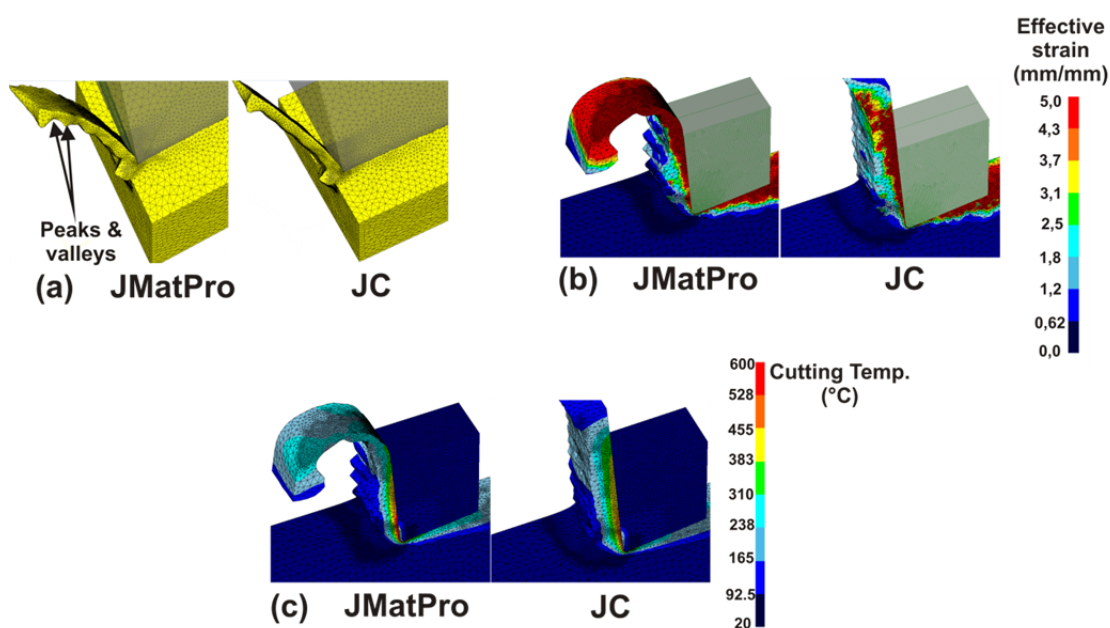


Figure 9.9: JMatPro and JC- based cutting simulation results.

9.3 Inverse identification of 3D FEM input parameters

The classical representation of cutting process by 2D models of chip formation suitable for orthogonal cutting has a limited assistance to tool and process designers. Moreover, the obtained final surface doesn't correspond to the final one that is obtained in 3D. Consequently, some prediction performances like residual stresses cannot have any realistic meaning. For these reasons, the oblique turning models are designed in 3D-FEM environment.

The simulations are carried out with commercial software DEFORM-3D v10.1. The software is based on the implicit updated Lagrangian formulation. The workpiece, each 10mm size, was considered as a plastic object and meshed with approximately 140,000 tetrahedral elements. The tool, considered a rigid object meshed with more than 100,000 tetrahedral elements (see Figure 2.6). It is oriented according to the cutting angles set in experimental test and moves along a straight path. The cutting tool material was uncoated tungsten carbide (WC) and assigned directly from the available material database of the software. Thermal and mechanical properties of WC tools are tabulated in Table 9.2.

Elastic Modulus	650 GPa
Poisson's ratio	0.25
Thermal conductivity	59 W/m.K
Specific heat capacity	15 J/kg.K
Thermal Expansion	$5 \cdot 10^{-6}$ 1/K

Table 9.2: Thermal and mechanical properties of WC.

To improve the gradients of temperature, stress, strain and strain rate distributions, the mesh is refined in the vicinity of areas of cutting tool and the workpiece where the primary and secondary shear zone will be located. However, fixing the minimum element size at a very fine one could make the computation very expensive in terms of running time and size of the final database. Therefore, the minimum mesh element size of the workpiece and aspect ratio were fixed at $\frac{1}{4}$ of the minimum uncut chip thickness and 7 respectively. The top sides of the workpiece as well as all sides of the cutting tool were allowed to exchange heat with the environment; the convection coefficient is considered constant at $0.02 \text{ N}/(\text{mm}\cdot\text{sec}\cdot\text{K})$, which is the default value for dry cutting in DEFORM 3D. On the other hand, meshing of the cutting tool model expected to be a decisive factor for the simulation of the heat flux, temperature and stresses in the material decohesion/deformation zone [NGCH14]. Therefore, the meshing density on the tool is increased in the potential chip-tool contact surface, while the rest of the tool is meshed with relatively coarser mesh. The mesh and boundary conditions for the finite element model are shown in Figure 9.10.

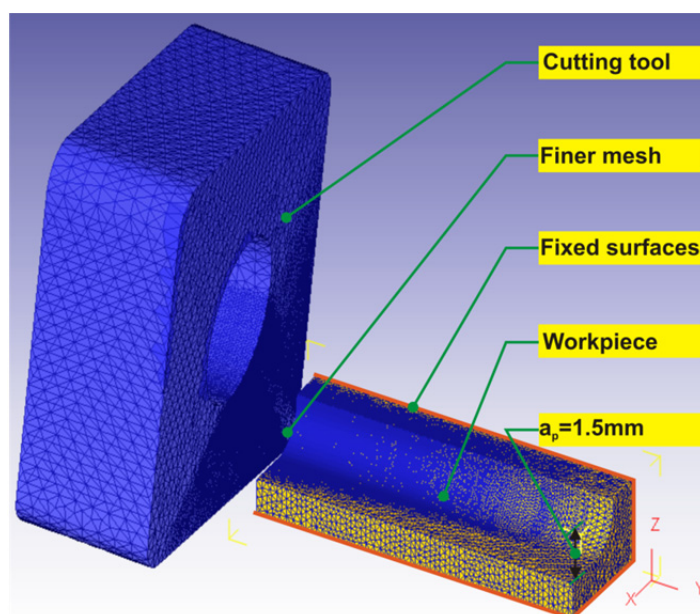


Figure 9.10: Objects of the FEM model.

In this study, the eight considered control factors are: h_{tc} , v_c , f_r , μ_c , μ_s , κ_t , $\%p_r$ and D_{crit} . The second and third control factors are referred to the cutting conditions and are included in the design to give the design more flexibility in dealing with other sets of cutting conditions that are planned in the second stage of the study. Taguchi mixed design $L_{18} (2^1 \times 3^7)$ is adopted so that the underestimation and overestimation problems are avoided by keeping the most parameter levels at three. Additional advantage of this factorial design is the reduction of exper-

imentation trials from 18 to 9, because cutting speed and feed rate are the only input variables that can be designated as controlled factors during experimentation phase of the study. The control factors and their levels are previously listed in Table 3.7.

Figure 9.11 depicts the impact of sets of control factors on the cutting temperature and chip morphology after cutting 8mm of the workpiece length. It is worth mentioning here that it is difficult to draw clear conclusion points on the parametric effect of each control factor based on the images shown, since at each cutting step the values of performances change considerably. Therefore, statistical tools have to be employed to analyze the results and help emphasizing the effect of control factors separately.

The next step after performing 3D-FEM is to postprocess numerous performance characteristics such as; F_c , F_f , F_t , h_{\max} , strain (ε), strain rate ($\dot{\varepsilon}$), effective stress (σ_{eff}), tool/ workpiece interface temperature (T_{TW}) and tool temperature (T_T). 3D-FEM simulation of randomly specified trials was also repeated and no difference between replications was noticed. Owing to the non-beneficial nature of the performances, the lowest value was always desirable. Therefore, Eq. (2.27) is directly employed to calculate the S/N ratios. ANOM is then applied to the computed S/N ratios using Eqs. (2.29) and (2.30). Thereafter, the optimum level is calculated utilizing Eq. (2.31).

Figure 9.12 shows the results of performing ANOM after normalization. The mean S/N ratios are normalized between the worst '0' and the best '1'. For instance, the optimum $factor^{level}$ combinations which minimize the main cutting force for machining EN 1.4462 and EN 1.4410 are $h_{tc}^1 v_c^3 f_r^2 \mu_c^1 \mu_s^1 \kappa_t^3 \% p_r^1 D_{crit}^1$ and $h_{tc}^1 v_c^3 f_r^1 \mu_c^2 \mu_s^1 \kappa_t^3 \% p_r^1 D_{crit}^1$ respectively. Another example, in the case of turning EN 1.4410, simulation results showed that increasing the cutting speed value from $v_c = 80\text{m/min}$ to 240m/min had reduced the main effects of F_c , F_f , F_t , h_{\max} and ε by 43.6%, 32.08%, 46.08%, 13.244% and 39.44% respectively. At the same time, the main effect of $\dot{\varepsilon}$, σ_{eff} and T_{TW} have increased by 37.98%, 7.25% and 19.045% respectively.

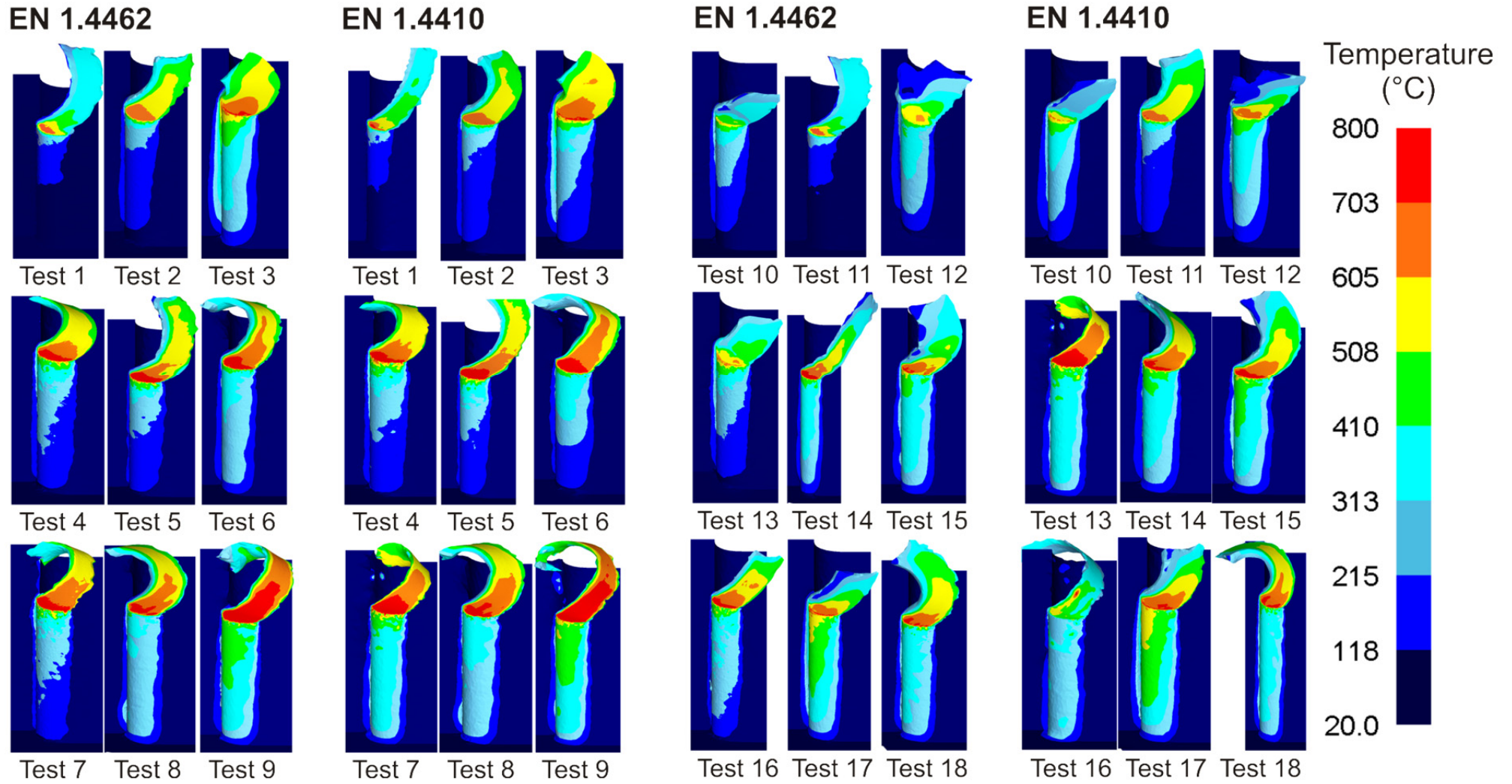


Figure 9.11: 3D-FEM temperature distributions.

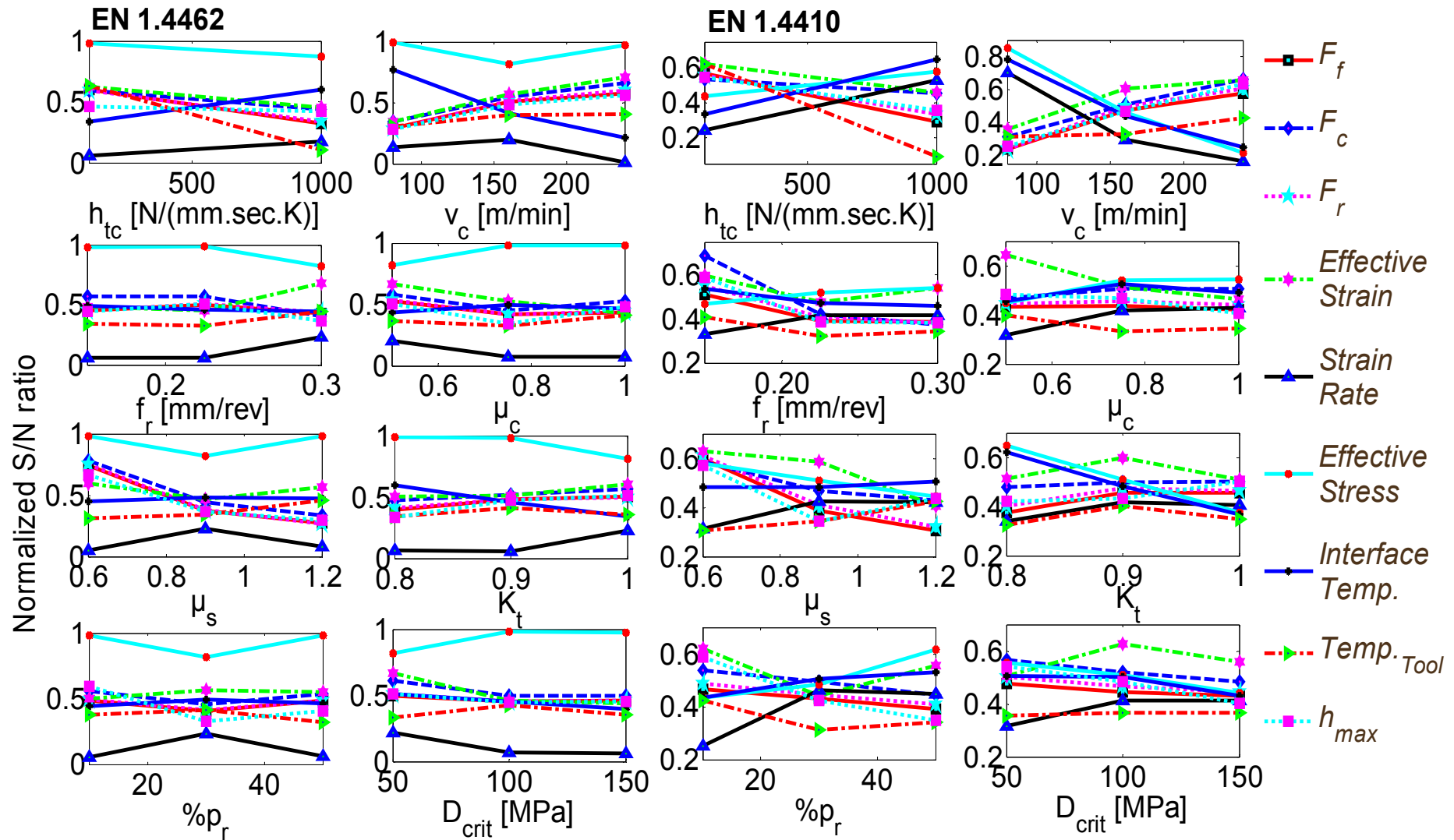


Figure 9.12: Main effect plots of the effect of control factors on the cutting performances during turning EN 1.4410 and EN 1.4462 DSS.

9.3.1 Proposed methodology

9.3.1.1 Analyses of the error percentages

The percentage of differences between the experimentally measured cutting forces, tool temperatures and thicknesses, and the FEM-predicted ones are computed using the percentage of difference expression ($\%E$):

$$\%E = \frac{Y_{EXP} - Y_{FEM}}{Y_{FEM}} \times 100 \quad (9.2)$$

where Y_{EXP} represents the experimental performance values and Y_{FEM} the simulated performance values. To estimate the effect of the control factors and important interactions on the $\%E$, percentage of contribution of each control factor on variance of the corresponding error percentage should be computed. The control factor that returns highest contribution percentage is designated as the prime factor. For the sake of more convenience, percentages are drawn in pie charts and shown in Figure 9.13. For instance, in the case of turning EN 1.4462, the control factors which are expected to play important roles in minimizing the percentage differences of feed force $\%E_f$, cutting force $\%E_c$, thrust force $\%E_t$, tool temperature $\%E_T$ and chip thickness $\%E_h$ were μ_s , κ_t , μ_s and $h_{tc} \times v_c$, μ_s and h_{tc} , and μ_s respectively.

Results of $\%E$ computations versus the experimental order are illustrated in Figure 9.14. It can be seen that the predicted feed and thrust force components are generally underestimated except for some few cases at $D_{crit.} = 150\text{MPa}$. Severe fluctuations of $\%E_f$ and $\%E_t$ were generally in the range of -40% to 195%. On the other hand, $\%E_c$ has shown better agreements with the range of approximately -40% to 45%. Furthermore, comparing the T_T and h_{max} , the $\%E$ between experimental and FEM values also fluctuate between over and under estimation, with very few cases in which absolute $\%E$ were less than 5%. These results show the strong impact of control factors on the outputs of the FEM. The next sections describe the study approach intended to simultaneously minimize all the differences between measured and predicted performances.

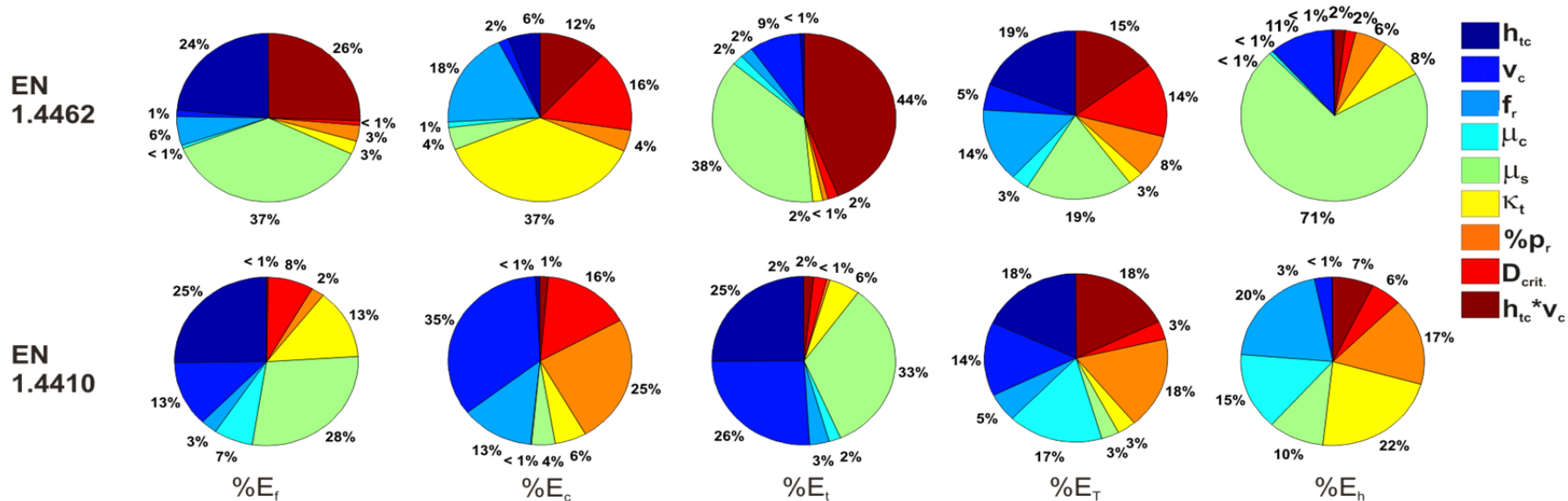


Figure 9.13: The percentage contribution of FEM control factors of the percentage error

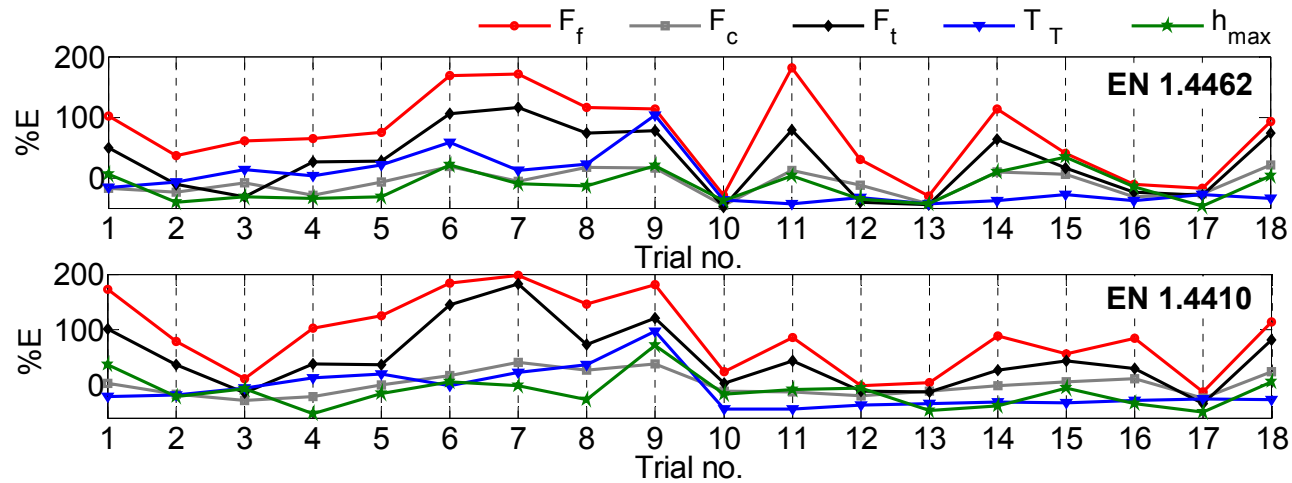


Figure 9.14: Percentage error between the experimentally measured and numerically predicted values for different cutting performances.

9.3.1.2 Application of VIKOR method

In order to simultaneously minimize the multiple error percentages and determine the best alternative (trial no.), VIKOR method is proposed. The procedure of calculating VIKOR indices for each workmaterial case is started with the representation of decision matrix through assigning $\%E_f, \%E_c, \%E_t, \%E_T$ and $\%E_h$ as attributes (columns) of the matrix. The criteria weights have are set using the standard deviation method as per equation (2.63). The best and the worst values of all the criteria in weighted normalized decision matrices are identified using Eqs. (2.79) and (2.80). The values of utility (S) and regret (R) measures are calculated using Eqs. (2.81) and (2.82), respectively. The VIKOR index values (Q_V) are then calculated using Eq. (2.83). For both work material cases, the values of the first and second ranked alternatives are in acceptable advantage range, i.e. $Q_V(A_{b_2}) - Q_V(A_{b_1})$ is always greater than $(1/(18-1)) = 0.05882$. For example, the $Q_V(A_{b_2})$ and $Q_V(A_{b_1})$ of EN 1.4462 are 0.106 and 0.012 respectively, which satisfies condition 1, i.e. $0.106 - 0.012 = 0.094$ is greater than 0.05882. Both regret and utility measure values by consensus prove the stability in decision making. Therefore, the values of Q_V are directly used in the next analyses. Based on the outcomes of the VIKOR method, the best alternatives during cutting EN 1.4410 and EN 1.4462 were alternatives no. 15 and no. 6 respectively. Performing the ANOM, it can be proved that the optimum $factor^{level}$ sets for machining EN 1.4462 and EN 1.4410 are:

$h_{ic}^2 v_c^1 f_r^1 \mu_c^2 \mu_s^2 \kappa_t^3 \% p_r^2 D_{crit}^3$ and $h_{ic}^2 v_c^2 f_r^3 \mu_c^2 \mu_s^3 \kappa_t^3 \% p_r^2 D_{crit}^3$ respectively.

The combination of these control factors should minimize the difference between experimental and numerical results. Figure 9.15 maps the effect of cutting speed interactions with the rest of control factors on the Q_V values. The dark blue areas represent the favored regions where the difference between experimental and numerical performances should be minimum.

9.3.1.3 Firefly Algorithm Neural Network System (FANNS)

To establish a useful relationship between independent variables ($h_{ic}, v_c, f_r, \mu_c, \mu_s, \kappa_t, \% p_r$ and D_{crit}) and dependent variable (Q_V), supervised feed-forward MLP-neural networks with back-propagation (BP) as learning algorithm were adopted. The MLP-neural networks used in this study have two layers: one hidden layer and one output layer. The hidden layer uses a sigmoid-type transference function and the output layer uses a linear function.

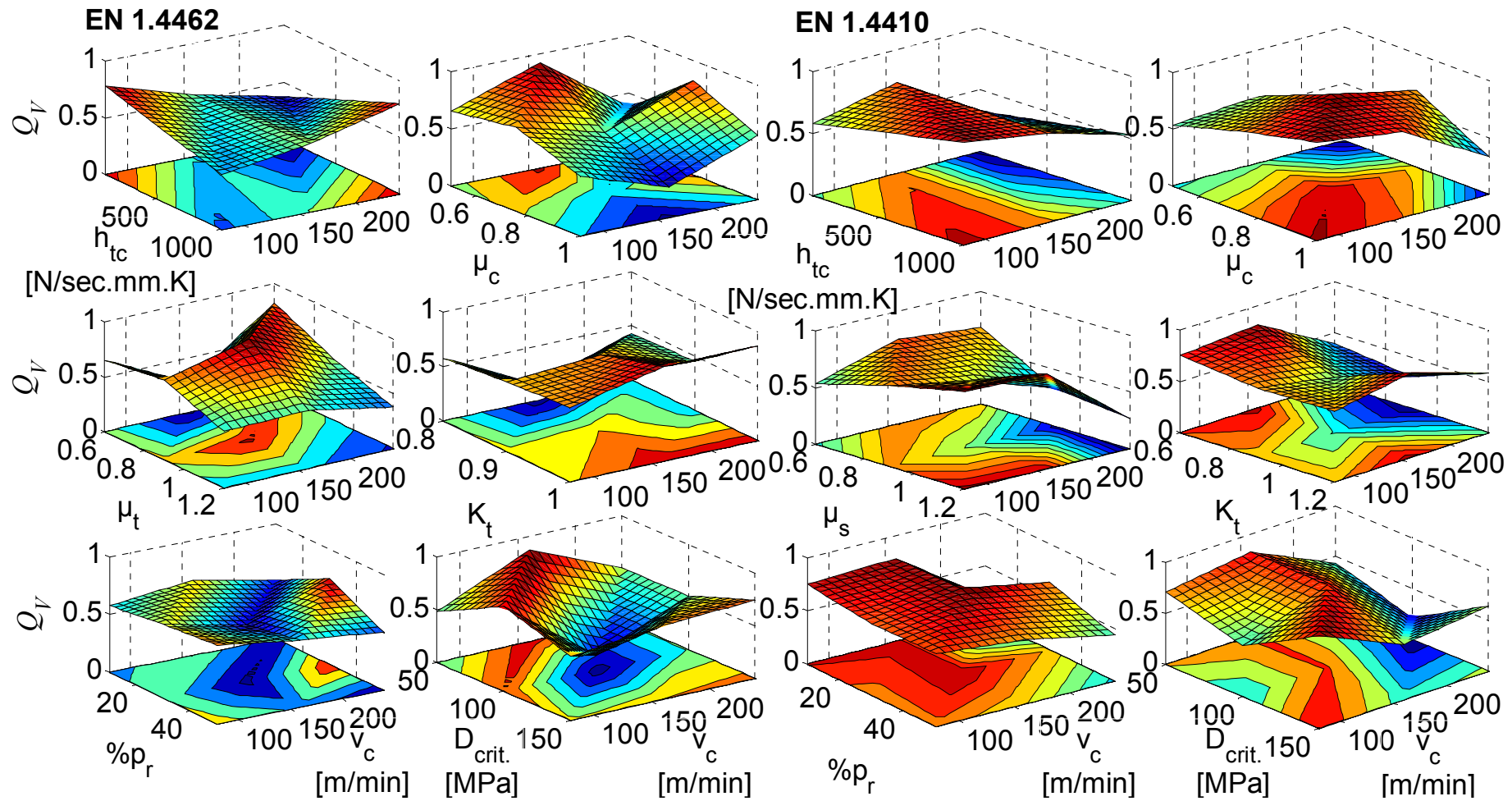


Figure 9.15: Surface and contour plots of the VIKOR indices (Q_v).

The final output (Q_{NN}) of feed forward neural network structure (input vector (8*1)-number of hidden neurons (N)-output) can be mathematically expressed as:

$$Q_{NN} = \log \operatorname{sig} \left(\begin{bmatrix} \omega_{11} & \cdot & \cdot & \omega_{18} \\ \cdot & \cdot & \cdot & \cdot \\ \cdot & \cdot & \cdot & \cdot \\ \omega_{81} & \cdot & \cdot & \omega_{88} \end{bmatrix} \times \begin{bmatrix} h_{ic} \\ \cdot \\ \cdot \\ D_{crit.} \end{bmatrix} + \begin{bmatrix} b_1 \\ \cdot \\ \cdot \\ b_N \end{bmatrix} \right) \times [\omega_1 \quad \cdot \quad \cdot \quad \omega_N] + b_{N+1} \quad (9.3)$$

where ω and b are the weights and biases of the network respectively.

In the present study, the MLP use sigmoid transfer functions in the hidden layers. These functions are often called "squashing" functions, because they compress an infinite input range into a finite output range. Sigmoid functions are characterized by the fact that their slopes must approach zero as the input gets large. This causes a problem when you use steepest descent to train a multilayer network with sigmoid functions, because the gradient can have a very small magnitude and, therefore, cause small changes in the weights and biases, even though the weights and biases are far from their optimal values. The purpose of the resilient back propagation training algorithm (RPROP) is to eliminate these harmful effects of the magnitudes of the partial derivatives. Only the sign of the derivative can determine the direction of the weight update; the magnitude of the derivative has no effect on the weight update. The size of the weight change is determined by a separate update value. The number of learning steps is significantly reduced in comparison to the original gradient-descent procedure as well as to other adaptive procedures, whereas the expense of computation of the RPROP adaptation process is held considerably small. Another important feature, especially relevant in practical application, is the robustness of the new algorithm against the choice of its initial parameter [RiBr93].

The scaling or normalization ensures that the ANN will be trained effectively without any particular variable skewing the results significantly. The weights and biases of the network are initialized to small random values to avoid immediate saturation in the activation functions. The neural networks trained by using the gradient descent with adaptive velocity and momentum back-propagation algorithm to model Q_V , where it is not easy to obtain analytical and good empirical relations. The optimum architecture was found out by varying network characteristics in MATLAB using trial and error technique. It was found that when the training function, RPROP; the number of hidden neurons, 13; maximum number of epochs to

train, 100; the learning rate, 0.01; the increment to weight change, 1.2; decrement to weight change, 0.5; initial weight change, 0.07; and maximum weight change, 50, the root mean square of errors were the minimum. Figure 9.16 shows the comparison of experimental results and ANN modeling ones in verifying the network generalization capabilities. The results are almost identical.

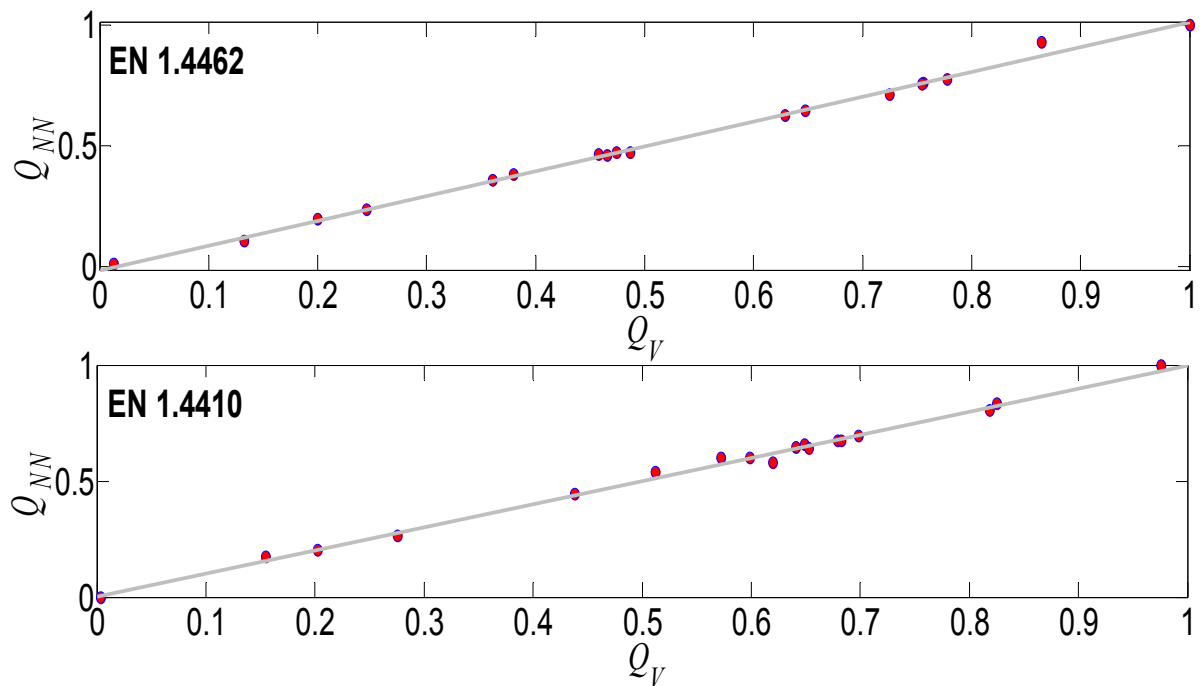


Figure 9.16: An actual versus predicted plot enabling correlating inspection of model predictions relative to actual data.

In order to obtain solutions that will provide useful information to the user during the phase of inverse identification of input parameters, neural network models should be integrated with the FA. The neural network models integrated with the FA optimizer was named Firefly Algorithm Neural Network System (FANNS) and its architecture is shown in Figure 9.17. The target of the optimization process in this study is to determine the optimal values of the input parameters that lead to the minimum value of ANN-predicted Q_{NN} at any given cutting condition. The optimization problem can be defined as:

$$\text{Objective} = \text{Max} (1 - Q_{NN}) \quad (9.4)$$

The decision variables are the defined control factors and are limited to the range of simulation experiments as:

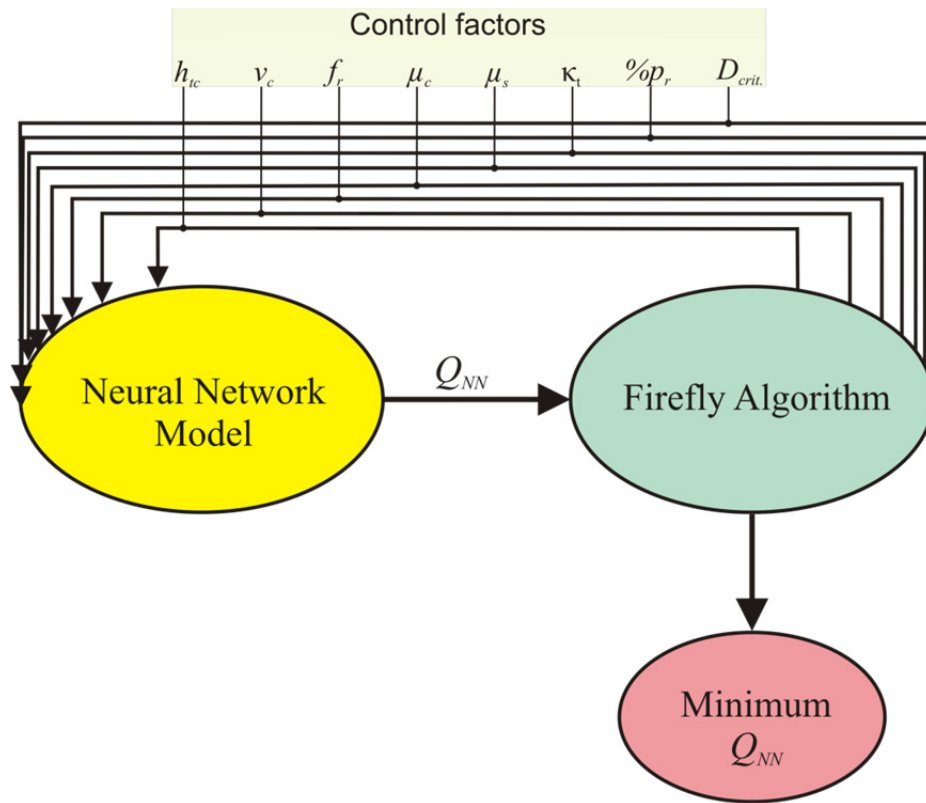


Figure 9.17: Firefly Algorithm Neural Network System (FANNS).

$$100 \leq h_{tc} \leq 1000 \text{ N}/(\text{sec}.\text{mm}.\text{K})$$

$$80 \leq v_c \leq 240 \text{ m / min}$$

$$0.10 \leq f_r \leq 0.30 \text{ mm/rev}$$

$$0.5 \leq \mu_c \leq 1.0$$

$$0.6 \leq \mu_s \leq 1.2$$

$$0.8 \leq \kappa_t \leq 1.0$$

$$10 \leq \%p_r \leq 50$$

$$50 \leq D_{crit.} \leq 150 \text{ MPa}$$

(9.5)

The proposed FANNS approach has been applied to effectively model and optimize the VI-KOR indices. The FA initializing optimization parameters were as follow; population size = 20, number of iterations = 2000, randomization $\alpha_{rand} = 0.5$, attractiveness $\beta_a = 0.2$ and attractiveness variation $\gamma_a = 1$. The optimal sets of control factors that lead to the optimum Q_{NN} values are tabulated in Table 9.3 and the results of the FANNS are shown in Figure 9.18. The obtained optimization results showed that FANNS is highly reliable, converge consistently and quickly (the computation time was less than 3 minutes) to the optimum solution.

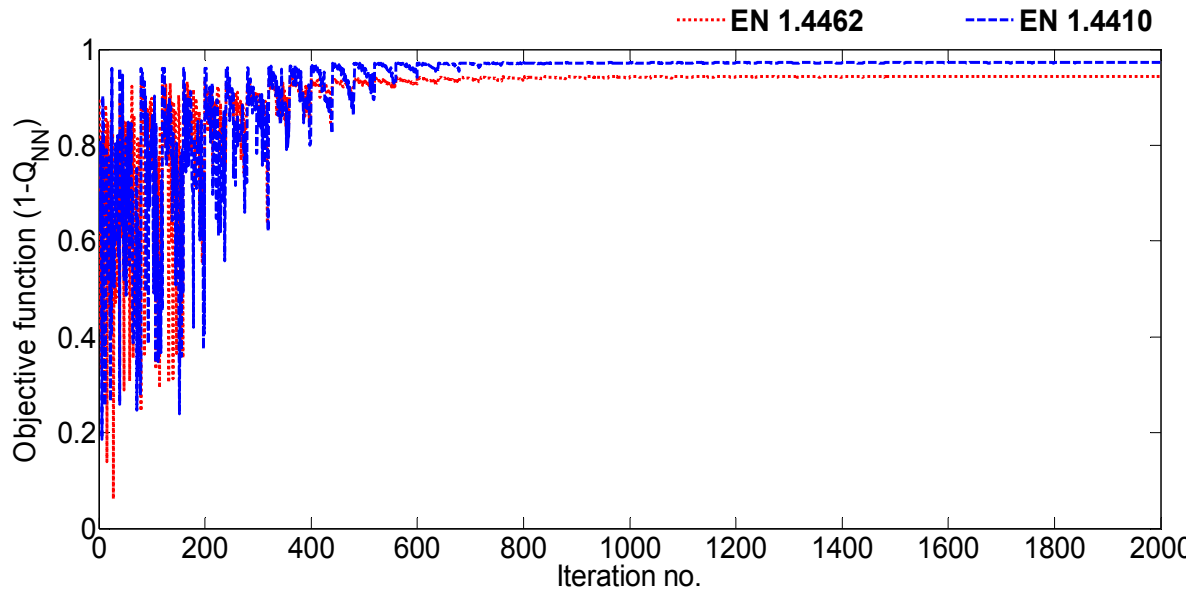


Figure 9.18: Minimization of VIKOR indices using FANNS.

Optimum control factor	Unit	EN 1.4462	EN 1.4410
Thermal contact conductance (h_{tc})	N/(sec.mm.K)	652.306	647.945
Cutting speed (v_c)	m/min	181.175	130.601
Feed rate (f_r)	mm/rev	0.21321	0.27441
Coulomb friction coefficient (μ_c)	-	0.63151	0.91255
Shear friction coefficient (μ_s)	-	0.74952	1.01455
Taylor-Quinney coefficient (κ_t)	-	0.95352	0.96525
Reduction in flow stress ($\%p_r$)	-	19.3549	28.8121
Critical damage value ($D_{crit.}$)	MPa	69.2885	89.1997
Minimum VIKOR index ($1-Q_{NN}$)	-	0.92211	0.95785

Table 9.3: Optimum sets of control factors.

To validate the global FANNS results, the experimental cutting conditions should be identical to the numerical ones. Therefore, three longitudinal turning experiments per each work material were carried out at the exact optimum cutting conditions as listed in Table 9. The averages of the measured performances are computed and used to calculate the percentage difference between the numerical and experimental ones using Eq. (9.2). The percentage difference between numerically obtained cutting forces, chip temperature and maximum chip thicknesses, and the experimental ones for each work material are tabulated in Table 9.4. It can be seen that the calculated performances are in close agreement to the experimental results. The global optimum difference percentages are also compared with difference percentages of the rank

no. 1. The lower percentages of difference confirm the advantage of FANNS application in identifying the input parameters while simulating the machining of duplex stainless steels.

Mat.	F_f [N]		F_c [N]		F_t [N]		T_T [°C]		h_{max} [mm]	
	Exp.	Num.	Exp.	Num.	Exp.	Num.	Exp.	Num.	Exp.	Num.
EN 1.4462	385.16	369.94	935.65	972.06	298.64	290.13	134.63	140.51	0.334	0.351
	%E = -4.116		%E = 3.745		%E = -2.139		%E = 4.187		%E = 5.125	
EN 1.4410	761.15	723.68	1485.63	1569.5	517.254	491.82	142.71	148.70	0.553	0.584
	%E = -5.177		%E = 5.346		%E = -5.169		%E = 4.031		%E = 5.254	

Table 9.4: Validation of the numerical results.

9.3.2 Extension of FANNS: a case study

One of the aims of conducting inverse identification was to define a robust approach, so that the optimum set of control factors at any given cutting speed and feed rate is accurately determined. In this subsection, the adaptability of the described approach to the changing cutting speeds and feed rates is examined. Three arbitrary experimental cutting tests per each work-material were conducted. The optimum sets of control factors at cutting speeds and feed rates combinations of 75m/min×0.325mm/rev, 150m/min×0.175mm/rev and 225m/min×0.2mm/rev were determined using the proposed FANNS; meanwhile numerical models, each at the exact optimum set of optimized control factors, were prepared and executed. Figure 9.19 shows the measured and predicted cutting performances for EN 1.4410 and EN 1.4462. The average of absolute percentage differences between the experimental and numerical results for each material case is 3.8652 % and 4.9956% respectively. Considering the wide range of applied cutting speeds and feed rates the proposed methodology of inversely identifying the simulation input factors shows excellent results with respect to the examined performances.

9.4 Inverse identification of Usui's wear model constants

In order to characterize tool wear for a cutting operation, there exist two main approaches; empirical tool life models and tool wear rate models. In order to derive a reliable empirical tool life model, a large number of experimental tests are essential which is usually time-consuming, cost-intensive, restricted to the investigated tool-workpiece combinations and cannot predict the influence of work material or tool materials on the values of constants in the models. On the other hand, tool wear rate models involve process variables that are not

- To estimate the variables in Eq. (9.6), prepare identical to the experimentations, fully coupled thermo-mechanical and FANNS-optimized 3D-FE models, and run the simulations.
- Collect the numerically estimated T , σ_n and v_s .
- Fit the nonlinear Usui's model to determine the constants A and B .

Seven arbitrary multi-pass dry turning tests of EN 1.4410 and EN 1.4462 DSS bars were performed on a variable spindle speed CNC lathe using rhombic CNMA 120412-IC20 uncoated cemented carbide inserts. Thereafter, logarithmic plots of tool wear versus cutting time were drawn and the slopes (dW/dt) were determined. Meanwhile, the 3D-FE cutting simulations were carried out based on the proposed procedure. The tool is considered rigid with no wearing possibility. Values of T , σ_n and v_s were directly extracted from simulation results. Matlab function NonLinearModel.fit was then utilized to fit the model and test its adequacy through various statistical diagnostic tools. The adjusted correlation factor ($R_{adj.}$) was in very good agreement with predicted correlation factor ($R_{pred.}$) which supports the prediction power of the model and were generally above 0.94. The RMSE for EN 1.4462 and EN 1.4410 Usui wear models were 0.000314 and 0.000469 respectively. The final form of the constants Usui's wear models can be constructed as;

$$\begin{aligned} \left(\frac{dW}{dt}\right)_{EN1.4462} &= 6.0478 \times 10^{-9} \sigma_n v_s \exp\left(-\frac{1172.8}{T}\right) \\ \left(\frac{dW}{dt}\right)_{EN1.4410} &= 7.1704 \times 10^{-9} \sigma_n v_s \exp\left(-\frac{992.5203}{T}\right) \end{aligned} \quad (9.7)$$

9.5 Numerical optimization of turning DSSs

In the second stage of the present study, a hypothetical benchmark-analysis based on the Taguchi optimization procedure is suggested. The objective is to select the best combination of criterions such as; chip breakers type (CB), tool geometry ($Geo.$), cooling medium application (CM), cutting conditions such as v_c and f_r , and tool orientation angles such as normal rake (α_n) and inclination angle (λ_i) for an effective machining of EN 1.4462 and EN 1.4410 DSSs. For this purpose, Taguchi's mixed design L_{18} ($2^1 \times 3^7$) is once again seen the most appropriate because of its attractive characteristics which combines the highest possible number of levels along with largest number of criterion and smallest number of experiments. Another

attractive characteristic of the design is that the interaction between column 1 and 2 is orthogonal to all columns and hence can be estimated without sacrificing any column. The interaction can be estimated from the 2-way table of columns 1 and 2. The studied criterion and their corresponding levels are listed in Table 3.8. Columns 1 and 2 of the design can be combined to form a 6-level column. Each level in column three represents an insert designation which is often commercially available.

9.5.1 Selective control factors

In the following subsections an introduction to the first three of above control factors is given. The reminder of the control factors have been previously described in Chapter 1 of the present dissertation.

9.5.1.1 Chip-breaker type

Especially designed for machining stainless steels, chip breakers such as M3M type is adapted with geometric features that improve the tool's life due to a reinforced cutting edge at the area where notch wear tends to occur when machining stainless steel, causing poor surface finish and risk of edge breakage (see Figure 9.20). On the other hand PP type chip breakers, which are also recommended for machining stainless steels, are characterized by having 3 step smart dot structures which provides smooth chip evacuation with a wide range of feed rates, and smooth taper cutting edge to reduce cutting forces.

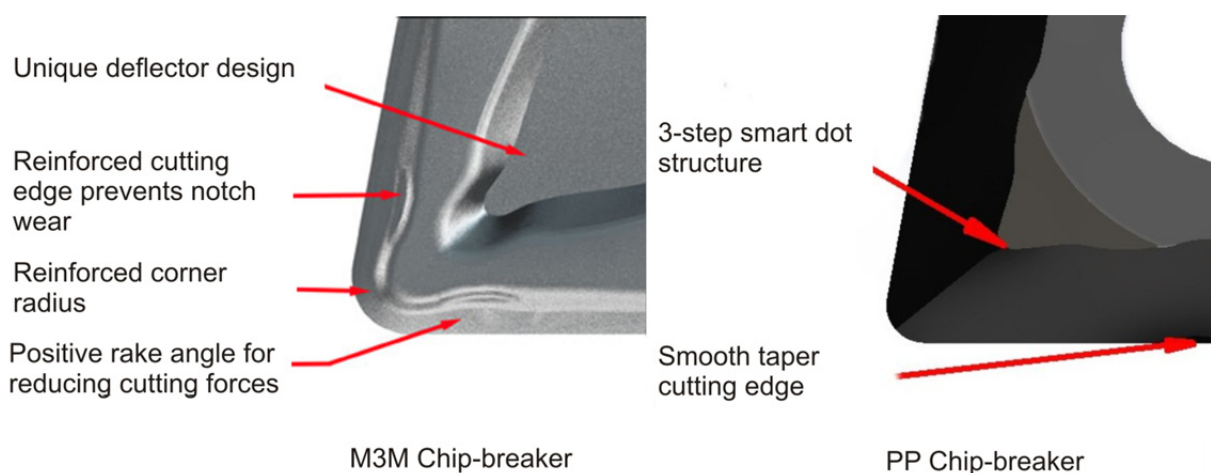


Figure 9.20: Adopted chip-breakers types.

9.5.1.2 Insert geometry

In metal cutting, the primary goal is to achieve the most efficient separation of chips from the workpiece. One of the main factors that contribute in optimizing chip morphology is the insert shape. For this reason, the selection of the right cutting tool geometry is critical. The three basic insert shapes which had to be investigated in the present hypothetical study were diamond 55° , rhombic 80° and trigon 80° . Other geometric features, such as clearance angle, tolerance, size, thickness, nose radius and cutting edge preparation were identical.

9.5.1.3 Cooling medium

Following the determination of the optimum thermal contact conductance of the tool-chip interface (h_{tc}) using the FANNS approach, the influence of environmental heat convection in dry, wet and cryogenic conditions on the cutting processes is investigated and optimized. A window for heat exchange was defined as shown in Figure 9.21. It was restricted to the secondary and tertiary deformation zones on the inserts using a cylindrical shape of 1.2mm radius and 3mm length and was not intended to change any other boundary conditions in the finite element model. Local convection coefficients in wet and cryogenic cutting were assigned in the areas covered by the window while the rest of the cutting tool is still subjected to air convection. The convection coefficients of dry, wet and cryogenic cutting mediums are taken from literature as; 0.02, 10 and 5000 N/(sec.mm.K) respectively [PUDJ14].

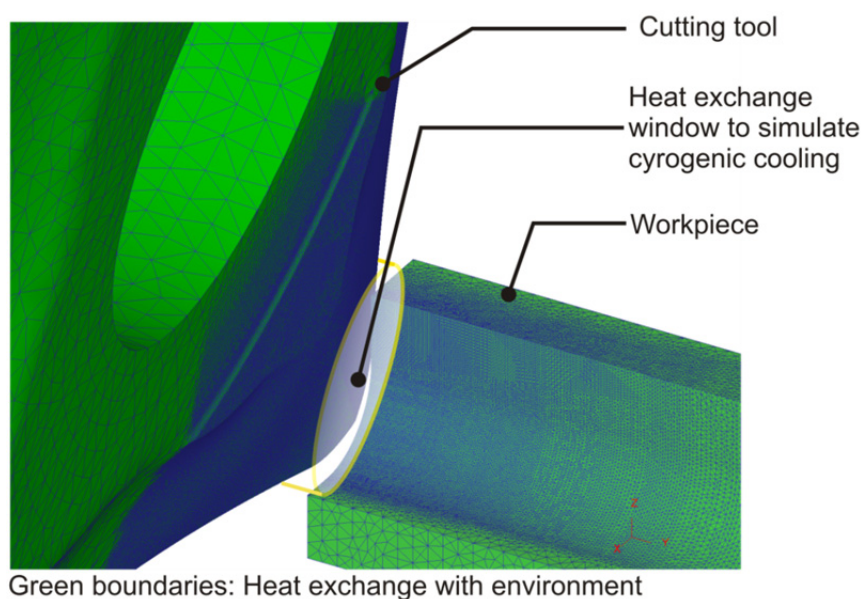


Figure 9.21: An illustrative thermal boundary condition using PP chip-breaker.

9.5.2 Results and discussions

Once the turning simulations has been finished, numerous cutting performances such as resultant cutting forces, temperatures,...,etc. have been extracted. The S/N ratio of each performance is computed and the main effect plots of the normalized S/N ratios are plotted as shown in Figure 9.22. The level which returns maximum normalized S/N ratio is assigned as the optimum level. Further statistical analyses are performed to specify statistically significant control factors. Figure 9.23 exhibits the percentage of contribution of each control factor on the variance of the corresponding cutting performance. The following sub-sections, the effects of control factors on each single cutting performance are briefly described.

9.5.2.1 Influence of control factors on the resultant cutting forces (R_c)

Based on a quick review of the 3D-FEM results, the following conclusion points can be drawn:

- The optimum insert designations which minimize R_c during turning EN 1.4462 and EN 1.4410 can be described in ISO norms as: WNMG 060408-PP and CNMG 120408-PP respectively.
- In spite of the advantageous aspects of increasing cutting speed, applying coolant and cryogenic conditions in increasing the productivity and reducing the overall R_c values, results has shown a limited influence of these control factors on the mean R_c values. This statement is supported by the slopes of the R_c curves in Figure 9.22
- Among the considered control factors, feed rate had shown the strongest impact on the resultant cutting forces (see Figure 9.23).
- The optimum values of cutting tool orientation angles expressed by ranges of investigated rake and inclination angles are -6° and 0° respectively.

9.5.2.2 Influence of control factors on the effective strain

Without relating the hardening parameters in the loading function to the experimental uniaxial stress-strain curve, the work-hardening theory of plasticity cannot be applied in practical terms. In order to correlate the test results obtained by different load programs, the introduction of any strain and stress variables, that are functions of plastic strain and plastic stress, and

can be plotted against each other is considered useful. These variables are often called effective strain and effective stress.

DSSs are a group of stainless steel alloys that are characterized by high work-hardening rate. They are machined at very high strain rates which increase the work hardening rate and causing higher resistance to plastic deformation. Generally, the following observation points can be made:

- The average effective plastic strain when machining EN 1.4462 was 13.2% lower than the corresponding EN 1.4410.
- Employing chip breaker type PP has generally caused lower effective strain values.
- Detrimental control factors vary considerably per work material family.
- Higher values of effective strains are observed when the cooling medium on the tool is cryogenic.
- Main effects of effective strain decreases with increasing cutting speed.
- Mean effective strains are found to be minimum at the feed rate range of 0.1-0.175 mm/rev and inclination angle range of 6°-12°.
- Minimum effective strain value when cutting EN 1.4462 and EN 1.4410 at $\alpha_n = 0^\circ$ and $\alpha_n = -12^\circ$ respectively.

9.5.2.3 Influence of control factors on the effective stress

Effective plastic stress is considered a relevant characteristic of the cutting process which characterizes the level of resistance to cutting. The correlation between the state of this performance imposed by the cutting tool in the layer being removed and the fracture strain of the work material could be used to estimate the physical efficiency of the cutting process. In summary to the results, the following conclusions can be drawn:

- The effective stress encountered in cutting EN 1.4410 was 12% higher than EN 1.4462.
- The optimum control *factor*^{level} combinations of cutting EN 1.4462 and EN 1.4410 were $CB^1 Geo.^1 CM^2 v_c^1 f_r^1 \alpha_n^3 \lambda_i^2$ and $CB^1 Geo.^2 CM^2 v_c^2 f_r^1 \alpha_n^3 \lambda_i^2$ respectively.
- Increasing the rake angle in negative direction and inclination angle in positive direction generally increases the effective stress.
- The minimum effective plastic stress of 1261.48MPa and 1492.01MPa when cutting EN 1.4462 and EN 1.4410 were respectively recorded at experiment no. 9.

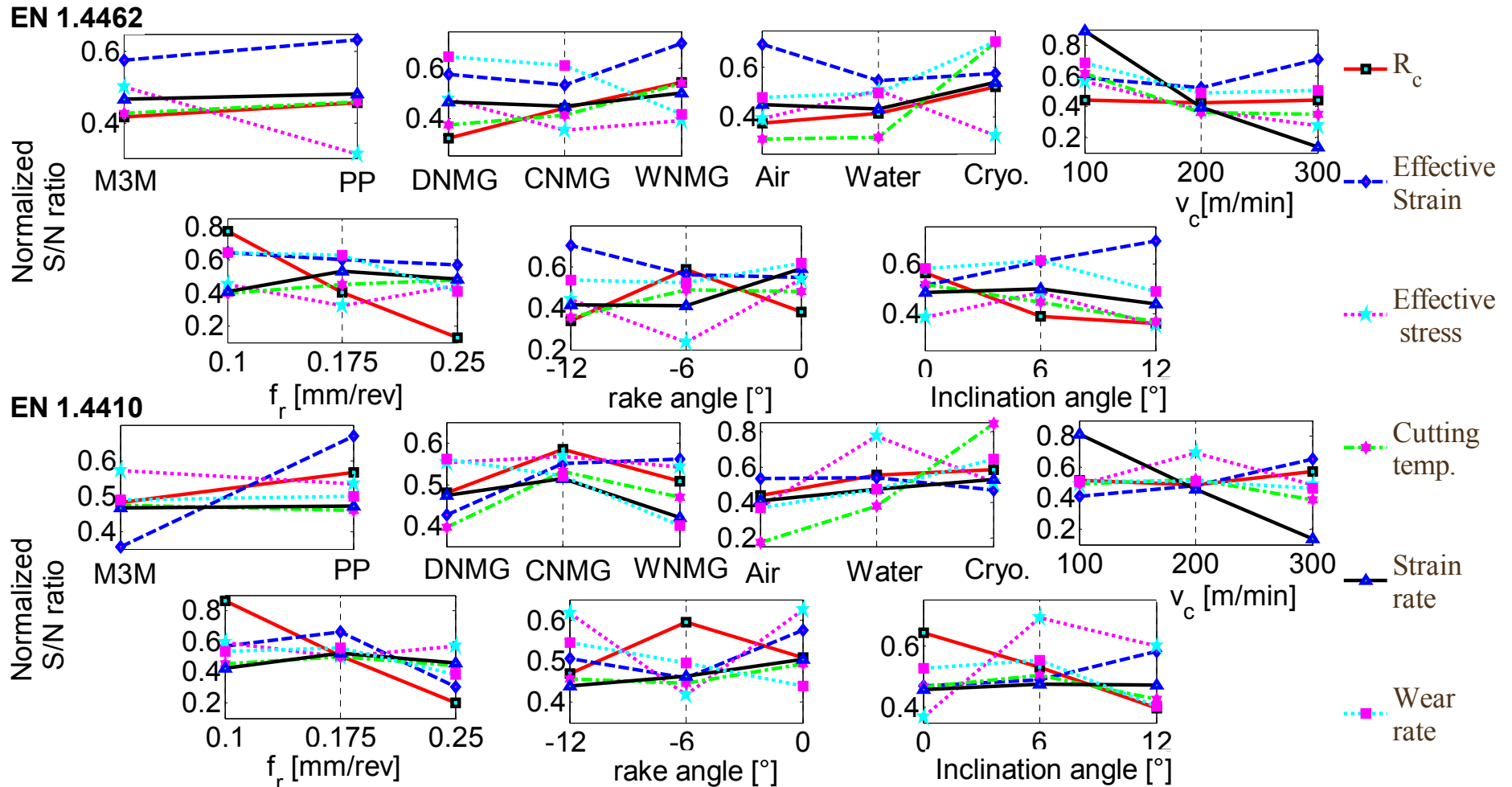


Figure 9.22: Main effect plots of the effect of control factors on the cutting performances during turning EN 1.4462 and EN 1.4410 DSSs.

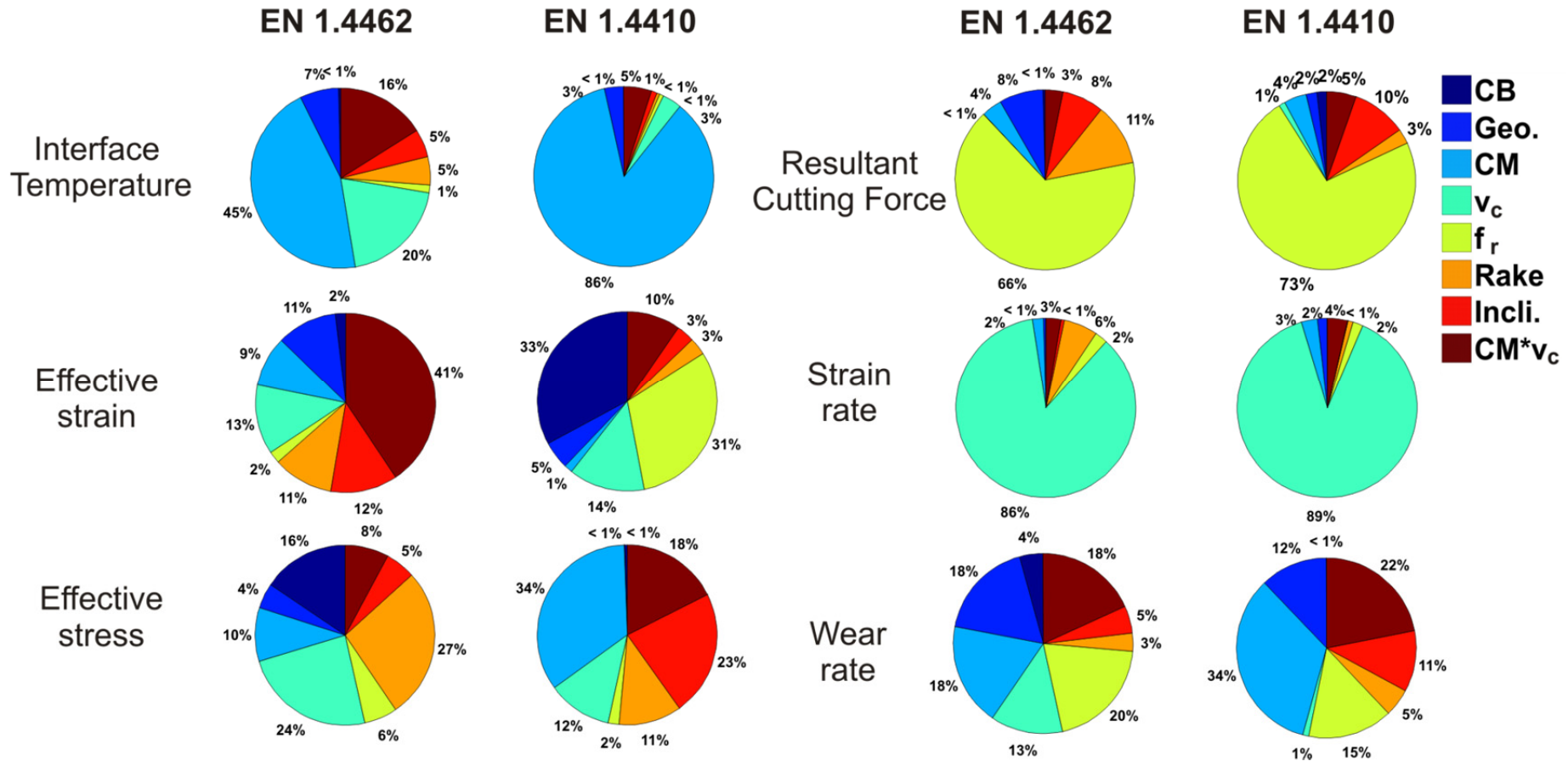


Figure 9.23: The percentage contribution of FEM control factors in the cutting performances variances.

- When cutting EN 1.4462, process conditions such as v_c, f_r, CM and $v_c \times CM$ interaction has contributed to the effective stress values by 48%. On the other hand, when cutting EN 1.4410, they had contributed by as much as 66%.

9.5.2.4 Influence of control factors on the cutting temperature

Mean contact temperature at the tool–chip interface (also is referred to as the cutting temperature) is the basic tribological characteristics of the tool–chip interface. It plays a major role in the formation of crater on the tool face and leads to failure of tool by softening and thermal stresses. This temperature is the most suitable parameter to correlate the tribological conditions with tool wear. Control factors that affect the tool–chip interface temperature are; work-piece and tool material, tool geometry, cutting conditions and cutting medium. Fortunately, most of these factors are included in the original design of simulation experimentations. Figure 9.24 depicts the state of cutting temperature distribution in the primary and secondary deformation zones of the workpiece. The results of the numerical studies on temperatures in cutting DSSs can be summarized as follows:

- Mean cutting temperatures at dry cutting when machining EN 1.4462 and EN 1.4410 were 36.3% and 53.5% higher than at corresponding cryogenic process conditions.
- The contribution of water-based coolant in lowering the average cutting temperature has not exceeded 7.8% in both material cases.
- Minimum mean cutting temperature when cutting EN 1.4462 and EN 1.4410 has been recorded at experimental run 16 and 15 respectively.
- Cooling medium, cutting condition and their interaction accounts for most of contributions in cutting temperature variations.
- The optimum control $factor^{level}$ combinations of cutting EN 1.4462 and EN 1.4410 were $CB^2Geo.^3CM^3v_c^1f_r^3\alpha_n^2\lambda_i^1$ and $CB^1Geo.^2CM^3v_c^1f_r^2\alpha_n^3\lambda_i^2$ respectively.
- The average cutting temperature when machining EN 1.4462 was 9.85% lower than the corresponding EN 1.4410.

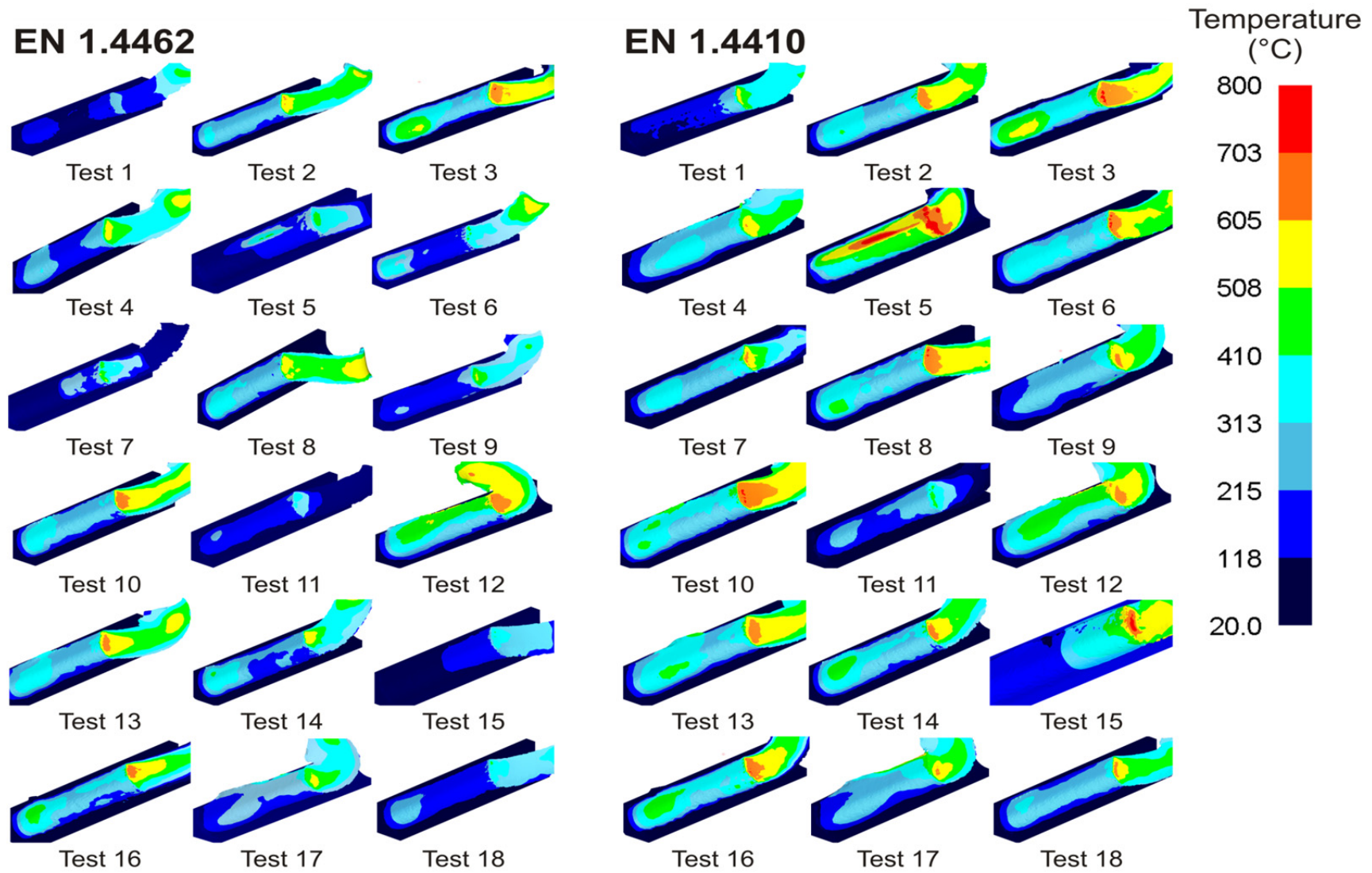


Figure 9.24: Contours of temperature distribution in 3D-FEM of cutting DSSs.

9.5.2.5 Influence of control factors on the strain rate

The flow stress curves shown in Figure 2.11 exhibit sensitivity to temperature and strain rate. This sensitivity is directly related with time and temperature dependency of the mechanisms that govern the deformation and the evolution of the deformation in the material. The main mechanism by which plastic strain takes place is thermally activated motion of dislocations past obstacles that exist within the lattice over a wide range of strain rates and cutting temperatures. The material response is significantly affected by the nature and density of the obstacles (which may change as the deformation takes place). When dealing with metals, experimental results show that the stress required for plastic strain often reduces with the increase of temperature and with the decrease of plastic strain rate [GiWu97]. It can then be said that temperature and plastic strain rate greatly influence the material response. In general, the stress decreases with the increasing of temperature and decreasing the plastic strain rate. Actually, temperature and strain rate effects are coupled, since one influences the other. Temperature affects the rate of deformation, which is controlled mainly by a thermally activated mechanism. On the other hand, plastic strain at high rate generates significant heating and cause an increase in temperature which leads to mechanical instability and the localization of deformation into narrow sheets of material (the adiabatic shear bands), which act as precursor for eventual material failure [DaMa09]. As generalization to the given results in Figure 9.22 and Figure 9.23, the following concluding points can be depicted:

- Average strain rate values under cutting EN 1.4462 and EN 1.4410 are of $2.067 \times 10^5 \text{ sec}^{-1}$ and $3.23 \times 10^5 \text{ 1/sec}$ respectively.
- Increasing cutting speeds from 100m/min to 300m/min at lower feed rates of 0.1mm/rev had drastically increased the strain rate values.
- Mean strain rate values in cryogenic cutting conditions during cutting EN 1.4462 and EN 1.4410 were respectively 9.158% and 11.863% lower than the corresponding still air conditions.
- $CB^2 Geo.^3 CM^3 v_c^1 f_r^2 \alpha_n^3 \lambda_i^3$ and $CB^2 Geo.^2 CM^3 v_c^1 f_r^2 \alpha_n^3 \lambda_i^3$ were the optimum control *factor*^{level} combinations which have minimized the strain rate when cutting EN 1.4462 and EN 1.4410, respectively.

9.5.2.6 Influence of control factors on the tool wear

Eq. (9.7) has been used in conjunction with finite element simulation to model wear of WC cutting tools. The simulation results related to the tool wear were obtained in terms of tool wear rate, total wear depth and tool temperature. Average values of tool wear rates are statistically analyzed and plotted as shown in Figure 9.22 and Figure 9.23. Figure 9.25 maps the contours of wear depth in the nose area of the employed cutting tools after 7mm longitudinal cutting. As it can be observed that the locations and intensity of tool wear depths are functions of work materials and control factors. Considering the effect of these factors, the summary of the findings are presented below.

- The optimum control *factor*^{level} combinations which have minimized the tool wear rate during cutting EN 1.4462 and EN 1.4410 were $CB^2Geo.^1CM^3v_c^1f_r^1\alpha_n^3\lambda_i^2$ and $CB^2Geo.^1CM^3v_c^1f_r^2\alpha_n^1\lambda_i^2$ respectively.
- For both workmaterials, major percentage of contributions of 69% and 72% in variance of tool wear rate were attributed to the process and cutting conditions and their subsequent interactions.
- The average tool wear rate when machining EN 1.4462 was 5.365% lower than the corresponding EN 1.4410.
- Contour profiles of tool wear depth shown in Figure 9.25 coincide with temperature distribution at rake and flank faces of the cutting tools in Figure 9.26. Maximum wear depths are occurred in positions at rake and flank surfaces where the tool temperature is the highest.

9.5.3 Numerical machining performance measure

The previous analyses of machining performances have showed different control *factor*^{level} preferences. This will cause confusions to the process designer or the machinist who interested in finding the best compromise combination of control factors which simultaneously optimize the machining of DSSs. Therefore, a new machining performance measure has to be defined. In this section of the work, fuzzy logic system is employed to combine the normalized performances, such as the resultant cutting force, effective stress, cutting temperature and tool wear rate into a single characteristics index called numerical machining performance measure (NMPM).

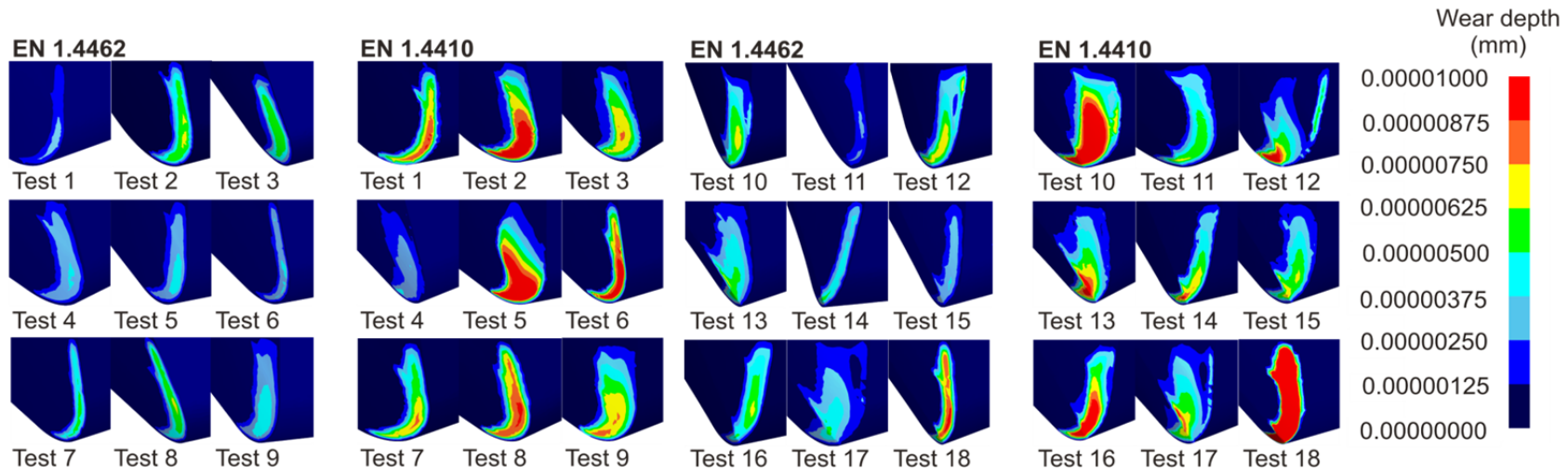


Figure 9.25: Contours of tool wear depth in 3D-FEM of cutting DSSs.

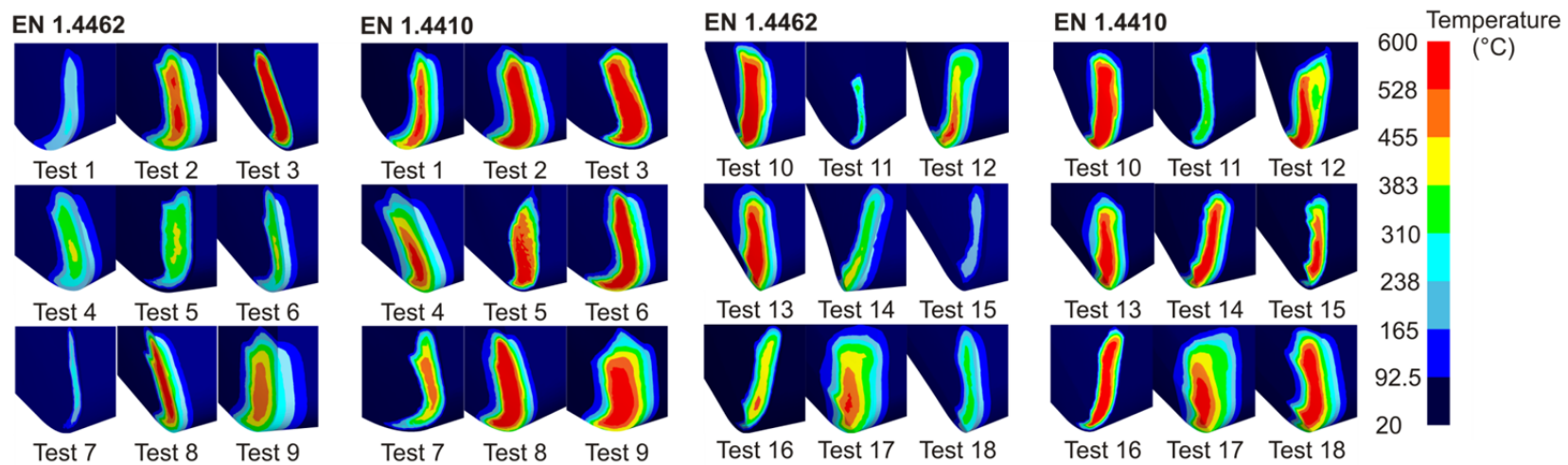


Figure 9.26: Contours of the cutting tools temperature distributions in 3D-FEM of cutting DSSs.

Matlab software was used to construct the inference model of the NMPM. The S/N ratios of performance values were first adjusted to a notionally common scale between null and one, so that the digit ‘one’ represents the most desirable and ‘null’ is the least desirable alternative. The four input variables are assigned with the following fuzzy sets: Small (S), Medium (M) and Large (Lg). The output variable has the following nine levels: Extremely Low (EL), Very Low (VL), Low (L), Lower Medium (LM), Medium (M), Upper Medium (UM), High (H), Very High (VH) and Extremely High (EH). Mamdani implication method is employed for the fuzzy inference reasoning. The relationship between system input and output is expressed by an “If-Then” type. Totally 3^4 fuzzy rules per material were formulated. Finally, the structural characteristics of the fuzzy inference system (FIS) in the present study can be plotted as shown in Figure 9.27.

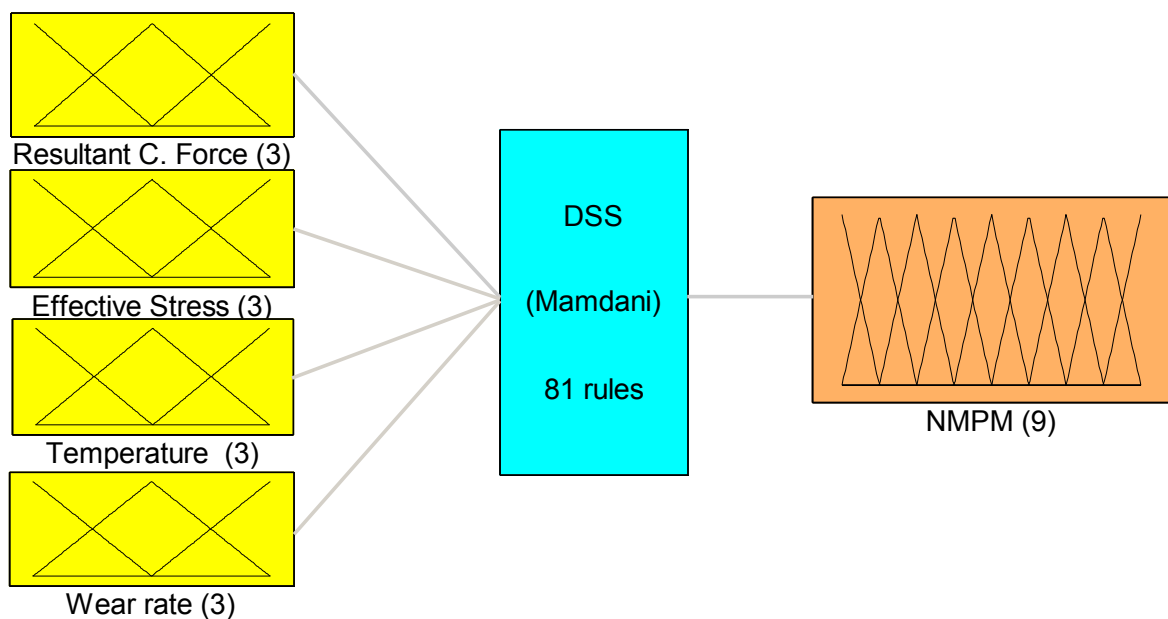


Figure 9.27: FIS-NMPM: 4 inputs, 1 output, 81 rules.

The main effect plots of the NMPM are presented in Figure 9.28. The figure indicates that the mean NMPM values of EN 1.4462 are generally higher than of EN 1.4410 and the final optimum $factor^{level}$ combinations for both materials are $CB^1Geo.^3CM^3v_c^1f_r^1\alpha_n^3\lambda_i^2$ and $CB^2Geo.^2CM^3v_c^1f_r^1\alpha_n^2\lambda_i^2$ respectively. Based on the NMPM values, it can be concluded that EN 1.4462 has better machinability in terms of the employed performances. Finally, performing ANOVA on the computed NMPMs, has confirmed the major effects of process and cutting conditions and their interactions on the overall performance of cutting DSSs (see Fig. 39).

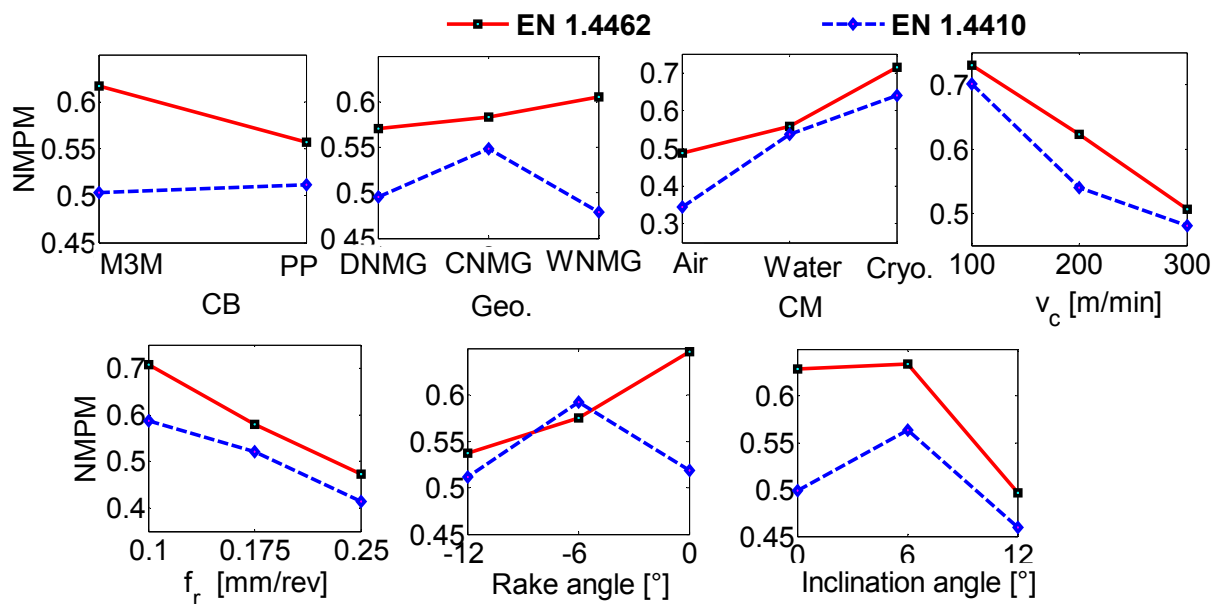


Figure 9.28: Main effect plots of the effect of control factors on the cutting performances during turning EN 1.4410 and EN 1.4462 DSSs.

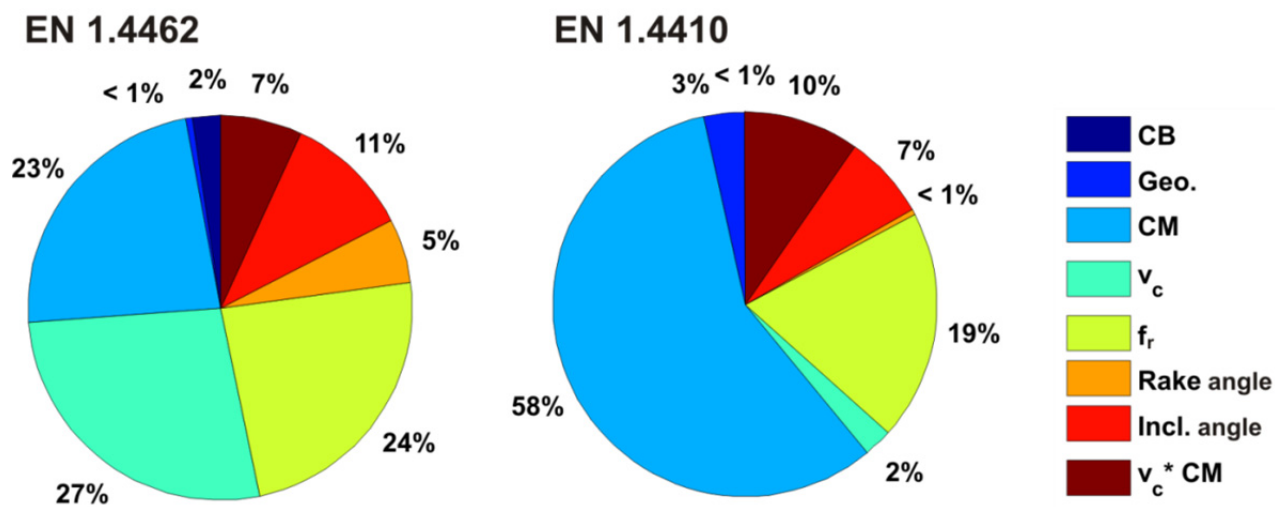


Figure 9.29: Percentage of contributions of FEM control factors in the NMPM variance.

9.6 Interim conclusions

The shortcomings of the machining analytical and empirical models in combination with the industry demands could be fulfilled using 3D-FEM. However, the challenging aspects which hinder its successful adoption in manufacturing process design practice have to be solved first. One of the greatest challenges is the identification of the correct set of machining simulation input parameters. The present chapter presented a new methodology to inversely calcu-

late the input parameters when simulating the machining of standard duplex EN 1.4462 and super duplex EN 1.4410 stainless steels. JMatPro software was first used to model elastic-viscoplastic and physical work material behavior. In order to effectively obtain an optimum set of inversely identified friction coefficients, thermal contact conductance, Cockcroft-Latham critical damage value, percentage reduction in flow stress and Taylor-Quinney coefficient, Taguchi-VIKOR coupled with Firefly Algorithm Neural Network System (FANNS) has been applied. The optimization procedure effectively minimized the overall differences between the experimentally measured performances such as cutting forces, tool nose temperature and chip thickness, and the numerically obtained ones at any specified cutting condition. The optimum set of input parameter were verified and used for the next step of 3D-FEM application. In the next stage of the study, design of experiments, numerical simulations and fuzzy rule modeling approaches were employed to optimize types of chip breaker, insert shapes, process conditions, cutting parameters and tool orientation angles based on many important performances. Based on the obtained experimental and numerical results, and the conducted extensive analyses, the main conclusion points that can be drawn in this chapter are:

- JMatPro-generated elasto-visco plastic and thermo-mechanical properties can be effectively used to numerically simulate the machining of DSSs.
- Using time-dependent damage criteria such Cockcroft-Latham damage criteria, JMatPro has outperformed the JC material model in prediction of chip serrations under similar thermo-mechanical material properties.
- Pre-processing FEM control factors such as; h_{tc} , v_c , f_r , μ_c , μ_s , κ_t , $\%p_r$ and D_{crit} have strong impacts on the percentage difference between experimental and numerical cutting performances.
- The lowest mean values of the overall error percentages for cutting EN 1.4462 and EN 1.4410 were, respectively, at the following pre-processing control *factor*^{level} combinations; $h_{tc}^2 v_c^1 f_r^1 \mu_c^2 \mu_s^2 \kappa_t^3 \%p_r^2 D_{crit}^3$ and $h_{tc}^2 v_c^2 f_r^3 \mu_c^2 \mu_s^3 \kappa_t^3 \%p_r^2 D_{crit}^3$.
- Validations of numerical results through experimentations have revealed that the proposed VIKOR-FANNS approach can efficiently minimize the overall percentage differences at any desired cutting conditions.

- Hypothetical benchmark-analysis based on the Taguchi optimization procedure can be numerically employed to select the best combination of criteria such as; CB , $Geo.$, CM , v_c , f_r , α_n and λ_i per cutting performance.
- Performing ANOM of the derived NMPM values has indicated that the final optimum $factor^{level}$ combinations during cutting EN 1.4462 and EN 1.4410 are $CB^1Geo.^3CM^3$ $v_c^1f_r^1\alpha_n^3\lambda_i^2$ and $CB^2Geo.^2CM^3v_c^1f_r^1\alpha_n^2\lambda_i^2$ respectively.

10 Conclusions

Recognizing the complexity of machinability investigations, the limitations of metal cutting theory and analytical modeling, the difficulties of modeling and optimization of machining process parameters and the necessity of extra knowledge to be gained from machining of ductile and strain hardening materials, the present dissertation has systematically investigated machining of DSSs through systematic application of advanced modeling and optimization techniques in turning processes. The ultimate goal of this dissertation was to provide the process planner and/ or the decision maker the selection capability of obtaining the optimum process parameters under the consideration of multiple and often conflicting performances. The application of input-output parameter relationship modeling and optimization tools and finite element simulations has been broadly demonstrated. MADM methods, often coupled with fuzzy set theory, are also proposed to perform multi-objective optimization and obtain different cutting performance measures. Hybridization of computational modeling and optimization techniques was another tool that has been effectively applied to the machining optimization problem. In conjunction with the research questions that motivated the present dissertation, the following concluding remarks can be drawn:

Research question 1:

Can the application of statistical regression and computational optimization techniques effectively obtain sets of non-dominated solutions in multi-objective optimization of machining DSSs?

In answer to the first research question, an experimental investigation on cutting of EN 1.4462 and EN 1.4410 DSSs is conducted. Statistical regression modeling techniques are adopted to model the performance characteristics and ANOVA tests were performed to check the models adequacies. Multi-objective optimization of machining DSSs based on the nature-inspired MOBA is performed to simultaneously minimize resultant cutting force and the maximum width of flank wear. Results of optimization have shown that MOBA is very efficient and highly reliable. It has provided Pareto frontiers of non-dominated solution sets for optimum cutting conditions, enabling decision makers and/or process planner with a resourceful and efficient means of achieving the optimum cutting conditions. Therefore, statistical regression

and meta-heuristics can be effectively applied to the multi-objective optimization of cutting processes.

Research question 2:

Is the application of fuzzy set theory advantageous in eliminating the discrepancy of ranking system among the MADM methods and obtain better results than other optimization approaches?

In response to the second research question, a comparative machining study of austenitic EN 1.4404, and EN 1.4462 and EN 1.4410 is primarily performed. Considering, chip volume ratio, resultant cutting forces, specific cutting pressures and net spindle powers potential performance characteristics, TOPSIS, VIKOR, GRA and UA were simultaneously applied to optimize the cutting of the stainless steels. Owing to the existing discrepancy among the above MADM methods, fuzzy rule modeling approach was proposed to derive a single characterization index called UCI. In comparison to the outcomes of other optimization approaches, a remarkable improvement in reduction of cutting power consumption, specific cutting pressure and resultant cutting forces has been reported when direct ranking system of predicted UCI indices are set as optimum. Hence, fuzzy set theory has not only proved to be advantageous in eliminating the discrepancy of ranking system among the MADM methods but also obtained better results than other optimization approaches.

Research question 3:

Can Taguchi-MADM-meta-heuristics concept be conveniently used for mono and multi-objective optimization of cutting stainless steels?

To answer the third research question, multi-performance optimization of turning of EN 1.4404, EN 1.4462 and EN 1.4410 has been first experimentally addressed. Utilizing Taguchi-VIKOR-Meta-heuristic as multi-performance optimization concept, performance characteristics such as; surface roughness, specific cutting energy, cutting power and resultant cutting forces are simultaneously and constrainedly optimized. Optimization performance of FA, APSO and CS algorithms are compared, and the exact settings of optimum cutting parameters are determined. The obtained optimization results showed that the algorithms are highly reliable and converge consistently to the optimum solution. However, when it comes to comparisons based on the iteration numbers required for convergence and computation results, APSO outperformed the FA and CS was seen far more efficient than both. Thus, the

proposed Taguchi-VIKOR-Meta-heuristic concept has enabled the decision maker and/or process planner with tools suitable for mono objective optimization using Taguchi optimization procedure, multi-objective optimization using VIKOR method and constrained optimization using the most efficient meta-heuristic algorithm.

Research question 4:

Can multiple machining surface quality characteristics be efficiently optimized when MADM methods are coupled with fuzzy set theory?

In order to answer the fourth research question, multiple surface quality characteristics of stainless steel grades such as; EN 1.4404, EN 1.4462 and EN 1.4410 have been systematically investigated under a constant cutting speed facing operation. MADM methods such as GTMA and AHP-TOPSIS are simultaneously adopted to combine well-known surface quality characteristics such as Ra , Rz and Rt into a single index called MSQCI. The differences in rankings between derived indices are solved through converting each crisp values into trapezoidal fuzzy number and unifying them using fuzzy simple additive weight method. The optimum $factor^{level}$ combinations have been defined and %Contribution of the control factors are determined. Confirmation test results have shown that the average percentage improvement in surface quality during facing EN 1.4404, EN 1.4462 and EN 1.4410 were: 26.302%, 10.62% and 12.679%, respectively. Thus, multiple machining surface quality performances could be efficiently optimized when MADM methods are coupled with fuzzy set theory.

Research question 5:

Would it be possible for multi-pass cutting operations to be sustainably optimized when the hybridization of input-output modeling and optimization tools and MADM methods is systematically performed?

In answer to the fifth research question, a systematic approach which employed different modeling and optimization tools under a three phase investigation scheme has been conducted to sustainably optimize the multi-pass constant cutting speed facing of DSSs. In the first phase of the investigation, D-optimal experimental design is used extensively to investigate the effect of process variables on performance characteristics such as percentage increase in thrust cutting force, effective cutting power, maximum tool flank wear and chip volume ratio. The models were then analyzed using 3D surface graphs and used to study the interaction effects of process parameters. At the end of the first phase, constrained Cuckoo Search algo-

rithm is selected to perform optimization of the performance characteristics thereby defining the optimum process conditions. In the second phase, the optimization conflict between machining economics attributes, such as simultaneous minimization of machine utilization time, main time-related costs and the tool related costs effectively solved employing TOPSIS. In the third phase of the study, the computed performances in the first and second phases were utilized to derive a new index of measuring machining sustainability called operational sustainability index (OSI). To accurately model and constrainedly optimize the highly nonlinear OSIs, CSNNS has been developed. The numerous conclusive results obtained in this extensive investigation has proved the potential of hybridization of input-output modeling and optimization tools and MADM methods when they systematically applied to the multi-pass cutting operations.

Research question 6:

Is it possible to apply JMatPro, DOE, MADM, computational modeling and meta-heuristic approach in inverse identification of the input parameters during finite element simulation of cutting processes? If it is possible, can a hypothetical numerical optimization study be performed as a case study?

In response to the last research question, a novel approach of inverse identification of input parameters in 3D-FEM of turning DSSs has been proposed. Adopting JMatPro software for generating of temperature dependent physical and elastic-viscoplastic properties of DSSs, the optimum 3D-FEM control $factor^{level}$ combination of h_{lc} , v_c , f_r , μ_c , μ_s , κ_t , $\%p_r$ and D_{crit} has been effectively defined under Taguchi-VIKOR-FANNS approach. Validations of the numerical results experimentally have proved the versatility of the approach accurately. The approach is then employed to define the optimum set of control factors for the rest of the planned investigations. In the next stage, a hypothetical 3D-FEM machining optimization study is then conducted and the optimum set of criteria such as; CB , $Geo.$, CM , v_c , f_r , α_n and λ_i per each cutting performance is defined using Taguchi optimization procedure. Finally, an expert system based on fuzzy rule modeling approach is adopted to simultaneously optimize resultant cutting forces, effective plastic stresses, chip-tool interface cutting temperatures and tool wear rate through deriving NMPMs and performing ANOM. Hence, the adopted hypothetical study can also act as a framework for investigating; ever widening spectrum of cutting tool and workpiece materials, new tool designs, including indexable inserts with complex chip forming

geometry, coatings cause new phenomena, new machining methods such as circular milling, and high speed machining.

11 References

- [ACRU08] ATTANASIO, A. ; CERETTI, E. ; RIZZUTI, S. ; UMBRELLO, D. ; MICARI, F.: 3D Finite Element Analysis of Tool Wear in Machining. In: *CIRP Annals - Manufacturing Technology* Bd. 57 (2008), S. 61–64 — ISBN 0007-8506
- [AhHo12] AHMADI, E. ; HOMAMI, R. M.: Experimental Investigation and Mathematical Modeling of Composite Ceramic Cutting Tools with Alumina Base in the Machining Process of PH- Hardened Austenitic-Ferritic (Duplex) Stainless Steel. In: *Int J Advanced Design and Manufacturing Technology* Bd. 5 (2012), Nr. 2
- [AkAs11] AKKUŞ, H. ; ASILTURK, I.: Predicting Surface Roughness of AISI 4140 Steel in Hard Turning Process through Artificial Neural Network, Fuzzy Logic and Regression Models. In: *Scientific Research and Essays* Bd. 6 (2011), S. 2729–2736
- [AlBe12] ALTINTAS, Y. ; BER, A. A.: *Manufacturing Automation: Metal Cutting Mechanics, Machine Tool Vibrations, and CNC Design*. Bd. 54. New York, USA, 2012 — ISBN 9780521172479
- [AnBM09] ANDERSON-COOK, C. M. ; BORROR, C. M. ; MONTGOMERY, D. C.: Response Surface Design Evaluation and Comparison. In: *Journal of Statistical Planning and Inference* Bd. 139 (2009), S. 629–641 — ISBN 0378-3758
- [AnKa96] ANTONY, J. ; KAYE, M.: Optimisation of Core Tube Life using Taguchi Experimental Design Methodology. In: *Quality World* Bd. 3 (1996), S. 42–50 — ISBN 1352-8769
- [AnPr02] ANTONY, J. ; PREECE, D.: *Understanding, Managing, and Implementing Quality: Frameworks, Techniques, and Cases*. London, UK : Routledge, 2002 — ISBN 0-415-22271-0
- [AÖUD13] ARRAZOLA, P. J. ; ÖZEL, T. ; UMBRELLO, D. ; DAVIES, M. ; JAWAHIR, I. S.: Recent Advances in Modelling of Metal Machining Processes. In: *CIRP Annals - Manufacturing Technology* Bd. 62 (2013), S. 695–718 — ISBN 0007-8506
- [ArDe09] ARMAS, I. A. ; DEGALAIX, S. M.: *Duplex Stainless Steels*. London, UK : ISTE Ltd., 2009 — ISBN 9781848211377
- [ArHe00] ARMAREGO, E. J. A. ; HERATH, A. B.: Predictive Models for Machining with Multi-Edge Form Tools Based on a Generalised Cutting Approach. In: *CIRP Annals - Manufacturing Technology* Bd. 49 (2000), S. 25–30
- [Arma00] ARMAREGO, E. J. A.: The Unified-Generalized Mechanics of Cutting Approach-A Step Towards a House of Predictive Performance Models for Machining Operations. In: *Machining Science and Technology* Bd. 4 (2000), S. 319–362

- [ArÖz09] ARRAZOLA, P. J. ; ÖZEL, T.: Finite Element Modeling of Machining Processes. In: ÖZEL, T. ; DAVIM, J. P. (Hrsg.): *Intelligent Machining Modeling and Optimization of the Machining Processes and Systems*. London, UK : ISTE Ltd. & John Wiley & Sons, Inc., 2009 — ISBN 9781848211292, S. 125–163
- [ArÖz10] ARRAZOLA, P. J. ; ÖZEL, T.: Investigations on the Effects of Friction Modeling in Finite Element Simulation of Machining. In: *International Journal of Mechanical Sciences* Bd. 52 (2010), S. 31–42 — ISBN 0020-7403
- [ArUD08] ARRAZOLA, P. J. ; UGARTE, D. ; DOMÍNGUEZ, X.: A New Approach for the Friction Identification during Machining through the Use of Finite Element Modeling. In: *International Journal of Machine Tools and Manufacture* Bd. 48 (2008), S. 173–183
- [AsCB07] ASLAN, E. ; CAMUŞCU, N. ; BIRGÖREN, B.: Design Optimization of Cutting Parameters when Turning Hardened AISI 4140 Steel (63 HRC) with Al₂O₃ + TiCN Mixed Ceramic tool. In: *Materials and Design* Bd. 28 (2007), S. 1618–1622
- [AsÇu11] ASILTÜRK, İ. ; ÇUNKAŞ, M.: Modeling and Prediction of Surface Roughness in Turning Operations using Artificial Neural Network and Multiple Regression Method. In: *Expert Systems with Applications* Bd. 38 (2011), S. 5826–5832 — ISBN 0957-4174
- [ASKS08] AGGARWAL, A. ; SINGH, H. ; KUMAR, P. ; SINGH, M.: Optimizing Power Consumption for CNC Turned Parts using Response Surface Methodology and Taguchi's Technique-A Comparative Analysis. In: *Journal of Materials Processing Technology* Bd. 200 (2008), S. 373–384
- [AsOu08] ASTAKHOV, V. P. ; OUTEIRO, J. C.: Metal Cutting Mechanics, Finite Element Modelling. In: DAVIM, J. P. (Hrsg.): *Machining: Fundamentals and recent advances*. London, UK, 2008 — ISBN 9781848002128, S. 1–25
- [Asta05] ASTAKHOV, V. P.: On the Inadequacy of the Single-Shear Plane Model of Chip Formation. In: *International Journal of Mechanical Sciences* Bd. 47 (2005), S. 1649–1672 — ISBN 0020-7403
- [Asta06] ASTAKHOV, V. P.: *Tribology of Metal Cutting*. Bd. 52. Oxford, UK : Elsevier, 2006 — ISBN 9780080451497
- [Asta98] ASTAKHOV, V. P.: *Metal Cutting Mechanics*. Boca Raton, USA : CRC Press LLC, 1998 — ISBN 9780849318955
- [AtMS14] ATHISANKAR, P. ; MACHAVARAM, R. ; SHANKAR, K.: System Identification of a Composite Plate using Hybrid Response Surface Methodology and Particle Swarm Optimization in Time Domain. In: *Measurement* Bd. 55 (2014), Nr. 0, S. 499–511
- [AtOB00] ATLAS, L. ; OSTENDORF, M. ; BERNARD, G. D.: Hidden Markov Models for Monitoring Machining Tool-Wear. In: *2000 IEEE International Conference on Acoustics, Speech, and Signal Processing. Proceedings (Cat. No.00CH37100)* Bd. 6 (2000) — ISBN 0-7803-6293-4

- [AtSt98] ATHAVALE, S. M. ; STRENKOWSKI, J. S.: Finite Element Modeling of Machining: from Proof-of-Concept to Engineering Applications. In: *Machining Science and Technology* Bd. 2, Taylor & Francis (1998), Nr. 2, S. 317–342
- [AuBi06] AURICH, J. C. C. ; BIL, H.: 3D Finite Element Modelling of Segmented Chip Formation. In: *CIRP Annals - Manufacturing Technology* Bd. 55 (2006), S. 47–50
- [BAPS05] BASKAR, N. ; ASOKAN, P. ; PRABHAHARAN, G. ; SARAVANAN, R.: Optimization of Machining Parameters for Milling Operations using Non-Conventional Methods. In: *International Journal of Advanced Manufacturing Technology* Bd. 25 (2005), S. 1078–1088 — ISBN 0017000319
- [BaRS02] BAKER, M. ; ROSLER, J. ; SIEMERS, C.: A Finite Element Model of High Speed Metal Cutting with Adiabatic Shearing. In: *Computers & Structures* Bd. 80 (2002), S. 495–513
- [BäRS03] BÄKER, M. ; RÖSLER, J. ; SIEMERS, C.: The Influence of Thermal Conductivity on Segmented Chip formation. In: *Computational Materials Science*. Bd. 26, 2003, S. 175–182
- [BASP06] BASKAR, N. ; ASOKAN, P. ; SARAVANAN, R. ; PRABHAHARAN, G.: Selection of Optimal Machining Parameters for Multi-Tool Milling Operations using a Memetic Algorithm. In: *Journal of Materials Processing Technology* Bd. 174 (2006), S. 239–249 — ISBN 0924-0136
- [BBCC09] BÖLLINGHAUS, T. ; BYRNE, G. ; CHERPAKOV, B. ; CHLEBUS, E. ; CROSS, C. ; DENKENA, B. ; DILTHEY, U. ; HATSUZAWA, T. ; U. A.: Manufacturing Engineering. In: GROTE, K.-H. ; ANTONSSON, E. K. (Hrsg.): *Springer Handbook of Mechanical Engineering*. Berlin, Germany : Springer, 2009 — ISBN 9783540491316, S. 523–785
- [BCLS02] BOROUCHEKI, H. ; CHEROUAT, A. ; LAUG, P. ; SAANOUNI, K.: Adaptive Remeshing for Ductile Fracture Prediction in Metal Forming. In: *Comptes Rendus - Mecanique* Bd. 330 (2002), S. 709–716
- [BCMC05] BERTELLI, R. ; CRISTEL, R. ; MELOTTI, G. ; CECCON, T.: Stainless Steels Machinability Assessment Model. In: KULJANIC, E. (Hrsg.): *AMST'05 Advanced Manufacturing Systems and Technology SE - 56, CISM International Centre for Mechanical Sciences*. Bd. 486 : Springer Vienna, 2005 — ISBN 9783211265376, S. 577–588
- [BeAR14] BELLOUFI, A. ; ASSAS, M. ; REZGUI, I.: Intelligent Selection of Machining Parameters in Multipass Turnings using Firefly Algorithm. In: *Modelling and Simulation in Engineering* (2014), S. 1–6
- [BeOk04] BENSON, D. J. ; OKAZAWA, S.: Contact in a Multi-Material Eulerian Finite Element Formulation. In: *Computer Methods in Applied Mechanics and Engineering* Bd. 193 (2004), S. 4277–4298 — ISBN 1619534592

- [BiFa95] BIGLARI, F. R. ; FANG, X. D.: Real-Time Fuzzy Logic Control for Maximising the Tool Life of Small-Diameter Drills. In: *Fuzzy Sets and Systems* Bd. 72 (1995), Nr. 1, S. 91–101
- [BiKT04] BIL, H. ; KILIÇ, S. E. ; TEKKAYA, A. E.: A Comparison of Orthogonal Cutting Data from Experiments with Three Different Finite Element Models. In: *International Journal of Machine Tools and Manufacture* Bd. 44 (2004), S. 933–944 — ISBN 08906955 (ISSN)
- [Blan04] LE BLANC, D. C.: *Statistics: Concepts and Applications for Science, Statistics: Concepts and Applications for Science*. London, UK : Jones and Bartlett, 2004 — ISBN 0-7637-4699-1
- [BIKo13] BLACK, J. T. ; KOHSER, R. A.: *DeGarmo's Materials and Processes in Manufacturing*. Hoboken, USA : John Wiley & Sons, Inc., 2013 — ISBN 9780470055120
- [BMUK12] BREZAK, D. ; MAJETIC, D. ; UDILJAK, T. ; KASAC, J.: Tool wear estimation using an analytic fuzzy classifier and support vector machines. In: *Journal of intelligent ...* Bd. 23, Springer US (2012), Nr. 3, S. 797–809
- [Bodn02] BODNER, S.: Formulation of a Unified Constitutive Theory of Elastic-Viscoplastic Behavior. In: *Unified Plasticity for Engineering Applications SE - 1, Mathematical Concepts and Methods in Science and Engineering*. Bd. 47 : Springer, 2002 — ISBN 9781461351283, S. 1–70
- [BoDr87] BOX, G. E. P. ; DRAPER, N. R.: *Empirical model-building and response surfaces, Wiley series in probability and mathematical statistics: Applied probability and statistics*. New York, USA : Wiley, 1987 — ISBN 9780471810339
- [Box88] BOX, G.: Signal-to-Noise Ratios, Performance Criteria, and Transformations. In: *Technometrics* Bd. 30 (1988), S. 1–17
- [Bram01] BRAMFITT, B. L.: *Metallographer's Guide: Practice and Procedures for Irons and Steels, EngineeringPro collection*. Metals Park .USA, USA : ASM International, 2001 — ISBN 0-87170-748-9
- [BrDR72] BROZZO, P. ; DELUCA, B. ; REDINA, R. A.: A New Method for the Prediction of the Formability Limits of Metals Sheets. In: *Proceeding 7th Biennial Conference Int. Deep Drawing Research Group* (1972), S. 3.1–3.5
- [BSVR13] BHARATHI, R., S. ; SRINIVAS, P., C. V. ; VAMSHEE, K., K. ; RAGUNATHAN, A. ; VINESH, S.: Optimization of Electrical Discharge Machining Parameters on Hardened Die Steel using Firefly Algorithm. In: *Engineering with Computers*, Springer-Verlag (2013), S. 1–9
- [BWLM14] BUCHKREMER, S. ; WU, B. ; LUNG, D. ; MÜNSTERMANN, S. ; KLOCKE, F. ; BLECK, W.: FE-Simulation of Machining Processes with a New Material Model. In: *Journal of Materials Processing Technology* Bd. 214 (2014), S. 599–611

- [CaCa75] CASTRO, R. ; CADENET, J. J.: *Welding Metallurgy of Stainless and Heat-resisting Steels* : Cambridge University Press, 1975 — ISBN 0-521-20431-3
- [CaCG08] CALAMAZ, M. ; COUPARD, D. ; GIROT, F.: A New Material Model for 2D Numerical Simulation of Serrated Chip formation when Machining Titanium Alloy Ti-6Al-4V. In: *International Journal of Machine Tools and Manufacture* Bd. 48 (2008), S. 275–288 — ISBN 0022-3115
- [ÇaEk12] ÇAYDAŞ, U. ; EKICI, S.: Support Vector Machines Models for Surface Roughness Prediction in CNC Turning of AISI 304 Austenitic Stainless Steel. In: *Journal of Intelligent Manufacturing* Bd. 23 (2012), S. 639–650
- [CaGu00] ÇAKIR, M. C. ; GURARDA, A.: Optimization of Machining Conditions for Multi-Tool Milling Operations. In: *International Journal of Production Research* Bd. 38, Taylor & Francis (2000), Nr. 15, S. 3537–3552
- [ÇaHa08] ÇAYDAŞ, U. ; HASÇALIK, A.: A Study on Surface Roughness in Abrasive Waterjet Machining Process using Artificial Neural Networks and Regression Analysis Method. In: *Journal of Materials Processing Technology* Bd. 202 (2008), S. 574–582 — ISBN 0878499180
- [CaLS14] CAMPATELLI, G. ; LORENZINI, L. ; SCIPPA, A.: Optimization of Process Parameters using a Response Surface Method for Minimizing Power Consumption in the Milling of Carbon Steel. In: *Journal of Cleaner Production* Bd. 66 (2014), S. 309–316
- [Cars02] CARSON, J. S.: Model Verification and Validation. In: *Proceedings of the 2002 Winter Simulation Conference* (2002), S. 52–58
- [CaSt88] CARROLL, J. T. ; STRENKOWSKI, J. S.: Finite Element Models of Orthogonal Cutting with Application to Single Point Diamond Turning. In: *International Journal of Mechanical Sciences* Bd. 30 (1988), S. 899–920
- [CBBM13] CHAGAS, G. M. P. ; BARBOSA, P. A. ; BARBOSA, C. A. ; MACHADO, I. F.: Thermal Analysis of the Chip formation in Austenitic Stainless Steel. In: *Procedia CIRP* Bd. 8 (2013), S. 293–298
- [CeLA99] CERETTI, E. ; LUCCHI, M. ; ALTAN, T.: FEM Simulation of Orthogonal Cutting: Serrated Chip formation. In: *Journal of Materials Processing Technology* Bd. 95 (1999), S. 17–26
- [Chan10] CHANG, C. L.: A Modified VIKOR Method for Multiple Criteria Analysis. In: *Environmental Monitoring and Assessment* Bd. 168, Springer Netherlands (2010), Nr. 1-4, S. 339–344
- [ChB194] CHEN, A. G. ; BLACK, J. T.: FEM Modeling in Metal Cutting. In: *Manufacturing Review* Bd. 7 (1994), Nr. 2, S. 120–133

- [ChCh01] CHIEN, W. -T. ; CHOU, C. Y.: The Predictive Model for Machinability of 304 Stainless Steel. In: *Journal of Materials Processing Technology* Bd. 118 (2001), Nr. 1–3, S. 442–447
- [ChCh13] CHINCHANIKAR, S. ; CHOUDHURY, S. K. K.: Effect of Work Material Hardness and Cutting Parameters on Performance of Coated Carbide Tool when Turning Hardened Steel: An Optimization Approach. In: *Measurement: Journal of the International Measurement Confederation* Bd. 46 (2013), S. 1572–1584
- [Chil06] CHILDS, T. H. C.: Numerical Experiments on the Influence of Material and other Variables on Plane Strain Continuous Chip formation in Metal Machining. In: *International Journal of Mechanical Sciences* Bd. 48 (2006), S. 307–322
- [ChLu07] CHING-KAO, C. ; LU, H. S.: The Optimal Cutting-Parameter Selection of Heavy Cutting Process in Side Milling for SUS304 Stainless Steel. In: *The International Journal of Advanced Manufacturing Technology* Bd. 34, Springer-Verlag (2007), Nr. 5-6, S. 440–447
- [ChMi11] CHICK, A. ; MICKLETHWAITE, P.: *Design for Sustainable Change: How Design and Designers Can Drive the Sustainability Agenda, Required reading range: Course reader*. Laussane, Switzerland : Bloomsbury Academic, 2011 — ISBN 9782940411306
- [Chry06] CHRYSOLOURIS, G.: *Manufacturing Systems: Theory and Practice, Mechanical Engineering Series*. New York, USA : Springer, 2006 — ISBN 9780387284316
- [ChSr13] CHITTARANJAN, D. ; SRINIVAS, C.: Evaluation of Metal Strip-Layout Selection using AHP and TOPSIS Method. In: *Advanced Materials Manufacturing & Characterization* Bd. 3 (2013), Nr. 1, S. 425–429
- [ChTo01] CHUNG, B. M. ; TOMIZUKA, M.: Fuzzy Logic Modeling and Control for Drilling of Composite Laminates. In: *10th IEEE International Conference on Fuzzy Systems* Bd. 1 (2001) — ISBN 0-7803-7293-X
- [ChTo07] CHAN, J. W. K. ; TONG, T. K. L.: Multi-Criteria Material Selections and End-of-Life Product Strategy: Grey Relational Analysis Approach. In: *Materials and Design* Bd. 28 (2007), S. 1539–1546 — ISBN 0261-3069
- [ChTs03] CHIEN, W. T. ; TSAI, C. S.: The Investigation on the Prediction of Tool Wear and the Determination of Optimum Cutting Conditions in Machining 17-4PH Stainless Steel. In: *Journal of Materials Processing Technology*. Bd. 140, 2003, S. 340–345
- [ChTs96] CHEN, M. -C. ; TSAI, D. -M.: A Simulated Annealing Approach for Optimization of Multi-Pass Turning Operations. In: *International Journal of Production Research* Bd. 34 (1996), Nr. 10, S. 2803–2825
- [ÇKKG13] ÇALIŞKAN, H. ; KURŞUNCU, B. ; KURBANOĞLU, C. ; GÜVEN, Y.: Material Selection for the Tool Holder Working under Hard Milling Conditions using Different

- Multi Criteria Decision Making Methods. In: *Materials and Design* Bd. 45 (2013), S. 473–479 — ISBN 3782235258
- [CMKD10] CHANDRASEKARAN, M. ; MURALIDHAR, M. ; KRISHNA, C. M. ; DIXIT, U. S.: Application of Soft Computing Techniques in Machining Performance Prediction and Optimization: A Literature Review. In: *The International Journal of Advanced Manufacturing Technology* Bd. 46, Springer-Verlag (2010), Nr. 5-8, S. 445–464 — ISBN 0268-3768
- [CMRM13] COURBON, C. ; MABROUKI, T. ; RECH, J. ; MAZUYER, D. ; D'ERAMO, E.: On the Existence of A Thermal Contact Resistance at the Tool-Chip Interface in Dry Cutting of AISI 1045: formation Mechanisms and Influence on the Cutting Process. In: *Applied Thermal Engineering*. Bd. 50, 2013, S. 1311–1325
- [Cobb99] COBB, H. M. (Hrsg.): *Steel Products Manual: Stainless Steels*. Warrendale, USA : Iron and Steel Society, 1999 — ISBN 1-886362-34-3
- [CoCF11] COSTA, A. ; CELANO, G. ; FICHERA, S.: Optimization of Multi-Pass Turning Economies through a Hybrid Particle Swarm Optimization Technique. In: *The International Journal of Advanced Manufacturing Technology* Bd. 53, Springer-Verlag (2011), Nr. 5-8, S. 421–433
- [Cock68] COCKCROFT, M. G., LATHAM, D. J.: Ductility and the Workability of Metals. In: *Journal of the Institute of Metals* Bd. 96 (1968), S. 33–39
- [Cocq51] COCQUILHAT, M.: Expériences sur la Resistance Utile Produite dans le Forage. In: *Annales Travaux Publics en Belgique* Bd. 10 (1851), S. 199–215
- [Coel99] COELLO, C. A. C.: An Updated Survey of Evolutionary Multiobjective Optimization Techniques: State of the Art and Future Trends. In: *Proceedings of the Congress on Evolutionary Computation*. Washington, DC : IEEE, 1999, S. 3–13
- [CoJS98] COIT, D. W. ; JACKSON, B. T. ; SMITH, A. E.: Static Neural Network Process Models: Considerations and Case Studies. In: *International Journal of Production Research* Bd. 36 (1998), Nr. 11, S. 2953–2967 — ISBN 0020754981
- [COKD11] CETIN, M. H. ; OZCELIK, B. ; KURAM, E. ; DEMIRBAS, E.: Evaluation of Vegetable based Cutting Fluids with Extreme Pressure and Cutting Parameters in Turning of AISI 304L by Taguchi Method. In: *Journal of Cleaner Production* Bd. 19 (2011), S. 2049–2056
- [DaMa09] DAVIM, J. P. ; MARANHÃO, C.: A Study of Plastic Strain and Plastic Strain Rate in Machining of Steel AISI 1045 using FEM Analysis. In: *Materials and Design* Bd. 30 (2009), S. 160–165 — ISBN 0261-3069
- [DaSa11] DANIEL, P. S. ; SAM, A. G.: *Research Methodology*. New Delhi, India : Chowla Offset Press, 2011 — ISBN 9788178359007

- [Davi03] DAVIS, J. R.: *Handbook of Materials for Medical Devices*. Materials Park, USA, USA : ASM International, 2003 — ISBN 0-87170-790
- [DaYS09] DARVISH, M. ; YASAEI, M. ; SAEEDI, A.: Application of the Graph Theory and Matrix Methods to Contractor Ranking. In: *International Journal of Project Management* Bd. 27 (2009), S. 610–619 — ISBN 02637863
- [Deb09] DEB, K.: *Optimization for Engineering Design: Algorithms and Examples*. New Delhi, India : Prentice-Hall of India, 2009 — ISBN 9788120309432
- [DeDi08] DEB, S. ; DIXIT, U. S.: Intelligent Machining: Computational Methods and Optimization. In: *Machining SE - 12* : Springer London, 2008 — ISBN 9781848002128, S. 329–358
- [DiCM01] DIRIKOLU, M. H. ; CHILDS, T. H. C. ; MAEKAWA, K.: Finite-Element Analysis of Machining with the Tool Edge Considered. In: *International Journal of Mechanical Sciences* Bd. 43 (2001), S. 2699–2713
- [DiDi08] DIXIT, P. M. ; DIXIT, U. S.: *Modeling of Metal Forming and Machining Processes by Finite Element and Soft Computing Methods, Engineering Materials and Processes*. London, UK : Springer, 2008 — ISBN 9781848001886
- [DoCa99] DORIGO, M. ; CARO, G. D.: Ant Colony Optimization: A New Meta-Heuristic. In: *Proceedings of the 1999 Congress on Evolutionary Computation-CEC99 (Cat. No. 99TH8406)* Bd. 2 (1999), S. 1470–1477 — ISBN 0-7803-5536-9
- [Dube09] DUBEY, A. K.: Optimization of Electro-Chemical Honing using Utility-based Taguchi Approach. In: *The International Journal of Advanced Manufacturing Technology* Bd. 41, Springer-Verlag (2009), Nr. 7-8, S. 749–759
- [DuRF14] DUCOBU, F. ; RIVIÈRE-LORPHEVRE, E. ; FILIPPI, E.: Numerical Contribution to the Comprehension of Saw-toothed Ti6Al4V Chip formation in Orthogonal Cutting. In: *International Journal of Mechanical Sciences* Bd. 81 (2014), S. 77–87
- [EIE108] EL-TAMIMI, A. M. ; EL-HOSSAINY, T. M.: Investigating the Tool Life, Cutting Force Components, and Surface Roughness of AISI 302 Stainless Steel Material under Oblique Machining. In: *Materials and Manufacturing Processes* Bd. 23 (2008), Nr. 4, S. 427–438
- [EnDK95] ENDRES, W. J. ; DEVOR, R. E. ; KAPOOR, S. G.: A Dual-Mechanism Approach to the Prediction of Machining Forces, Part 1: Model Development. In: *Journal of Engineering for Industry* Bd. 117 (1995), S. 534–541
- [ErLO01] ERTUNC, H. M. ; LOPARO, K. A. ; OCAK, H.: Tool Wear Condition Monitoring in Drilling Operations Using Hidden Markov Models (HMMs). In: *International Journal of Machine Tools and Manufacture* Bd. 41 (2001), S. 1363–1384

- [ErOz10] EREN, T. ; OZBAYOGLU, M. E. E.: Real Time Optimization of Drilling Parameters During Drilling Operations. In: *SPE Oil and Gas India Conference and Exhibition*, 2010, S. 1–14
- [ErŞe09] ERDIK, T. ; ŞEN, Z.: Prediction of Tool Wear using Regression and ANN Models in End-Milling Operation A Critical Review. In: *International Journal of Advanced Manufacturing Technology* Bd. 43 (2009), S. 765–766
- [ETGZ13] ESCAMILLA-SALAZAR, I. G. ; TORRES-TREVIÑO, L. M. ; GONZÁLEZ-ORTÍZ, B. ; ZAMBRANO, P. C.: Machining Optimization using Swarm intelligence in Titanium (6Al 4V) Alloy. In: *The International Journal of Advanced Manufacturing Technology* Bd. 67, Springer-Verlag (2013), Nr. 1-4, S. 535–544
- [FaJa94] FAND, X. D. ; JAWAHIR, I. S.: Predicting Total Machining Performance in Finish Turning using Integrated Fuzzy-Set Models of the Machinability Parameters. In: *International Journal of Production Research* Bd. 32 (1994), Nr. 4, S. 833–849
- [FAMS12] FATHI, J. ; ASHRAFI, S. ; MOVLA, H. ; SOBHAIAN, S.: A Novel Method to Determine Poisson's Ratio by Beta-Ray Absorption Experiment. In: *Applied Radiation and Isotopes* Bd. 70 (2012), S. 823–826
- [FaZe05] FANG, G. ; ZENG, P.: Three-Dimensional Thermo-Elastic-Plastic Coupled FEM Simulations for Metal Oblique Cutting Processes. In: *Journal of Materials Processing Technology* Bd. 168 (2005), S. 42–48
- [Finn56] FINNIE, I.: Review of the Metal Cutting Analyses of the Past Hundred Years. In: *Mech Eng* Bd. 78 (1956), Nr. 8, S. 715–721
- [FiYB13] FISTER, I. ; YANG, X. -S. ; BREST, J.: A Comprehensive Review of Firefly Algorithms. In: *Swarm and Evolutionary Computation* Bd. 13 (2013), S. 34–46
- [Fran08] FRANCOIS C.: *Ferrous Metals and Their Alloys*. London, UK : Springer, 2008 — ISBN 9781846286681
- [Fung03] FUNG, C. P.: Manufacturing Process Optimization for Wear Property of Fiber-Reinforced Polybutylene Terephthalate Composites with Grey Relational Analysis. In: *Wear* Bd. 254 (2003), S. 298–306
- [FYBF13] FISTER, I. ; YANG, X. -S. ; BREST, J. ; FISTER, D.: A Brief Review of Nature-inspired Algorithms for Optimization. In: *Elektrotehniski Vestnik/Electrotechnical Review* Bd. 80 (2013), S. 116–122
- [GaKD08a] GAITONDE, V. N. ; KARNIK, S. R. ; DAVIM, J. P.: Taguchi Multiple-Performance Characteristics Optimization in Drilling of Medium Density Fibreboard (MDF) to Minimize Delamination using Utility Concept. In: *Journal of Materials Processing Technology* Bd. 196 (2008), S. 73–78

- [GaKD08b] GAITONDE, V. N. ; KARNIK, S. R. ; DAVIM, J. P.: Selection of Optimal MQL and Cutting Conditions for Enhancing Machinability in Turning of Brass. In: *Journal of Materials Processing Technology* Bd. 204 (2008), S. 459–464
- [GaKD09] GAITONDE, V. N. ; KARNIK, S. R. ; DAVIM, J. P.: Design of Experiments. In: ÖZEL, T. ; DAVIM, J. P. (Hrsg.): *Intelligent Machining Modeling and Optimization of the Machining Processes and Systems*. London, UK : ISTE Ltd. & John Wiley & Sons, Inc., 2009 — ISBN 9781848211292, S. 216–243
- [GePo10] GENDREAU, M. ; POTVIN, J. -Y.: Tabu Search. In: GLOVER, F. ; KOCHENBERGER, G. A. (Hrsg.): *Handbook of Metaheuristics*. Bd. 146. Dordrecht, Holland, 2010 — ISBN 9781441916631, S. 648
- [GhCH04] GHANI, J. A. ; CHOUDHURY, I. A. ; HASSAN, H. H.: Application of Taguchi Method in the Optimization of End Milling Parameters. In: *Journal of Materials Processing Technology* Bd. 145 (2004), S. 84–92
- [Gilb50] GILBERT, W. W.: Economics of Machining. In: *In Machining Theory and Practice*. Materials Park, USA : American Society of Metals, 1950, S. 465–485
- [GiWu97] GILAT, A. ; WU, X.: Plastic Deformation of 1020 Steel over a Wide Range of Strain Rates and Temperatures. In: *International Journal of Plasticity* Bd. 13 (1997), S. 611–632
- [GKAS06] GAITONDE, V. N. ; KARNIK, S. R. ; ACHYUTHA, B. T. ; SIDDESWARAPPA, B.: Taguchi Approach with Multiple Performance Characteristics for Burr Size Minimization in Drilling. In: *Journal of Scientific and Industrial Research* Bd. 65 (2006), S. 977–981 — ISBN 0836237498
- [GKAS09] GAITONDE, V. N. ; KARNIK, S. R. R ; ACHYUTHA, B. T. T. ; SIDDESWARAPPA, B. ; DAVIM, J. P.: Predicting Burr Size in Drilling of AISI 316L Stainless Steel using Response Surface Analysis. In: *International Journal of Materials and Product Technology* Bd. 35 (2009), S. 228–245
- [GoMG09] GOPALSAMY, B. M. ; MONDAL, B. ; GHOSH, S.: Taguchi Method and ANOVA: An Approach for Process Parameters Pptimization of Hard Machining while Machining Hardened Steel. In: *Journal of Scientific and Industrial Research* Bd. 68 (2009), S. 686–695 — ISBN 9474112444
- [GrBN05] GRZESIK, W. ; BARTOSZUK, M. ; NIESLONY, P.: Finite Element Modelling of Temperature Distribution in the Cutting Zone in Turning Processes with Differently Coated Tools. In: *Journal of Materials Processing Technology* Bd. 164–165 (2005), S. 1204–1211
- [Groo10] GROOVER, M. P.: *Fundamentals of Modern Manufacturing: Materials, Processes, and Systems*. Hoboken, USA : John Wiley & Sons, Inc., 2010 — ISBN 9780470467002

- [Grou11] GROUS, A.: *Applied Metrology for Manufacturing Engineering*, ISTE. London, UK : ISTE Ltd. & John Wiley & Sons, Inc., 2011 — ISBN 9781848211889
- [Grze08] GRZESIK, W.: *Advanced Machining Processes of Metallic Materials: Theory, Modelling and Applications*. Amsterdam, Holland : Elsevier Science, 2008 — ISBN 9780080445342
- [Grze09] GRZESIK, W.: Analytical and Mechanistic Modeling of Machining Processes. In: ÖZEL, T. ; DAVIM, J. P. (Hrsg.): *Intelligent Machining Modeling and Optimization of the Machining Processes and Systems*. London, UK : ISTE Ltd. & John Wiley & Sons, Inc., 2009 — ISBN 978-1-84821-129-2, S. 72–121
- [GuBa09] GUJARATHI, A. M ; BABU, B. V.: Improved Strategies of Multi-objective Differential Evolution (MODE) for Multi-objective Optimization. In: *Indian International Conference on Artificial Intelligence 2009* (2009), S. 933–948 — ISBN 9780972741279
- [GuDo00] GUO, Y. B. ; DORNFELD, D. A.: Finite Element Modeling of Burr formation Process in Drilling 304 Stainless Steel. In: *Journal of Manufacturing Science and Engineering, Transactions of the ASME* Bd. 122 (2000), S. 612–619
- [GuLi02] GUO, Y. B. ; LIU, C. R.: 3D FEA Modeling of Hard Turning. In: *Journal of Manufacturing Science and Engineering* Bd. 124 (2002), S. 189–199 — ISBN 10871357
- [GuMu80] GUPTA, V. ; MURTHY, P. N.: *An introduction to Engineering Design Method*. New Delhi, India, India : Tata McGraw-Hill, 1980 — ISBN 9780070964419
- [GuWW06] GUO, Y. B. ; WEN, Q. ; WOODBURY, K. A.: Dynamic Material Behavior Modeling Using Internal State Variable Plasticity and Its Application in Hard Machining Simulations. In: *Journal of Manufacturing Science and Engineering* Bd. 128 (2006), S. 749–759
- [HaBR99] HASHMI, K. ; EL BARADIE, M. A. ; RYAN, M.: Fuzzy-Logic Intelligent Selection of Machining Parameters. In: *Journal of Materials Processing Technology* Bd. 94 (1999), S. 94–111
- [HaKR08] HAGLUND, A. J. ; KISHAWY, H. A. ; ROGERS, R. J.: An Exploration of Friction Models for the Chip-Tool Interface using an Arbitrary Lagrangian-Eulerian Finite Element Model. In: *Wear* Bd. 265 (2008), S. 452–460 — ISBN 0043-1648
- [HaNo13] HADDAG, B. ; NOUARI, M.: Tool Wear and Heat Transfer Analyses in Dry Machining based on Multi-Steps Numerical Modelling and Experimental Validation. In: *Wear* Bd. 302 (2013), S. 1158–1170
- [Hart73] HARTIG, E.: *Versuche über Leistung und Arbeitsverbrauch der Werkzeugmaschine*. 3. Aufl. Leipzig, Germany, Germany : Druck und Verlag von B. G. Teubner, 1873

- [HaSu90] HASSAN, G. A. ; SULIMAN, S. M. A.: Experimental Modelling and Optimization of Turning Medium Carbon Steel. In: *International Journal of Production Research* Bd. 28 (1990), Nr. 6, S. 1057–1065
- [Hayk99] HAYKIN, S. S.: *Neural Networks: A Comprehensive Foundation, International edition*. Upper Saddle River, USA, USA : Prentice Hall, 1999 — ISBN 81-7808-300-0
- [Hedb89] HEDBERG, J.: *Oxford Advanced Learner's Dictionary of Current English*. Bd. 83. 4. Aufl. Oxford, UK : Oxford University Press, 1989 — ISBN 0194001024
- [HeSK13] HEISEL, U. ; STORCHAK, M. ; KRIVORUCHKO, D.: Thermal Effects in Orthogonal Cutting. In: *Production Engineering* Bd. 7, Springer-Verlag (2013), Nr. 2-3, S. 203–211
- [HoCh08] HORNG, J. T. ; CHIANG, K. T.: A Grey and Fuzzy Algorithms integrated Approach to the Optimization of Turning Hadfield Steel with Al₂O₃/TiC Mixed Ceramic Tool. In: *Journal of Materials Processing Technology* Bd. 207 (2008), S. 89–97
- [HoNg13] HOSSEINKHANI, K. ; NG, E.: Analysis of the Cutting Mechanics under the Influence of Worn Tool Geometry. In: *Procedia CIRP*. Bd. 8, 2013, S. 117–122
- [HPSS11] HEISEL, U. ; PASTERNAK, S. ; STORCHAK, M. ; SOLOPOVA, O.: Optimal Configurations of the Machine Tool Structure by Means of Neural Networks. In: *Production Engineering* Bd. 5, Springer-Verlag (2011), Nr. 2, S. 219–226
- [HuBl96] HUANG, J. M. ; BLACK, J. T.: An Evaluation of Chip Separation Criteria for the FEM Simulation of Machining. In: *Journal of Manufacturing Science and Engineering* Bd. 118 (1996), S. 545–554
- [Hueb01] HUEBNER, K. H.: *The Finite Element Method for Engineers, A Wiley-Interscience publication*. 4. Aufl. Rosewood Drive, USA : John Wiley & Sons, Inc., 2001 — ISBN 0-471-37078-9
- [HuLL01] HUI, Y. V. ; LEUNG, L. C. ; LINN, R.: Optimal Machining Conditions with Costs of Quality and Tool Maintenance for Turning. In: *International Journal of Production Research* Bd. 39 (2001), Nr. 4, S. 647–665
- [HuSh04] HUA, J. ; SHIVPURI, R.: Prediction of Chip Morphology and Segmentation during the Machining of Titanium Alloys. In: *Journal of Materials Processing Technology*. Bd. 150, 2004 — ISBN 1614292787, S. 124–133
- [IHLD07] IQBAL, A. ; HE, N. ; LI, L. ; DAR, N. U.: A Fuzzy Expert System for Optimizing Parameters and Predicting Performance Measures in Hard-Milling Process. In: *Expert Systems with Applications* Bd. 32 (2007), S. 1020–1027 — ISBN 0957-4174
- [Issf13] ISSF: *Stainless Steel in Figures*. Brussels, Belgium, Belgium, 2013

- [IwOT84] IWATA, K. ; OSAKADA, K. ; TERASAKA, Y.: Process Modeling of Orthogonal Cutting by the Rigid-Plastic Finite Element Method. In: *Journal of Engineering Materials and Technology, Transactions of the ASME* Bd. 106 (1984), S. 132–138 — ISBN 00944289 (ISSN)
- [JaEd13a] JAHAN, A. ; EDWARDS, K. L.: *Multi-criteria Decision Analysis for Supporting the Selection of Engineering Materials in Product Design*, 2013 — ISBN 9780080993867
- [JaEd13b] JAHAN, A. ; EDWARDS, K. L.: VIKOR Method for Material Selection Problems with Interval Numbers and Target-based Criteria. In: *Materials and Design* Bd. 47 (2013), S. 759–765
- [Jawa88] JAWAHIR, I. S.: The Chip Control Factor in Machinability Assessments: Recent Trends. In: *Journal of Mechanical Working Technology* Bd. 17 (1988), S. 213–224
- [JiLi12] JIN, D. ; LIN, S.: *Advances in Computer Science and Information Engineering: Volume 2, Advances in Intelligent and Soft Computing*. Heidelberg, Germany : Springer, 2012 — ISBN 9783642302237
- [JIUA14] JAFARIAN, F. ; IMAZ CIARAN, M. ; UMBRELLO, D. ; ARRAZOLA, P. J. ; FILICE, L. ; AMIRABADI, H.: Finite Element Simulation of Machining Inconel 718 Alloy including Microstructure Changes. In: *International Journal of Mechanical Sciences* Bd. 88 (2014), Nr. 0, S. 110–121
- [Jkau08] J. KAUSHISH: *Manufacturing Processes*. 2. Aufl. New Delhi, India, India : Prentice-Hall of India Pvt. Limited, 2008 — ISBN 9788120333529
- [JNUM13] JOHANSSON, M. P. ; NORRBY, N. ; ULLBRAND, J. ; M'SAOUBI, R. ; ODÉN, M.: Effects on Microstructure and Properties in Decomposed Arc Evaporated Ti_{1-x}Al_xN Coatings during Metal Cutting. In: *Surface and Coatings Technology* Bd. 235 (2013), S. 181–185
- [JoCo83] JOHNSON, G. R. ; COOK, W. H.: A Constitutive Model and Data for Metals Subjected to Large Strains, High Strain Rates and High Temperatures. In: *7th International Symposium on Ballistics* (1983), S. 541–547
- [JoCo85] JOHNSON, G. R. ; COOK, W. H.: Fracture Characteristics of Three Metals Subjected to Various Strains, Strain Rates, Temperatures and Pressures. In: *Engineering Fracture Mechanics* Bd. 21 (1985), S. 31–48 — ISBN 0013-7944
- [JoDJ94] JOSHI, V. S. ; DIXIT, P. M. ; JAIN, V. K.: Viscoplastic Analysis of Metal Cutting by Finite Element Method. In: *International Journal of Machine Tools and Manufacture* Bd. 34 (1994), S. 553–571
- [Julo82] JU-LONG, D.: Control Problems of Grey Systems. In: *Systems & Control Letters* Bd. 1 (1982), S. 288–294 — ISBN 0167-6911

- [Julo89] JULONG, D.: Introduction to Grey System Theory. In: *The Journal of Grey System* Bd. 1 (1989), S. 1–24
- [JuYL03] JUAN, H. ; YU, S. F. ; LEE, B. Y.: The Optimal Cutting-Parameter Selection of Production Cost in HSM for SKD61 Tool Steels. In: *International Journal of Machine Tools and Manufacture* Bd. 43 (2003), S. 679–686
- [KaCh08] KALYAN, K. ; CHOUDHURY, S. K. K.: Investigation of Tool Wear and Cutting Force in Cryogenic Machining using Design of Experiments. In: *Journal of Materials Processing Technology* Bd. 203 (2008), S. 95–101 — ISBN 0924-0136
- [KaGC13] KARANDE, P. ; GAURI, S. K. ; CHAKRABORTY, S.: Applications of Utility Concept and Desirability Function for Materials Selection. In: *Materials and Design* Bd. 45 (2013), S. 349–358
- [KaHo03] KAO, P. S. ; HOCHENG, H.: Optimization of Electrochemical Polishing of Stainless Steel by Grey Relational Analysis. In: *Journal of Materials Processing Technology*. Bd. 140, 2003 — ISBN 0924-0136, S. 255–259
- [Kahr08] KAHRAMAN, C.: Multi-Criteria Decision Making Methods and Fuzzy Sets. In: *Fuzzy Multi-Criteria Decision Making*. Bd. 16, 2008 — ISBN 9780387768137, S. 1–18
- [Karp11] KARPAT, Y.: . Temperature Dependent Flow Softening of Titanium Alloy Ti6Al4V: An Investigation using Finite Element Simulation of Machining. In: *Journal of Materials Processing Technology* Bd. 211 (2011), S. 737–749
- [KaSc06] KALPAKJIAN, S. ; SCHMIT, S. R.: *Manufacturing Engineering and Technology*. 5. Aufl. Upper Saddle River, USA : Pearson Education, Inc., 2006 — ISBN 0-13-148965-8
- [KaSc08] KALPAKJIAN, S. ; SCHMIT, S. R.: *Manufacturing Processes for Engineering Materials*. 5. Aufl. Upper Saddle River, USA : Pearson Education Inc, 2008 — ISBN 9789810679538
- [KaSR10] KALADHAR, M. ; SUBBAIAH, K. V. ; RAO, K. N.: Optimization of Process Parameters Inturning of AISI202 Austenitic Stainless Steel. In: *ARPJ Journal of Engineering and Applied Sciences* Bd. 5 (2010), Nr. 9, S. 79–87
- [KaTU83] KATSUHIRO, M. ; TAKAHIRO, S. ; USUI, E.: . Flow Stress of Low Carbon Steel at High Temperature and Strain Rate (Part 2) - Flow Stress under Variable Temperature and Variable Strain Rate. In: *Bulletin of the Japan Society of Precision Engineering* Bd. 17 (1983), Nr. 3, S. 167–172
- [KeEb95] KENNEDY, J. ; EBERHART, R.: Particle Swarm Optimization. In: *Neural Networks, 1995. Proceedings., IEEE International Conference on*. Bd. 4, 1995 — ISBN VO - 4, S. 1942–1948 vol.4

- [KhPS97] KHAN, Z. ; PRASAD, B. ; SINGH, T.: Machining Condition Optimization by Genetic Algorithms and Simulated Annealing. In: *Computers & Operations Research* Bd. 24 (1997), Nr. 7, S. 647–657
- [KiCh07] KIRBY, E. D. ; CHEN, J. C.: Development of a Fuzzy-Nets-based Surface Roughness Prediction System in Turning Operations. In: *Computers and Industrial Engineering* Bd. 53 (2007), S. 30–42 — ISBN 0360-8352
- [KiGV83] KIRKPATRICK, S. ; GELATT, C. D. ; VECCHI, M. P.: Optimization by Simulated Annealing. In: *Science* Bd. 220 (1983), S. 671–680 — ISBN 1095-9203 (Electronic)r0036-8075 (Linking)
- [KiLS99a] KIM, K. W. ; LEE, W. Y. ; SIN, H. C.: Finite Element Analysis of Machining with the Tool Edge Considered. In: *Journal of Materials Processing Technology* Bd. 86 (1999), S. 45–55
- [KiLS99b] KIM, K. W. ; LEE, W. Y. ; SIN, H.: A Finite Element Analysis for the Characteristics of Temperature and Stress in Micro-Machining Considering the Size Effect. In: *International Journal of Machine Tools and Manufacture* Bd. 39 (1999), S. 1507–1524 — ISBN 0890-6955
- [KiPa05] KIM, B. ; PARK, K.: Modeling Plasma Etching Process using a Radial Basis Function Network. In: *Microelectronic Engineering* Bd. 77 (2005), S. 150–157
- [KIBW05] KLOCKE, F. ; BRINKSMEIER, E. ; WEINERT, K.: Capability Profile of Hard Cutting and Grinding Processes. In: *CIRP Annals - Manufacturing Technology* Bd. 54 (2005), S. 22–45 — ISBN 0007-8506
- [KIKr05] KLOCKE, F. ; KRATZ, H.: Advanced Tool Edge Geometry for High Precision Hard Turning. In: *CIRP Annals - Manufacturing Technology* Bd. 54 (2005), S. 47–50
- [KILB13] KLOCKE, F. ; LUNG, D. ; BUCHKREMER, S.: Inverse Identification of the Constitutive Equation of Inconel 718 and AISI 1045 from FE Machining Simulations. In: *Procedia CIRP*. Bd. 8. Turin, Italy, 2013, S. 212–217
- [Kloc11] KLOCKE, F.: *Manufacturing Processes I: Cutting, RWTHedition*. Heidelberg, Germany, Germany : Springer, 2011 — ISBN 9783642119798
- [KnBo05] KNIGHT, W. A. ; BOOTHROYD, G.: *Fundamentals of Metal Machining and Machine Tools, Third Edition, Manufacturing engineering and materials processing*. Boca Raton, USA, USA : Taylor & Francis, 2005 — ISBN 9781574446593
- [KoCS06] KONAK, A. ; COIT, D. W. ; SMITH, A. E.: Multi-Objective Optimization using Genetic Algorithms: A Tutorial. In: *Reliability Engineering & System Safety* Bd. 91 (2006), S. 992–1007 — ISBN 0951-8320
- [KoDi05] KOHLI, A. ; DIXIT, U. S.: A Neural-Network-based Methodology for the Prediction of Surface Roughness in a Turning Process. In: *International Journal of Advanced Manufacturing Technology* Bd. 25 (2005), S. 118–129

- [KoKS08] KOSE, E. ; KURT, A. ; SEKER, U.: The Effects of the Feed Rate on the Cutting Tool Stresses in Machining of Inconel 718. In: *Journal of Materials Processing Technology* Bd. 196 (2008), S. 165–173
- [Koth04] KOTHARI, C. R.: *Research Methodology: Methods and Techniques*. New Delhi, India : New Age International Publishers, 2004 — ISBN 9788122424881
- [KrLG13] KROLCZYK, G. ; LEGUTKO, S. ; GAJEK, M.: Predicting the Surface Roughness in the Dry Machining of Duplex Stainless Steel (DSS). In: *METALURGIJA* Bd. 52 (2013), Nr. 2, S. 259–262
- [Kron66] KRONENBERG, M.: *Machining Science and Application: Theory and Practice for Operation and Development of Machining Processes*. London, UK, UK : Pergamon Press, 1966 — ISBN 9780080116273
- [Krus12] KRUSE, F. C.: *Predictions, Nonlinearities and Portfolio Choice, Reihe: Katallaktik*. Kologne, Germany : Josef Eul Verlag GmbH, 2012 — ISBN 9783844101850
- [KuHM10] KUNDISCH, D. ; HERRMANN, P. ; MEIER, C.: Sustainable Process Management - Status Quo and Perspectives. In: DANGELMAIER, W. ; BLECKEN, A. ; DELIUS, R. ; KLÖPFER, S. (Hrsg.): *Advanced Manufacturing and Sustainable Logistics SE - 9, Lecture Notes in Business Information Processing*. Bd. 46 : Springer Berlin Heidelberg, 2010 — ISBN 9783642124617, S. 94–106
- [KwFT02] KWON, Y. ; FISCHER, G. W. ; TSENG, T. L.: Fuzzy Neuron Adaptive Modeling to Predict Surface Roughness under Process Variations in CNC Turning. In: *Journal of Manufacturing Systems* Bd. 21 (2002), S. 440–450
- [LaHw96] LAI, Y. J. ; HWANG, C. L.: *Fuzzy Multiple Objective Decision Making: Methods and Applications*. Berlin, Germany : Springer Verlag, 1996 — ISBN 9783540575955
- [LaSe10] LATHA, B. ; SENTHILKUMAR, V. S.: Modeling and Analysis of Surface Roughness Parameters in Drilling GFRP Composites Using Fuzzy Logic. In: *Materials and Manufacturing Processes* Bd. 25 (2010), S. 817–827 — ISBN 10426914
- [Lazi06] LAZIC, Z. R.: *Design of Experiments in Chemical Engineering: A Practical Guide*. Weinheim,, Germany : Wiley-VCH Verlag, 2006 — ISBN 3-527-31142-4
- [LCHC09] LU, H. S. ; CHANG, C. K. ; HWANG, N. C. ; CHUNG, C. T.: Grey Relational Analysis Coupled with Principal Component Analysis for Optimization Design of the Cutting Parameters in High-Speed End Milling. In: *Journal of Materials Processing Technology* Bd. 209 (2009), S. 3808–3817 — ISBN 0924-0136
- [Leon08] LEON, M. P.: *Full Wafer Map Response Surface Models for Combinatorial Chemical Vapor Deposition Reactor Operations*, University of Maryland, College Park, 2008

- [LeSc51] LEE, E. H. ; SCHAFFER, B. W.: The Theory of Plasticity Applied to a Problem of Machining. In: *Transactions of ASME, Journal of Applied Mechanics* Bd. 18 (1951), S. 405–413
- [LiBK03] LIN, J. T. ; BHATTACHARYYA, D. ; KECMAN, V.: Multiple Regression and Neural Networks Analyses in Composites Machining. In: *Composites Science and Technology* Bd. 63 (2003), S. 539–548
- [LiCh11] LIN, Y.C. ; CHEN, X. -M.: A Critical Review of Experimental Results and Constitutive Descriptions for Metals and Alloys in Hot Working. In: *Materials & Design* Bd. 32 (2011), S. 1733–1759 — ISBN 02613069
- [LiGS02] LI, K. ; GAO, X. L. ; SUTHERLAND, J. W.: Finite Element Simulation of the Orthogonal Metal Cutting Process for Qualitative understanding of the Effects of Crater Wear on the Chip formation Process. In: *Journal of Materials Processing Technology* Bd. 127 (2002), S. 309–324 — ISBN 1906487189
- [LiKh99] LIANG, R. ; KHAN, A. S.: A Critical Review of Experimental Results and Constitutive Models for BCC and FCC Metals over a Wide Range of Strain Rates and Temperatures. In: *International Journal of Plasticity* Bd. 15 (1999), S. 963–980 — ISBN 0749-6419
- [LiLi92] LIN, Z. C. ; LIN, S. Y.: A Coupled Finite Element Model of Thermo-Elastic-Plastic Large Deformation for Orthogonal Cutting. In: *Journal of Engineering Materials and Technology* Bd. 114 (1992), Nr. 2, S. 218–226
- [LiLo01] LIN, Z. C. ; LO, S. P.: 2-D Discontinuous Chip Cutting Model by using Strain Energy Density Theory and Elastic-Plastic Finite Element Method. In: *International Journal of Mechanical Sciences* Bd. 43 (2001), S. 381–398 — ISBN 8862737645
- [Lin04] LIN, C. L.: Use of the Taguchi Method and Grey Relational Analysis to Optimize Turning Operations with Multiple Performance Characteristics. In: *Materials and Manufacturing Processes* Bd. 19 (2004), S. 209–220
- [Loga01] LOGANATHAN, G. V.: A New Heuristic Optimization Algorithm: Harmony Search. In: *Simulation* Bd. 76 (2001), S. 60–68
- [LoJJ09] LORENTZON, J. ; JÄRVSTRÄT, N. ; JOSEFSON, B. L.: Modelling Chip Formation of Alloy 718. In: *Journal of Materials Processing Technology* Bd. 209 (2009), S. 4645–4653 — ISBN 0924-0136
- [LoMT07] LORONG, P. ; MICARI, F. ; TOURATIER, M.: Modelling of Cutting and Machining: 10 Years of ESAFORM Activity. In: *Advances in Material Forming SE - 13* : Springer Paris, 2007 — ISBN 9782287721427, S. 225–236
- [Lula86] LULA, R. A.: *Stainless Steels*. Metals Park .USA : American Society for Metals, 1986 — ISBN 9780871702081

- [LuSp95] LUONG, L. H. S. ; SPEDDING, T. A.: A Neural-Network System for Predicting Machining Behaviour. In: *Journal of Materials Processing Technology* Bd. 52. Hoboken, USA (1995), S. 585–591
- [MaAd05] MADHAVAN, V. ; ADIBI-SEDEH, A. H.: Understanding of Finite Element Analysis Results under the Framework of Oxley's Machining Model. In: *Machining Science and Technology* Bd. 9 (2005), S. 345–368
- [MaBh04] MANNA, A. ; BHATTACHARYYA, B.: Investigation for Optimal Parametric Combination for Achieving better Surface Finish during Turning of Al/SiC-MMC. In: *The International Journal of Advanced Manufacturing Technology* Bd. 23 (2004), S. 658–665 — ISBN 02683768
- [MaBM02] MAMALIS, A. G. ; BRANIS, A. S. ; MANOLAKOS, D. E.: Modelling of Precision Hard Cutting using Implicit Finite Element Methods. In: *Journal of Materials Processing Technology* Bd. 123 (2002), S. 464–475
- [Mack03] MACKERLE, J.: Finite Element Analysis and Simulation of Machining: An Addendum. In: *International Journal of Machine Tools and Manufacture* Bd. 43 (2003), S. 103–114 — ISBN 0890-6955
- [Mack98] MACKERLE, J.: Finite-Element Analysis and Simulation of Machining: A Bibliography (1976–1996). In: *Journal of Materials Processing Technology* Bd. 86 (1998), S. 17–44 — ISBN 0924-0136
- [Mall81] MALLOCK, A.: The Action of Cutting Tools. In: *Proc Roy Soc Lond* Bd. 33 (1881), S. 127–139
- [MaOk83] MAEKAWA, K. ; OKAMURA, H.: Deformational Behavior and Constitutive Equation of Concrete using the Elasto-Plastic and Fracture Model. In: *Journal of the Faculty of Engineering, University of Tokyo, Series B* Bd. 37 (1983), Nr. 2, S. 253–328
- [MaOr95] MARUSICH, T. D. ; ORTIZ, M.: Modelling and Simulation of High Speed Machining. In: *international journal for numerical methods in engineering* Bd. 38 (1995), S. 3675–3694
- [MaPa06] MAHAPATRA, S. S. ; PATNAIK, A.: Optimization of Wire Electrical Discharge Machining (WEDM) Process Parameters using Taguchi Method. In: *The International Journal of Advanced Manufacturing Technology* Bd. 34 (2006), S. 911–925 — ISBN 0268-3768
- [MaRi06] MABROUKI, T. ; RIGAL, J. F.: A Contribution to a Qualitative understanding of Thermo-Mechanical Effects during Chip formation in Hard Turning. In: *Journal of Materials Processing Technology* Bd. 176 (2006), S. 214–221
- [Mark13] MARKOPOULOS, A. P.: *Finite Element Method in Machining Processes*, SpringerBriefs in Applied Sciences and Technology. London, UK : Springer, 2013 — ISBN 9781447143291

- [MaSa08] MANNA, A. ; SALODKAR, S.: Optimization of Machining Conditions for Effective Turning of E0300 Alloy Steel. In: *Journal of Materials Processing Technology* Bd. 203 (2008), S. 147–153
- [MaSO96] MAEKAWA, K. ; SHIRAKASHI, T. ; OBIKAWA, T.: Recent Progress of Computer Aided Simulation of Chip Flow and Tool Damage in Metal Machining. In: *Proceedings of the Institution of Mechanical Engineers, Part B: Journal of Engineering Manufacture* Bd. 210 (1996), S. 233–242
- [Mccl68] MC-CLINTOCK, F. A.: A Criterion for Ductile Fracture by the Growth of Holes. In: *Journal of Applied Mechanics* Bd. 35 (1968), S. 363–371
- [Mcgu08] MCGUIRE, M. F.: *Stainless Steels for Design Engineers*. Materials Park, USA, USA : ASM International, 2008 — ISBN 9780871707178
- [Merc44] MERCHANT, M. E.: Basic Mechanics of the Metal-Cutting Process. In: *Journal of Applied Mech* Bd. 11 (1944), S. 168–175
- [MeWi14] MELLAL, M. ; WILLIAMS, E.: Cuckoo Optimization Algorithm for Unit Production Cost in Multi-Pass Turning Operations. In: *The International Journal of Advanced Manufacturing Technology*, Springer London (2014), S. 1–10
- [MHBM01] MAMALIS, A. G. ; HORVÁTH, M. ; BRANIS, A. S. ; MANOLAKOS, D. E.: Finite Element Simulation of Chip formation in Orthogonal Metal Cutting. In: *Journal of Materials Processing Technology* Bd. 110 (2001), S. 19–27
- [MiPe63] MICHAELS, S. F. ; PENGILLY, P. J.: Maximum yield for specific cost. In: *Applied Statistics* Bd. 12 (1963), S. 189–193
- [MoGA00] MOVAAHEDY, M. ; GADALA, M. S. ; ALTINTAS, Y.: Simulation of the Orthogonal Metal Cutting Process using An Arbitrary Lagrangian-Eulerian Finite-Element Method. In: *Journal of Materials Processing Technology* Bd. 103 (2000), S. 267–275 — ISBN 0924-0136
- [MOJH04] MAGHSOODLOO, S. ; OZDEMIR, G. ; JORDAN, V. ; HUANG, C.: Strengths and Limitations of Taguchi's Contributions to Quality, Manufacturing, and Process Engineering. In: *Journal of Manufacturing Systems* Bd. 23 (2004), Nr. 2, S. 73–126
- [MoNE12] MOHAMMED, W. M. ; NG, E. ; ELBESTAWI, M. A.: Modeling the Effect of Compacted Graphite Iron Microstructure on Cutting Forces and Tool Wear. In: *CIRP Journal of Manufacturing Science and Technology* Bd. 5 (2012), S. 87–101
- [Monr09] MONROE, E. M.: *Optimal Experimental Designs for Accelerated Life Tests with Censoring and Constraints*, Arizona State University, 2009
- [Mont09] MONTGOMERY, D. C.: *Design and Analysis of Experiments*. Cary, USA : John Wiley & Sons, Inc., 2009 — ISBN 9780470398821

- [MoPV12] MONTGOMERY, D. C. ; PECK, E. A. ; VINING, G. G.: *Introduction to Linear Regression Analysis, Wiley Series in Probability and Statistics*. Hoboken, USA : John Wiley & Sons, Inc., 2012 — ISBN 9780470542811
- [MoSw99] MOONEY, D. D. ; SWIFT, R. J.: *A Course in Mathematical Modeling, Classroom resource materials*. Washington D.C., USA : Mathematical Association of America, 1999 — ISBN 0-88385-712-X
- [MSTM14] MARKO, H. ; SIMON, K. ; TOMAZ, I. ; MATEJ, P. ; JOZE, B. ; MIRAN, B.: Turning Parameters Optimization using Particle Swarm Optimization. In: *Procedia Engineering*. Bd. 69, 2014, S. 670–677
- [MuRa06] MUKHERJEE, I. ; RAY, P. K.: A Review of Optimization Techniques in Metal Cutting Processes. In: *Computers and Industrial Engineering* Bd. 50 (2006), S. 15–34 — ISBN 9780470686652
- [MyMA09] MYERS, R. H. ; MONTGOMERY, D. C. ; ANDERSON-COOK, C. M.: *Response Surface Methodology: Process and Product Optimization Using Designed Experiments, Wiley Series in Probability and Statistics*. 3. Aufl. Rosewood Drive, USA, USA : John Wiley & Sons, Inc., 2009 — ISBN 9780470174463
- [NaDa09] NANDI, A. K. ; DAVIM, J. P.: A Study of Drilling Performances with Minimum Quantity of Lubricant using Fuzzy Logic Rules. In: *Mechatronics* Bd. 19 (2009), S. 218–232
- [Nahk13] NAHKALA, S.: Aligning Product Design Methods and Tools for Sustainability. In: NEE, A. Y. C. ; SONG, B. ; ONG, S.-K. (Hrsg.): *Re-engineering Manufacturing for Sustainability SE - 9* : Springer Singapore, 2013 — ISBN 9789814451475, S. 53–58
- [NaNE07] NASR, M. ; NG, E.-G. ; ELBESTAWI, M.: Effects of Workpiece Thermal Properties on Machining-induced Residual Stresses - Thermal Softening and Conductivity. In: *Proceedings of the Institution of Mechanical Engineers, Part B: Journal of Engineering Manufacture* Bd. 221 (2007), Nr. 9, S. 1387–1400
- [NGCH14] NIEŚŁONY, P. ; GRZESIK, W. ; CHUDY, R. ; HABRAT, W.: Meshing Strategies in FEM Simulation of the Machining Process. In: *Archives of Civil and Mechanical Engineering* (2014)
- [NoMa13] NOUARI, M. ; MAKICH, H.: Experimental Investigation on the Effect of the Material Microstructure on Tool Wear when Machining Hard Titanium Alloys. In: *International Journal of Refractory Metals and Hard Materials* Bd. 41 (2013), S. 259–269
- [NPDG14] NAYAK, S. K. ; PATRO, J. K. ; DEWANGAN, S. ; GANGOPADHYAY, S.: Multi-objective Optimization of Machining Parameters During Dry Turning of AISI 304 Austenitic Stainless Steel Using Grey Relational Analysis. In: *Procedia Materials Science* Bd. 6 (2014), Nr. 0, S. 701–708

- [ObUs96] OBIKAWA, T. ; USUI, E.: Computational Machining of Titanium Alloy - Finite Element Modeling and a few Results. In: *Journal of Manufacturing Science and Engineering, Transactions of the ASME* Bd. 118 (1996), S. 208 — ISBN 10871357
- [OdAB05] ODESHI, A. G. ; AL-AMEERI, S. ; BASSIM, M. N.: Effect of High Strain Rate on Plastic Deformation of a Low Alloy Steel Subjected to Ballistic Impact. In: *Journal of Materials Processing Technology* Bd. 162–163 (2005), Nr. 0, S. 385–391
- [Oful13] OFULLA, A. V. O.: *The Secrets of Hidden Knowledge: How Understanding Things in the Physical Realm Nurtures Life*. Bloomington, USA : Abbott Press, 2013 — ISBN 9781458209306
- [OHAS12] OLOVSJÖ, S. ; HAMMERSBERG, P. ; AVDOVIC, P. ; STÅHL, J. E. ; NYBORG, L.: Methodology for Evaluating Effects of Material Characteristics on Machinability - Theory and Statistics-based Modelling Applied on Alloy 718. In: *The International Journal of Advanced Manufacturing Technology* Bd. 59, Springer-Verlag (2012), Nr. 1-4, S. 55–66
- [OhOb05] OHBUCHI, Y. ; OBIKAWA, T.: Adiabatic Shear in Chip formation with Negative Rake Angle. In: *International Journal of Mechanical Sciences* Bd. 47 (2005), S. 1377–1392
- [ÖKFD07] ÖZEL, T. ; KARPAT, Y. ; FIGUEIRA, L. ; DAVIM, J. P.: Modelling of Surface Finish and Tool Flank Wear in Turning of AISI D2 Steel with Ceramic Wiper Inserts. In: *Journal of Materials Processing Technology* Bd. 189 (2007), S. 192–198
- [OkKa71] OKUSHIMA, K. ; KAKINO, Y.: The Residual Stress Produced by Metal Cutting. In: *Annals of the CIRP* Bd. 20 (1971), Nr. 1, S. 13–14
- [OINS99] OLOVSSON, LA. ; NILSSON, L. ; SIMONSSON, K.: ALE Formulation for the Solution of Two-Dimensional Metal Cutting Problems. In: *Computers and Structures* Bd. 72 (1999), S. 497–507 — ISBN 0045-7949
- [OpTz04] OPRICOVIC, SE. ; TZENG, G. H.: Compromise Solution by MCDM Methods: A Comparative Analysis of VIKOR and TOPSIS. In: *European Journal of Operational Research* Bd. 156 (2004), S. 445–455 — ISBN 0377-2217
- [OSSU97] OBIKAWA, T. ; SASAHARA, H. ; SHIRAKASHI, T. ; USUI, E.: Application of Computational Machining Method to Discontinuous Chip Formation. In: *Journal of Manufacturing Science and Engineering* Bd. 119 (1997), S. 667
- [Oxle64] OXLEY, P. L. B.: Introducing Strain-Rate Dependent Work Material Properties into the Analysis of Orthogonal Cutting. In: *CIRP Annals - Manufacturing Technology* Bd. 13 (1964), S. 127–138
- [Oxle89] OXLEY, P. L. B.: *The Mechanics of Machining: An Analytical Approach to Assessing Machinability, Ellis Horwood series in mechanical engineering*. New York, USA : Halsted Press, 1989 — ISBN 9780745800073

- [Oxle98] OXLEY, P. L. B.: Development and Application of a Predictive Machining Theory. In: *Machining Science and Technology* Bd. 2 (1998), S. 165–189
- [ÖZA100a] ÖZEL, T. ; ALTAN, T.: Process Simulation using Finite Element Method - Prediction of Cutting Forces, Tool Stresses and Temperatures in High-Speed Flat End Milling. In: *International Journal of Machine Tools and Manufacture* Bd. 40 (2000), S. 713–738
- [ÖZA100b] ÖZEL, T. ; ALTAN, T.: Determination of Workpiece Flow Stress and Friction at the Chip-Tool Contact for High-Speed Cutting. In: *International Journal of Machine Tools and Manufacture* Bd. 40 (2000), S. 133–152
- [ÖzCD09] ÖZEL, T. ; CORREIA, A. E. ; DAVIM, J. P.: Neural Network Process Modelling for Turning of Steel Parts using Conventional and Wiper Inserts. In: *International Journal of Materials and Product Technology* Bd. 35 (2009), S. 246
- [Özel06] ÖZEL, T.: The Influence of Friction Models on Finite Element Simulations of Machining. In: *International Journal of Machine Tools and Manufacture* Bd. 46 (2006), S. 518–530 — ISBN 0890-6955
- [Özel09] ÖZEL, T.: Single and Multi-Objective Optimization Methods. In: ÖZEL, T. ; DAVIM, J. P. (Hrsg.): *Intelligent Machining Modeling and Optimization of the Machining Processes and Systems*. London, UK : ISTE Ltd. & John Wiley & Sons, Inc., 2009 — ISBN 9781848211292, S. 245–267
- [ÖzKa05] ÖZEL, T. ; KARPAT, Y.: Predictive Modeling of Surface Roughness and Tool Wear in Hard Turning using Regression and Neural Networks. In: *International Journal of Machine Tools and Manufacture* Bd. 45 (2005), S. 467–479 — ISBN 0890-6955
- [ÖzKS08] ÖZEL, T. ; KARPAT, Y. ; SRIVASTAVA, A.: Hard Turning with Variable Micro-Geometry PcBN Tools. In: *CIRP Annals - Manufacturing Technology* Bd. 57 (2008), S. 73–76 — ISBN 0007-8506
- [ÖzNa02] ÖZEL, T. ; NADGIR, A.: Prediction of Flank Wear by using Back Propagation Neural Network Modeling when Cutting Hardened H-13 Steel with Chamfered and Honed CBN Tools. In: *International Journal of Machine Tools and Manufacture* Bd. 42 (2002), S. 287–297
- [ÖzSS10] ÖZEL, T. ; SIMA, M. ; SRIVASTAVA, A. K.: Finite Element Simulation of High Speed Machining Ti–6Al–4V Alloy using Modified Material Models. In: *Transactions of the NAMRI/SME* Bd. 38 (2010), S. 49–56
- [OzZe06] ÖZEL, T. ; ZEREN, E.: A Methodology to Determine Work Material Flow Stress and Tool-Chip Interfacial Friction Properties by Using Analysis of Machining. In: *Journal of Manufacturing Science and Engineering* Bd. 128 (2006), S. 119

- [ÖzZe07] ÖZEL, T. ; ZEREN, E.: Finite Element Modeling the Influence of Edge Roundness on the Stress and Temperature Fields induced by High-Speed Machining. In: *Int J Adv Manuf Tech* Bd. 35 (2007), S. 255–267 — ISBN 02683768
- [PAMC07] PUJANA, J. ; ARRAZOLA, P. J. ; M'SAOUBI, R. ; CHANDRASEKARAN, H.: Analysis of the Inverse Identification of Constitutive Equations Applied in Orthogonal Cutting Process. In: *International Journal of Machine Tools and Manufacture* Bd. 47 (2007), S. 2153–2161
- [Pant04] PANTALE, O.: 2D and 3D Numerical Models of Metal Cutting with Damage Effects. In: *Computer Methods in Applied Mechanics and Engineering* Bd. 193 (2004), S. 4383–4399
- [Phad89] PHADKE, M. S.: *Quality Engineering Using Robust Design*. Englewood Cliffs, USA : Prentice-Hall, 1989 — ISBN 0-13-745167-9
- [PhCM14] PHILIP, S. D. ; CHANDRAMOHAN, P. ; MOHANRAJ, M.: Optimization of Surface Roughness, Cutting Force and Tool Wear of Nitrogen Alloyed Duplex Stainless Steel in A Dry Turning Process using Taguchi Method. In: *Measurement* Bd. 49 (2014), S. 205–215
- [PHLT08] PAUCKSCH, E. ; HOLSTEN, S. ; LINß, M. ; TIKAL, F.: *Zerspantechnik: Prozesse, Werkzeuge, Technologien*. Wiesbaden, Germany : Vieweg Teubner Verlag, 2008 — ISBN 9783834802798
- [PiAS05] PIENDL, S. ; AURICH, J. C. ; STEINICKE, M.: 3D Finite-Element Simulation of Chip Formation in Turning. In: *Proceedings of the 8th CIRP international workshop on modelling of machining operations, Chemnitz, Germany, 2005*, S. 225–234
- [PUDJ14] PU, Z. ; UMBRELLO, D. ; DILLON, O. W. ; JAWAHIR, I. S.: Finite Element Simulation of Residual Stresses in Cryogenic Machining of AZ31B Mg Alloy. In: *Procedia CIRP*. Bd. 13, 2014, S. 282–287
- [QuDa09] QUIZA, R. ; DAVIM, J. P.: Computational Modelling of Machining Systems. In: ÖZEL, T. ; DAVIM, J. P. (Hrsg.): *Intelligent Machining Modeling and Optimization of the Machining Processes and Systems*. London, UK : ISTE Ltd. & John Wiley & Sons, Inc., 2009 — ISBN 978-1-84821-129-2, S. 174–209
- [QuDa11] QUIZA, R. ; DAVIM, J. P.: Computational Methods and Optimization. In: DAVIM, J. P. (Hrsg.): *Machining of hard materials*. London, UK : Springer-Verlag London Limited, 2011 — ISBN 9781849964494, S. 191–208
- [RaDa08] RAO, R. V. ; DAVIM, J. P.: A Decision-Making Framework Model for Material Selection using A Combined Multiple attribute Decision-Making Method. In: *The International Journal of Advanced Manufacturing Technology* Bd. 35, Springer-Verlag (2008), Nr. 7-8, S. 751–760

- [RaDo89] RANGWALA, S. S. ; DORNFELD, D. A.: Learning and Optimization of Machining Operations using Computing Abilities of Neural Networks. In: *IEEE Transactions on Systems, Man and Cybernetics* Bd. 19 (1989), S. 299–314
- [RaGa01] RAO, R.V. ; GANDHI, O P: Digraph and Matrix Method for the Selection, Identification and Comparison of Metal-Cutting Fluids. In: *Proceedings of the Institution of Mechanical Engineers* Bd. 215 (2001), Nr. 1, S. 25–33
- [RaJT93] RAKOTOMALALA, R. ; JOYOT, P. ; TOURATIER, M.: Arbitrary Lagrangian-Eulerian Thermomechanical Finite-Element Model of Material Cutting. In: *Communications in numerical methods in engineering* Bd. 9 (1993), Nr. January, S. 975–987
- [RaKu10] RAJU, K. S. ; KUMAR, D. N.: *Multicriterion Analysis in Engineering and Management*. New Delhi, India : Prentice-Hall Of India Pvt. Limited, 2010 — ISBN 9788120339767
- [RaLB05] RATCHEV, S. ; LIU, S. ; BECKER, A. A.: Error Compensation Strategy in Milling Flexible Thin-Wall Parts. In: *Journal of Materials Processing Technology*. Bd. 162–163, 2005 — ISBN 0924-0136, S. 673–681
- [Rao06a] RAO, R. V.: A Material Selection Model using Graph Theory and Matrix Approach. In: *Materials Science and Engineering A* Bd. 431 (2006), S. 248–255
- [Rao06b] RAO, R.V.: A Decision-Making Framework Model for Evaluating Flexible Manufacturing Systems using Digraph and Matrix Methods. In: *The International Journal of Advanced Manufacturing Technology* Bd. 30, Springer-Verlag (2006), Nr. 11-12, S. 1101–1110
- [Rao11a] RAO, R.V. V.: Advanced Modeling and Optimization of Manufacturing Processes. In: *Springer Series in Advanced Manufacturing*. London, UK, UK : Springer, 2011 — ISBN 9780857290144, S. 1–54
- [Rao11b] RAO, S. S. ; RAO, S. S. (Hrsg.): *The Finite Element Method in Engineering*. Fifth Edit. Aufl. Boston, USA : Butterworth-Heinemann, 2011 — ISBN 9781856176613
- [Rao13] RAO, R. V.: *Decision Making in Manufacturing Environment using Graph Theory and Fuzzy Multiple attribute Decision Making Methods*. London, UK : Springer London, 2013 — ISBN 9781447143758
- [RaRA09] RAMESH, R. ; RAVI KUMAR, K. S. ; ANIL, G.: Automated Intelligent Manufacturing System for Surface Finish Control in CNC Milling using Support Vector Machines. In: *The International Journal of Advanced Manufacturing Technology* Bd. 42, Springer-Verlag (2009), Nr. 11-12, S. 1103–1117
- [Rasc12] RASCH, M.: *100 Jahre nichtrostender Stahl: Historisches und Aktuelles*. 1. Aufl. Aufl. Essen, Germany : Klartext Verlag, 2012 — ISBN 9783837500950

- [RaSe11] RANGANATHAN, S. ; SENTHILVELAN, T.: Multi-Response Optimization of Machining Parameters in Hot Turning using Grey Analysis. In: *International Journal of Advanced Manufacturing Technology* Bd. 56 (2011), S. 455–462 — ISBN 0017001131985
- [Reul00] REULEAUX, F.: Über den Taylor whiteschen Werkzeugsstahl. In: *Verein zur Beförderung des Gewerbefleißes in Preussen* Bd. 79 (1900), S. 179
- [RFJM02] REDHE, M. ; FORSBERG, J. ; JANSSON, T. ; MARKLUND, P. O. ; NILSSON, L.: Using the Response Surface Methodology and the D-Optimality Criterion in Crashworthiness Related Problems. In: *Structural and Multidisciplinary Optimization* Bd. 24, Springer-Verlag (2002), Nr. 3, S. 185–194
- [RhOh06] RHIM, S. H. ; OH, S. I. I.: Prediction of Serrated Chip formation in Metal Cutting Process with New Flow Stress Model for AISI 1045 Steel. In: *Journal of Materials Processing Technology* Bd. 171 (2006), S. 417–422 — ISBN 0924-0136
- [RiBr93] RIEDMILLER, M. ; BRAUN, H.: A Direct Adaptive Method for Faster Backpropagation Learning: The RPROP Algorithm. In: *Proceedings of the IEEE International Conference on Neural Networks (ICNN)*. San Francisco, 1993, S. 586–591
- [RLHB06] RATCHEV, S. ; LIU, S. ; HUANG, W. ; BECKER, A. A.: . An Advanced FEA based Force induced Error Compensation Strategy in Milling. In: *International Journal of Machine Tools and Manufacture* Bd. 46 (2006), Nr. 5, S. 542–551
- [RoAK00] ROWLANDS, H. ; ANTONY, J. ; KNOWLES, G.: An Application of Experimental Design for Process Optimisation. In: *The TQM Magazine* Bd. 12, Emerald (2000), Nr. 2, S. 78–84
- [RoBC03] ROSOCHOWSKA, M. ; BALENDRA, R. ; CHODNIKIEWICZ, K.: Measurements of Thermal Contact Conductance. In: *Journal of Materials Processing Technology* Bd. 135 (2003), S. 204–210
- [Ross95] ROSS, P. J.: *Taguchi Techniques for Quality Engineering: Loss Function, Orthogonal Experiments, Parameter and Tolerance Design*. 2. Aufl. New York, USA : McGraw Hill Professional, 1995 — ISBN 0-07-100884-5
- [Ruth01] RUTHERFORD, A.: *ANOVA and ANCOVA: A GLM Approach*. Gateshead, UK : SAGE Publications Ltd, 2001 — ISBN 0-7619-5160-1
- [SaAG05] SARTKULVANICH, P. ; ALTAN, T. ; GÖCMEN, A.: Effects of Flow Stress and Friction Models in Finite Element Simulation of Orthogonal Cutting—A Sensitivity Analysis. In: *Machining Science and Technology* Bd. 9 (2005), S. 1–26
- [ScEH05] SCHEFFER, C. ; ENGELBRECHT, H. ; HEYNS, P. S.: A Comparative Evaluation of Neural Networks and Hidden Markov Models for Monitoring Turning Tool Wear. In: *Neural Computing & Applications* Bd. 14, Springer-Verlag (2005), Nr. 4, S. 325–336

- [SeCh06] SEAH, M. ; CHIFFRE, L.: Surface and Interface Characterization. In: CZICHOS, H. ; SAITO, T. ; SMITH, L. (Hrsg.): *Springer Handbook of Materials Measurement Methods SE - 6*. Berlin, Germany : Springer, 2006 — ISBN 9783540207856, S. 229–280
- [SeRS06] SENTHILKUMAR, A. ; RAJA, D. A. ; SORNAKUMAR, T.: The Effect of Tool Wear on Tool Life of Alumina-Based Ceramic Cutting Tools while Machining Hardened Martensitic Stainless Steel. In: *Journal of Materials Processing Technology* Bd. 173 (2006), S. 151–156
- [SGLM03] SAUNDERS, N. ; GUO, U. K. Z. ; LI, X. ; MIODOWNIK, A. P. ; SCHILLÉ, J. -PH.: Using JmatPro to Model Materials Properties and Behavior. In: *Jom* Bd. 55 (2003), Nr. 12, S. 60–65
- [Shaw89] SHAW, M. C.: *Metal Cutting Principles*. 3. Aufl. Oxford, UK, UK : Oxford Clarendon Press, 1989 — ISBN 9780195142068
- [ShBä11] SHROT, AV. ; BÄKER, M.: How to Identify Johnson-Cook Parameters from Machining Simulations. In: *AIP Conference Proceedings*. Bd. 1353, 2011 — ISBN 9780735409118, S. 29–34
- [ShBä12] SHROT, A. ; BÄKER, M.: Determination of Johnson–Cook Parameters from Machining Simulations. In: *Computational Materials Science* Bd. 52 (2012), Nr. 1, S. 298–304
- [Sher94] SHERIDAN, T. B.: Human Supervisory Control. In: SALVENDY, G. ; KARWOWSKI, W. (Hrsg.): *Design of Work and Development of Personnel in Advanced Manufacturing, Wiley-Interscience publication*. New York, USA : Wiley, 1994 — ISBN 0-471-59447-4, S. 79–103
- [ShGi06] SHI, D. ; GINDY, N. N.: Tool Wear Predictive Model Based on Least Squares Support Vector Machines. In: *Mechanical Systems and Signal Processing* Bd. 21 (2006), S. 1799–1814
- [Shih96] SHIH, A. J.: Finite Element Analysis of the Rake Angle Effects in Orthogonal Metal Cutting. In: *International Journal of Mechanical Sciences* Bd. 38 (1996), S. 1–17 — ISBN 0791810291
- [ShKA01] SHATLA, M. ; KERK, C. ; ALTAN, T.: Process Modeling in Machining. Part II: Validation and Applications of the Determined Flow Stress Data. In: *International Journal of Machine Tools and Manufacture* Bd. 41 (2001), S. 1659–1680 — ISBN 0890-6955
- [SHMS02] SHIVPURI, R. ; HUA, J. ; MITTAL, P. ; SRIVASTAVA, A. K. ; LAHOTI, G. D.: Microstructure-Mechanics Interactions in Modeling Chip Segmentation during Titanium Machining. In: *CIRP Annals - Manufacturing Technology* Bd. 51 (2002), S. 71–74 — ISBN 00078506

- [Shor11] SHORE, H.: Response Modeling Methodology: Empirical Modeling for Engineering and Science. In: *Wiley Interdisciplinary Reviews: Computational Statistics* Bd. 3. Rosewood Drive, USA, World Scientific Publishing Co. (2011), S. 357–372
- [ShVi96] SHIN, Y. C. ; VISHNUPAD, P.: Neuro-Fuzzy Control of Complex Manufacturing Processes. In: *International Journal of Production Research* Bd. 34, Taylor & Francis (1996), Nr. 12, S. 3291–3309
- [ShWe49] SHANNON, C. E. ; WEAVER, W.: *The Mathematical Theory of Communication*. Bd. 27, 1949 — ISBN 0252725484
- [SiDM11] SINGH, AN. ; DATTA, S. ; MAHAPATRA, S. S.: Application of TOPSIS in the Taguchi Method for Optimal Machining Parameter Selection. In: *Journal for Manufacturing Science & Production* Bd. 11 (2011), Nr. 1-3, S. 49–60
- [SiKu06] SINGH, H. ; KUMAR, P.: Optimizing Multi-Machining Characteristics Through Taguchi's Approach and Utility Concept. In: *Journal of Manufacturing Technology Management* Bd. 17 (2006), Nr. 2, S. 255–274
- [SiMS11] SIVAPIRAKASAM, S. P. ; MATHEW, J. ; SURIANARAYANAN, M.: Multi-attribute Decision Making for Green Electrical Discharge Machining. In: *Expert Systems with Applications* Bd. 38 (2011), S. 8370–8374
- [SiNE07] SIMONEAU, A. ; NG, E. ; ELBESTAWI, M. A.: Modeling the Effects of Microstructure in Metal Cutting. In: *International Journal of Machine Tools and Manufacture* Bd. 47 (2007), S. 368–375 — ISBN 0890-6955
- [Sing11] SINGH, S.: *Handbook of Mechanical Engineering*. New Delhi, India : S. Chand & Company Ltd., 2011 — ISBN 9788121935876
- [SiÖz10] SIMA, M. ; ÖZEL, T.: Modified Material Constitutive Models for Serrated Chip formation Simulations and Experimental Validation in Machining of Titanium Alloy Ti-6Al-4V. In: *International Journal of Machine Tools and Manufacture* Bd. 50 (2010), S. 943–960 — ISBN 0890-6955
- [SLCM01] SZYMURA-OLEKSIK, J. ; LÓSARCZYK, A. ; CIOS, A. ; MYCEK, B. ; PASZKIEWICZ, Z. ; SZKLARCZYK, S. ; STANKIEWICZ, D.: Process Modeling in Machining. Part I: Determination of Flow Stress Data. In: *International Journal of Machine Tools and Manufacture* Bd. 41 (2001), S. 1511–1534 — ISBN 0890-6955
- [SMBS10] SAMANTARAY, D. ; MANDAL, S. ; BHADURI, A. K. ; SIVAPRASAD, P. V.: An Overview on Constitutive Modelling to Predict Elevated Temperature Flow Behaviour of Fast Reactor Structural Materials. In: *Transactions of the Indian Institute of Metals* Bd. 63, Springer-Verlag (2010), Nr. 6, S. 823–831
- [SoAD04] SOO, S. L. ; ASPINWALL, D. K. ; DEWES, R. C.: 3D FE Modelling of the Cutting of Inconel 718. In: *Journal of Materials Processing Technology*. Bd. 150, 2004, S. 116–123

- [SPBA14] SAMANTARAY, D. ; PATEL, A. ; BORAH, U. ; ALBERT, S. K. ; BHADURI, A. K.: Constitutive Flow Behavior of IFAC-1 Austenitic Stainless Steel Depicting Strain Saturation over a Wide Range of Strain Rates and Temperatures. In: *Materials and Design* Bd. 56 (2014), S. 565–571
- [TaLa72] TARAMAN, K. S. ; LAMBERT, B. K.: Application of Response Surface Methodology to the Selection of Machining Variables. In: *A I I E Transactions* Bd. 4 (1972), Nr. 2, S. 111–115
- [Tara74] TARAMAN, K. S.: Multi Machining Output—Multi independent Variable Turning Research by Response Surface Methodology. In: *International Journal of Production Research* Bd. 12 (1974), Nr. 2, S. 233–245
- [TaSD74] TAY, A. O. ; STEVENSON, M. G. ; DAVIS, G. V.: Using the Finite Element Method to Determine Temperature Distributions in Orthogonal Machining. In: *Proceedings of the Institution of Mechanical Engineers* Bd. 188 (1974), S. 627–268
- [Tayl07] TAYLOR, F. W.: *On the Art of Cutting Metals*. New York, USA : American society of mechanical engineers, 1907
- [ThSe13] THIRUMALAI, R. ; SENTHILKUMAAR, J. S.: Multi-Criteria Decision Making in the Selection of Machining Parameters for Inconel 718. In: *Journal of Mechanical Science and Technology* Bd. 27, Korean Society of Mechanical Engineers (2013), Nr. 4, S. 1109–1116
- [Tosu06] TOSUN, N.: Determination of Optimum Parameters for Multi-Performance Characteristics in Drilling by using Grey Relational Analysis. In: *International Journal of Advanced Manufacturing Technology* Bd. 28 (2006), S. 450–455
- [Tres73] TRESKA, H.: Mémoires sur le Rabotage des Métaux. In: *Bulletin de la Société d' Encouragement pour l' Industrie Nationale* (1873), S. 585–607
- [TrWr00] TRENT, E. M. ; WRIGHT, P. K. ; BUTTERWORTH-HEINEMANN (Hrsg.): *Metal Cutting*. 4. Aufl. Boston, USA, 2000 — ISBN 9780750670692
- [TsRe09] TSCHÄTSCH, H. ; REICHEL, A.: *Applied Machining Technology*. 8. Aufl. Heidelberg, Germany, Germany : Springer, 2009 — ISBN 9783642010071
- [TSTY93] TESHIMA, T. ; SHIBASAKA, T. ; TAKUMA, M. ; YAMAMOTO, A. ; IWATA, K.: Estimation of Cutting Tool Life by Processing Tool Image Data with Neural Network. In: *CIRP Annals - Manufacturing Technology* Bd. 42 (1993), S. 59–62 — ISBN 0007-8506
- [TSVO76] TAY, A. O. ; STEVENSON, M. G. ; DE VAHL DAVIS, G. ; OXLEY, P. L. B.: A Numerical Method for Calculating Temperature Distributions in Machining, from Force and Shear Angle Measurements. In: *International Journal of Machine Tool Design and Research* Bd. 16 (1976), S. 335–349 — ISBN 00207357

- [UhSZ07] UHLMANN, E. ; VON DER SCHULENBURG, M. G. ; ZETTIER, R.: Finite Element Modeling and Cutting Simulation of Inconel 718. In: *CIRP Annals - Manufacturing Technology* Bd. 56 (2007), S. 61–64
- [Umbr08] UMBRELLO, D.: Finite Element Simulation of Conventional and High Speed Machining of Ti6Al4V Alloy. In: *Journal of Materials Processing Technology* Bd. 196 (2008), S. 79–87 — ISBN 0924-0136
- [UmMO07] UMBRELLO, D. ; M'SAOUBI, R. ; OUTEIRO, J. C.: The Influence of Johnson-Cook Material Constants on Finite Element Simulation of Machining of AISI 316L Steel. In: *International Journal of Machine Tools and Manufacture* Bd. 47 (2007), S. 462–470 — ISBN 0890-6955
- [UmSm59] UMLAND, A. W. ; SMITH, W. N.: The Use of LaGrange Multipliers with Response Surfaces. In: *Technometrics* Bd. 1 (1959), Nr. 3, S. 289–292
- [Unng87] UN-NGO: *Our Common Future: World Commission on Environment and Development*. Oxford, UK, 1987
- [UsSh82a] USUI, E. ; SHIRAKASHI, T.: Mechanics of Metal Cutting—from “Description” to “Predictive” Theory. In: *On the art of cutting metals—75 years later*. Phoenix, USA : Production Engineering Division (PED), ASME, 1982
- [UsSh82b] USUI, E. ; SHIRAKASHI, T.: Mechanics of machining - from „Descriptive“ to „Predictive“ Theory. In: *American Society of Mechanical Engineers, Production Engineering Division (Publication) PED* Bd. 7 (1982), S. 13–35
- [Usui88] USUI, E.: Progress of „Predictive“ Theories in Metal Cutting. In: *JSME international journal. Ser. 3*, Bd. 31 (1988), Nr. 2, S. 363
- [VeGa02] VENKATA, R. R. ; GANDHI, O. P.: Digraph and Matrix Methods for the Machinability Evaluation of Work Materials. In: *International Journal of Machine Tools and Manufacture* Bd. 42 (2002), S. 321–330
- [VeMM14] VENKATA, R. K. ; MURTHY, B. S. N. ; MOHAN, R. N.: Prediction of Cutting Tool Wear, Surface Roughness and Vibration of Work Piece in Boring of AISI 316 Steel with Artificial Neural Network. In: *Measurement: Journal of the International Measurement Confederation* Bd. 51 (2014), S. 63–70
- [VePa10] VENKATA, R. R. ; PAWAR, P. J.: Parameter Optimization of a Multi-pass Milling Process Using Non-traditional Optimization Algorithms. In: *Applied Soft Computing Journal* Bd. 10 (2010), S. 445–456 — ISBN 1568-4946
- [VoAb05] VOYIADJIS, G. Z. ; ABED, F. H.: Microstructural based Models for BCC and FCC Metals with Temperature and Strain Rate Dependency. In: *Mechanics of Materials*. Bd. 37, 2005 — ISBN 0167-6636, S. 355–378
- [VOKL07] VAZ JR., M. ; OWEN, D. R. J. ; KALHORI, V. ; LUNDBLAD, M. ; LINDGREN, L.-E. E. ; VAZ, M.: Modelling and Simulation of Machining Processes. In: *Archives of*

- Computational Methods in Engineering* Bd. 14, Kluwer Academic Publishers (2007), Nr. 2, S. 173–204
- [VPAS03] VIJAYAKUMAR, K. ; PRABHAHARAN, G. ; ASOKAN, P. ; SARAVANAN, R.: Optimization of Multi-Pass Turning Operations using Ant Colony System. In: *International Journal of Machine Tools and Manufacture* Bd. 43 (2003), S. 1633–1639
- [WaCh13] WANG, Q. J. ; CHUNG, Y.-W.: Encyclopedia of Tribology. In: . Bd. 193. New York, USA : Springer Science & Business Media, 2013 — ISBN 9780387928968
- [WaMK02] WANG, L. ; MEHRABI, M. G. ; KANNATEY, A. E.: Hidden Markov Model-based Tool Wear Monitoring in Turning. In: *Journal of Manufacturing Science and Engineering* Bd. 124 (2002), S. 651
- [WaOh02] WARNECKE, G. ; OH, J. -D.: A new Thermo-viscoplastic Material Model for Finite-Element-Analysis of the Chip Formation Process. In: *CIRP Annals - Manufacturing Technology* Bd. 51 (2002), S. 79–82
- [WaSK06] WALIA, R. S. ; SHAN, H. S. ; KUMAR, P.: Multi-Response Optimization of CFAAFM Process Through Taguchi Method and Utility Concept. In: *Materials and Manufacturing Processes* Bd. 21 (2006), Nr. 8, S. 907–914
- [WaWa14] WANG, Z. X. ; WANG, Y. Y.: Evaluation of the Provincial Competitiveness of the Chinese High-Tech industry using An Improved TOPSIS Method. In: *Expert Systems with Applications* Bd. 41 (2014), S. 2824–2831
- [WaWR04] WANG, Z. G. ; WONG, Y. S. ; RAHMAN, M.: Optimisation of Multi-Pass Milling using Genetic Algorithm and Genetic Simulated Annealing. In: *International Journal of Advanced Manufacturing Technology* Bd. 24 (2004), S. 727–732
- [WKFL13] WANG, X. ; KANG, M. ; FU, X. ; LI, C.: Predictive Modeling of Surface Roughness in Lenses Precision Turning Using Regression and Support Vector Machines. In: *The International Journal of Advanced Manufacturing Technology*, Springer London (2013), S. 1–9
- [WuDL96] WU, J. -S. ; DILLON JR., O. W. ; LU, W. -Y.: Thermo-Viscoplastic Modeling of Machining Process using a Mixed Finite Element Method. In: *Journal of Manufacturing Science and Engineering, Transactions of the ASME* Bd. 118 (1996), S. 470
- [WuJF03] WU, W. T. ; JINN, J. T. ; FISCHER, C. E.: Handbook of Workability and Process Design. In: DIETER, G. E. ; KUHN, H. A. ; SEMIATIN, S. L. (Hrsg.): . Materials Park, USA, USA : ASM International, 2003 — ISBN 9780871707789, S. 220–231
- [XLZG05] XUE, Q. ; LIAO, X. Z. ; ZHU, Y. T. ; GRAY, G. T.: Formation Mechanisms of Nanostructures in Stainless Steel during High-Strain-Rate Severe Plastic Deformation. In: *Materials Science and Engineering* Bd. 410–411 (2005), S. 252–256 — ISBN 0921-5093

- [YaDe09] YANG, X. -S. ; DEB, S.: Cuckoo Search via Lévy Flights. In: *2009 World Congress on Nature and Biologically Inspired Computing, NABIC 2009 - Proceedings*. Coimbatore, India, 2009 — ISBN 9781424456123, S. 210–214
- [YaHo12] YANG, X. -S. ; HOSSEIN, G. A.: Bat Algorithm: A Novel Approach for Global Engineering Optimization. In: *Engineering Computations* Bd. 29 (2012), Nr. 5, S. 464–483
- [YaKa13] YANG, X. -S. ; KARAMANOGLU, M.: Swarm Intelligence and Bio-Inspired Computation: An Overview. In: *Swarm Intelligence and Bio-Inspired Computation*, 2013 — ISBN 978-0-12405-163-8, S. 3–23
- [YaLi02] YANG, X. ; LIU, C. R.: A New Stress-based Model of Friction Behavior in Machining and its Significant Impact on Residual Stresses Computed by Finite Element Method. In: *International Journal of Mechanical Sciences* Bd. 44 (2002), S. 703–723
- [YaLi13] YAN, J. ; LI, L.: Multi-Objective Optimization of Milling Parameters – the Trade-offs Between Energy, Production Rate and Cutting Quality. In: *Journal of Cleaner Production* Bd. 52 (2013), S. 462–471
- [Yang09] YANG, X. -S.: Firefly Algorithms for Multimodal Optimization. In: *Lecture Notes in Computer Science (including subseries Lecture Notes in Artificial Intelligence and Lecture Notes in Bioinformatics)*. Bd. 5792 LNCS. Heidelberg, Germany, 2009 — ISBN 3642049435, S. 169–178
- [Yang10a] YANG, X. -S.: *Engineering Optimization: An Introduction with Metaheuristic Applications*. Hoboken, USA : John Wiley & Sons, Inc., 2010 — ISBN 9780470582466
- [Yang10b] YANG, X. -S.: A New Metaheuristic Bat-inspired Algorithm. In: *Studies in Computational Intelligence*. Bd. 284, 2010 — ISBN 9783642125379, S. 65–74
- [Yang11] YANG, X. -S.: Bat Algorithm for Multi-Objective Optimisation. In: *International Journal of Bio-Inspired Computation* Bd. 3 (2011), S. 267–274
- [Yang14a] YANG, X. -S.: *Nature-Inspired Optimization Algorithms*. London, UK : Elsevier Science, 2014 — ISBN 9780124167438
- [Yang14b] YANG, X. -S.: Cuckoo Search and Firefly Algorithm: Overview and Analysis. In: *Studies in Computational Intelligence* Bd. 516 (2014), S. 1–26 — ISBN 9783319021409
- [YaTa98] YANG, W. H. ; TARNG, Y. S.: Design Optimization of Cutting Parameters for Turning Operations based on the Taguchi Method. In: *Journal of Materials Processing Technology* Bd. 84 (1998), S. 122–129

- [Yild13a] YILDIZ, A. R.: Optimization of Cutting Parameters in Multi-Pass Turning using Artificial Bee Colony-based Approach. In: *Information Sciences*. Bd. 220, 2013, S. 399–407
- [Yild13b] YILDIZ, A. R.: Cuckoo Search Algorithm for the Selection of Optimal Machining Parameters in Milling Operations. In: *The International Journal of Advanced Manufacturing Technology* Bd. 64, Springer-Verlag (2013), Nr. 1-4, S. 55–61
- [Yin13] YIN, M. -S.: Fifteen Years of Grey System Theory Research: A Historical Review and Bibliometric Analysis. In: *Expert Systems with Applications* Bd. 40 (2013), S. 2767–2775 — ISBN 0957-4174
- [YoBT94] YOUSSEF, Y. A. ; BEAUCHAMP, Y. ; THOMAS, M.: Comparison of a Full Factorial Experiment to Fractional and Taguchi Designs in A Lathe Dry Turning Operation. In: *Computers & Industrial Engineering* Bd. 27 (1994), Nr. 1–4, S. 59–62
- [YoEA11] YOUSSEF, H. A. ; EL-HOFY, H. A. ; AHMED, M. H.: *Manufacturing Technology: Materials, Processes, and Equipment*. Boca Raton, USA, USA : Taylor & Francis, 2011 — ISBN 9781439810859
- [Yu73] YU, P. L.: A Class of Solutions for Group Decision Problems. In: *Management Science* Bd. 19 (1973), S. 936–946
- [YuZH12] YUSUP, N. ; ZAIN, A. M. ; HASHIM, S. Z. M.: Overview of PSO for Optimizing Process Parameters of Machining. In: *Procedia Engineering*. Bd. 29, 2012, S. 914–923
- [Zade65] ZADEH, L. A.: Fuzzy Sets. In: *Information and Control* Bd. 8 (1965), S. 338–353 — ISBN 0019-9958
- [ZaHS10] ZAIN, A. M. ; HARON, H. ; SHARIF, S.: Simulated Annealing to Estimate the Optimal Cutting Conditions for Minimizing Surface Roughness in End Milling Ti-6Al-4V. In: *Machining Science and Technology* Bd. 14 (2010), Nr. 1, S. 43–62
- [ZeAr87] ZERILLI, F. J. ; ARMSTRONG, R. W.: Dislocation-Mechanics-based Constitutive Relations for Material Dynamics Calculations. In: *Journal of Applied Physics* Bd. 61 (1987), S. 1816–1825 — ISBN 0021-8979
- [ZeLe98] ZELENY, M.: Multiple Criteria Decision Making: Eight Concepts of Optimality. In: *Human Systems Management* Bd. 17 (1998), S. 97–107 — ISBN 9780070727953
- [Zeri04] ZERILLI, F. J.: Dislocation mechanics-based constitutive equations. In: *Metallurgical and Materials Transactions A* Bd. 35 (2004), S. 2547–2555 — ISBN 1073-5623
- [ZhCP07] ZHENG, C. ; CESAR DE SA, J. M. A. ; PIRES, F.: A Comparison of Models for Ductile Fracture Prediction in forging Processes. In: *Computer Methods in Materials Science* Bd. 7 (2007), Nr. 4, S. 389–396

- [ZhSS14] ZHANG, X. P. ; SHIVPURI, R. ; SRIVASTAVA, A. K.: Role of Phase Transformation in Chip Segmentation during High Speed Machining of Dual Phase Titanium Alloys. In: *Journal of Materials Processing Technology* Bd. 214 (2014), S. 3048–3066
- [ZhWH09] ZHU, K. ; WONG, Y. S. ; HONG, G. S.: Multi-Category Micro-Milling Tool Wear Monitoring with Continuous Hidden Markov Models. In: *Mechanical Systems and Signal Processing* Bd. 23 (2009), S. 547–560
- [ZhXi14] ZHANG, L. ; XIE, L.: *Modeling and Computation in Engineering III*. London, UK : Taylor & Francis, 2014 — ISBN 9781138026803
- [ZiTZ13] ZIENKIEWICZ, O. C. C. ; TAYLOR, R. L. L. ; ZHU, J. Z. Z.: *The Finite Element Method: Its Basis and Fundamentals*. 6. Aufl. Oxford, UK : Elsevier Science, 2013 — ISBN 0-7506-6320-0
- [ZMYP11] ZHANG, Q. ; MAHFOUF, M. ; YATES, J. R. ; PINNA, C. ; PANOUTSOS, G. ; BOUMAIZA, S. ; GREENE, R. J. ; DE LEON, L.: Modeling and Optimal Design of Machining-Induced Residual Stresses in Aluminium Alloys Using a Fast Hierarchical Multiobjective Optimization Algorithm. In: *Materials and Manufacturing Processes* Bd. 26 (2011), S. 508–520 — ISBN 1042-6914
- [Zore63] ZOREV, N.: Inter-Relationship Between Shear Processes Occurring along Tool Face and on Shear Plane in Metal Cutting. In: *ASME International Research in Production Engineering* (1963), S. 42–49
- [ZRSD09] ZEMZEMI, F. ; RECH, J. ; BEN SALEM, W. ; DOGUI, A. ; KAPSA, P.: Identification of a Friction Model at Tool/Chip/Workpiece Interfaces in Dry Machining of AISI4142 Treated Steels. In: *Journal of Materials Processing Technology* Bd. 209 (2009), S. 3978–3990
- [Zvor96] ZVORYKIN, K. A.: On the Force and Energy Necessary to Separate the Chip from the Workpiece (in Russian). In: *Vetnik Promyslennostie* (1896), S. 123

12 Appendix A: Supplementary tabulations

Pareto points	EN 1.4462				EN 1.4410			
	Dry		Wet		Dry		Wet	
	v_c [m/min]	f_r [mm/rev]	v_c [m/min]	f_r [mm/rev]	v_c [m/min]	f_r [mm/rev]	v_c [m/min]	f_r [mm/rev]
1	100.019	0.200	174.046	0.150	179.984	0.152	100.004	0.174
2	173.193	0.151	143.854	0.150	100.002	0.201	107.497	0.156
3	167.437	0.151	121.146	0.156	138.808	0.157	177.114	0.152
4	169.429	0.157	174.046	0.150	100.002	0.201	132.746	0.158
5	134.816	0.156	102.310	0.161	102.522	0.180	166.641	0.153
6	103.408	0.195	164.364	0.150	155.850	0.154	114.347	0.158
7	100.019	0.200	126.393	0.153	119.773	0.174	122.355	0.153
8	106.685	0.182	154.713	0.150	126.411	0.160	158.811	0.152
9	173.193	0.151	100.245	0.176	100.619	0.190	121.981	0.162
10	120.206	0.152	100.498	0.173	100.837	0.181	150.066	0.152
11	144.103	0.1547	136.370	0.151	179.984	0.152	100.004	0.174
12	119.304	0.158	100.010	0.179	100.002	0.172	102.748	0.165
13	111.892	0.162	163.478	0.150	136.836	0.153	100.504	0.174
14	152.364	0.1526	100.237	0.177	151.121	0.159	174.408	0.152
15	150.742	0.155	127.148	0.153	137.698	0.163	138.973	0.153
16	109.020	0.181	129.206	0.150	171.648	0.154	131.180	0.153
17	101.039	0.185	116.964	0.160	137.552	0.160	145.943	0.152
18	135.316	0.156	107.993	0.163	120.767	0.1649	100.803	0.160
19	105.785	0.162	112.535	0.162	108.919	0.170	164.439	0.155
20	100.519	0.200	101.524	0.169	179.922	0.152	100.511	0.169

Table A1: Sets of non-dominated optimal solutions

NO.	f_r [mm/r]	a_p [mm]	EN 1.4404						EN 1.4462						EN 1.4410					
			R	R_c [N]	k_c [N/mm ²]	P_{sp} [W]	UCI	Rank	R	R_c [N]	k_c [N/mm ²]	P_{sp} [W]	UCI	Rank	R	R_c [N]	k_c [N/mm ²]	P_{sp} [W]	UCI	Rank
1	0.1	0.5	43	451	7574	166	0.578	17	100	590	9962	108	0.604	10	100	620	10249	187	0.449	22
2	0.1	1.0	43	576	4794	142	0.779	5	62	560	4614	131	0.887	1	118	680	5551	200	0.619	13
3	0.1	1.5	32	718	3906	172	0.959	1	118	799	4258	157	0.627	8	118	859	4564	192	0.642	9
4	0.1	2.0	62	935	3787	195	0.695	8	118	1131	4327	188	0.553	11	118	1132	4514	226	0.581	14
5	0.1	2.5	118	1207	3766	229	0.312	28	118	1336	4075	316	0.393	22	118	1384	4206	266	0.518	17
6	0.1	3.0	118	1594	3810	268	0.266	30	118	1615	3740	412	0.329	24	118	1870	4328	310	0.393	25
7	0.1	3.5	118	1710	3564	291	0.260	31	118	2413	4513	349	0.271	30	118	2549	4798	349	0.294	29
8	0.175	0.5	32	739	7252	152	0.617	14	62	740	7178	182	0.735	3	62	800	7852	216	0.663	7
9	0.175	1.0	21	877	4332	234	0.801	3	62	1364	7012	284	0.542	12	62	973	4737	154	0.846	2
10	0.175	1.5	21	1129	3650	264	0.848	2	78	1244	3949	274	0.627	8	78	1254	4010	251	0.727	4
11	0.175	2.0	21	1361	3297	311	0.794	4	78	1540	3572	365	0.508	15	78	1754	4024	314	0.648	8
12	0.175	2.5	43	1592	3070	372	0.620	13	118	1646	3164	328	0.420	20	118	2099	3906	399	0.343	27
13	0.175	3.0	78	1814	2920	366	0.362	24	78	1893	3011	365	0.505	16	118	1992	3192	397	0.417	24
14	0.175	3.5	78	2054	2828	345	0.357	26	118	2165	2937	470	0.316	26	78	2248	3080	391	0.625	11
15	0.25	0.5	32	825	5803	186	0.683	9	32	843	5823	359	0.719	4	32	897	6208	183	0.886	1
16	0.25	1.0	32	1225	4274	226	0.722	7	43	1205	4128	313	0.708	5	43	1408	4835	335	0.784	3
17	0.25	1.5	21	1534	3533	309	0.752	6	62	1685	3802	386	0.518	13	62	2027	4429	478	0.545	15
18	0.25	2.0	21	1812	3135	474	0.640	11	78	1930	3301	393	0.446	19	100	1965	3419	405	0.475	19
19	0.25	2.5	43	2091	2888	460	0.478	21	118	2282	3123	435	0.310	28	118	2320	3185	463	0.342	28
20	0.25	3.0	78	2407	2734	492	0.275	29	118	2516	2809	546	0.282	29	118	2536	2811	472	0.353	26
21	0.25	3.5	78	2603	2549	310	0.359	25	118	2880	2840	569	0.261	31	118	2989	2942	628	0.284	30
22	0.325	0.5	12	1038	5721	418	0.625	12	32	1096	5917	333	0.702	6	32	1135	6109	396	0.718	5
23	0.325	1.0	12	1724	4438	421	0.651	10	43	1908	4902	425	0.517	14	43	1776	4716	507	0.623	12

Table A2: Performance characteristics and predicted UCI values.

NO.	f_r [mm/r]	a_p [mm]	EN 1.4404						EN 1.4462						EN 1.4410					
			R	R_c [N]	k_c [N/mm ²]	P_{sp} [W]	UCI	Rank	R	R_c [N]	k_c [N/mm ²]	P_{sp} [W]	UCI	Rank	R	R_c [N]	k_c [N/mm ²]	P_{sp} [W]	UCI	Rank
24	0.325	1.5	21	2472	4070	523	0.386	23	62	2459	4102	525	0.399	21	43	2587	4286	593	0.480	18
25	0.325	2.0	21	2276	3069	481	0.587	16	43	2595	3352	453	0.454	17	78	2652	3497	483	0.469	20
26	0.325	2.5	32	2899	3004	549	0.346	27	118	3020	3121	649	0.454	17	118	3191	3291	584	0.266	31
27	0.325	3.0	43	3116	2723	679	0.260	31	118	3387	2894	602	0.241	32	118	3603	3059	594	0.266	31
28	0.325	3.5	78	3263	2521	690	0.091	35	118	3484	2688	669	0.235	33	118	3680	2813	759	0.250	33
29	0.4	0.5	12	1335	5749	418	0.574	18	32	983	4127	379	0.741	2	32	1248	5492	466	0.711	6
30	0.4	1.0	12	1868	4142	497	0.603	15	12	2068	4275	488	0.669	7	32	2331	4768	493	0.638	10
31	0.4	1.5	12	2329	3450	578	0.538	20	21	3313	4352	645	0.358	23	21	3102	4480	647	0.541	16
32	0.4	2.0	12	2651	2948	583	0.561	19	43	3262	3416	673	0.318	25	43	3311	3562	602	0.438	23
33	0.4	2.5	21	2759	2444	689	0.405	22	43	3836	3108	608	0.316	26	43	3551	3078	605	0.458	21
34	0.4	3.0	32	3637	2574	698	0.207	33	118	4294	2990	720	0.091	34	118	4414	3116	854	0.099	34
35	0.4	3.5	43	4255	2614	806	0.099	34	118	4670	2814	770	0.041	35	118	4860	2933	910	0.039	35

Table A2: Contd.

Alter.	Cutting Parameters			EN 1.4404			EN 1.4462			EN 1.4410		
	v_c [m/min]	f_r [mm/r]	a_p [mm]	R_a [μm]	R_z [μm]	R_t [μm]	R_a [μm]	R_z [μm]	R_t [μm]	R_a [μm]	R_z [μm]	R_t [μm]
A ₁	50	0.1	0.5	0.496	2.364	2.709	0.584	2.783	3.025	0.482	2.474	2.438
A ₂	50	0.25	1.5	2.986	12.01	12.68	2.799	10.46	10.86	2.655	11.88	12.47
A ₃	50	0.4	2.5	4.602	18.22	18.85	4.705	19.67	20.90	4.939	20.01	20.67
A ₄	50	0.55	3.5	6.867	26.15	27.72	6.277	29.24	30.34	8.447	34.98	37.73
A ₅	100	0.1	1.5	0.453	2.355	2.637	0.694	2.506	2.697	0.784	3.458	3.784
A ₆	100	0.25	0.5	1.678	7.711	7.861	1.918	9.480	9.661	2.117	9.325	9.501
A ₇	100	0.4	3.5	3.853	16.98	19.36	4.441	18.70	19.63	5.131	20.62	21.50
A ₈	100	0.55	2.5	6.318	25.01	26.64	6.071	24.89	26.75	6.861	26.15	26.94
A ₉	150	0.1	2.5	0.641	3.857	4.175	0.594	2.688	2.884	0.558	2.461	2.667
A ₁₀	150	0.25	3.5	2.316	9.187	9.489	2.208	9.054	9.348	2.281	9.841	10.01
A ₁₁	150	0.4	0.5	3.411	16.11	16.36	4.371	15.75	15.92	4.215	15.82	16.25
A ₁₂	150	0.55	1.5	5.149	23.73	24.33	5.902	22.69	23.36	4.435	16.26	16.49
A ₁₃	200	0.1	3.5	0.518	2.398	2.613	0.558	2.680	2.971	0.515	2.711	2.771
A ₁₄	200	0.25	2.5	2.482	8.636	8.850	2.471	8.897	9.385	2.452	9.273	9.692
A ₁₅	200	0.4	1.5	4.239	16.15	16.30	4.075	15.50	15.86	3.981	16.13	16.81
A ₁₆	200	0.55	0.5	4.185	19.61	20.15	5.111	20.64	20.94	6.277	28.79	29.12

Table A3: Taguchi L₁₆ experimental results.

Alter.	\tilde{R}			Mode			Spread			Rank		
	EN 1.4404	EN 1.4462	EN 1.4410	EN 1.4404	EN 1.4462	EN 1.4410	EN 1.4404	EN 1.4462	EN 1.4410	EN 1.4404	EN 1.4462	EN 1.4410
A ₁	0.386	0.386	0.393	0.987	0.988	1.005	1.276	1.278	1.300	2	4	1
A ₂	0.146	0.174	0.180	0.374	0.445	0.461	0.484	0.575	0.596	8	8	8
A ₃	0.080	0.078	0.108	0.205	0.200	0.277	0.265	0.259	0.358	12	12	12
A ₄	0.000	0.000	0.000	0.000	0.000	0.000	0.000	0.000	0.000	16	16	16
A ₅	0.393	0.388	0.328	1.005	0.992	0.840	1.300	1.283	1.086	1	3	4
A ₆	0.213	0.199	0.209	0.543	0.510	0.535	0.703	0.659	0.692	5	5	5
A ₇	0.091	0.089	0.103	0.234	0.227	0.263	0.303	0.293	0.340	11	11	13
A ₈	0.013	0.029	0.061	0.033	0.075	0.156	0.043	0.097	0.202	15	15	14
A ₉	0.317	0.391	0.381	0.810	0.999	0.974	1.048	1.292	1.260	4	2	2
A ₁₀	0.184	0.198	0.202	0.470	0.506	0.517	0.607	0.654	0.669	7	6	7
A ₁₁	0.111	0.113	0.139	0.283	0.290	0.356	0.366	0.375	0.461	9	10	9
A ₁₂	0.039	0.050	0.135	0.099	0.128	0.346	0.128	0.165	0.448	14	14	11
A ₁₃	0.385	0.393	0.378	0.984	1.005	0.966	1.273	1.300	1.250	3	1	3
A ₁₄	0.187	0.194	0.204	0.477	0.495	0.521	0.617	0.640	0.674	6	7	6
A ₁₅	0.101	0.118	0.138	0.258	0.301	0.355	0.334	0.389	0.459	10	9	10
A ₁₆	0.076	0.071	0.053	0.194	0.182	0.135	0.251	0.235	0.174	13	13	15

Table A4: Area between centroid of centroids (\tilde{R}), mode and spread values.

Exp No.	Design variables					EN 1.4462				EN 1.4410			
	v_c [m/min]	f_r [mm/rev]	a_p [mm]	L_c [mm]	CM	$\%F_t$	P_e [W]	VB_{max} [μ m]	R	$\%F_t$	P_e [W]	VB_{max} [μ m]	R
1	200	0.25	1.5	12	Wet	21.7	4236.4	193.7	32.02	30.18	4451.4	186.8	37.48
2	75	0.25	1.5	7.5	Dry	18.3	1815.05	117.8	159.05	20.39	2222.0	134.6	157.9
3	75	0.25	1.5	3	Wet	9.66	1000.04	70.96	116.7	10.41	1063.8	85.75	141
4	200	0.25	0.5	12	Wet	26.4	3489.3	211.6	105.6	32.82	3566.5	225.9	115.2
5	200	0.25	0.5	3	Wet	12.5	3234.7	109.01	96.06	16.31	3467.2	111.4	100.1
6	200	0.10	0.5	12	Wet	10.3	3545.7	93.15	105.9	13.73	3887.2	93.81	114
7	75	0.17	1	7.5	Wet	15.9	923.63	101.3	99.36	15.10	1011.2	137.9	105.8
8	137.5	0.17	1.5	7.5	Wet	5.60	1904.1	75.31	91.59	10.48	2018.5	57.27	111.8
9	75	0.25	1	3	Dry	15.2	958.95	98.64	24.01	11.97	980.69	92.11	71.80
10	200	0.10	1.5	3	Wet	11.2	3143.7	93.78	59.86	14.30	3356.9	98.18	66.07
11	75	0.10	1.5	12	Wet	19.0	968.77	154.6	97.27	23.86	1100.7	164.2	106.9
12	200	0.25	0.5	12	Wet	26.4	3487.5	211.6	106.9	32.82	3586.3	225.9	117.5
13	200	0.10	1.5	12	Wet	16.7	3294.3	131.5	63.95	19.96	3489.5	145.6	76.15
14	200	0.10	0.5	3	Wet	11.7	3155.3	137.0	101.3	21.27	3489.6	103.6	123.8
15	75	0.25	1.5	12	Wet	20.7	1306.6	134.2	128.9	20.59	1512.8	176.4	155.1
16	75	0.10	0.5	3	Dry	20.4	912.85	130.3	88.14	24.50	831.53	160.1	91.10
17	75	0.25	0.5	3	Wet	14.3	912.03	91.20	98.67	13.59	998.23	124	113.8
18	200	0.25	1.5	3	Dry	25.0	4556.1	178.5	33.88	31.56	5748.8	203.6	39.96
19	200	0.25	1	12	Dry	36.7	4621.1	230.09	17.75	41.41	5493.9	284.1	29.79
20	200	0.25	1.5	3	Wet	10.7	4072.7	93.30	21.02	13.95	4189.5	95.44	25.09
21	75	0.10	1.5	3	Wet	14.3	793.15	114.3	92.39	17.75	842.73	122.3	105.4
22	137.5	0.17	1	3	Wet	2.26	1781.6	59.64	50.50	8.10	1884.7	29.15	75.02
23	137.5	0.17	1	12	Wet	10.5	1616.5	89.17	55.12	12.97	1745.2	95.35	82.56
24	75	0.25	0.5	3	Wet	14.3	913.13	88.60	97.67	13.05	985.85	124.5	112.1
25	75	0.10	0.5	12	Wet	25.6	838.76	146.1	74.07	22.04	996.36	218.8	81.36
26	137.5	0.10	1	7.5	Wet	12.7	1592.8	82.71	69.12	11.73	1606.8	114.1	83.55
27	200	0.10	1.5	7.5	Dry	26.4	3634.8	167.5	121.9	30.39	3848.5	216.6	119.5
28	106.2	0.21	0.75	7.5	Dry	15.1	1558.2	97.76	69.05	19.01	1547.8	126.1	86.65
29	137.5	0.10	1.5	3	Dry	10.5	1946.8	79.49	115.7	14.38	2052.2	97.11	123.7
30	200	0.25	1.5	3	Dry	27.0	4556.1	180.6	34.01	30.55	5739.2	197.4	38.26
31	75	0.17	1.5	3	Dry	10.8	1206.5	71.18	139.8	13.05	1332.6	88.75	147.9
32	200	0.17	1	7.5	Wet	14.4	3672.3	112.9	48.02	16.72	4016.4	128.3	60.46
33	200	0.17	1.5	12	Dry	28.6	3330.2	180.7	29.87	35.53	3622.9	234	57.99
34	75.0	0.10	0.5	7.5	Dry	21.1	996.49	234.6	111.2	26.13	1027.2	170.2	155.7
35	137.5	0.25	1.5	12	Dry	16.1	2718.01	124.2	65.04	20.38	2812.9	134.6	30.17
36	200	0.10	0.5	12	Dry	55.2	3293.1	448.01	119.7	61.41	3579.6	579.1	138.5
37	75	0.10	1	12	Dry	32.3	1146.7	203.02	104.2	11.02	1071.2	81.97	122.9
38	168.7	0.14	0.75	7.5	Dry	19.2	2197.6	127.08	98.87	23.35	2201.8	153	117.1
39	75	0.17	0.5	12	Dry	24.6	959.55	156.4	126.06	29.41	913.94	190.4	145
40	200	0.10	0.5	12	Dry	55.9	3313.1	446.4	121.6	61.41	2934.2	586.8	139.9
41	200	0.25	0.5	7.5	Dry	37.1	3557.2	232.3	116.8	42.08	3557.3	268	135.3
42	137.5	0.25	0.5	3	Dry	13.7	2240.7	109.3	56.32	22.93	1971.5	150.4	84.12

Table A5: D-Optimal results.

Exp No.	Design variables					EN 1.4462				EN 1.4410			
	v_c [m/min]	f_r [mm/rev]	a_p [mm]	L_c [mm]	CM	$\%F_t$	P_e [W]	VB_{max} [μm]	R	$\%F_t$	P_e [W]	VB_{max} [μm]	R
43	200	0.10	1	3	Dry	24.2	3207.7	152.5	64.14	26.89	3514.1	185	91.98
44	75	0.25	0.5	12	Wet	25.4	998.86	122.3	107.10	18.37	1208.4	215.8	118
45	75	0.10	0.5	3	Wet	17.4	759.17	132.5	70.77	20.11	845.42	151.7	80.75
46	75	0.25	0.5	12	Dry	29.5	1052.5	216.3	119.9	34.71	955.32	205.8	128.6
47	75	0.10	1.5	12	Dry	17.5	1051.1	113.0	112.5	23.05	1075.7	153.2	140.9
48	200	0.17	0.5	3	Dry	18.2	3232.6	119.0	69.33	22.81	3447.9	153.7	65.26

Table A5: Contd.

Coef.	EN 1.4462								EN 1.4410							
	%F _r		P _e		VB _{max}		R		%F _r		P _e		VB _{max}		R	
	Wet	Dry	Wet	Dry	Wet	Dry	Wet	Dry	Wet	Dry	Wet	Dry	Wet	Dry	Wet	Dry
c ₀	70.6	69.4	1700.9	2165.7	467.2	604.2	29.8	88.9	75.8	22.3	1765.7	2013.1	576.9	176.2	-16.31	76.65
c ₁	-0.59	-0.48	-20.63	-5.30	-3.03	-1.91	0.67	0.32	-0.51	0.21	-25.55	18.75	-4.70	1.64	1.56	0.71
c ₂	-386.	-435	-1384	-23259	-1550	-4341.5	412.3	-401.5	-253.	160.1	5243	14453	-3123	1265.2	732.1	550.24
c ₃	9.22	-0.74	-811.2	-0.52	-69.37	-257.56	-144.9	-173.5	-10.1	21.75	-1274	1963.4	65.42	171.8	-143.2	74.7
c ₄	1.58	1.70	61.81	46.41	-10.37	19.05	13.30	31.54	-1.94	2.01	59.15	181.15	13.86	15.86	6.91	6.90
c ₁₁	0.00	0.00	0.13	0.07	0.01	0.01	0.00	0.00	0.00	0.00	0.16	0.06	0.01	0.01	0.00	0.00
c ₂₂	931	1235	-3539	50842	2176	11795	95.65	737.5	358.9	425.8	-21964	8438.1	7473.3	3365	-666.4	1463.4
c ₃₃	-6.29	1.34	88.09	8.97	27.36	103.39	118.20	166.96	4.15	9.63	236.10	869.17	-47.89	76.09	119.06	33.09
c ₄₄	-0.10	0.08	-3.74	-0.54	-0.08	0.44	-0.90	-1.60	0.03	0.11	-2.81	9.98	-0.88	0.87	-0.58	0.38
c ₁₂	0.38	-0.01	11.96	36.67	3.88	-0.95	-2.46	-1.27	0.62	0.28	3.69	25.30	3.24	2.21	-3.27	0.96
c ₁₃	0.03	-0.03	1.78	0.23	-0.06	-0.16	-0.65	-0.65	-0.01	0.04	1.52	3.76	0.28	0.33	-0.74	0.14
c ₁₄	0.00	0.01	0.08	-0.06	0.01	0.07	0.00	-0.02	0.00	0.00	-0.04	0.42	-0.01	0.04	0.00	0.02
c ₂₃	-22.1	31.8	3421.3	3590.9	-73.52	580.6	-117.5	-93.95	-12.2	35.85	4036.3	3235.8	-176.9	283.2	-77	123.2
c ₂₄	5.81	-5.36	-16.90	97.45	48.25	-58.30	5.89	26.88	8.00	4.00	-9.61	360.96	46.71	31.60	9.78	13.74
c ₃₄	-0.02	-1.64	3.13	-36.41	3.56	-14.68	-0.02	-7.57	0.58	0.60	11.06	54.40	-0.07	4.76	0.52	2.07
ANOVA																
R ²	0.96	0.97	0.99	0.98	0.92	0.98	0.97	0.93	0.92	0.95	0.99	0.97	0.96	0.97	0.97	0.94
R _{adj.}	0.90	0.93	0.98	0.95	0.80	0.95	0.91	0.83	0.80	0.87	0.97	0.93	0.89	0.92	0.93	0.85
RMSE	2.09	3.2	179	274	18.6	21.4	8.33	16.8	3.01	4.86	212	423	17.4	37	8.27	16.1
A _{prec.}	14.9	17.7	24.5	17.1	9.82	22.91	15.57	9.66	9.82	12.67	21.59	14.67	14.53	17.33	19.1	9.465
F-value	15	22.3	79.9	34.8	7.57	32.9	17.8	8.89	7.62	12.4	61.3	21.9	14.5	19.2	21.6	10.6
R. DOF	14	14	14	14	14	14	14	14	14	14	14	14	14	14	14	14
Err. DOF	9	9	9	9	9	9	9	9	9	9	9	9	9	9	9	9

RMSE: Root Mean Squared Error, R. DOF: Regression Degrees of Freedom, Err. DOF: Error Degrees of Freedom

Table A6: Models coefficients estimates and ANOVA.

Component	Independent variables					EN 1.4462				EN 1.4410			
	v_c [m/min]	f_r [mm/rev]	a_p [mm]	L_c [mm]	CM	t_{bb} [hrs/year]	K_I [€/unit]	K_3 [€/unit]	C_i^*	t_{bb} [hrs/year]	K_I [€/unit]	K_3 [€/unit]	C_i^*
1	200	0.25	1.5	12	Wet	734.47	2.54	1.58	0.845	748.02	2.543	1.86	0.886
2	75	0.25	1.5	12	Dry	959.73	4.88	1.04	0.885	985.958	4.880	1.59	0.882
3	75	0.25	1.5	12	Wet	959.22	4.91	1.03	0.886	971.80	4.910	1.30	0.904
4	200	0.25	0.5	12	Wet	1261.2	7.62	1.33	0.791	1288.9	7.629	1.91	0.792
5	200	0.25	0.5	12	Wet	1261.2	7.62	1.33	0.791	1288.9	7.629	1.91	0.792
6	200	0.10	0.5	12	Wet	1969.4	14.65	0.58	0.609	1985.9	14.65	0.93	0.607
7	75	0.17	1	12	Wet	1496.2	10.13	0.68	0.749	1512.1	10.13	1.02	0.748
8	137	0.17	1.5	12	Wet	877.47	4.205	0.88	0.918	884.97	4.205	1.04	0.941
9	75	0.25	1	12	Dry	1230.4	7.320	1.27	0.804	1252.4	7.320	1.73	0.810
10	200	0.10	1.5	12	Wet	943.05	4.884	0.75	0.914	952.16	4.884	0.94	0.924
11	75	0.10	1.5	12	Wet	1562.3	10.80	0.60	0.729	1571.2	10.80	0.78	0.728
12	200	0.25	0.5	12	Wet	1261.2	7.629	1.33	0.791	1288.9	7.629	1.91	0.792
13	200	0.10	1.5	12	Wet	943.05	4.884	0.75	0.914	952.16	4.884	0.94	0.924
14	200	0.10	0.5	12	Wet	1969.4	14.65	0.58	0.609	1985.9	14.65	0.93	0.607
15	75	0.25	1.5	12	Wet	959.22	4.910	1.03	0.886	971.80	4.910	1.30	0.904
16	75	0.10	0.5	12	Dry	3910.6	32.20	1.88	0.389	3922.9	32.20	2.14	0.385
17	75	0.25	0.5	12	Wet	1990.1	14.73	0.85	0.604	2016.4	14.73	1.40	0.602
18	200	0.25	1.5	12	Dry	748.01	2.527	1.86	0.813	795.55	2.527	2.86	0.799
19	200	0.25	1	12	Dry	901.82	3.791	2.26	0.764	942.67	3.791	3.12	0.771
20	200	0.25	1.5	12	Wet	734.47	2.543	1.58	0.845	748.02	2.543	1.86	0.886
21	75	0.10	1.5	12	Wet	1562.3	10.80	0.60	0.729	1571.2	10.80	0.78	0.728
22	137	0.17	1	12	Wet	1095.5	6.308	0.78	0.869	1109.3	6.308	1.07	0.873
23	137	0.17	1	12	Wet	1095.5	6.308	0.78	0.869	1109.3	6.308	1.07	0.873
24	75	0.25	0.5	12	Wet	1990.1	14.73	0.85	0.604	2016.4	14.73	1.40	0.602
25	75	0.10	0.5	12	Wet	3842.9	32.40	0.45	0.370	3860.7	32.40	0.83	0.373
26	137	0.10	1	12	Wet	1443.5	9.692	0.57	0.766	1455.1	9.692	0.81	0.765
27	200	0.10	1.5	12	Dry	992.90	4.854	1.80	0.800	1031.2	4.854	2.60	0.799
28	106	0.21	0.75	12	Dry	1379.1	8.578	1.58	0.748	1402.5	8.578	2.07	0.758
29	137	0.10	1.5	12	Dry	1140.8	6.422	1.39	0.814	1167.9	6.422	1.96	0.818
30	200	0.25	1.5	12	Dry	748.01	2.527	1.86	0.813	795.55	2.527	2.86	0.799
31	75	0.17	1.5	12	Dry	1155.7	6.717	1.05	0.838	1178.4	6.717	1.52	0.839
32	200	0.17	1	12	Wet	956.20	4.916	0.95	0.894	972.60	4.916	1.30	0.904
33	200	0.17	1.5	12	Dry	819.29	3.257	1.72	0.825	860.45	3.257	2.59	0.817
34	75.0	0.10	0.5	12	Dry	3910.6	32.20	1.88	0.389	3922.9	32.20	2.14	0.385
35	137	0.25	1.5	12	Dry	791.46	3.155	1.37	0.869	826.79	3.155	2.11	0.860
36	200	0.10	0.5	12	Dry	2082.0	14.56	2.95	0.566	2128.4	14.56	3.93	0.569
37	75	0.10	1	12	Dry	2173.9	16.10	1.43	0.558	2188.2	16.10	1.73	0.561
38	168	0.14	0.75	12	Dry	1383.1	8.394	2.07	0.715	1412.7	8.394	2.69	0.728
39	75	0.17	0.5	12	Dry	2614.1	20.15	1.62	0.472	2631.9	20.15	2.00	0.472
40	200	0.10	0.5	12	Dry	2082.2	14.56	2.95	0.566	2128.4	14.56	3.93	0.569
41	200	0.25	0.5	12	Dry	1334.4	7.582	2.87	0.675	1383.3	7.582	3.90	0.681
42	137	0.25	0.5	12	Dry	1497.9	9.464	2.09	0.693	1530.6	9.464	2.78	0.701

Table A7: Results of multi-objective optimization using TOPSIS

Component	Independent variables					EN 1.4462				EN 1.4410			
	v_c [m/ min]	f_r [mm /rev]	a_p [mm]	L_c [mm]	CM	t_{bb} [hrs/ year]	K_1 [€/ unit]	K_3 [€/ unit]	C_i^*	t_{bb} [hrs /year]	K_1 [€/ unit]	K_3 [€/ unit]	C_i^*
43	200	0.10	1	12	Dry	1272.3	7.28	2.24	0.723	1305.	7.281	2.93	0.737
44	75	0.25	0.5	12	Wet	1990.1	14.7	0.85	0.604	2016	14.73	1.40	0.602
45	75	0.10	0.5	12	Wet	3842.9	32.4	0.45	0.370	3860	32.40	0.83	0.373
46	75	0.25	0.5	12	Dry	2026.1	14.6	1.60	0.592	2047	14.64	2.06	0.595
47	75	0.10	1.5	12	Dry	1588.6	10.7	1.15	0.714	1608	10.73	1.57	0.716
48	200	0.17	0.5	12	Dry	1558.5	9.77	2.67	0.653	1603	9.772	3.62	0.658

Table A7: Contd.